HYDROLYTIC STRIPPING OF MIXED METAL CARBOXYLATES

by

FIONA MARY DOYLE
M.A.(Cantab) M.Sc. D.I.C.

A thesis submitted for the
Degree of Doctor of Philosophy
of the University of London
and for the
Diploma of Membership of the Imperial College

March 1983

Department of Metallurgy and Materials Science
Royal School of Mines
Imperial College of Science and Technology
University of London

To my parents and Des

ABSTRACT

Hydrolytic stripping is the process whereby metal ions in an organic solution are hydrolysed by water at 150°-200°C. Iron(III), nickel(II) and copper(II), for example, are hydrolysed in carboxylate solutions and precipitate hematite, nickel hydroxide and copper(I) oxide respectively.

The carboxylic acid used was Versatic 10, a tertiary aliphatic monobasic acid. Screening tests were done on Versatic solutions of Mg, Ca, Sr, Al, Ti, Cr, Mn, Fe, Co, Ni, Cu, Zn and Cd, singly and in mixtures at 200°C. Single solutions of Mg, Mn, Fe, Ni and Cu precipitated $Mg(OH)_2$, Mn_2O_3, Fe_2O_3, $Ni(OH)_2$ and Cu_2O respectively during hydrolytic stripping. In general, mixed solutions gave a mixture of precipitates, according to the metals in solution. However, some mixtures containing iron precipitated magnetic ferrites $MFeO_4$, with the spinel structure.

The precipitation of nickel ferrite was studied in sealed tube and kinetic tests. The rate of heterogeneous precipitation appeared to be proportional to seed area, and inversely proportional to free Versatic acid concentration. The rate increased with increasing iron concentration but decreased with increasing nickel concentration, and was independent of water concentration and stirring speed. The activation energy was 124.4 kJ mol^{-1}.

High temperature infrared spectrophotometry was used to measure free Versatic concentrations, and gave evidence of mixed iron-nickel carboxylate complexes in mixed solutions. Thin layer chromatography gave further evidence of mixed species. Surface area analysis and electron microscopy indicated that the precipitated ferrite typically comprised chains of clusters, each of diameter .07-.1μm, containing randomly oriented crystallites of about 50-100Å radius.

CONTENTS

	Page
Abstract	2
Contents	3
List of Figures	8
List of Tables	10
List of Abbreviations	12
CHAPTER 1 INTRODUCTION	14
CHAPTER 2 LITERATURE SURVEY	22
2.1 The Use of Carboxylic Acids as Solvent Extraction Reagents	22
2.1.1 Properties of Carboxylic Acids	22
2.1.2 Extraction of Metals by Carboxylic Acids	25
2.1.3 Influence of Other Ions in Solution on the Extraction of Metals by Carboxylic Acids	29
2.1.4 Determination of the Mechanism of Extraction	32
2.1.5 Composition of Metal-Carboxylate Complexes	33
2.2 Aqueous Phase Hydrolysis	38
2.2.1 Precipitation of Metal Hydroxides	38
2.2.2 Factors Influencing the Hydrolysis Behaviour of Iron	41
2.2.3 The Mechanism of Hydrolysis of Iron(III)	48
2.2.4 The Crystal Structure of Iron Oxides and Oxide Hydroxides	56
2.3 Spinel Ferrites: Their Structure, Properties and Uses	60
2.3.1 The Structure of Spinel Ferrites	60
2.3.2 Magnetic Properties of the Spinel Ferrites	65
2.3.3 Uses of the Spinel Ferrites	68
2.3.4 Manufacture of Spinel Ferrites	69

Page

PART I EQUILIBRIUM STUDIES OF THE HYDROLYTIC STRIPPING OF METAL CARBOXYLATES AND THEIR MIXTURES

CHAPTER 3 EXPERIMENTAL PROCEDURE 72

3.1 Introduction 72
3.2 Materials Used 74
3.3 Exchange Extraction of Iron 74
3.3.1 Factorial Design 74
3.3.2 Staged Washing of Iron-Versatic Solution 78
3.3.3 Continuous Washing of Iron-Versatic Solution 79
3.4 Preparation of Metal-Versatic Solutions 79
3.5 Chemical Analysis of Metal-Versatic Solutions 81
3.5.1 EDTA Titrations 81
3.5.2 Atomic Absorption Spectrophotometry 82
3.5.3 Analysis of Strontium-Versatic Solution 84
3.6 Sealed Tube Screening Tests 85
3.6.1 Hydrolytic Stripping 85
3.6.2 Identification of Precipitates by X-Ray Powder Diffraction 86
3.6.3 Chemical Analysis of Precipitates 86

CHAPTER 4 RESULTS FOR THE PREPARATION AND ANALYSIS OF METAL-VERSATIC SOLUTIONS 87

4.1 Exchange Extraction of Iron 87
4.1.1 Factorial Design 87
4.1.2 Staged Washing of Iron-Versatic Solution 90
4.1.3 Continuous Washing of Iron-Versatic 92
4.2 Preparation of Metal-Versatic Solutions 93
4.3 Chemical Analysis of Metal-Versatic Solutions 95
4.3.1 EDTA Titrations 95
4.3.2 Atomic Absorption Spectrophotometry 95
4.3.3 Concentration of Metal-Versatic Solutions 95

Page

CHAPTER 5 RESULTS FROM SEALED TUBE SCREENING TESTS 97

5.1 Identification of Precipitates by X-ray Powder Diffraction 97
5.2 Hydrolytic Stripping of Metal Carboxylates 98
5.2.1 Solutions Containing a Single Metal 98
5.2.2 Solutions Containing Two Metals 98
5.2.3 Solutions Containg Three Metals 101
5.3 Chemical Analysis of Spinel Ferrites 101
5.4 Discussion of Results 102
5.4.1 Solutions Containing a Single Metal 102
5.4.2 Solutions Containing Two and Three Metals 106

PART II THE HYDROLYTIC STRIPPING OF IRON-NICKEL CARBOXYLATE SOLUTIONS

CHAPTER 6 EXPERIMENTAL PROCEDURE 112

6.1 Introduction 112
6.2 Screening Tests 113
6.3 Kinetic Studies: Apparatus and Materials 113
6.4 Kinetic Studies: Routine Procedure 119
6.4.1 Preparation of Versatic Solutions 120
6.4.2 Hydrolytic Stripping Runs 122
6.4.3 Analysis of Samples 123

CHAPTER 7 SCREENING OF VARIABLES 124

7.1 Introduction 124
7.2 Plackett-Burman Design 124
7.3 Resolution IV Fractionated Factorial Design 127
7.4 Selection of Variables for Kinetic Studies 133

CHAPTER 8 KINETIC TESTS 134

8.1 Introduction 134
8.2 Measurement of Initial Reaction Rates 135
8.3 Unseeded Runs 138
8.4 Effect of Different Seed Materials 140
8.5 Effect of the Age of Metal Versatic Solutions 145

		Page
8.6	Effect of Water Volume and Stirring Speed	148
8.7	Effect of Temperature on Initial Rate	149
8.8	Effect of Nickel Ferrite Seed on Initial Rate	153
8.9	Effect of Iron, Nickel and Versatic Concentration: Factorial Design	156
8.10	Organic Injection Runs	162
8.11	Effect of Versatic Concentration on Initial Rate	165
CHAPTER 9	INFRARED SPECTROPHOTOMETRY	167
9.1	Introduction	167
9.2	Measurement of Free Versatic Acid in Organic Solutions	172
9.2.1	Determination of the Monomer and Dimer Extinction Coefficients	173
9.2.2	Determination of the Dimer Dissociation Constant	177
9.2.3	Effect of Dilution on Free Versatic in Iron-Nickel Solutions	180
9.2.4	Examination of Organic Samples from Kinetic Runs	184
9.3	Composition of Mixed-Metal Versatic Complexes	189
9.4	Infrared Spectra of Metal Versatic Solutions	193
CHAPTER 10	ADDITIONAL EXPERIMENTAL WORK	200
10.1	Surface Area Measurements	200
10.1.1	Experimental Method	200
10.1.2	Results of Surface Area Measurements	200
10.2	X-ray Powder Diffraction Analysis	202
10.3	Electron Microscopy	203
10.3.1	Specimen Preparation	203
10.3.2	Examination of Precipitates	204
10.4	Thin Layer Chromatography	210
CHAPTER 11	GENERAL DISCUSSION	212

Page

CHAPTER 12 CONCLUSIONS AND SUGGESTIONS FOR FURTHER WORK 223

12.1 Conclusions from Experimental Work 223

12.1.1 Part I: Preparation of Metal-Versatic Solutions and Hydrolysis of Single and Mixed Solutions in Sealed Tubes 223

12.1.2 PartII: Hydrolytic Stripping of Iron-Nickel Versatic Solutions 224

12.1.3 Infrared Spectrophotometry 226

12.1.4 Additional Experimental Work 227

12.2 Suggestions for Further Work 228

APPENDICES

APPENDIX A Calibration of Variable Diluter 230

APPENDIX B X-ray Powder Diffraction Patterns 232

APPENDIX C Results fron Kinetic Runs 245

APPENDIX D Precipitation of Cobalt Ferrite 252

APPENDIX E Estimate of Thickness of Ferrite Layer Precipitated During Seeded Kinetic Run 254

APPENDIX F Estimate of the Radius of Seed Particles 255

References 256

Acknowledgements 264

LIST OF FIGURES

		Page
Figure 2.1	Extraction of Metals by Versatic 10	26
Figure 2.2	The Structure of the Dimeric Copper Complex	33
Figure 2.3	The Structure of $[Cr_3O(CH_3COO)_6(H_2O)_3]^+$	37
Figure 2.4	Hydroxide Precipitation Diagram, 25°C	39
Figure 2.5	(a) Precipitation Temperature for Ferric Nitrate Solutions, Showing Compounds Precipitated (b) Phase Diagram for the System Fe^{3+}-Fe_2O_3-H_2O	42
Figure 2.6	Part of the Fe_2O_3-H_2O-SO_3 Phase System at 100°C as a Function of Iron Concentration and pH	46
Figure 2.8	(a) Species Distribution Diagrams for Ferric-Hydroxo Complexes (b) Species Distribution Diagrams for Ferric-Hydroxo and Sulphato Complexes	50
Figure 2.9	(a) Polynuclear Cation Formed in Ferric Nitrate and Sulphate Solutions (b) Polynuclear Cation Formed in Ferric Chloride Solns	52
Figure 2.10	Proposed Scheme of Hydrolysis-Precipitation	53
Figure 2.11	Projected Atom Positions in Hematite, Goethite, Lepidocrocite and Magnetite/maghemite	59
Figure 2.12	Unit Cell of Nickel Ferrite	62
Figure 2.13	The Structure of the Spinel Unit Cell	63
Figure 6.1	Front View of Experimental Apparatus	115
Figure 6.2	Rear View of Experimental Apparatus	117
Figure 7.1	Normal Probability Plot of Effects	132
Figure 8.1	Unseeded Runs	139
Figure 8.2	Effect of Activated Carbon, Silica and Sintered Nickel Ferrite on Precipitation Rate	143
Figure 8.3	Effect of Seeding with Hematite and Nickel Hydroxide	144
Figure 8.4	Effect of Precipitated Nickel Ferrite on Rate	146
Figure 8.5	Effect of Temperature on Rate of Hydrolytic Stripping	150
Figure 8.6	Arrhenius Plot	151
Figure 8.7	Effect of Seed Level on Initial Rate	154
Figure 8.8	Factorial Design: Concentration-Time Curves for [V]=50%, Varying $[Fe]_o$ and $[Ni]_o$	157
Figure 8.9	Effect of Versatic, Iron and Nickel on Initial Rate	161

		Page
Figure 8.10	Injection Runs (a)Injection of Versatic Acid (b)Injection of Iron Versatic Solution	164
Figure 8.11	Effect of Versatic Concentration on Initial Rate	166
Figure 9.1	Infrared Spectrum of a 2.5% Solution of Versatic 10 at 25°C and 165°C	169
Figure 9.2	(a) Predicted $\hat{C}_v$ versus actual C_v (b) Plot of residuals versus predicted $\hat{C}_v$	176
Figure 9.3	Determination of Dissociation Constant: ln r against 1/T	179
Figure 9.4	Effect of Dilution on Concentration of Free Versatic Acid	183
Figure 9.5	Initial Rate against Free Versatic Concentration for Kinetic Runs	187
Figure 9.6	Initial Rate against $1/[HV]_f$	188
Figure 9.7	Versatic to Metal Charge Ratio in Complexes as a Function of Total Metal Charge	191
Figure 9.8	Plots of Free Versatic Acid against Total Metal	192
Figure 9.9	Infrared Spectrum of Iron-Versatic	194
Figure 9.10	Infrared Spectrum of Nickel-Versatic	195
Figure 9.11	Infrared Spectrum of Iron-Nickel Versatic	196
Figure 9.12	Infrared Spectra of 33% Versatic Solutions with Varying Iron and Nickel Concentrations	198
Figures 10.1 - 10.12	Electron Micrographs of Material Precipitated During Hydrolytic Stripping	206 207 208
Figure 11.1	Schematic Distribution of Fe(III) and Ni(II) Species over Active Surface Sites (first model proposed)	219
Figure 11.2	Schematic Distribution of Fe(III) and Ni(II) Species over Active Surface Sites (second model proposed)	221
Figure D	Precipitation of Cobalt Ferrite Under Different Seeding Conditions	253

LIST OF TABLES

		Page
2.1.1	Experimentally Determined Composition of Metal-Carboxylate Complexes	34
2.2.1	Comparison of 'Goethite' Precipitates from E.Z. and V.M. Processes in Sulphate and Chloride Solutions	47
2.2.2	Summary of the Crystal Structures of Iron Oxides and Oxide Hydroxides	57
2.3.1	Commercially Important Ferrites	61
2.3.2	Lattice Parameters of Single Ferrite Spinels $M^{2+}Fe_2O_4$	64
2.3.3	Ion Distribution and Net Moment per Molecule for Some Typical Ferrites	67
2.3.4	Market Value of U.S. Production of Magnetic Materials in 1968	69
3.2.1	Reagents Used in the Preparation of Metal-Versatic Solutions	75
3.2.2	Reagents Used in the EDTA Analysis of Metal-Versatic Solutions	75
3.2.3	Atomic Absorption Standard Solutions	76
3.2.4	Miscellaneous Reagents Used	76
3,4.1	Preparation of Metal-Versatic Solutions	80
3.5.1	Metals Analysed by EDTA Titrations	82
3.5.2	Standard Conditions Used for Atomic Absorption Spectrophotometry	83
4.1.1	Variables Studied in Factorial Design	87
4.1.2	Exchange Extraction of Iron: Factorial Design; Yates' Algorithm and Effects	88
4.1.3	Results of Staged Washing Tests on Iron-Versatic Solution	91
4.3.1	Concentration of Metal in 1.7492M Versatic Acid Solutions	96
5.2.1	Hydrolytic Stripping of Single Metal Carboxylates	99
5.2.2	Hydrolytic Stripping of Metal Carboxylates: Two Metals	100
5.4.1	Chemical Analysis of Precipitates from Hydrolytic Stripping	108
6.3.1	Materials Tested as Seeds for Precipitation of Nickel Ferrite	118
6.3.2	Size Analysis of Nickel Ferrite Used to Seed Main Kinetic Runs	119
7.2.1	Results from Plackett-Burman Design	125
7.2.2	Confounding within the 8 Experiment Plackett-Burman Design	127

	Page
7.3.1 Resolution IV Fractionated Factorial Design - Responses, Main Effects and Design Matrix	129
7.3.2 Resolution IV Fractionated Factorial Design - Two Factor Effects	130
8.2.1 Computer Output of Polynomial Fitting Routine	137
8.3.1 Initial Rates of Unseeded Runs	140
8.4.1 Effect of Different Seed Materials on Rates of Precipitation	141
8.5.1 Effect of the Age of Metal-Versatic Solutions on Rate	147
8.6.1 Effect of Water Volume and Stirring Speed on Rate	148
8.7.1 Effect of Temperature on Initial Rate of Precipitation	152
8.8.1 Effect of Nickel Ferrite Seed Level on Initial Rate	155
8.9.1 Levels of the Variables Studied in Factorial Design	156
8.9.2 Factorial Design: Initial Rates, Yates' Algorithm and Effects	159
8.10.1 Injection Runs: Compositions Before and During Runs, and Initial Rates	162
8.11.1 Effect of Versatic Concentration on Initial Rate	165
9.1.1 Carboxyl Dimer Spectral Regions	168
9.1.2 Carboxyl Monomer Spectral Regions	168
9.2.1 OD_{HV} versus C_v in the range 25-165°C	174
9.2.2 $OD_{(HV)_2}$ versus C_v in the range 25-165°C	174
9.2.3 ln r values for nominal temperatures 130°, 150° and 165°C	178
9.2.4 Calculated Dissociation Constants for Various Temperatures	180
9.2.5 Effect of Dilution on Concentration and Dissociation Constant of Free Versatic Acid at 160°C	182
9.2.6 Organic Samples from Kinetic Runs	185
9.2.7 Free Acid Concentration and Initial Rate of Selected Kinetic Runs	186
10.1.1 Surface Area of Seed, and Precipitates from Factorial Design	201
10.4.1 Thin Layer Chromatography Results: Retention Factors	211

LIST OF ABBREVIATIONS

R	carboxylate ion
HR	carboxylic acid
$\overline{MR_n}$	bar over a species indicates that it is present in the organic phase
{ }	activity
[ ]	concentration
$[\ ]_{org}$	concentration in organic phase
$[\ ]_{aq}$	concentration in aqueous phase
$[\ ]_o$	concentration at time zero
D_M	distribution constant of metal M
$pH_{0.5}$	pH at which there is 50% extraction of a metal For equal phase volumes
TBP	tributyl phosphate
D2EHPA	di-(2-ethylhexyl)-phosphoric acid
x	degree of polymerisation
s	solvation number
m	degree of hydrolysis
q	hydration number
E.Z.	Electrolytic Zinc Co of Australasia (Goethite) Process
V.M.	Vieille Montagne (Goethite) Process
μ	ionic strength
□	lattice vacancy
μ_B	Bohr magneton
M	molar
V	Versatic ion
HV	Versatic acid
A.A.	atomic absorption spectrophotometer/spectrophotometry
R^2	squared correlation coefficient
t	Students t
$t_{90\%}$	t-value for 90% probability
O.E	oxygen equivalent (= Ni + 3/2 Fe)
k	initial rate
E_a	activation energy
R	gas constant
RF	retention factor

Abbreviations Used in Chapter 9

IR	infrared
OD_{HV}	
$OD_{(HV)_2}$	optical density of Versatic acid dimer
C_V	total Versatic in acid solutions
C_V	predicted total Versatic
ε_{HV}	extinction coefficient of Versatic acid monomer
$\varepsilon_{(HV)_2}$	extinction coefficient of Versatic acid dimer
l	pathlength of IR cell
r	$OD_{HV}^2/OD_{(HV)_2}$
K_{diss}	dissociation constant
$[HV]_f'$	free acid in diluted sample
$[HV]_f$	free acid in undiluted metal-Versatic sample
D	dilution
M_t	total metal charge (=2xO.E)
$(V/M_t)_{cmp}$	average Versatic to metal charge ratio in complexes

CHAPTER 1

INTRODUCTION

During the last thirty years, solvent extraction has proved to be a useful technique for separating metals in hydrometallurgical operations. In most solvent extraction processes the organic phase is an intermediate: metals are extracted from the process stream into an immiscible organic solution, then are stripped from the organic phase into another aqueous solution. The metal is then recovered from the aqueous strip solution, for example by electrowinning, or precipitation of the metal or a compound.

It was recognised by Burkin in the late 1960's that in some solvent extraction processes it could be feasible to recover metals directly from the organic solution, thereby obviating separate stripping and recovery stages in the process flowsheet[1,2,3]. Burkin investigated the reduction and precipitation of metals by hydrogen in organic solutions, and found that although many solvent extraction reagents were chemically unstable under the conditions required, it was possible to precipitate nickel from carboxylates and D2EHPA (di-(2-ethylhexyl)-phosphoric acid). Iron (in the presence of ammonia), cobalt and copper could be precipitated from carboxylate solutions. The process regenerated the organic acid for recycle to the extraction stage, i.e.

$$\overline{MR_n} + \frac{n}{2} H_2 = nM + n\overline{HR} \qquad 1.1$$

where R represents an organic acid anion, and a bar above a species indicates that it is present in the organic phase.

It is not possible to reduce iron(III) to iron metal by hydrogen in aqueous solution, because iron precipitates as hydroxide at low pH values; at the pH required for reduction by hydrogen, the activity of iron(III) in solution is very low. This limitation is not thermodynamic: iron(III) can be reduced by hydrogen, but the chemical properties of water, the solvent, introduce a kinetic limitation. When the solvent is carboxylic acid in an inert diluent, this does not react with iron(III) in solution, so the iron activity is high

and reduction can occur. Thus organic phase hydrogen reduction offers two advantages; simplification of the process flowsheet, and the possibility of reducing metals such as iron which cannot be reduced in aqueous solutions.

Thorsen and Monhemius recognised the advantages of organic phase reduction, but noted that in some hydrometallurgical operations it is not always necessary or even desirable to obtain a metallic product[4]. They investigated hydrolysis, a chemical process widely used for the removal of impurity metals from process streams. They found that it is possible to precipitate oxides and hydroxides of some metals directly from a loaded carboxylate solution, by hydrolysis at temperatures in the region of 150°-200°C. Only small quantities of water, present as a separate phase, were needed for hydrolysis. Here a single stage operation replaces the conventional stripping and hydrolysis steps; hence the process was named hydrolytic stripping.

Large quantities of hematite, nickel hydroxide and copper(I) oxide were precipitated from carboxylate solutions of iron(III), nickel(II) and copper(II) respectively. The idealised reactions are:

$$2\overline{FeR_3} + 3H_2O = \alpha Fe_2O_3 + 6\overline{HR} \qquad 1.2$$

$$\overline{NiR_2} + 2H_2O = Ni(OH)_2 + 2\overline{HR} \qquad 1.3$$

$$2\overline{CuR_2} + 2H_2O = Cu_2O + 4\overline{HR} + [O] \qquad 1.4$$

Slight precipitation from organic solutions of aluminium, titanium and zinc was observed, while solutions of cadmium, cobalt, chromium, manganese and lead gave no precipitation.

The behaviour exhibited by iron during hydrolytic stripping generated most interest initially, because of the potential application of hydrolytic stripping for removing waste iron in hydrometallurgical processes[6].

Iron is present in the ores of most metals, and must be separated from the metal values during processing. In pyrometallurgical processes, conditions are selected to ensure that

the iron reports to the slag phase, in which it is physically and chemically inert. There are therefore no environmental hazards associated with dumping such slags[7].

In hydrometallurgical processes there is no analogous method of removing iron from process streams in a satisfactory way. The Jarosite, goethite and hematite processes offer a means of precipitating iron from the feed in a filterable form. However, in these processes impurities are carried down with the iron, either substituted into the crystal lattice of the precipitate, adsorbed onto the surface, as occluded solid residue from the neutralising solution or as occluded leach liquor. Cationic impurities represent a loss of values, and also render the precipitates unacceptable for iron making, since many of the base metals which cannot be oxidised out during refining have a deleterious effect on the properties of iron and steel. The impurities also present problems if the iron waste is dumped, because the impurities tend to be slowly leached from the waste, causing severe pollution. In terms of cationic impurities the hematite process is a marked improvement on the earlier Jarosite and goethite processes, but the products of all these processes contain appreciable levels of sulphate[8]. The Jarosite process has been improved to increase metal recoveries, which results in significantly lower levels of cationic impurities[9] but the contaminants are still environmentally undesirable. It seems to be inevitable that an iron product precipitated from a concentrated leach liquor will be contaminated to some extent.

Solvent extraction offers a means of separating iron from leach liquors. For example, in the Falconbridge Matte Leach process, iron is removed from the chloride leach solution by tributyl phosphate (TBP), then is stripped with water to yield a solution of $FeCl_3$[10].

Cation exchange extractants, such as carboxylic and alkyl phosphoric acids, are particularly suited to the extraction of iron, because with these reagents the extraction of metals is pH dependent, with iron(III) being extracted at lower pH values than other base metals. Acid leach solutions therefore require little or no pH adjustment for iron extraction, and base is required only to neutralise the H^+ ions released during the extraction reaction:

$$Fe^{3+} + 3\overline{HR} = \overline{FeR_3} + 3H^+ \qquad 1.5$$

If a low pH is maintained, only iron is extracted into the organic phase, so a clean separation from the non-ferrous metals can be achieved.

Iron is stripped from cation exchangers with mineral acid, usually HCl, to reverse reaction 1.5, i.e.

$$\overline{FeR_3} + 3HCl = FeCl_3 + 3\overline{HR} \qquad 1.6$$

to give a pure concentrated solution of a ferric salt. It is easier to strip iron from carboxylic acids than from alkyl phosphoric acids such as D2EHPA because the latter are stronger acids, and are generally used with a modifier such as isodecanol, which has been reported to re-extact iron from the strip solution[11]. Much work has been done on the solvent extraction of iron with carboxylic acids, but the limitation in using conventional solvent extraction for a waste material lies with the utilisation of the strip solution. The acid in this cannot be regenerated in an electrowinning stage, as is done for values separated by solvent extraction. For chloride solutions there is a process termed pyrohydrolysis, whereby a concentrated solution of $FeCl_3$ is burned in air with a fuel to give hematite and hydrochloric acid:

$$2FeCl_3 + 3H_2O = \alpha Fe_2O_3 + 6HCl \qquad 1.7$$

The hematite is uncontaminated, so can be used for iron-making, but the process is very energy intensive, and is therefore unlikely to be economically viable.

Hydrolytic stripping of iron from carboxylate solutions is clearly an attractive alternative to stripping followed by pyrohydrolysis. It can be seen from equation 1.2 that the hydrolytic stripping process combines equations 1.6 and 1.7, without the need for hydrochloric acid as an intermediate reagent. Teixeira has studied the kinetics of the process in detail[12], and has concluded that the process is likely to be commercially feasible. Although precipitation is under surface control for all but the most concentrated solutions, suitable recycle of solids is expected to give

short residence times during commercial operation of the process.

Thorsen, Svendsen and Grislingås have developed a detailed flowsheet for incorporating solvent extraction-hydrolytic stripping in the Electrolytic Zinc Process, to replace jarosite, goethite or hematite precipitation[13]. Zinc oxide in the calcine is used as an indirect neutralising agent during extraction: the calcine is leached by the carboxylic acid, in the presence of a little aqueous sulphate solution which minimises contamination of the leach residue by the organic phase:

$$ZnO + 2\overline{HR} = \overline{ZnR_2} + H_2O \qquad 1.8$$

The zinc carboxylate solution is then contacted with leach liquor containing iron. Because of the relative positions of the extraction isotherms, iron replaces the zinc in the organic, by a process termed exchange extraction:

$$3\overline{ZnR_2} + 2Fe^{3+} = 2\overline{FeR_3} + 3Zn^{2+} \qquad 1.9$$

The system is self-buffering, and no extraneous cations enter the aqueous leach solution.

The overall advantage of the integrated organic leaching-solvent extraction-hydrolytic stripping operation is that a saleable iron product is formed without a high energy input. By virtue of being produced via a solvent extraction route, the hematite precipitated by hydrolytic stripping is very pure chemically. In 1975, Mühl et al reported that although hydrometallurgical processes are not usually economically viable for the winning of iron, the situation alters when the application, for example the production of magnetic materials in metallic or oxide form, requires a level of purity which cannot be achieved in pyrometallurgical processes. The cost of such high grade iron may be comparable with that of the usual non-ferrous metals, or even higher[14]. Iron powder metallurgy is another application where high purity is essential. By directing the hematite to such applications, it should be possible to recover some of the additional process costs associated with solvent extraction-hydrolytic stripping.

These additional costs represent the main disadvantage of the operation, and stem from the increased complexity of the flowsheet, and from solvent losses. The solvent wets the surface of the hematite, so some is lost when the oxide is filtered from solution. Even though carboxylic acids are relatively inexpensive extractants, some would have to be recovered in a washing stage. Fortunately, any residual organic which cannot be economically recovered will not be detrimental to the product; it will assist pelletising or compacting and will be oxidised during reduction or sintering.

In hydrolytic stripping, metal ions are hydrolysed in the organic phase; the water needed is probably dissolved in the organic phase. A closely related process which has been shown to be applicable to iron(III) is precipitation stripping[6,15]. In this process, iron (III) carboxylate solution is contacted with a dilute sulphuric acid solution (typically 10g/l H_2SO_4) at about 100°C. Some iron is stripped from the organic solution, reaction 1.10, and under these conditions is rapidly hydrolysed to form a crystalline precipitate, for example goethite, as in reaction 1.11

$$\overline{FeR_3} + 3H^+ = 3\overline{HR} + Fe^{3+} \qquad 1.10$$

$$Fe^{3+} + 2H_2O = \alpha FeOOH + 3H^+ \qquad 1.11$$

The H^+ ions released in 1.11 are then available to strip more iron from the organic phase, so as with hydrolytic stripping, the system is self-buffering. No neutralising agent is required for hydrolysis, therefore no extraneous cations which could contaminate the product are present. Unlike hydrolytic stripping, however, hydrolysis and precipitation occur in the aqueous phase. If the sulphate to iron ratio is high, basic sulphates are produced instead of goethite. Additionally, in practice there is usually some sulphate in the product, so it is not suitable for iron-making. The precipitates are suitable for dumping, however, because they contain no cationic impurities. In this respect, solvent extraction-precipitation stripping is a significant improvement on the existing Jarosite, goethite and hematite processes.
Precipitation stripping has the advantages over hydrolytic stripping that pressure equipment is not necessary for the process, and that solvent loss is negligible because hydrolysis occurs in the aqueous

phase and the precipitates are not wetted by the organic.

Hydrolytic stripping and precipitation stripping could find application for iron-removal in a large number of hydrometallurgical processes. Hydrolytic stripping of other metals, although unlikely to become important in process flowsheets, could prove to be an important means of producing specialised materials, because of the intrinsic high purity of the products. The formation of Cu_2O and $Ni(OH)_2$, for example, could be of interest for the production of pigments and chemicals. Cu_2O in particular is used as a fungicide for crops and seed treatment, as a catalyst and in large quantities as an antifouling additive to marine paints[5].

During the preliminary studies of hydrolytic stripping, a little work was done on stripping organic solutions containing mixtures of cations[4]. For example, it was shown that during hydrolytic stripping, nickel precipitates as hydroxide whereas cobalt remains in solution, so it was thought that cobalt and nickel might be separated by hydrolytic stripping. In fact hydrolytic stripping of a carboxylate solution containing both nickel and cobalt gave nickel hydroxide containing significant levels of substituted cobalt. Although the organic solution was enriched in cobalt after hydrolytic stripping, the separation was not significantly better than that achieved in existing processes[4].

A more interesting result was observed for a mixed carboxylate solution of cobalt and iron, which precipitated cobalt ferrite, $CoFe_2O_4$, with the spinel structure[16]. Crystallographically, this is completely different from hematite, αFe_2O_3, which is formed by iron alone. The appearance of a mixed oxide suggested that it might be possible to prepare other commercially useful mixed oxides by hydrolytic stripping.

The purpose of this project was to study the behaviour of a number of different metals, singly and in mixtures, during hydrolytic stripping, to establish the range of single and mixed oxides which can be formed by this method.

Mixtures containing iron were of particular interest for the following reasons:

(1) Iron(III) is extensively hydrolysed in aqueous solutions and in iron-carboxylate solution. It is therefore likely to be hydrolysed in mixed carboxylate solutions, giving extensive precipitation.

(2) It is conceivable that in specific hydrometallurgical operations, precipitation of commercially useful mixed oxides containing iron could be a useful way of removing iron from process streams.

(3) There was evidence that magnetic ferrites could be precipitated. These materials are used in large tonnages, but their current methods of production are costly and energy intensive. Therefore hydrolytic stripping could be useful as a materials preparation process.

The project was organised in two distinctly different sections of work; in the first section, organic solutions containing mixtures of metals were heated to 200°C with water, to establish the nature of any precipitates formed within a period of three hours. In the second section, the iron-nickel system, which precipitated nickel ferrite, $NiFe_2O_4$, was selected for kinetic study. The results from the kinetic studies of the hydrolytic stripping reaction, together with results from infrared spectrophotometry, thin layer chromatography and electron microscopy gave some indication of the mechanism of hydrolysis in organic solution. The two sections of experimental work are presented separately here, as Parts I and II.

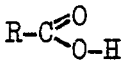
CHAPTER 2

LITERATURE SURVEY

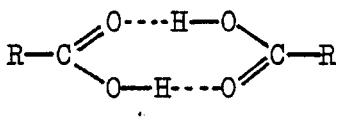
2.1 THE USE OF CARBOXYLIC ACIDS AS SOLVENT EXTRACTION REAGENTS

2.1.1 Properties of Carboxylic Acids

The saturated monocarboxylic acids are an homologous series with the general formula $C_nH_{2n+1}COOH$. They are also referred to as the fatty acids, because natural fats are esters of some of the higher members of the series[17]. Denoting the alkyl group as R, the structure of these acids is represented by



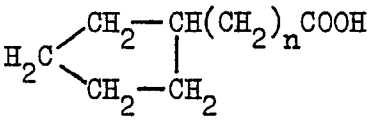
Although the lower members of the series are soluble in water, with the hydrophilic nature of the carboxyl group predominating over the hydrophobic nature of the alkyl group, the higher members, with large alkyl groups, have low aqueous solubilities. The acids tend to dimerise by hydrogen bonding of the carboxyl groups, to form planar eight-membered rings, i.e.



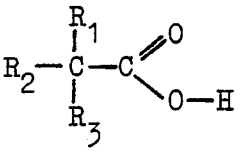
The lower members of the series form these dimers in the vapour phase, and in aqueous solution, forming higher polymers in the liquid phase. The higher members are largely dimerised in the liquid phase, but the undissociated acid is not dimerised in aqueous solution, since the limited solubility is due to the interaction of the polar carboxyl group with water. Conductivity measurements indicate that the acids dissociate slightly in aqueous solution. The anionic species thought to be present are singly charged anions, singly charged anion-molecule dimers, and doubly charged dimers[18]. There appears to be no dissociation in non-polar organic solutions.

All of the acids react with metal ions, to form salts or soaps. The monocarboxylic acids are monobasic, with only the hydrogen atom on the carboxyl group replaceable by a metal ion. The heavy metal soaps of higher acids are used as paint driers, pigment dispersers and fungicides. Although generally prepared for such uses by an aqueous metathetic reaction, in which the insoluble soaps are precipitated from aqueous solutions of the required metal ions by the soluble alkali metal soaps,[19] a process for preparing them by solvent

extraction has been patented[20]. Originally the naphthenic acids were used to make such soaps; these are carboxyl derivatives of saturated cyclic hydrocarbons of the type:



These acids have now been replaced for this function by the Versatic acids, marketed by the Shell Chemical Co. Ltd. These are saturated tertiary acids, that is, they have three alkyl groups on the α carbon as shown:



The acids are synthesised by reaction between alkenes, carbon monoxide and water, in the presence of an acid catalyst such as BF_3, i.e.

$$C_nH_{2n} + CO + H_2O = C_nH_{2n+1}COOH \qquad 2.1.1$$

This reaction yields a small percentage of secondary acid[21], that is, an acid with two alkyl groups on the α carbon. Although Burkin reported that the secondary acid in Versatic 911 was reduced by hydrogen pressures of about 75 atmospheres, at about 250°C, and the alcohol formed then esterified a little of the tertiary acid[3], there are no reports of the secondary acid being problematic under less extreme conditions. It is the unusual stability of the Versatic acids, combined with their commercial availability, which renders them suitable for high temperature stripping processes.

As the higher acids have only limited aqueous solubility, metal soaps are probably formed by solvent extraction at the aqueous-organic interface. The soaps are almost completely dissociated in the aqueous phase, and associated in the organic[22,23]. It is the ability to extract metals from an aqueous solution into an immiscible organic phase which makes these acids useful as solvent extraction reagents.

Denoting the carboxylic acid as RH, for simplicity, the extraction can be represented as:

$$n\overline{RH} + M^{n+} \overset{K_{ex}}{=} \overline{R_nM} + nH^+ \qquad 2.1.2$$

$$K_{ex} = \frac{\{\overline{R_nM}\}\{H^+\}^n}{\{\overline{RH}\}^n\{M^{n+}\}} \qquad 2.1.3$$

It can therefore be seen that high organic concentrations of metal can only be achieved if the hydrogen ions released in equation 2.1.2 are neutralised. Furthermore, if R_nM is the only species in the organic phase which contains M, then the distribution constant, D_M, defined as the ratio of metal concentration in the organic and aqueous phases at equilibrium, can be denoted by

$$D_M = \frac{[\overline{R_nM}]}{[M^{n+}]} \qquad 2.1.4$$

If the solution is near ideal, that is, the concentration of M^{n+} is low, and the ionic strength high, the activities of M^{n+}, R_nM and RH in 2.1.3 can be replaced by concentrations. Thus

$$D_M = \frac{K_{ex}[\overline{RH}]^n}{\{H^+\}^n} \qquad 2.1.5$$

and $$\log D_M = \log K_{ex} + n \log \overline{RH} + n\,pH \qquad 2.1.6$$

Although the assumptions made mean that equation 2.1.6 is a simplification of the behaviour of a real system, it can be seen that the distribution of a given metal between the aqueous and organic phases is determined by the extraction constant for that metal, the concentration of carboxylic acid in the organic phase, and the pH of the aqueous phase. Because the extraction constants vary for different metals, the pH at which a given percentage is extracted, generally taken as 50% and denoted as $pH_{0.5}$, will vary, so that separations can be effected by these extractants.

The acids which are useful for commercial applications are those with a carbon chain length of 6 to 13; the lower acids are unsuitable because their high aqueous solubility leads to large losses in the raffinate, while the higher acids are rather viscous at ambient temperatures, and, having a high molecular weight, have a limited loading capacity. Although early research was done on natural carboxylic acids, with straight alkyl chains, these have been superseded by synthetic acids, notably the Versatic acids in Western

Europe and North America, where they are commercially available.

2.1.2 Extraction of Metals by Carboxylic Acids

The extraction of base metals from aqueous solutions by carboxylic acids was first studied extensively in the 1950's, although a few examples of extraction had been reported earlier. Gindin and co-workers in the U.S.S.R. studied the extraction of a large number of metals with industrial monocarboxylic acids of the C_7-C_9 fraction, as a 400 g/l (approx. 2.8M) solution in kerosene[22,23,24], after ascertaining that the separation factors of metals are independent of the aliphatic fraction used, and of its concentration in an inert solvent. Initially they added alkali to the aqueous phase to neutralise the protons released during extraction[22], but after studying the distribution of the soaps of different metals between the phases[24], they concluded that a metal will be displaced from an aqueous solution by one whose soap is more soluble in water. They proved that the solubility of the soaps is determined by the solubility products of the hydroxides; thus copper is displaced by the soap of cobalt, which has a higher solubility product for its hydroxide. They named this displacement technique exchange extraction. The extraction order which they determined experimentally, in order of decreasing extractability, is

Sn(IV), Bi(III), Fe(III), Pb(II), Al(III), Cu(II), Cd(II), Zn(II), Ni(II), Co(II), Mn(II), Mg(II), Na(I)

At approximately the same time, workers in Britain were using naphthenic acid in kerosene as an extractant. Fletcher and Wilson studied the extraction of metals from 0.1M solutions by 1M naphthenic acid. They observed that extraction is pH dependent, appreciable extraction only occurring at pH values very close to the point at which hydroxides are precipitated[20], an observation consistent with the results of Gindin et al. For the metals investigated, the order of extraction from sulphate solutions agreed with that given by Gindin. Although naphthenic acids of different molecular weight were found to have different $pH_{0.5}$ values for a given metal, these increasing with molecular weight, the separation of different metals appeared to be similar for the acids tested.

Although naphthenic acid seemed suitable for the separation of copper and nickel, it was not considered to be suitable for iron, because of the low solubility of ferric naphthenate in kerosene. As the Versatic soaps are more soluble than the naphthenates in non-polar diluents, the extraction of iron(III) with Versatic 911 was studied by Fletcher, Flett and Wilson[21]. Studies made with a large excess of the acid indicated that the log D_{Fe}/pH curve was linear, with a gradient of 3, which implied the extraction reaction to be stoichiometric. Nevertheless, in loading tests involving stagewise contact of a 1M Versatic 911 solution with portions of ferric sulphate solution preneutralised to a pH of 3.59, the maximum loading achieved was well below the stoichiometric concentration. Neutralisation during contacting was found to be more effective than preneutralisation, because the latter led to a build-up of inextractable, aged iron hydroxide precipitates during continuous separation of iron from copper.

The curves for the extraction of several metals by Versatic 10 are shown below in Figure 2.1[54]

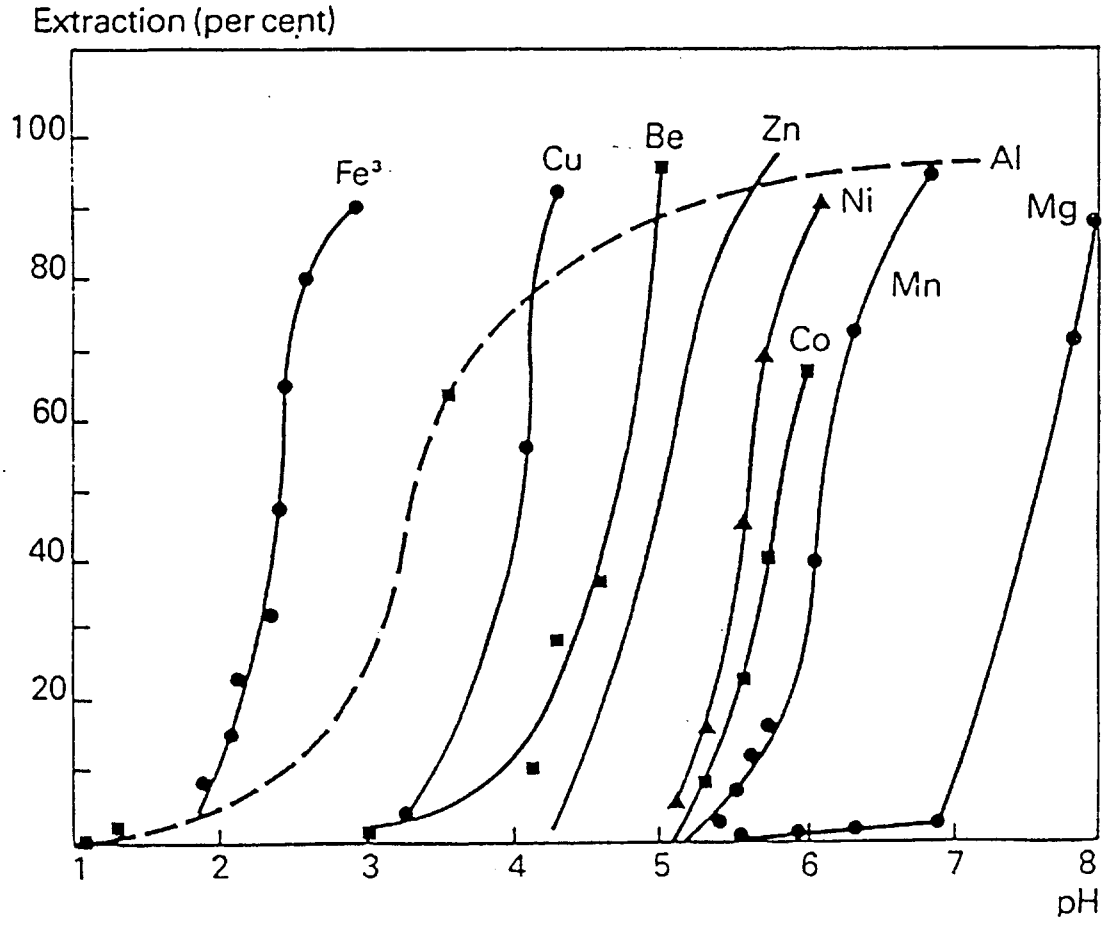


Figure 2.1 Extraction of Metals by Versatic 10

Spitzer, Radder and Muys investigated extraction from mixed sulphate solutions with Versatic 9, and successfully separated iron from copper, copper from nickel and cobalt, and zinc from cadmium[25].

Mikhailichenko, Klimenko and Bulgakova studied the extraction of alkaline earth metals and magnesium, using C_7-C_9 aliphatic acids. The order of extraction from 1M aqueous solutions was Ba, Sr, Ca, and Mg[26].

Mühl, Gindin, Kholkin, Gloe and Luboshnikova used n-caprylic acid, $C_7H_{15}COOH$, in n-decane, to investigate the mechanism of iron(III) extraction[27]. A noteable observation made in this study was that although 'equilibrium' was reached after fifteen minutes shaking, the concentration of iron in the aqueous phase rose after four hours, with a corresponding drop in the distribution ratio, and that after a longer period ferric hydroxides appeared. This is almost certainly due to slow hydrolysis of the small amount of iron in the aqueous phase at equilibrium. This lowers its activity, causing more iron to be stripped from the organic to maintain the partition coefficient, which is a thermodynamic constant defined as $\{M^{n+}\}_{org}/\{M^{n+}\}_{aq}$. The process must proceed until there is sufficient hydrolysed iron in the aqueous phase for precipitation to occur, although the thermodynamic activity of iron has been low throughout. This behaviour is clearly the low temperature equivalent of the precipitation stripping process mentioned earlier[6].

For the application of solvent extraction of iron to the production of high purity compounds, Mühl and co-workers used a C_6-C_{10} fraction of acids, commercially available as 'PC acid'[14]. Mühl, Gloe, Fischer, Ziegenbalg and Hoffmann also tested this reagent, as well as amines and TBP for the separation of iron during the production of alumina[28], and concluded that separation could be achieved with careful pH control, but that this became difficult with decreasing iron concentration, and was never as good as the separation possible with TBP.

Van der Zeeuw applied exchange extraction to the purification of zinc leach solutions, using the zinc salt of Versatic 10[29]. The

problems of iron hydroxide precipitation reported by earlier authors [20,21,27] were not encountered using this technique. It was possible to extract 95% of the iron before coextraction of copper began, while coextraction of cobalt and manganese could not be detected, and arsenic was only detected in the Versatic solution at nearly complete iron extraction. Van der Zeeuw states that Cr(III) is not extracted at all by Versatic, only forming a hydroxide on neutralisation, whereas Mühl et al reported the coextraction of this ion with Fe(III) [14]. Wood and Rycroft measured the aggregation of the myristate, palmitate and stearate soaps of Cr(III) in toluene, but since they prepared these soaps by aqueous metathesis, their observations are not necessarily applicable to solvent extraction phenomena[30].

Several reviews of carboxylic acids as solvent extractants have been published[18,31,32,33], as well as more general surveys of solvent extraction reagents[34,35]. With regard to carboxylic acids, the need for an equivalent amount of alkali to effect extraction was expected to impose economic limitations on the use of these reagents [35], though the later work of Van der Zeeuw[29] and Thorsen[13] has shown this not always to be the case, since materials like zinc calcine may be used for neutralisation.

Flett and Jaycock discussed the single and multiple equilibrium models which can be used in slope analysis, and discussed the likely composition of copper complexes[18]. Ashbrook discussed much of the work published on the use of carboxylic acids, and considered many characteristics of these reagents, including their aqueous solubility, loading behaviour, extraction properties and effect on the environment, in many cases comparing these characteristics with those of D2EHPA. He concluded that the case for the use of carboxylic acids in commercial liquid-liquid extraction processes was not very strong[32].

Rice, however, after an extensive review of the literature up to 1977, found that some modification of Ashbrook's conclusions would be appropriate, because although inferior to D2EHPA and chelating reagents in many respects, there are some applications in which carboxylic acids are more effective[33]. These include the extraction of cobalt from ammoniacal media, the direct reduction of

metals in the organic phase, and exchange extraction for the removal of impurities, especially iron, which after solvent extraction might be more readily recoverable in a useable form than the jarosites, goethite and hematite currently precipitated in zinc hydrometallurgy.

Rice's review preceded the first published account of the hydrolytic stripping process, therefore does not include this process as an application in which carboxylic acids are effective reagents. Carboxylic acids are particularly suitable for hydrolytic stripping because, unlike many other extractants, they are chemically stable at the high temperatures needed[2,3,4], while although the lower temperatures used for precipitation stripping do not preclude the use of D2EHPA, this reagent has been found to be too acidic for this purpose[15].

2.1.3 Influence of Other Ions in Solution on the Extraction of Metals by Carboxylic Acids

Although in early work Gindin et al stated that the mineral acid anion was without influence on the extraction process[22], it was soon recognised that this was not so. The extraction order obtained by these workers, showing Pb, Cd and Zn extracted ahead of Co, referred to sulphate solutions. In concentrated chloride solutions these three ions are extracted after Co, because of the formation of stable complex anions[23].

In their extraction tests using naphthenic acid in kerosene, Fletcher and Wilson compared the extraction of Cu, Ni, Co, Zn and Mg from 0.1M solutions of their sulphates, with and without large additions of $(NH_4)_2SO_4$ (30-160 g/l)[20]. There were slight differences in the extraction isotherms, with most metals being extracted from the heavily salted solutions at a slightly lower pH than from the solutions containing no ammonium sulphate, the exception being Mn, for which this trend was reversed. These effects could be due to the sulphate ion, the ammonium ion, or to increased ionic strength.

Flett reported that with the extractive separation of cadmium and zinc with naphthenic acid, there is a selectivity reversal

on changing the anion from sulphate to chloride[36]. Thus, although zinc is extracted before cadmium from chloride solutions, as would be expected from the pH at which the hydroxides of these two metals are precipitated, in sulphate media the cadmium is extracted first. The $pH_{0.5}$ values obtained for 5 x 10^{-3}M solutions of the metals in M/3 $NaSO_4$ or 1M NaCl, using 1M naphthenic acid in kerosene, are 5.04, 5.36, 5.48 and 5.58 for $ZnCl_2$, $CdSO_4$, $ZnSO_4$ and $CdCl_2$ respectively. This result is attributed to strong complexing of zinc by sulphate, while cadmium is more strongly complexed by chloride than by sulphate. This result is not consistent with that of Gindin et al, who found that chloride complexed both zinc and cadmium more strongly than sulphate[23], or with the order of extraction; Fe, Cu, Zn, Cd, Ni/Co given by Van der Zeeuw[29] and Spitzer, Radder and Muys[25] for extraction from sulphate solutions by Versatic. Since the effect which an anion exerts is determined by the formation constants of both the metal-anion and the metal-carboxylate complex[32], this discrepancy is probably due to the different carboxylic acids used by these workers.

Mikhailichenko et al determined the extraction isotherms of Mg, Ca, Sr and Ba from both chloride and nitrate solutions[26]. These metals were extracted from chloride solutions at lower pH than from nitrate solutions, with $pH_{0.5}$ = 4.33 for calcium chloride and 4.72 for calcium nitrate, but the order of extraction was the same for both anions. The log $D_M 2+/pH$ plots for calcium nitrate, bromide, perchlorate and thiocyanate were all very similar, and lower than the line for calcium chloride, from which it was concluded that there was less extensive association of alkaline earth metal ions with chloride than with the other anions.

Ammonium salts can profoundly affect the extraction of some metals by carboxylic acids. Haffenden and Lawson established that when Cu(II), Ni(II) and Co(II) are extracted by excess Versatic 9 in toluene, from ammonium solutions, the extraction initially increases with increase in pH, as expected, but then falls, because free ammonia is formed at high pH, and this forms inextractable ammines. A theoretical model of the behaviour when the extractant was in excess was proposed[37]. Lawson and Pridden then extended this model to 'non-ideal' conditions, required for the practical application of solvent extraction, and determined the behaviour of copper, nickel and cobalt,

using Versatic 911 in toluene[38]. An unexpectedly high separation factor was observed for cobalt and nickel, because of preferential complexing of the nickel by ammonia.

Mühl et al plotted log D_{Fe}/pH curves for the extraction of iron from aluminium chloride and aluminium sulphate solutions of varyious aluminium concentrations[28]. Iron is separated from chloride solutions at a much lower pH than from sulphates, with $pH_{0.5}$ values of about 0.5 and 2 respectively, because of the greater stability of the iron(III) sulphate complexes. The variation in D_{Fe} with aluminium salt concentration was similar for both anions. For D_{Fe} less than 10, iron extraction was enhanced with increasing aluminium salt concentration, because of a salting out effect. This contrasts the effect of increasing alkali metal salts, which lower iron extraction by forming, for example, iron sulphate complexes[39]. At higher pH values the log D_{Fe}/pH curves reached a maximum D_{Fe} value, which decreased with increasing aluminium salt concentration, because of increasing hydrolysis of iron.

Cations can also modify the extraction behaviour. Mühl et al showed that the distribution ratio of iron fell with increasing iron concentration in a chloride solution, and that although the distribution ratio of many trace impurities varies similarly, giving a constant separation factor, there are some anomalies[14]. The separation of iron from Mo(VI) and As(V) improves, but that from Cr(III) Mn(II), Cu(II) and Ni(II) becomes poorer as the iron concentration increases. The latter behaviour was considered to be due to co-extraction, by the formation of mixed organic complexes. This co-extraction behaviour was investigated for copper and nickel, both with iron[39]. For both systems the log D_{Fe}/pH curve was slightly higher when extracting from mixed solutions, than from solutions containing only iron, but the log $D_{M}2+$/pH curve was much higher for mixtures than for single solutions at low pH values, only coinciding with the curves for single M^{2+} solutions at higher pH values, when $D_{M}2+$ was 0.1 - 1.0. Zinc was later shown to behave similarly to copper and nickel, but the extraction of lead appeared to be independent of iron concentration. The iron-nickel mixed complexes were estimated to have an iron to nickel ratio of 3:1[40].

It is clear from the literature that the influence of other ions in solution on the extraction of a metal by carboxylic acids is very complex in nature, and can really only be evaluated by experimental techniques.

2.1.4 Determination of the Mechanism of Extraction

Much of the early work done to elucidate the mechanism of the extraction of metals was based on slope analysis, or variations of this technique. According to equation 2.1.6, a plot of log $D_{M^{n+}}$ against pH will be a straight line, with gradient n. This was indeed found to be so, in many cases, for aqueous solutions with a high ionic strength, and low concentration of M^{n+}, in contact with a large excess of extractant[21,22,26]. However, the extraction equation 2.1.2 is an oversimplification, since the reacting species may be carboxylic acid dimers, and the product may be a polymeric complex, containing carboxylate ions, solvating carboxylic acid, and sometimes water and hydroxyl ions. The more realistic equation is:

$$xM^{n+} + (x/2)(n-m+s)(\overline{HR})_2 + x(q+m)H_2O = \overline{[M(OH)_m R_{n-m} . sHR . qH_2O]}_x + nxH^+ \qquad 2.1.7$$

where HR indicates the carboxylic acid, x the degree of polymerisation, s the solvation number, m the degree of hydrolysis and q the hydration number.

Slope analysis has been applied to extraction equations of varying complexity, yielding, for example, the single and multiple equilibrium models discussed by Flett and Jaycock[18]; but the composition of complexes determined by such analysis is only applicable to the conditions for which the approximations and assumptions needed for slope analysis are valid. Examples have been reported where theoretical loading, based on the stoichiometry ascertained by slope analysis, could not be achieved, because of a change in the extraction equation under 'realistic' conditions[20,21]. Other techniques, such as spectroscopy and Karl Fischer titrations have been used to complement slope analysis techniques[109].

Van der Zeeuw recognised the limitations of slope analysis, and using a log D/pH curve measured for the system of interest, under realistic conditions, applied a statistical technique to determine the likely composition of complexes within the organic phase[41,42]

2.1.5 Composition of Metal-Carboxylate Complexes

Some of the complexes determined by workers for copper, cobalt, nickel and iron are shown in Table 2.1.1. It can be seen that there is fairly good agreement throughout on the complexes formed under conditions where the ratio of extractant to metal was high. Those determined by Van der Zeeuw, using a statistical method differ most from the others. The structure of the dimeric copper complex, as given by Graddon[43], is shown in Figure 2.2. Tanaka et al[44], and Van der Zeeuw[41], have suggested that nickel also forms similar twinned octahedral structures.

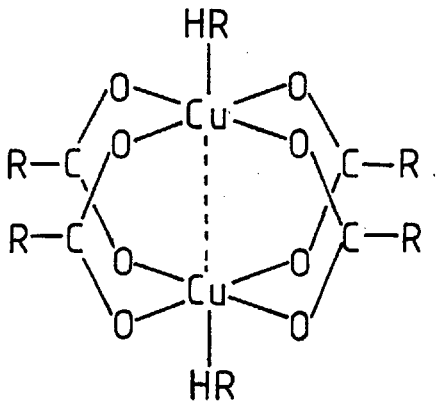


Figure 2.2 The structure of the dimeric copper complex

It can be seen from Table 2.1.1, that at lower overall extractant to metal ratios, this ratio falls in the complex, the valency of the metal being satisfied by hydroxyl ions, sometimes with water replacing the solvating carboxylic acid. There is some inherent ambiguity in the literature, when water is stated as being present in the organic phase. This has generally been determined by Karl Fischer titration, which, according to Flett and Jaycock[18], cannot differentiate between OH^- and water, but according to Stefanakis determines only water[49].

High $[HR]/[M^{n+}]$ WORKERS AND CARBOXYLIC ACID USED

Metal	Fletcher & Flett (31)	Haffenden & Lawson Pivalic acid (45)	Tanaka Capric acid (44)	Jaycock et al Versatic & naphthenic (47)	Van der Zeeuw Versatic 10 (41)
Cu	$(CuR_2.HR)_2$	$(CuR_2.HR)_2$ + 10% monomer	$(CuR_2.HR)_2$	$(CuR_2HR)_2$	
Co	$(CoR_2.2HR)_2$		$(CoR_2.2HR)_2$ + $CoR_2.4HR$	$(CoR_2.2HR)_2$	$(CoR_2)_2$
Ni	$(NiR_2.2HR)_2$		$(NiR_2.2HR)_2$ + $NiR_2.4HR$	$(NiR_2.2HR)_2$	$(NiR_2.2HR)_2$
Fe					$(FeR_3.3HR)_2$

Metal	Low $[HR]/[M^{n+}]$ Van der Zeeuw(41)	Lawson & Pridden(38)	Fletcher & Flett(31)	Medium $[HR]/[M^{n+}]$ Van der Zeeuw(41)
Cu				
Co	$(CoR(OH).1or2HR)_2$	$(CoR_2.HR)_2H_2O$	evidence	$Co_2R_3(OH).2-4HR$
Ni	$(NiR(OH).2HR)_2$	$(NiR_2.HR)_2H_2O$	for	$Ni_2R_3(OH).4HR$
Fe	$(FeR_2(OH))_3$		polymerisation	

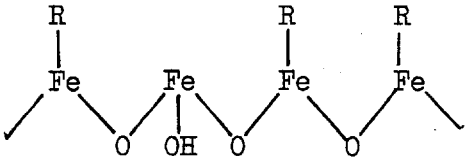
Table 2.1.1 Experimentally Determined Composition of Metal-Carboxylate Complexes

Fletcher and Flett reported that nickel and cobalt can be loaded to 0.70M and 0.66M respectively with 1.0M naphthenic acid, well above the stoichiometric level. Karl Fischer titration showed these complexes to contain 0.85M and 0.53M water[31], which may include the OH^- needed to balance the charge in the complexes. These authors stated that there was evidence of an increase in polymerisation of the complexes with increase in metal concentration, as well as with ageing, although none of the complexes shown in Table 2.1.1 verify this.

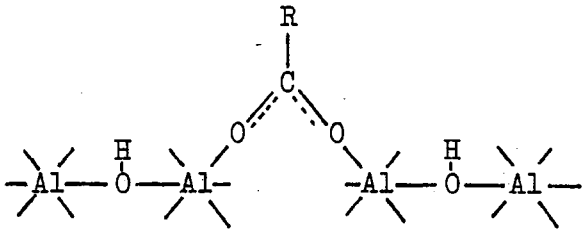
Mühl et al found the composition of the iron(III) complex extracted by n-caprylic acid in n-decane, from dilute solutions, to be $(Fe(C_7H_{15}COO)_3.H_2O)_3$[27], and have assumed that the same type of complex was formed by the 'PC acids'[14,28]. Bartecki and Apostuluk studied the extraction of iron(III) with capric acid, using graphical techniques, and found that the probable complexes were $(Fe(OH)R_2)_2$, $(Fe(OH)_2R.HR)_2$, $Fe_2(OH)_3R_3HR$ and $Fe_2(OH)_5R.HR$.[48].

Stefanakis used a statistical method to determine the composition of iron-Versatic 10 complexes, and found them to be of the form $(FeR_n(OH)_{3-n}.sRH)_x$, where n=1to 2, s=0.5 to 5 and x=1,2 and 3; n and s often adopting non-integral values, indicating the existence of more than one species[49]. The composition of these complexes was found to be very sensitive to the concentration of iron in the organic solution.

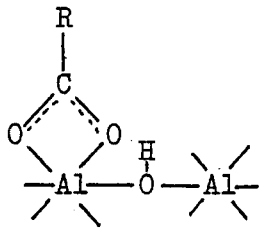
Tikhomirov investigated the extraction of iron by oleic acid, or C_7-C_9 acids, in systems where the iron was in a large excess (0.01M acid per mole of Fe)[50]. The formation of polymeric adsorption layers on the surface of the organic droplets was proposed, to account for the retention of colloidally precipitated iron hydroxide, which was observed. These layers are of the type



Tanaka, Nakasuka and Yamada found that aluminium forms hexameric complexes with capric acid, of the form $(AlR_2(OH))_6$[51]. Leger et al found that the polymerisation of aluminium-laurate complexes is much more extensive than this[19]. Although aluminium will form a tri-soap $(AlR_3)_x$, this is readily hydrolysed to the di-soap $(AlR_2(OH))_x$, which is encountered following solvent extraction from aqueous solutions. No evidence of hydrogen bonding was observed in the gels which are formed by the organic solution, even at low aluminium concentrations, and it was concluded that the carboxylate ion forms a bidentate coordination bridge of the form;



The cross linking gives a gel with an average molecular weight of 1,000,000. On ageing, the molecular weight falls, and the structure changes to the following, in which the carboxylate ion is involved in intramolecular, bidentate chelating.



McDowell and Harmon found that the complexes formed by strontium with a tertiary monocarboxylic acid of molecular weight 262, were probably $SrR_2.2HR$ and $SrR_2.3HR$, probably with water octahedrally coordinated to Sr, and possibly $SrR_2.4HR$[52]. Mikhailichenko et al, however, found that Mg, Ca, Sr and Ba all form complexes $(MR_2.4HR.qH_2O)$ over a wide range of compositions[26], but ascribed the differences between their results and those of McDowell and Harmon to the fact that McDowell and Harmon were working at higher pH, and using a tertiary acid which is bulky, so that steric

hindrance could limit the solvation number. The values of q in the complex ($MR_2.4HR.qH_2O$) were 22,6.3,4.4 and 2 for Mg, Ca, Sr and Ba.

Van der Zeeuw investigated the effect of temperature on the extraction of Cu, Ni, Co(II), Zn, Fe(III) and Co(III) from dilute solutions[42]. The distribution coefficients of Cu, Ni, Co(II) and Zn only changed slightly on heating from 20° to 80°C, but that of Fe(III) increased markedly. At 60°C the complexes likely in solution were monomers, FeV_3, $FeV_3.HV$ and $FeV_2.2HV$. On cooling, the distribution coefficient falls, indicating that there is a reversible depolymerisation of the form

$$(FeV_3.xHV)_y \underset{-T}{\overset{+T}{\rightleftharpoons}} yFeV.xHV \qquad 2.1.8$$

With trivalent cobalt, which has complexes of the form $CoV(OH)_2xHV$, (x= 0,1,2 and 3) at room temperature and $CoV_2(OH)yHV$, (y= 0,1,2 and3) at 80°C, the distribution constant does not revert to its original value on cooling, implying that the change, 2.1.9, involving both the character and number of ligands, is irreversible.

$$CoV(OH)_2xHV \overset{+T}{\rightarrow} CoV_2OH\ yHV \qquad 2.1.9$$

Cotton and Wilkinson describe an oxo-centered basic acetate ion formed by Mn(III), Cr(III) and Fe(III), shown in Figure 2.3[53]. It is feasible that similar structures are formed by the higher carboxylic acids.

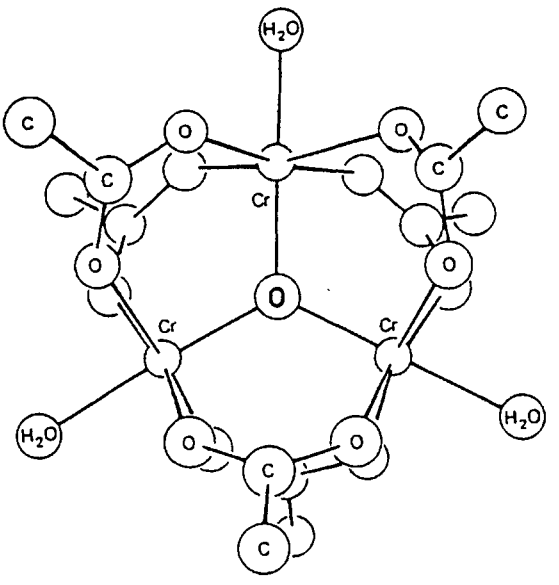


Figure 2.3 The structure of $[Cr_3O(CH_3COO)_6(H_2O)_3]^+$ (53)

2.2 AQUEOUS PHASE HYDROLYSIS

2.2.1 Precipitation of Metal Hydroxides

The precipitation of hydroxides by hydrolysis of metal cations in solution can be represented simplistically as

$$M^{n+} + nH_2O = M(OH)_n + nH^+ \qquad 2.2.1$$

$$K = \frac{\{M(OH)_n\}\{H^+\}^n}{\{M^{n+}\}\{H_2O\}^n} = \frac{\{H^+\}^n}{\{M^{n+}\}} \qquad 2.2.2$$

The solubility product, K_{so}, of a sparingly soluble hydroxide is defined as

$$K_{so} = \{M^{n+}\}\{OH^-\}^n \qquad 2.2.3$$

The dissociation constant of water, K_w, can then be used to relate the activities of OH^- and H^+ in aqueous solution, so that

$$K_{so} = \frac{\{M^{n+}\}K_w^n}{\{H^+\}^n} = \frac{K_w^n}{K} \qquad 2.2.4$$

Taking logs of 2.2.2 and 2.2.4

$$-\log K = \log K_{so} - n\log K_w \qquad 2.2.5$$

$$= \log\{M^{n+}\} - n\log\{H^+\} \qquad 2.2.6$$

Thus K can be eliminated, and the activity of a metal ion can be related to the solution pH by the relationship

$$pH = \frac{1}{n}(\log K_{so} - n\log K_w - \log\{M^{n+}\}) \qquad 2.2.7$$

Figure 2.4 shows this relationship plotted for a variety of metals at 25°C[54,55]; from this the pH range over which amorphous metal hydroxides precipitate at 25°C can be read. Such a diagram is useful on a qualitative basis, showing, for example, which metal ions may be separated by hydroxide precipitation, but it does suffer from certain

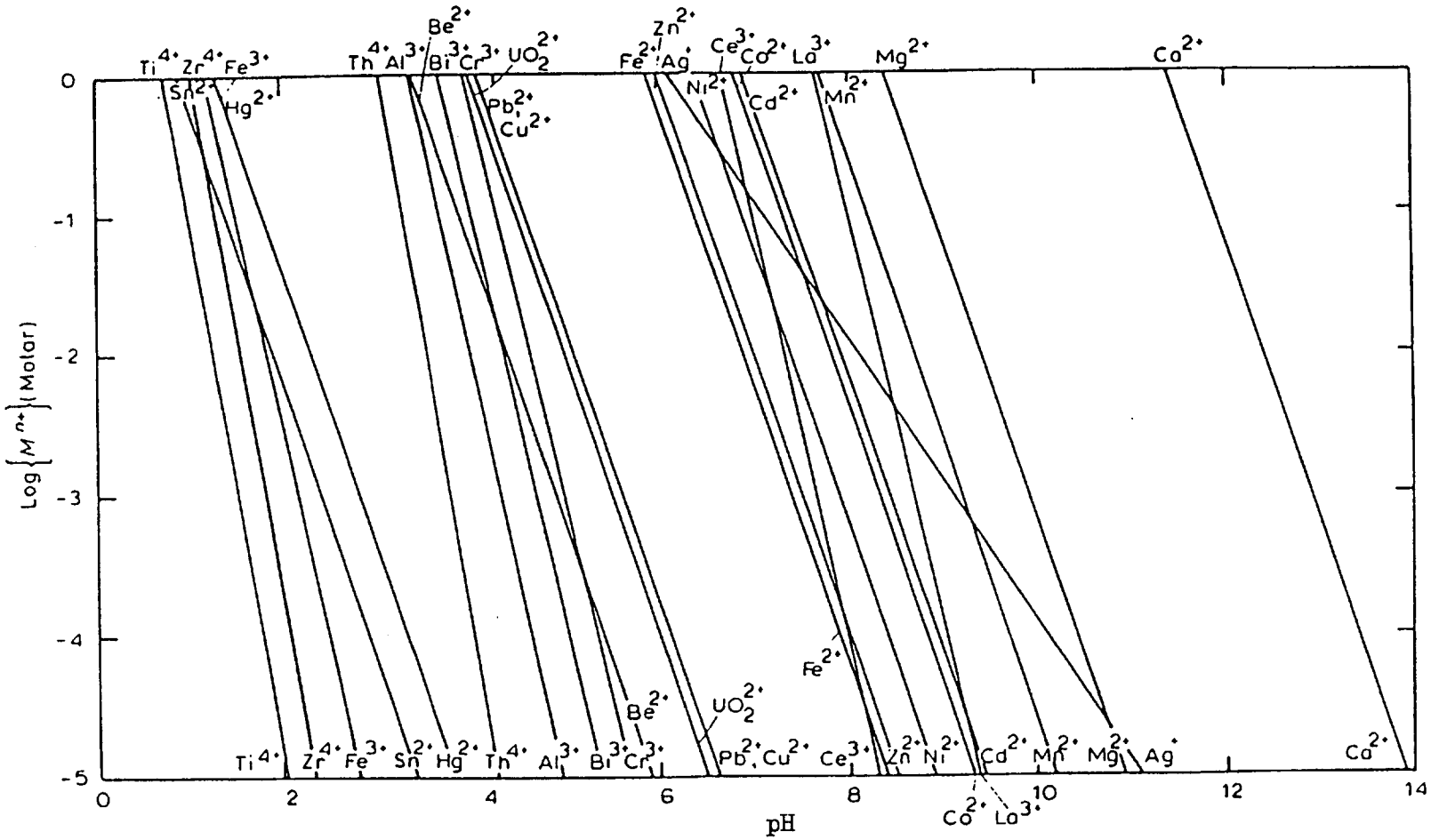


Figure 2.4 Hydroxide Precipitation Diagram, 25°C (55)

limitations. These include:

(1) The fact that equations 2.2.1-2.2.3 only take into account the simple M^{n+} ion, whereas a variety of metal-hydroxyl and metal-anion species are likely to exist in solution.

(2) The diagram shows metal ion activity as a function of pH, but the relationship between activity and concentration is not simple for the concentrated solutions typically encountered in hydrometallurgical processes.

(3) The diagram shows only the position of thermodynamic equilibrium, although the kinetics of the precipitation/dissolution equilibrium strongly influence the behaviour at 25°C.

(4) Only the solubility product of hydroxides has been considered, although other species can precipitate, for example, basic sulphates from sulphate solutions.

At the elevated temperatures required for hydrolytic stripping, there are likely to be marked deviations from the behaviour predicted by Figure 2.4, because of the temperature dependence of the thermodynamic quantities included in equation 2.2.7, and because other solid phases will be stable at high temperature.

The hydrolysis of iron(III) is particularly complex because of the large number of soluble species containing the Fe^{3+} ion, the large number of solid phases which can be formed on hydrolysis, the dependence of the relative stabilities of these on pH, temperature, pressure, particle size and anions in solution, and the slow rate at which thermodynamically unstable phases transform to stable phases. Nevertheless, the hydrolysis of iron has been studied more extensively than the hydrolysis of other metals, because of its importance, not only in hydrometallurgical processes, but also in geological processes. Comprehensive reviews of these studies have been made by Dias[56] and Agatzini[57]. A discussion of the salient results of some of the studies is appropriate here, because the only mixed carboxylate solutions to precipitate mixed oxides by hydrolytic stripping were the solutions which included iron. Although the published work on aqueous phase hydrolysis of iron cannot explain all of the experimental observations made in this project, some of the results in the literature are important in understanding the processes operative in hydrolytic stripping.

2.2.2 Factors Influencing the Hydrolysis Behaviour of Iron

Depending on conditions such as temperature, pH, iron concentration, and the nature of other ions in solution, hydrolysis of iron(III) can yield either amorphous hydroxide gel, crystalline oxyhydrates, of which there are four polymorphs; α FeOOH (goethite), β FeOOH (akaganeite), γ FeOOH (lepidocrocite) and δ FeOOH, or ferric oxide, of which there are two forms; hematite, α Fe_2O_3, and maghemite, γ Fe_2O_3[58]. Basic iron sulphates may also precipitate from sulphate solutions; the most common of these being $Fe_4(SO_4)(OH)_{10}$ and hydronium jarosite, $(H_3O)Fe_3(SO_4)_2(OH)_6$[59,60].

Robins studied hydrothermal precipitation from ferric nitrate solution; the relationship between precipitation temperature and concentration is shown in Figure 2.5(a), and the temperature-pH dependence is shown in Figure 2.5(b)[61]. It is clear that the temperature at which goethite transforms to hematite is very sensitive to pH and concentration.

Christensen examined the precipitates formed by hydrolysis of 0.1M ferric nitrate solutions of varying pH, at temperatures in the range 104°-190°C[62]. Hematite was the only product after 48 hours in samples with a final pH of 0.8-2.6, and goethite the only product in samples with a final pH of 10.5-10.8. Mixtures of these products were found in the intermediate pH range, the relative proportion of goethite increasing with increasing pH. Within the range studied, the relative proportions of hematite and goethite were not altered by temperature.

These results are consistent with those of Smith and Kidd, who by heating gels of very fine hematite or goethite, determined that goethite transforms to hematite at 125°±15°C in pure water, and at 165°±5°C in 0.1M NaOH[63]. The effect of pressure up to 2000 atm. was found to be small, with the decomposition temperature raised less than 5°C per 1000 atm. in 0.1M NaOH solution. The enhanced stability of goethite in alkaline solutions is considered by these authors to be evidence of a structure FeO(OH), containing hydroxyl groups, rather than $HFeO_2$ as proposed by Bragg.

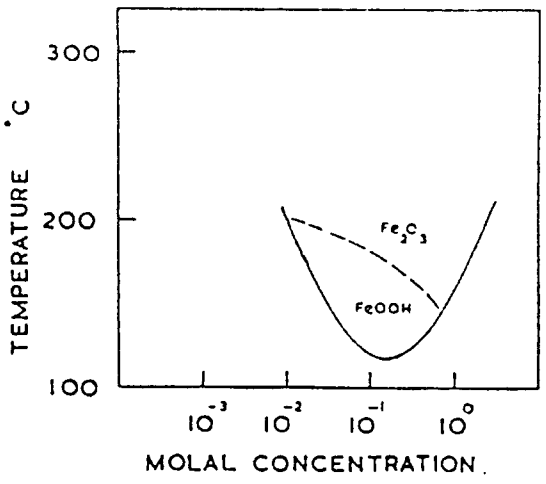


Figure 2.5(a) Precipitation Temperature for Ferric Nitrate Solutions, Showing Compounds Precipitated

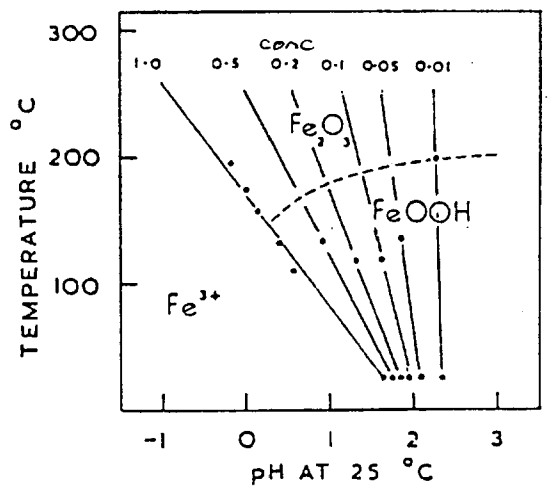


Figure 2.5(b) Phase Diagram for the System Fe^{3+}-Fe_2O_3-H_2O

Langmuir determined that particle size is very important in dictating the goethite-hematite stability limits[64]. In water at 25°C, goethite of particle size down to 0.08μ is more stable than hematite of greater or equal particle size, but hematite is more stable if finer than goethite.

The transformation of amorphous iron(III) hydroxide to goethite by ageing in 2M KOH (pH15) at 20°C and 100°C was studied by Van der Kraan and Medema[65]. At 100°C, only crystalline goethite

needles, 120Å in length, were present after 15 minutes. These grew to 220Å after 60 mins. For the samples aged at 20°C, the amorphous material was only completely transformed after 300 mins, although the sample taken after 180 mins had a fairly sharp X-ray pattern. The sample taken after 2 mins was very fine (50Å), with a poorly defined X-ray pattern, and lost far more water at low temperatures during differential thermal analysis than the more crystalline samples. This material was considered to be a labile arrangement of iron atoms, oxygen atoms and water molecules, poorly ordered in the form of an iron-oxide-hydrate in which water is only weakly bound.

The studies mentioned so far were carried out either in nitrate solutions, in which iron-anion complexing is acknowledged as being minimal, or with gels washed free of anion. Collepardi, Massida and Rossi investigated the effect of salts, as well as pH and temperature, on the ageing of iron oxide gels[66,67]. They compared the ageing of ferric hydroxide in water and in 1.8M chloride solutions, at different temperatures. In water there was an induction period, which was reduced with rise in temperature, after which hematite and goethite appeared together. Both phases then formed at a similar rate at 60°C, but at higher temperatures hematite formed at a faster rate than goethite. In the chloride solutions the induction periods observed were similar to those for water, but after these hematite was formed at an accelerated rate. No goethite, α FeOOH, was formed, but electron microscopy suggested that very small amounts of β FeOOH were present in the precipitate[66]. Hydroxide gels washed free of chloride were then aged at different pH at 100°C. At pH 5.3 and 8.2, α FeOOH formed after an induction period of 10 hours, whereas hematite appeared after only about 2 hours, and formed faster than the goethite. At pH 10,12 and 13.8 both solid phases appeared immediately. The total amount of α FeOOH formed reached a maximum at pH 12; less formed at 13.8 because the solubility of goethite rises with the formation of $Fe(OH)_4^-$ at high pH. The rate of formation of hematite was highest at pH 10, but the total amount formed after 2 days was independent of pH in the range 5-10. The enhanced rate of formation of hematite with increasing pH was thought to be due to the associated reduction in size, and hence faster dissolution, of hydroxide particles in this range. This is a kinetic effect only, and so did not affect the total

amount eventually formed.

Gels were then prepared at pH 5.3 and 12, given a variable number of washes to reduce progressively the chloride in the gel, and aged at 100°C with different electrolytes. At pH 5.3, increased washing increased the induction time, and reduced the rate of formation of hematite. α FeOOH was detected only in the gel containing no chloride. Electrolyte additions to gels containing residual chloride generally enhanced the rate of transformation, this effect falling with decreasing residual chloride, to the extent of slowing down transformation in chloride-free gels. Fluoride and tartrate slowed down transformation, regardless of the chloride content of the gel. Since these ions complex iron(III) in solution, the authors assumed that the transformation proceeds by dissolution of the hydroxide, followed by nucleation of hematite. Divalent cations were more effective than monovalent cations in enhancing the transformation. At pH 12, however, the addition of chloride to unwashed gel did not inhibit the formation of α FeOOH[67]. The general conclusion drawn from this work was that the formation of hematite is favoured by high temperature, low pH and the presence of electrolytes, although no suggestions were made on the role of these, whereas the formation of α FeOOH is favoured by temperatures of about 60°C and a pH of 12.

It should be noted that Collepardi et al were observing the transformation of an amorphous iron hydroxide gel, formed rapidly by the addition of excess base to ferric chloride solution. Different behaviour may be exhibited if ferric solutions are hydrolysed by sub-stoichiometric additions of base, since ferric hydroxy cations can form by slow polymerisation. These cations generally inhibit the formation of crystalline species, but the behaviour is sensitive to the anion in solution, sulphate solutions precipitating basic sulphates, chlorides forming β FeOOH, nitrates α FeOOH, while perchlorates give α and γ FeOOH at room temperature.

Atkinson, Posner and Quirk allowed hydrolysed species to develop in ferric solutions with OH/Fe ratios of 0-2.75, by ageing for different time periods, then precipitated gels by further addition of base[68]. These gels were then maintained at 65°C, to allow crystalline phases to develop. At pH 12, goethite was formed, but

whereas in nitrate solutions the size of the acicular crystals formed decreased with increasing hydrolysis of the parent solution, this effect was not observed in chloride solutions. Extensively hydrolysed nitrate solutions formed twinned goethite crystals, derived from hematite nuclei, but comparable chloride solutions did not. The difference in behaviour seemed to be due to the inhibition of nucleation in chloride solutions. At pH 1 - 2, chloride gels gave β FeOOH after 6 days, in contrast to nitrate systems which formed hematite and goethite, the latter predominating in extensively hydrolysed solutions. After periods exceeding 6 days, the β FeOOH in chloride solutions slowly transformed to hematite and goethite. Addition of hematite and goethite seed to ageing chloride solutions promoted the formation of these phases, indicating that their usual absence is due to the lack of suitable nuclei, whereas the β FeOOH is readily nucleated. Addition of seed also enhanced the transformation of β FeOOH to hematite or goethite, which suggests that this proceeds by dissolution and reprecipitation.

Matijevic et al investigated the hydrolysis of iron sulphate solutions, with the aim of producing monodispersed colloidal particles of basic sulphates[69, 70], and found that the concentration of iron (III) and sulphate, pH, temperature and rate of heating all affect the chemical composition or morphology of the precipitated species. By maintaining the concentration of ferric sulphate at 0.08-0.10M, the pH at 1.5-1.7, and ageing for 3-4 hours, it was possible to form monodispersed particles of $Fe_4(SO_4)(OH)_{10}$ and hydronium jarosite. Monodispersed hydrous oxides of chromium(III), aluminium, zirconium(III) and copper(I) oxides were also formed by similar, controlled hydrolysis.

The hydrolysis of iron in sulphate solution has been extensively studied because of its application in the Electrolytic Zinc Process. Figure 2.6 shows part of the Fe_2O_3-H_2O-SO_3 system at 100°C (from reference[59]). From the tie lines it is clear that hydronium jarosite will precipitate from fairly concentrated solutions, over a wide composition range, while $Fe_4(SO_4)(OH)_{10}$ forms from more dilute solutions, over a narrow composition range. Goethite, α FeOOH, can be seen to form only from solutions with very low iron concentration. At higher temperatures, hematite can be precipitated directly from such solutions. There are three main processes for removing iron

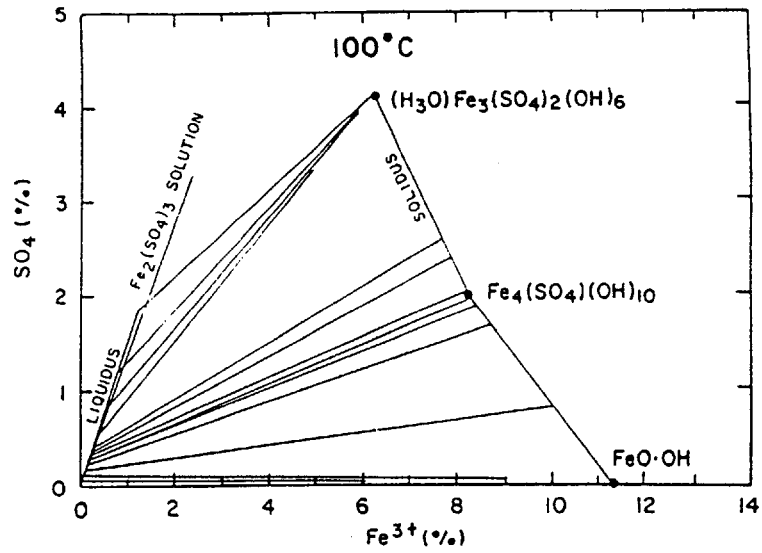


Figure 2.6 Part of the Fe_2O_3-H_2O-SO_3 Phase System at 100°C[59]

from sulphate solutions; the Jarosite, goethite and hematite processes, named after the principal phases formed.

In the Jarosite process, either hydronium jarosite or $MFe_3(SO_4)_2(OH)_6$, where M= NH_4^+, Na^+, K^+ etc., is precipitated. One of the main drawbacks of the process is the fact that a large number of metals can be substituted into the jarosite lattice; for example, lead will substitute for alkali metals, divalent base metals such as Cu, Zn, Co, Ni and Mn substitute for Fe to a minor extent, while trivalent Al, In and Ga all substitute for Fe to give solid solutions. The extent of substitution increases with increasing pH, and can lead to significant loss of values[71].

The physical chemistry of the processes involved in jarosite precipitation has been discussed by McAndrew, Wang and Brown[60], and Haigh[72].

As shown in Figure 2.6, goethite can only be precipitated from very dilute iron(III) solutions. In practice the pH is maintained at 2-4, and the ferric concentration is kept below 1g/l.[59,73]. In the Electrolytic Zinc Company of Australasia (E.Z.) process, this is achieved by feeding leach solution, typically with 30g/l Fe(III), into

a precipitation vessel at a rate which keeps pace with precipitation. In the Vieille Montagne (V.M.) process, the iron in the leach solution is reduced to ferrous with zinc sulphide, then slowly oxidised with oxygen while precipitating goethite[73,74]. Davey and Scott examined the precipitates formed by the V.M. and E.Z. variations, in both chloride and sulphate media[73]. Their results are summarised in Table 2.2.1, which shows the nature of the precipitates, as identified by X-ray diffraction, and by differential thermal, and thermal gravimetric analyses. Only the Vieille Montagne process in sulphate solution actually gave pure goethite; under other conditions β FeOOH and hematite appeared. These results demonstrate the effect of pH, and anion on the nature of the iron precipitate, as previously discussed.

Table 2.2.1 Comparison of 'Goethite' Precipitates from E.Z. and V.M. Processes in Sulphate and Chloride Solutions[73]

Process	Anion	pH	XRD & Crystallinity	DTA - TGA	Wt Loss at 500°C %
V.M.	SO_4^{2-}	3.5	α FeOOH good	α FeOOH	13.5
E.Z.	SO_4^{2-}	3	α FeOOH poor	$\alpha+\beta$ FeOOH	19.5
E.Z.	SO_4^{2-}	3	α FeOOH v.poor	mostly β FeOOH	21.5
E.Z.	Cl^-	3	β FeOOH good	β FeOOH	14.7
V.M.	Cl^-	3.5	α Fe_2O_3 good +minor α FeOOH	—	6.0

Although the V.M. process has been found to give lower final iron concentrations than the E.Z. process, in sulphate solutions the product from the former was more heavily contaminated by Co, Cu and Zn than the product from the latter[75]. This could be due to the higher pH used in the V.M. process, since coprecipitation of divalent metals with iron is known to increase greatly with increasing pH[97]. Davey and Scott showed that chloride solutions precipitated β FeOOH at low pH, whereas hematite and possibly δFeOOH appeared at higher pH. The addition of different seed materials was found to have no significant effect on the nature of the products[75], which contrasts with

the results of Atkinson, Posner and Quirk[68].

In the hematite process, the iron(III) is reduced by SO_2, the pH is raised to 4.5, then αFe_2O_3 is precipitated at 180°-200°C, under 18 atm O_2 pressure, to give a relatively uncontaminated product.

A variety of hydrolysis processes have been studied in the work presented in this section; therefore the results cannot be summarised in a simple manner. Nevertheless, the general conclusions which can be drawn are:

(1) The formation of goethite, whether by precipitation or transformation of amorphous hydroxide, is favoured by nitrate (or dilute sulphate) solutions, at relatively low temperatures and high pH values.
(2) The formation of β FeOOH is favoured by chloride solutions, at relatively low temperatures and low pH values.
(3) The formation of hematite is favoured by relatively high temperature and low pH values.

It is not possible to quantify temperature and pH in the above conclusions, because their effects appear to be inter-related.

2.2.3 The Mechanism of Hydrolysis of Iron(III)

The behaviour of iron(III) on hydrolysis under different conditions has been described in the previous section. In the context of accounting for the behaviour during hydrolytic stripping, however, the fundamental mechanism of hydrolysis is required. Most authors have reported experimental results without attempting an explanation for the results. Fortunately, many of the results can be interpreted in the light of those mechanisms which have been proposed.

The nature of the phases precipitated by hydrolysis is widely considered to be determined by the nature of the ferric complexes in solution before precipitation. In the absence of strong complexing anions, the simple hydrated Fe^{3+} ion is stable in dilute solutions at low pH. As the pH is raised, a series of hydroxy complexes forms, i.e. $Fe(OH)^{2+}$, $Fe(OH)_2^{+}$ etc. At higher iron concentrations a dimeric species $Fe_2(OH)_2^{4+}$ exists. This is formed

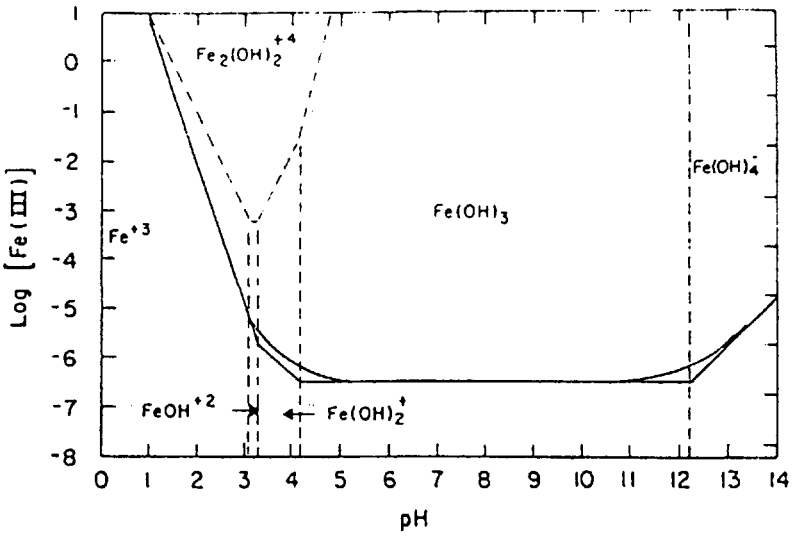


Figure 2.7 Solution species present in the Fe^{3+}-H_2O system at 25°C as a function of iron concentration and pH[60]

by hydroxyl bridging[59,76]:

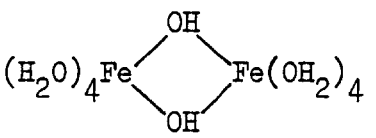


Figure 2.7 shows the species present in the iron(III)-water system at 25°C, as given by McAndrew et al[60]. The dotted lines indicate equal concentrations of neighbouring hydroxyl complexes, and define the areas of predominance for each species. The solubility of goethite is shown (solid line) and demonstrates how the existence of anion complexes causes departures from the ideal behaviour illustrated in Figure 2.4.

Figure 2.8(a) shows the distribution of ferric hydroxo complexes at low pH and $[Fe^{3+}]_{tot}$=0.18M, at 25°, 55° and 80°C, as given by Sapieszko, Patel and Matijevic[77]. A comparison of this with Figure 2.8(b), which shows the distribution of complexes in a sulphate solution, indicates the effect which a complexing anion can exert on the species present.

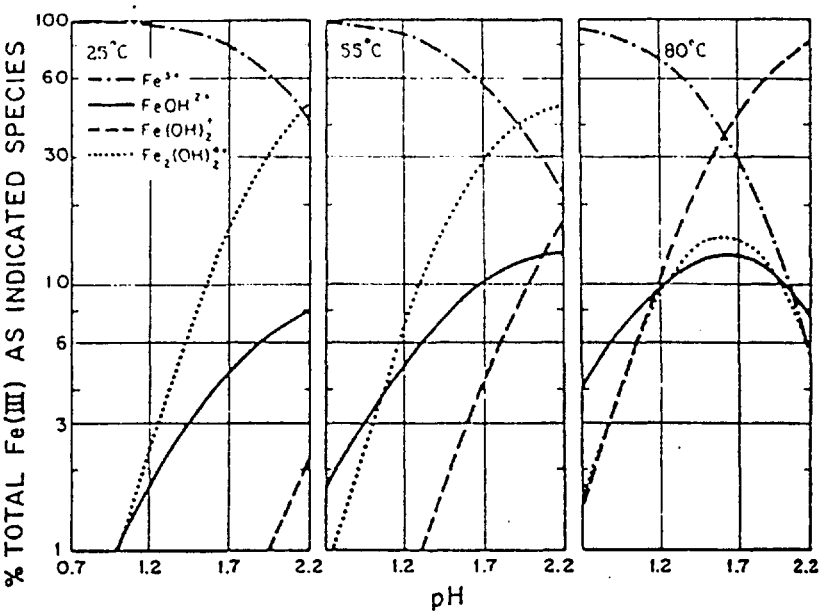


Figure 2.8(a) Species distribution diagrams as a function of pH at 25°, 55° and 80°C for ferric hydroxo complexes. $[Fe^{3+}]_{tot}$ = 0.18M and μ= 2.67M in all cases(77)

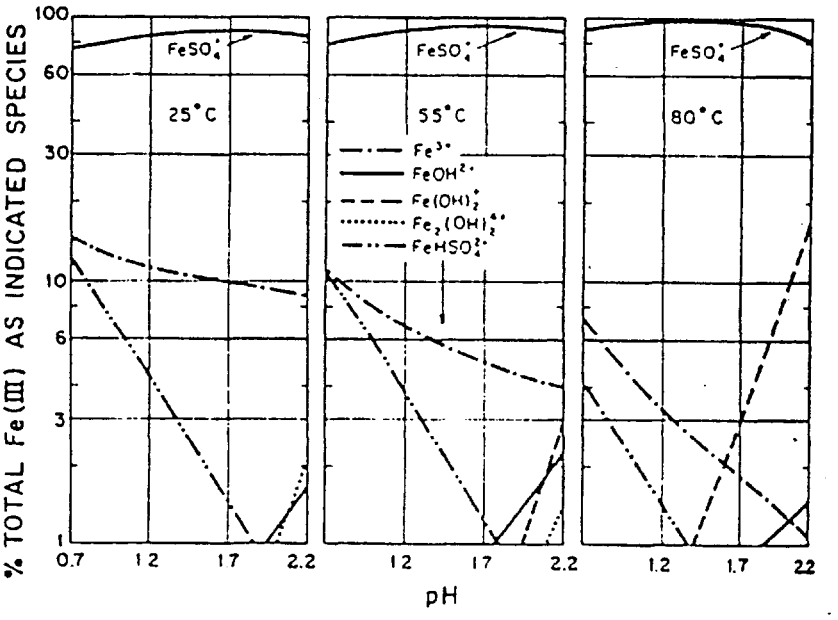


Figure 2.8(b) Species distribution diagrams as a function of pH at 25°, 55° and 80°C for ferric hydroxo and sulphato complexes. $[Fe^{3+}]_{tot}$=0.18M $[SO_4^{2-}]_{tot}$=0.53M and μ= 2.67M(77)

Kiyama and Takada stated that at low pH, solutions of iron(III) chloride, sulphate and nitrate contain ferric chloro, sulphato and aquo complexes respectively[78]. As the acidity of the solutions was decreased, spectrophotometric measurements indicated that a polynuclear complex, containing a large number of ferric ions, was formed in each type of solution. The concentration of the complex increased with decreasing acidity. Magnetic susceptibility measurements suggested that the polynuclear complex formed by hydrolysis of the aquo ferric complex in nitrate solutions contains $[Fe_2(OH)_3]^{3+}$ cations, that in sulphate solutions the polynuclear complexes contain $[Fe_2(OH)_3]^{3+}$ and/or $[Fe_3(OH)_2]^{7+}$, depending on the pH, while $[Fe(OH)_2]^{+}$ cations are present in chloride solutions. The polynuclear complexes containing $[Fe_2(OH)_3]^{3+}$ cations seemed to contain dihydroxo-bridged structural units. It was proposed that edge-shared octahedral dimers $[Fe_2(OH)_2(H_2O)_8]^{4+}$ are bound together in nitrate or sulphate solutions by monohydroxo-bridging, to give a zig-zag polynuclear cation with the structure shown in Figure 2.9(a). From the crystal structure and magnetic properties of the β FeOOH which is formed from chloride solutions, it was presumed that edge-shared octahedral dimers are bound by oxo-bridging in these solutions, to give the ring structure shown in Figure 2.9(b). Polynuclear complexes consist of such polynuclear cations and the acid anions; their formation is roughly described by equations 2.2.8-2.2.11, which omit the water ligands for simplicity:

$$2Fe(NO_3)_3 + 3H_2O = Fe_2(OH)_3(NO_3)_3 + 3HNO_3 \qquad 2.2.8$$

$$Fe_2(SO_4)_3 + 3H_2O = Fe_2(OH)_3(SO_4)_{3/2} + 3/2H_2SO_4 \qquad 2.2.9$$

$$3/2Fe_2(SO_4)_3 + 2H_2O = Fe_3(OH)_2(SO_4)_{7/2} + H_2SO_4 \qquad 2.2.10$$

$$2FeCl_3 + 3H_2O = Fe_2(OH)_2Cl_2O + 4HCl \qquad 2.2.11$$

On heating, the nitrate and sulphate polynuclear complexes were hydrolysed to α FeOOH, whereas the chloride complex gave β FeOOH. Hematite was formed at higher temperatures; 60°C in nitrate solutions and 90° in chloride and sulphate solutions, indicating that the structure of the complexes is temperature dependent.

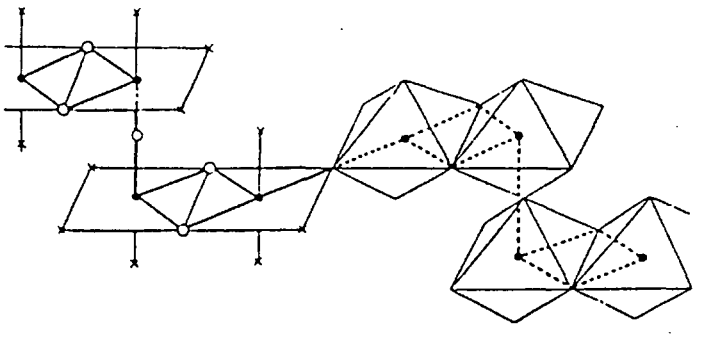


Figure 2.9(a) Polynuclear cation formed in ferric nitrate and sulphate solutions[78]
•-Fe^{3+}, o-OH^-, ×-H_2O

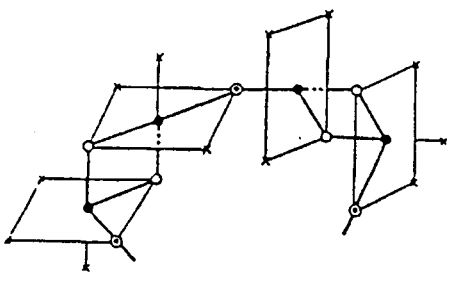
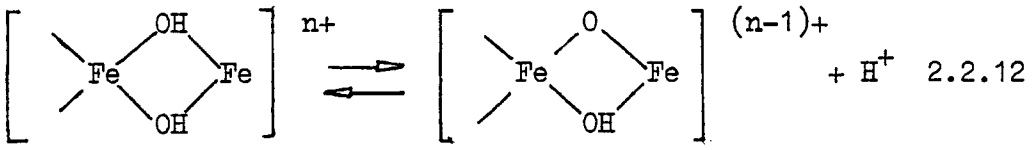


Figure 2.9(b) Polynuclear cation formed in ferric chloride solutions[78] • -Fe^{3+}, o -OH^-, ⊙ -O^{2-}, × -H_2O

From kinetic studies, Dousma and de Bruyn divided hydrolysis in nitrate solutions into four stages;

(1) Hydrolysis to monomers and dimers
(2) Reversible, rapid growth to small polymers
(3) Formation of slowly reacting, large polymers
(4) Precipitation of a solid phase[76]

In developing a model to explain these stages, they used the fact that hydrolysis occurs by olation, which is the linking of metal ions by hydroxyl groups, and by oxolation, which is represented by;



2.2.12

They postulated that oxolation of large hydroxy-complexes occurs at all temperatures, and that once formed, the oxybridges react only slowly with acid, to reverse the process. Their proposed scheme of hydrolysis is shown below in Figure 2.10.

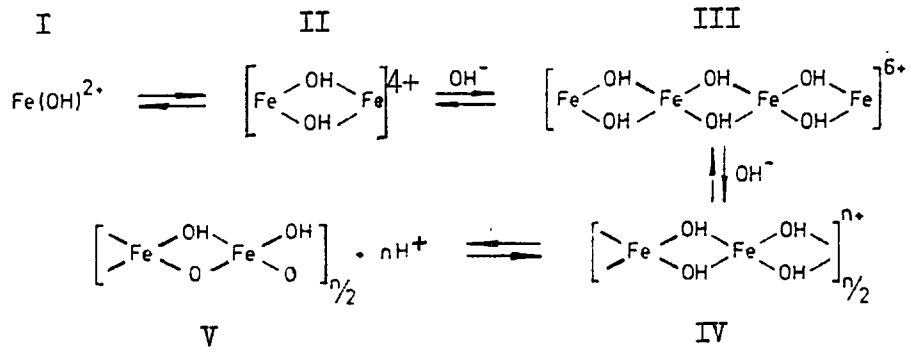
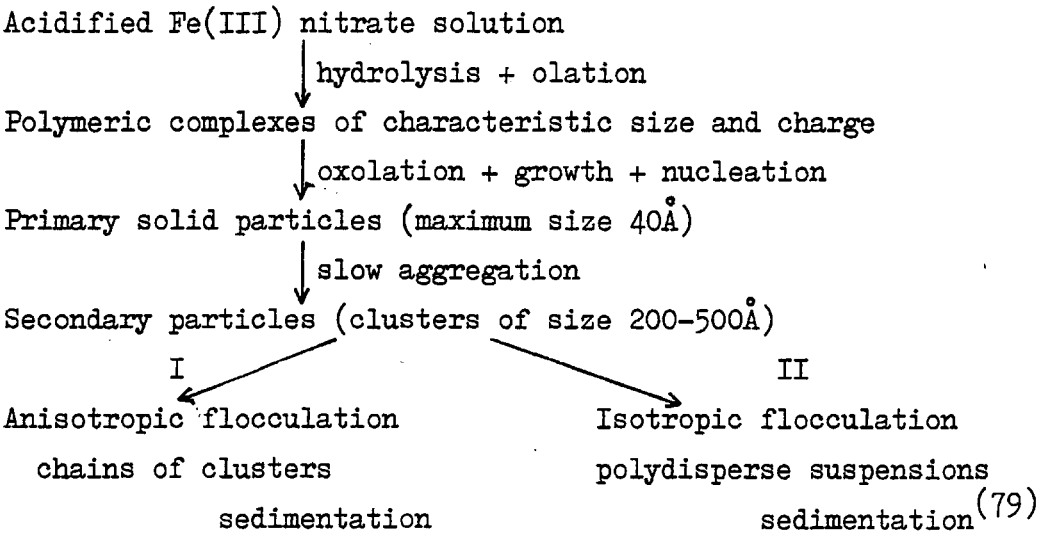


Figure 2.10 Proposed Scheme of Hydrolysis-Precipitation(76)

III is a small polymer, the formation of which is easily reversible, whereas IV is a large polymer, which is oxolated in a series of steps to form the unreactive, uncharged polymer V.

These authors studied the process by which the unreactive polymers IV and V are aged to give finally precipitates, and were able to amplify and extend the original model(79). At low OH/Fe ratios, there was an induction time before oxolation of species IV occurred. As the pH was virtually constant during this period, the kinetic barrier must be related to a compositional change which does not consume OH^-; it could be the olation of two polymeric species, or a reaction between a monomer and polymer, to form a larger polymeric species of increased charge. Samples with a higher OH/Fe ratio did not have an induction time; a sharp pH drop was evident as soon as ageing started. The steepness of the curve was interpreted as resulting from a cooperative mechanism, involving oxolation and a hydroxyl consuming process. Oxolation, which lowers the surface charge by eliminating H^+, was envisaged as being followed by addition of monomers

or dimers to increase the surface charge. Continued growth was thought to be facilitated by binding OH^- to the growing, partly oxolated species. Because oxolation changes the environment of Fe^{3+}, these theories can be supported by spectrophotometric measurements which were made. The cooperative process appeared to lead to nucleation and growth of small particles, 40-60Å in diameter. At this point secondary particles of about 200Å appeared; the lack of particles of intermediate size suggests that the secondary particles were clusters of primary particles. Aggregation could be the result of hydrolysis or oxolation of the primary particles, which would lower the surface charge, and make clustering possible. In a stable sol, of low ionic strength, the secondary clusters flocculated by attachment at the ends of particles, forming chains of clusters. In solutions of higher ionic strength, isotropic flocculation occurred. The hydrolysis and precipitation processes were summarised by the authors as:



(79)

When the pH of an iron solution is rapidly increased, large polymers become cross-linked by hydroxyl bridges, and large hydroxide gel colloids form; these coagulate before oxolation can occur, to give bulky gel precipitates(59).

From pH studies, and electron micrographs of samples taken during hydrolysis of ferric chloride and ferric nitrate solutions, Fryer, Gildawie and Paterson found that hydrolysis was virtually complete when the solutions were still optically clear. At this stage thin films were present in both solutions. In nitrate solutions these

films then thickened evenly, eventually forming lath shaped crystals of α FeOOH[80]. In chloride solutions the films thickened unevenly, with pod-like structures developing, eventually precipitating β FeOOH. In mixed solutions, with anion ratios of 0-50% Cl^-/NO_3^-, the precipitate had the crystal structure of α FeOOH, but the pod-like morphology of β FeOOH. At higher Cl^-/NO_3^- ratios, only β FeOOH formed. The final crystalline product is clearly determined by the manner in which the anions affect film thickening. Initial hydrolysis was envisaged by the authors as forming films in which four equatorial OH^- ions are shared by four Fe(III) ions, these films being stabilised by anion ligands in both of the axial positions of the octahedral Fe(III) ions. Since Cl^- is a stronger complexing agent than NO_3^-, it is thought to stabilise the film to a greater extent, so that it is more likely to crystallise by rolling up, than by thickening, which requires displacement of the ligand. Growth was considered to result from elimination of water from hydroxyl bridges to give an oxide structure, i.e.:

$$p[(MH_2O)_x]^{n+} \xrightarrow[pH\ drop]{rapid} \underset{\text{thin film}}{[M(OH)_y(H_2O)_{x-y}]_p^{p(n-y)+}} + pyH^+$$

$$\downarrow \text{dehydration}$$

$$pMO_{n/2} + (p/2)(2x-n)H_2O + pnH^+$$

Murphy, Posner and Quirk observed spherical ferric hydroxy polycations of diameter 15-30Å as initial products of iron(III) hydrolysis in nitrate, chloride and perchlorate solutions. Polycations, isolated from a nitrate solution, were aged in nitrate or chloride solutions. α FeOOH precipitated from the nitrate solutions, whereas β FeOOH formed in the chloride solutions. This indicates that the ferric hydroxy polycations have the same structure in all solutions, and the divergence in structure, due to the nature of the anion, only occurs on ageing[81]. β FeOOH was considered to develop in chloride solutions because penetration of chloride ions into the polycations interrupts the development which would otherwise occur. These authors regarded the size of polycations to be highly sensitive to the ionic strength of the solution, so their observations of spherical crystal precursors are not necessarily contradictory to the observations of film precursors made by Fryer et al[80]. Both groups of workers

concluded that anions affect only the growth of polymers, not their formation. This conclusion explains the effect of the anion observed by many workers, and also accounts for the incorporation of the counter anion in the final iron precipitate, which renders the products of the goethite process unsuitable for iron-making.

In hydrolytic stripping, the carboxylate ions may be expected to exert some effect on the hydrolysis of metals. This cannot be predicted theoretically, but since, as discussed in section 2.1.3, solvent extraction by carboxylic acids is possible because of the formation of metal-carboxylate complexes in preference to metal-anion complexes in aqueous solution, the effect of the carboxylate ions might be expected to be substantial. The polymers which are widely considered to be the first hydrolysis products in aqueous solution may be modified, for example, by carboxylate bridging as in the aluminium carboxylate gel structure described in section 2.1.5. The structure of the metal carboxylate complexes prior to hydrolysis may also exert an effect on the development of hydrolysis products, and this is known to be sensitive to the concentration of metal and carboxylate in the organic phase.

2.2.4 The Crystal Structure of Iron Oxides and Oxide Hydroxides

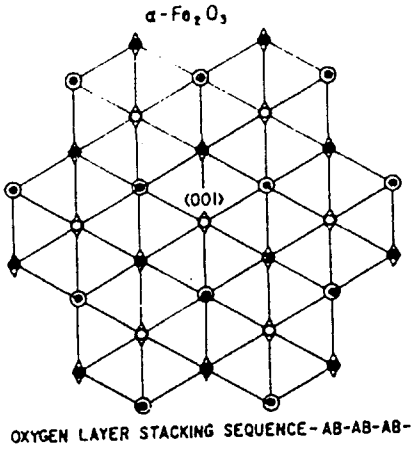
The crystal structures of iron oxides and oxide hydroxides are shown in Table 2.2.2, compiled from references[58,82]. There is apparently very little similarity between these structures, apart from Fe_3O_4 and γFe_2O_3, which both possess the spinel structure, and are easily interconvertible[83]. Nevertheless, many of the transformations between these structures are topotactic, that is, they occur by a rearrangement such that the two phases have a definite structural relationship[58]. The relationship arises because the structures may all be described in terms of stacked 'almost close packed' layers of oxygen or OH^- ions, with the iron atoms behaving as interstitials of atomic radius such that they almost fit into the available sites without distortion of the oxygen lattice. The distances between the oxygen planes are essentially the same, 2.3-2.5Å. The stacking sequences are ABC-ABC in the <111> direction for magnetite and maghemite, with cubic symmetry, and AB-AB-AB in <001> for goethite and

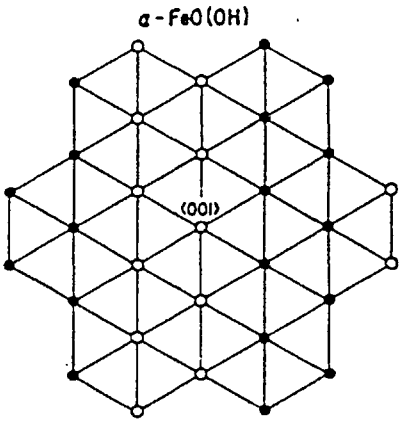
Composition	Mineral Name	System	Space Group	Cell Constants Å	Notes *
αFe_2O_3	hematite	Trigonal (hexagonal unit cell)	$R\bar{3}\bar{c}$	a_o=5.035±0.0005 c_o= 13.72±0.01	H.c.p.oxygen with Fe^{3+} in octahedral positions
γFe_2O_3	maghemite	Cubic(spinel)	Fd3m	a_o=8.33- 8.38±0.01	Spinel-various degrees of ordering
Fe_3O_4	magnetite	Cubic(fcc-inverse spinel)	Fd3m	a_o=8.397- 8.394±0.005	Inverse spinel
αFeOOH	goethite	Orthorhombic	Pnma	a_o=10.0±0.1 b_o= 3.03±0.01 c_o= 4.64±0.01	Based on h.c.p. oxygen
βFeOOH	akaganeite		I4/m(?)*	a_o= 10.48* b_o= 3.06	Laue gp I4/m or I4/mmm F^-or Cl^- necessary for formation. αMnO_2 structure
γFeOOH	lepidocrocite	Orthorhombic	Cmcm	a_o= 3.06±0.01 b_o=12.4 ±0.1 c_o= 3.87±0.01	Based on c.c.p. oxygen
δFeOOH			P312(?)*	a_o=2.941, c_o=4.58*	H.c.p.oxygen. Disordered CdI_2 structure

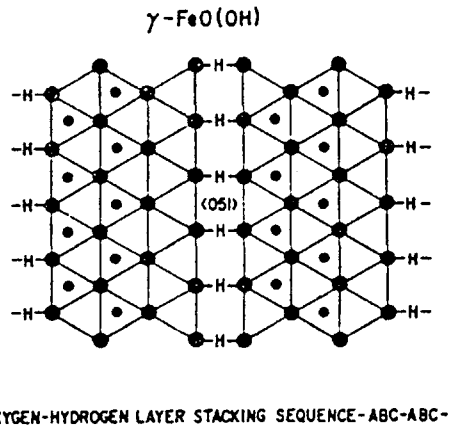
TABLE 2.2.2 SUMMARY OF THE CRYSTAL STRUCTURES OF IRON OXIDES AND OXIDE HYDROXIDES (82, 58(*))

hematite. Lepidocrocite has ABC-ABC in the <051> direction of the orthorhombic cell, which corresponds to the <111> direction of the distorted cubic cell which can also be used to describe this phase. β FeOOH cannot be described in terms of a close packed oxygen-hydroxide lattice. It is thought to have a structure like that of αMnO_2, in which there are open channels along the c-axis of an otherwise cubic body-centred arrangement of oxygen atoms. Chloride or fluoride ions, which are necessary for the formation of this phase, are thought to be incorporated in the lattice. The transformation of β FeOOH to αFe_2O_3 is therefore non-topotactic; the literature indicates that in solution the transformation proceeds by dissolution and reprecipitation, while on heating the transformation only occurs at 280°C, and seems to entail recrystallisation[58].

The differences between the structures having the same oxygen layer packing sequences result from the differences in position of the iron atoms, as is shown in Figure 2.11, taken from reference[82], which shows the positions of the iron, projected onto the plane of the oxygen layers. In hematite, goethite and lepidocrocite the iron atoms occupy the layer octahedral sites, whereas in magnetite and maghemite, with the spinel structure, both octahedral and tetrahedral sites are occupied. The spinel structure is described in detail in the next section.







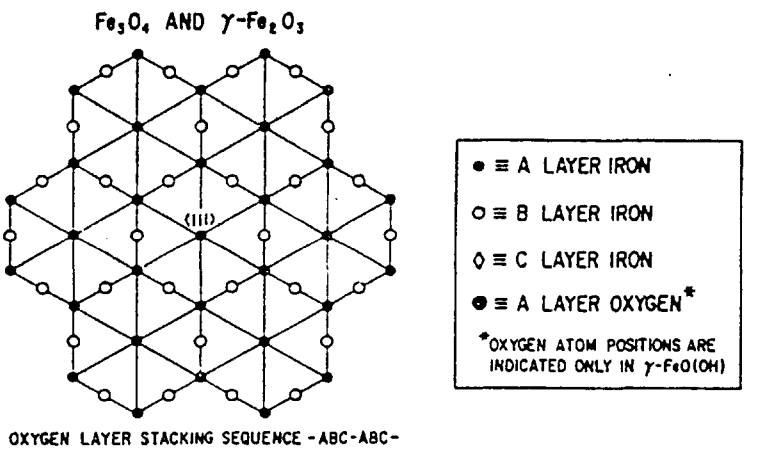


Figure 2.11 Projected atom positions in hematite, goethite, lepidocrocite, and magnetite/maghemite[82]

2.3 SPINEL FERRITES: THEIR STRUCTURE, PROPERTIES AND USES

2.3.1 The Structure of Spinel Ferrites

The spinel structure, AB_2Z_4, is shown by a large number of compounds. The anion Z may be;

$Z = O^{2-}$, S^{2-}, Se^{2-} and Te^{2-}

The divalent metals, A^{2+}, which are found in the oxide spinels are;

A = Mg, Cr, Mn, Fe, Co, Ni, Cu, Zn, Cd and Sn (all M^{2+})

The trivalent metals, B^{3+}, found in the oxide spinels are;

B = Al, Ga, In, Ti, V, Cr, Mn, Fe, Co, Ni and Rh (all M^{3+})

Only some combinations of these metals are known[84]. Only the spinel ferrites, with the formula AFe_2O_4, were formed by hydrolytic stripping, so discussion will be confined to this class of compound. The spinel ferrites are an important class of ferrites, which are defined as magnetic oxides containing iron oxide as a main constituent. The main classes are shown in Table 2.3.1, from reference[85]. The synthesis of the other ferrites, namely garnets, hexaferrites and orthoferrites was not investigated in this work.

The structure of the ferrite spinels is closely related to the structure of the mineral spinel, $MgAl_2O_4$, which crystallises in a cubic system with 8 formula units in the unit cell. Iron(III) is substituted for Al in the ferrites. Mg(II) may be replaced by divalent cations with radius 0.6-1.0Å. The larger oxygen ions, radius 1.32Å, are almost close packed in a face-centred cubic arrangement, and the metal ions fit into the interstices, forming additional face-centred cubic sub-lattices interlaced with the oxygen lattice. Only 8 of the 64 tetrahedral, and 16 of the 32 octahedral sites are occupied. These are commonly referred to as the A and B sites respectively[85,86,87,88,89,90]. The structure is shown in Figure 2.12, which shows the relative sizes of the ions in the unit cell, and in Figure 2.13, which shows the coordination of the ions. In spinel all of the Mg(II) ions are on the tetrahedral (A) sites, and all of the Al(III) ions are on the octahedral (B) sites. This is termed the 'normal' spinel structure, and is shown by some ferrites, such as $ZnFe_2O_4$ and $CdFe_2O_4$, which are both paramagnetic.

Table 2.3.1 Commercially Important Ferrites[85]

Class of Ferrite	Crystal Structure	Composition
Spinels	Cubic spinel	$M^{2+}Fe_2^{3+}O_4$ where M= Ni,Zn,Fe,Mn, Cu,Cd,Mg,Co singly or as mixtures
Garnets	Cubic garnet	$R_3^{3+}Fe_5^{3+}O_{12}$ where R is a rare earth, generally Y or Gd
Hexaferrite	Hexagonal magnetoplumbite	$BaFe_{12}O_{19}$ (M type) $BaM^{2+}Fe_{12}O_{22}$ (Y type) $BaM_2^{2+}Fe_{16}O_{27}$ (W type) $Ba_3M_2^{2+}Fe_{24}O_{41}$ (Z type) $Ba_2M_2^{2+}Fe_{28}O_{46}$ (X type) $Ba_4M_2^{2+}Fe_{36}O_{60}$ (U type) M= Ni,Co,Zn,Mg or mixtures
Orthoferrites	Orthorhombic perovskite	$R^{3+}Fe^{3+}O_3$ R= rare earth or mixtures

Other ferrites have the so-called 'inverse' spinel structure, in which the M(II) ions are all on B sites, so that 8 of the Fe(III) ions are on A sites, and 8 on B sites, e.g. Fe(II), Co(II) and Ni(II) ferrites, which are all strongly magnetic. The ions on the octahedral sites are probably statistically distributed[91], although in magnetite, $Fe^{2+}Fe_2^{3+}O_4$ the electrical resistance increases markedly below 120°K, which indicates that there is long range ordering of the cations at this temperature, which limits the semi-conductor properties[87]. The normal and inverse spinel structures are best regarded as extremes, since intermediate structures are known; for example, in $MnFe_2O_4$, 80% of the Mn(II) ions are on the A sites and 20% on the B sites, with Fe(III) making up the balance on the A and B sites, and in $MgFe_2O_4$ only 10% of the Mg(II) is on the A sites, the remaining 90% being on the B sites. It is conventional to indicate the cation distribution by writing the composition with those ions on

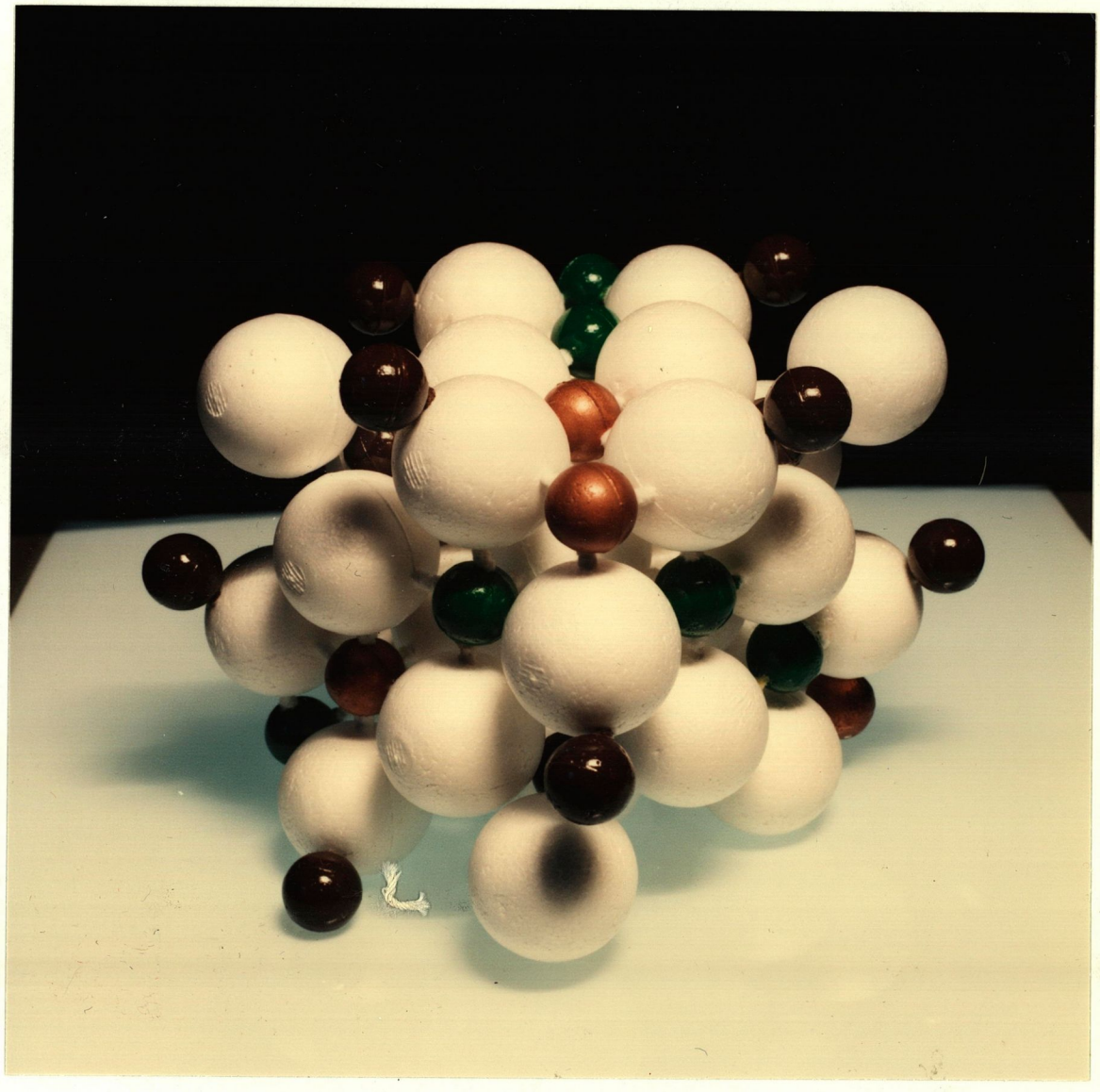


Figure 2.12 Unit Cell of Nickel Ferrite

Key: Large white spheres - oxygen
Small green spheres - nickel(octahedral coordination)
Small bronze spheres - iron(octahedral coordination)
Small dark brown spheres - iron(tetrahedral coordination)

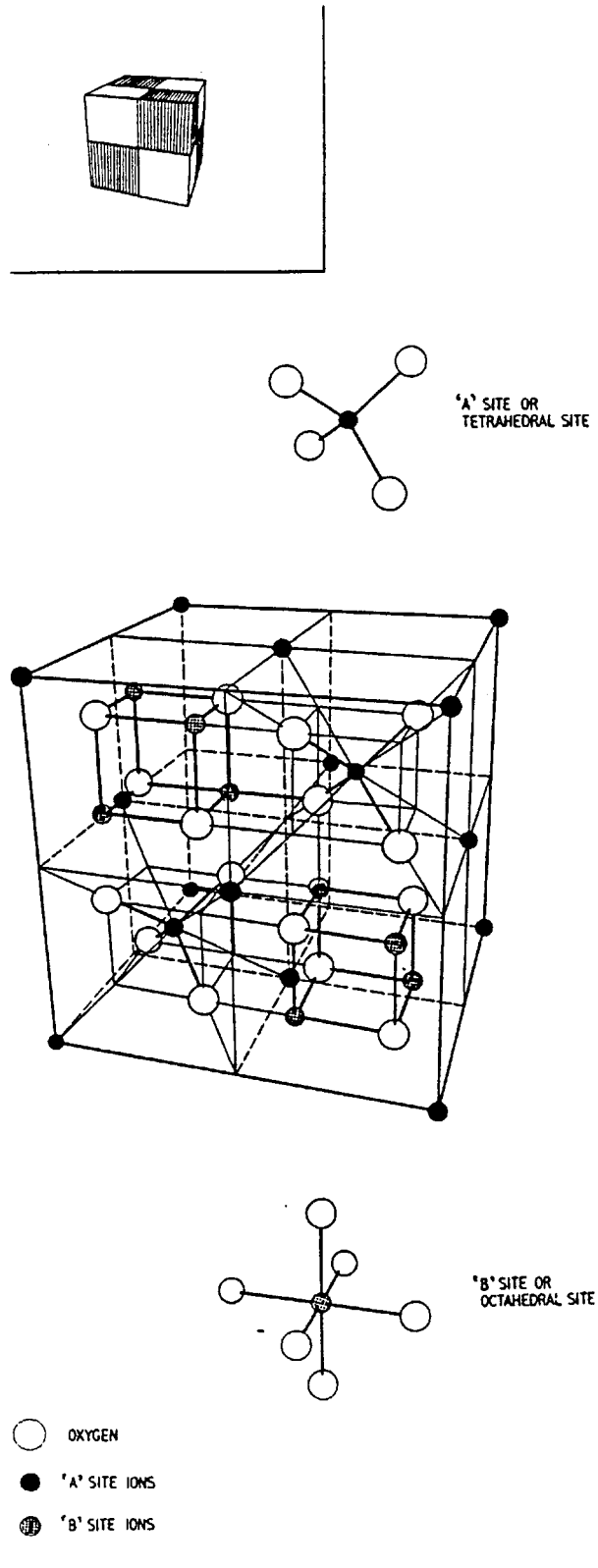


Figure 2.13 The Structure of the Spinel Unit Cell[86]

the B sites within brackets; thus zinc, nickel and manganese ferrites are written as $Zn[Fe_2]O_4$, $Fe[NiFe]O_4$ and $Mn_{0.8}Fe_{0.2}[Mn_{0.2}Fe_{1.8}]O_4$ respectively.

It was stated in section 2.2.4 that maghemite, γFe_2O_3 has the spinel structure. This is generally regarded as $Fe[Fe_{1.67}\square_{0.33}]O_4$, where $\square$ indicates a vacancy. At low temperatures these vacancies are usually ordered on the octahedral sites, but a disordered distribution on octahedral sites has been reported for particles less than 200Å, and for epitaxially grown films. Distribution of the vacancies over A and B sites has been reported for γFe_2O_3 prepared by dehydrating γ FeOOH, or oxidising Fe_3O_4 prepared by treatment of ferrous/ferric chloride with NaOH[82,92], which suggests that the structure is determined by the preparation method.

Table 2.3.2 shows the crystal ionic radius of the divalent metal[93], the cell edge and cation distribution, for the ferrites. The ionic radius of Fe^{3+} is 0.64Å, and that of O^{2-} is 1.32Å. The structure of the spinel is clearly not determined by the ionic radius

Table 2.3.2 Lattice Parameters of Single Ferrite Spinels $M^{2+}Fe_2O_4$ [89,93]

Formula	Ionic Radius M^{2+} Å	Cell Edge a_o Å	Cation Distribution
$MgFe_2O_4$	0.66	8.36	$Mg_{0.1}Fe_{0.9}[Mg_{0.9}Fe_{1.1}]$
$MnFe_2O_4$	0.80	8.507	$Mn_{0.8}Fe_{0.2}[Mn_{0.2}Fe_{1.8}]$
Fe_3O_4	0.74	8.394	$Fe^{3+}[Fe^{2+}Fe^{3+}]$
$CoFe_2O_4$	0.72	8.38	$Fe[CoFe]$
$NiFe_2O_4$	0.69	8.325	$Fe[NiFe]$
$CuFe_2O_4$	0.72	a_o=8.22* c_o=8.71	$Fe[CuFe]$
$ZnFe_2O_4$	0.74	8.44	$Zn[Fe_2]$
$CdFe_2O_4$	0.97	8.69	$Cd[Fe_2]$

*copper ferrite shows a tetragonal deformation below 760°C because of the Jahn-Teller effect

of the divalent ion, since the largest ions, Cd and Mn, are predominantly found on the smaller, tetrahedral sites. The adoption of the normal or inverse structure seems to be dictated by any pronounced preference for a given environment, for example the tendency of zinc to be tetrahedrally coordinated and that of nickel to be octahedrally coordinated, in conjunction with magnetic interactions, which are discussed below.

2.3.2 Magnetic Properties of the Spinel Ferrites

Individual atoms and ions may, or may not possess a magnetic moment. Any magnetic moment results from unpaired electrons, and is generally only due to the spin of the electrons, though in rare earths the orbital angular momentum usually contributes to the magnetic moment. In a solid the outer orbits are generally perturbed by neighbouring ions, resulting in the quenching of the orbital angular momentum, leaving only the spin momentum. Materials are divided into five classes, according to their magnetic properties, as follows:

(1) Diamagnetic - the material contains atoms or ions with all electrons paired and their orbital moments so oriented that the particles have no net magnetic moment.

(2) Paramagnetic - the particles of the material each have the same net magnetic moment. The moments are usually randomly distributed, so that the magnetic moment of the bulk material is zero. The application of an external field produces some alignment of the moments, leading to a small, positive susceptibility. The magnitude of this is limited by thermal agitation, which also randomises the magnetic moments when the applied field is removed.

(3) Ferromagnetic - the particles have a fairly large net magnetic moment. At $0^{\circ}K$ these moments are all aligned by exchange interactions, in the same direction, in magnetic domains in the crystal, giving the material a large net magnetisation e.g. Fe, Co and Ni. Above $0^{\circ}K$ thermal vibration progressively reduces the magnetisation, until at the Curie point, which is characteristic of the material, the material exhibits paramagnetic behaviour.

(4) Antiferromagnetic - although each particle has a large magnetic moment, half are aligned in one direction in the crystal, and half in the other, so the material has no net magnetic moment.

(5) Ferrimagnetic - as in antiferromagnetic materials, the atomic moments are antiparallel. Since the alternate particles have different magnetic moments, these do not cancel each other out, so there is a residual intensity of magnetisation. Spinel ferrites are in this class of meterial[89].

For the elements of the first transition series, the magnetic moments of the atoms and ions are determined by the number of unpaired electrons. The magnetic dipole moment due to the spin of a single electron is μ_B, the Bohr magneton. Thus the magnetic moments of the atoms of the first series are:

Element:	Sc	Ti	V	Cr	Mn	Fe	Co	Ni	Cu	Zn
Moment μ_B:	1	2	3	5	5	4	3	2	0	0

In calculating the magnetisation of ferrites, however, it is the number of unpaired electrons in the relevant ions, and the distribution of these ions in the sub-lattices of the spinel which is of interest. The alignment of the sub-lattices is determined by the exchange interaction between the A and B sub-lattices, and that within each sub-lattice, denoted by AB, AA and BB interactions[90]. These all tend to be negative, but cannot all be so simultaneously, so the strongest interaction predominates; this is usually the AB interaction which results in the ions on the A and B sites being aligned in opposite directions. Table 2.3.3 shows how the net moment of some ferrites is calculated from the moment and distribution of the ions. In zinc ferrite the A lattice has no moment, so the negative BB interaction comes into play in the absence of the AB interaction. The calculated and measured magnetic moments of the ferrites are shown below:

Ferrite:	Mn	Fe	Co	Ni	Cu	Zn
Calculated μ_B:	5	4	3	2	1	0
Measured μ_B:	4.6	4.1	3.7	2.3	1.3	0

The differences are due to either

(1) Incomplete quenching of the orbital momentum, which then contributes to the total magnetic moment, and/or

(2) The structures may not be completely inverse, as assumed.

Table 2.3.3 Ion Distribution and Net Moment per Molecule for Some Typical Ferrites[90]

Formula	Structure	Tetrahedral A sites	Octahedral B sites	Net moment (μ_B/molecule)
$NiFe_2O_4$	inverse	Fe^{3+} 5 →	Ni^{2+} ← 2 Fe^{3+} ← 5	2
$ZnFe_2O_4$	normal	Zn^{2+} 0	Fe^{3+} ← 5 Fe^{3+} → 5	0
$MgFe_2O_4$	mostly inverse	Mg^{2+} 0 Fe^{3+} 4.5 →	Mg^{2+} 0 Fe^{3+} ← 5.5	1
0.9 $NiFe_2O_4$ + 0.1 $ZnFe_2O_4$	inverse	Fe^{3+} 4.5 →	Ni^{2+} ← 1.8 Fe^{3+} ← 4.5	
	normal	Zn^{2+} 0	Fe^{3+} ← 0.5 Fe^{3+} ← 0.5	
	Total	4.5 →	← 7.3	2.8

The addition of up to 50% of the non-magnetic zinc ferrite to other ferrites actually increases their saturation magnetisation. The example in Table 2.3.3 shows why: the zinc ions go onto A sites, displacing Fe^{3+} and hence weakening the A site moment. As the AB interaction is still strong, the ferric ions from the zinc ferrite go onto the B sites with their moments parallel to the others; hence the expected overall moment increases. At over 50% zinc ferrite the A site moment falls to such an extent that the BB interaction predominates over the AB interaction, so the saturation magnetisation falls off.

The ferrites are all magnetically soft, with their moments in the <111> direction, with the exception of $CoFe_2O_4$, which is magnetically hard and magnetised in the <100> direction.

2.3.3 Uses of the Spinel Ferrites

The spinels have a domain structure similar to that of ferromagnetics, and a hysteresis loop resulting from this. The soft ferrites have a low coercive force and narrow hysteresis loop. Since they also have high resistivities and high initial relative permeability, the eddy current and hysteresis losses are lower than for ferromagnetic materials, so they are suitable for use as core materials in high frequency inductors and transformers. Mixed ferrites are used for such applications; for frequencies of around 500kHz the Mn-Zn ferrites are suitable, whereas for V.H.F. applications, at frequencies of about 100MHz, the Ni-Zn ferrites are used because they have a higher initial permeability than the Mn-Zn ferrites at high frequency.

Because the saturation magnetisation per unit volume is less than that of the ferromagnetic metals, the ferrites are not suitable for high field or high power applications, such as motors, generators and power transformers. They are widely used, however, in low power applications, such as television receivers, radios, memory devices and microwave devices. Although cobalt ferrite is magnetically hard, it is not suitable alone for magnetic recording tape, because the coercive force is highly temperature dependent, falling from 6000 Oe to 440 Oe between 90° and 200°C. It can now be used to dope the surface of acicular γFe_2O_3 particles, which are used for recording tape, with a resultant improvement in performance. The importance of both soft ferrites and the oxides used for recording tapes can be judged from Table 2.3.4, which shows the market value of the U.S. production of magnetic materials in 1968.

The spinel ferrites also find application, along with other spinels, as catalysts for oxidation reactions, such as the oxidative dehydrogenation of hydrocarbons to form unsaturated compounds suitable for subsequent syntheses[84].

Because of the semi-conductor properties of some of the ferrites, which result from a defect structure such as that in maghemite, they are of potential use as solid-state battery materials when doped with Li^+ [94].

Table 2.3.4 Market Value of U.S. Production of Magnetic Materials in 1968[90]

			Millions of dollars	Percent of market	
Soft Magnetic Materials	Electrical steel		180	28	49
	Soft ferrites		110	17	
	Nickel-iron alloys		25	4	
Hard Magnetic Materials	Magnetic Recording Materials	Tape	180	28	51
		Discs & drums	100	15	
	Permanent magnets		55	8	
Total			650	100	100

2.3.4 Manufacture of Spinel Ferrites

There are two interrelated steps in the production of polycrystalline ferrites, that is, the chemical preparation of the ferrite in powder form, and the fabrication of the component by pressing and sintering.

The fundamental reaction for the formation of a simple spinel ferrite is

$$MO + Fe_2O_3 = MFe_2O_4 \qquad 2.3.1$$

Sometimes the relevant oxides are used as raw materials, but frequently salts such as oxalates, carbonates and hydroxides, which decompose to oxides on heating, are used, as they are easier to prepare in a suitable form. Intimate mixtures of the salts may be prepared by spraying mixed solutions into an oven at 400°C, freeze drying or by coprecipitation techniques. The full details of ferrite manufacture are not relevant to this work, but the essential points are as follows.

The mixture of salts, however prepared, is calcined at between 900° and 1200°C, typically for 20 hours total residence in a

tunnel kiln. The kiln has a thermal gradient, so that the material is only at the maximum temperature for a few hours. Spinels begin to form by solid state diffusion. Although particle sizes of 1μm are reached, the reaction is rarely taken to completion at this stage. The calcined material is then milled for up to 12 hours to reduce the particle size and mix any unreacted oxides. The powders are then compacted by appropriate techniques, and sintered to convert unreacted oxide to ferrite while developing the microstructure of the ceramic. Variations in the exact treatment can strongly influence the physical properties of the ferrite, and are therefore utilised, but a typical maximum temperature in the sintering kiln is 1400°C[86,88,90].

This production method is clearly very laborious and energy intensive. Cobalt and nickel ferrites have been prepared by coprecipitation of hydroxides from chloride solutions containing Co(II) or Ni(II) and Fe(III) in a 1:2 ratio, by treatment with excess NaOH. If precipitation is done at room temperature, it is followed by dehydration at 100°C[95], and if done at 100°C it is followed by ageing, to achieve larger particle sizes[96]. Such preparations only give very fine particle sizes, with surface areas of typically $100m^2/g$, but the magnetic properties of ferrites are highly dependent on particle size and morphology, and the optimum size is about 1μm. Furthermore, when the experimental method of Schuele and Deetscreek[96] was followed in the course of this work, a bulky, non-magnetic iron precipitate was formed instead of nickel ferrite. Whatever the reason, aqueous precipitation methods have not been adopted on a widespread basis for manufacturing ferrites.

Han, Narita and Lawson reported on the coprecipitation behaviour of cobalt and nickel with Fe(III) from aqueous ammoniacal solutions[97]. Cobalt was found to coprecipitate to a greater extent than nickel, this effect being higher in 1M ammonia than in 5M solutions, in which extensive ammine formation occurs. Although the authors report the formation of spinels when coprecipitation occurs, their X-ray data reveal some discrepancies between the pattern of the precipitates and that of Fe_3O_4 or $CoFe_2O_4$ which suggests that these phases are not well developed.

From references[95,96 97] it can be deduced that a mixed ferrite is more stable, thermodynamically, than a mixture of the single hydrolysis products of the constituent metals, even at temperatures of about 100°C. The usual absence of these ferrite phases must, therefore, be attributed to a kinetic barrier to their formation.

PART I

EQUILIBRIUM STUDIES OF THE HYDROLYTIC STRIPPING OF METAL CARBOXYLATES AND THEIR MIXTURES

CHAPTER 3

EXPERIMENTAL PROCEDURE

3.1 INTRODUCTION

A variety of metals were selected for screening, to ascertain their behaviour, singly and in mixtures, during hydrolytic stripping. As discussed in Chapters 1 and 2, iron(III) was of particular interest, and all of the metals known to form spinel ferrites were tested. Trivalent Al, Cr, Mn and Co were tested because they can form spinels. Ca(II), Sr(II) and Ti(IV) were also selected, because of their ability to form complex oxides, such as $SrTiO_3$ and $CaTiO_3$ with the perovskite structure.

Organic solutions of these metals were prepared, and subjected to hydrolytic stripping. Any solids precipitated were identified by X-ray powder diffraction, and in same cases it was necessary to carry out chemical analysis, because of the ambiguity of the X-ray results.

In earlier work[15], practical problems had been encountered with the preparation of ferric solutions of Versatic 10, the carboxylic acid used throughout this work, and further work was deemed necessary. All metals are extracted by Versatic solutions at pH values very close to the pH at which their hydroxides precipitate, and some precipitation is inevitable as a result of the addition of base to effect extraction. For most metals these precipitates readily redissolve with the pH drop which accompanies extraction;

$$M^{n+} + n\overline{HV} = \overline{MV_n} + nH^+ \qquad 3.1.1$$

(where V represents the Versatic ion), but iron rapidly hydrolyses to form unreactive polymers, as discussed in 2.2.3. Once formed, these polymers do not redissolve. Continuous neutralisation is therefore only suitable for iron extraction in apparatus such as the AKUFVE[49], where mixing is sufficiently rapid to ensure that no large, local pH rises accompany the addition of alkali.

For routine preparation of iron-Versatic, exchange extraction from aqueous ferric solutions with calcium-Versatic solutions has proved to be effective. The overall reaction of this process is

$$2Fe^{3+} + 3\overline{CaV_2} = 3Ca^{2+} + 2\overline{FeV_3} \qquad 3.1.2$$

Ferric chloride solutions are used in preference to ferric sulphate, because the $CaSO_4$ which precipitates in the latter system stabilises the organic-aqueous emulsion, preventing separation. The most effective method of contacting the two phases had been found to be shaking in a separating funnel.

The problems encountered with this preparation method were:

(1) Occasionally aqueous phase hydrolysis occurred during exchange extraction, despite vigorous agitation. The ferric hydroxide which formed hindered or prevented separation of the two phases, and decreased the final concentration of iron in the organic solution.

(2) Although the procedure of washing the organic solution 3 times with dilute HCl, pH 2.5, had been adopted, analysis indicated the presence of residual calcium in the organic solution. Clearly this would be unacceptable in a study of the stripping of mixed Versatic solutions.

(3) The 3 contacts with HCl left chloride ions in the organic phase. As a stainless steel autoclave was to be used in Part II, it was imperative that all traces of chloride were removed.

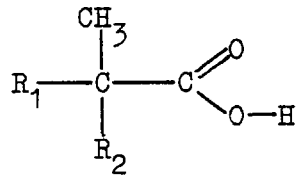
(4) There was evidence that recycled Versatic solutions had a slightly lower loading capacity than fresh material.

The first three of these problems were investigated before the main screening tests were made.

3.2 MATERIALS USED

Organic Solutions

Versatic 10, a synthetic tertiary aliphatic monocarboxylic acid manufactured by Shell was used as the extractant. This has the structure



R_1 and R_2 with 3-4 C atoms

The material contains 97.5% C_{10} acid, and has an average molecular weight of 174.3, and specific gravity 0.915[12]. The Versatic 10 was used as received, without further purification, as a 33% v/v solution in Escaid 110, a commercial blend of aliphatic hydrocarbons manufactured by Esso.

The reagents used in the preparation of metal Versatic solutions are shown in Table 3.2.1, while Tables 3.2.2 and 3.2.3 show the reagents used for the analysis of these solutions. Miscellaneous reagents used are given in Table 3.2.4.

3.3 EXCHANGE EXTRACTION OF IRON

3.3.1 Factorial Design

Because precipitation of iron hydroxide sometimes spoilt the exchange extraction of iron for no apparent reason, a 2^5 factorial design was used to try to identify the variables which cause this behaviour. Unlike most factorial designs, only a qualitative result was recorded for each trial. If extraction was clean, the trial was regarded as successful, and denoted numerically by a '1'; if hydroxides precipitated during extraction, the trial was regarded as unsuccessful, and denoted by '0'.

Five independent variables; temperature, pH, concentration

Table 3.2.1 Reagents Used in the Preparation of Metal-Versatic Solutions

Reagent	Grade	Quality	Supplier
MgO	GPR	light	H & W
CaO	laboratory reagent		H & W
$SrCl_2 6H_2O$	GPR	Assay 98-101%	BDH
$Al(NO_3)_3 9H_2O$	Analar		H & W
$Ti(SO_4)_2$ sol	technical	~15% w/v $Ti(SO_4)_2$	BDH
$Cr(OH)_3 + H_2O$	GPR	Min assay as $Cr(OH)_3$ 70%	H & W
$MnSO_4 4H_2O$	Analar	Min assay 98.0%	H & W
$FeCl_3 6H_2O$	GPR	Min assay 96%	H & W
$CoSO_4 7H_2O$	GPR	Min assay 97%	H & W
$NiSO_4 + H_2O$	GPR	Assay as Ni: 20.8-22.4%	H & W
$CuSO_4 5H_2O$	GPR	Assay 98.5-101%	H & W
ZnO	Analar	Min assay 99.7% ZnO	H & W
CdO*	laboratory reagent	Min assay 99.5%	BDH
NaOH	Analar	Min assay 98.0% NaOH	BDH

* + H_2SO_4 to give sulphate

GPR - general purpose reagent

H & W - Hopkin & Williams Ltd

Table 3.2.2 Reagents used in the EDTA Analysis of Metal-Versatic Solutions

Reagent	Grade	Quality	Supplier
EDTA	GPR	Sequestric Acid, Disodium Salt (Diaminoethanetetra-acetic acid, disodium)	H & W
NH_4Cl	GPR	Min assay 99.5%	H & W
NH_3	Analar	Ammonia .88	BDH
$MgSO_4 7H_2O$	Analar	Assay 99.5-103.0%	BDH
Eriochrome Black T		Metal indicator	H & W
Murexide		Metal indicator	H & W
Xylenol Orange		Metal indicator	H & W
Hexamine	GPR	Min assay 99.0% $C_6H_{12}N_4$	H & W
HCl	Analar	sp. gr. 1.18	BDH

Table 3.2.3 Atomic Absorption Standard Solutions

Element	Concentration	Matrix	Supplier
*Co	1000 ppm w/v	0.1N $HClO_4$	H & W
Cu	1000 ppm w/v	0.1N $HClO_4$	H & W
Ca	1000 ppm w/v	1N HCl	BDH
*Fe	1000 ppm w/v	0.1N $HClO_4$	H & W
Mn	1000 ppm w/v	1N HNO_3	BDH
Ni	1000 ppm w/v	1N HNO_3	Fisons
Zn	1000 ppm w/v	0.1N $HClO_4$	H & W
Mg	1000 ppm w/v	1NHNO_3	BDH

* - prepared from H & W Conion concentrated solution

Table 3.2.4 Miscellaneous Reagents Used

Reagent	Grade	Quality	Supplier
H_2SO_4	Analar	S.G. 1.84	BDH
Acetic acid, glacial	Analar	Min assay 99.7%	BDH
Sodium acetate $CH_3COONa\ 3H_2O$,	Analar	Min assay 99.0%	H & W
KH_2PO_4	Analar		H & W
Na_2HPO_4	Analar		H & W
KH phthalate	Analar		BDH
K tetroxalate	Analar		H & W
Hydrogen peroxide, 20 vol	GPR	Min assay 6% w/v	H & W

of calcium in the organic phase, concentration of iron in the aqueous phase, and aqueous:organic volume ratio, were tested at two different levels. A sixth variable was of interest, the overall ratio

$$S = \frac{\text{total no of moles of Ca}}{\text{total no of moles of Fe}}$$

This could not be fixed independently, however, as it is determined by the concentrations of calcium and iron, and the aqueous:organic phase ratio. The levels of these three variables were selected to give four different values of S, which is the minimum possible number. The values were distributed around the stoichiometric value of 1.5, as determined by equation 3.1.2.

The 32 different trials of the design were written in standard order, then randomised by the method recommended by Duckworth[98]. The tests were then performed in this random order, in two blocks which were performed on separate days.

A batch of calcium-loaded Versatic solution was prepared by sieving 100g CaO into 2 litres of 33% Versatic 10 in Escaid 110, preheated to 50°C. The oxide dissolves directly in the organic solution

$$CaO + 2\overline{HV} = \overline{CaV_2} + H_2O \qquad 3.3.1$$

After stirring for 2 hours, the organic solution was filtered under vacuum, using Whatman 540 paper, to remove any undissolved CaO. The solution was then analysed for Ca(II) by EDTA titration, as described in section 3.5.1. This was taken as the upper level of calcium concentration. A stock for the lower level was prepared by dilution with 33% Versatic in Escaid.

The iron solutions were prepared each day by dissolving accurately weighed quantities of $FeCl_3 6H_2O$ in water, in 500ml volumetric flasks. The upper level of pH used was that of the ferric chloride solution. The lower level was achieved by addition of HCl before making the solution up to volume.

The extraction tests were performed by pipetting either

25 mls each, or 30 and 20 mls, of ferric chloride and calcium-Versatic solution into a 100 ml separating funnel. For the higher temperature, the appropriate volume of ferric solution was pipetted into a small beaker, covered, and heated to 60°C, then transferred to the separating funnel. The organic phase was not heated, because there would have been large volume losses on the beaker due to the high viscosity of this phase.

As soon as both phases were contacted, the separating funnel was stoppered and shaken vigorously for 3 minutes. Where loading was successful, the dark brown layer of iron(III) Versatic rapidly separated from the colourless $CaCl_2$ solution. When hydroxide was precipitated there was poor separation of the phases.

The results are discussed fully in section 4.1.1, but in summary they indicated that for successful loading, it is necessary to have the ratio of total calcium to total iron greater than or equal to the stoichiometric level of 1.5.

3.3.2 Staged Washing of Iron-Versatic Solutions

A series of washing tests was performed, to find a suitable method for removing all residual calcium and chloride from iron-Versatic solutions. A solution containing 20.7 g/l Fe^{3+} and 3-4 g/l residual Ca^{2+} was used throughout. 25 ml aliquots were subjected to different washing procedures, consisting of a number of contacts with different reagents and water. Each contact was made by vigorously shaking the organic solution with the appropriate aqueous solution for 2 minutes in a separating funnel. The aqueous phase from the final contact was reserved and tested with 0.1M $AgNO_3$ solution, to detect any residual chloride.

The organic solutions were analysed for iron and calcium, using the atomic absorption spectrophotometry method described in section 3.5.2.

3.3.3 Continuous Washing of Iron-Versatic Solutions

Staged washing did not appear to be satisfactory, so a continuous washing procedure was tested.

Iron-Versatic solution was mixed with an equal volume of distilled water, using a magnetic stirrer. The pH of the mixture was measured with a Russell CTW 72 electrode, connected to a Philips PW 9409 pH meter. The meter was standardised before use against buffers of pH 6.88, 4.00 and 1.68, prepared by the methods given by Vogel[99]. When a steady pH was recorded, about 10 mls of 0.1M HCl were added; the pH fell sharply, then slowly increased as Ca^{2+} was stripped from the organic solution. Acid was gradually added until a steady pH of about 3.2 was recorded. The aqueous solution was then run off, in a separating funnel, and the organic solution was mixed 3 times with distilled water, to remove all chloride.

This washing procedure was used throughout the project.

3.4 PREPARATION OF METAL-VERSATIC SOLUTIONS

The organic solutions prepared are listed in Table 3.4.1, together with the materials from which they were prepared, the extraction method, the colour of the solutions, and any appropriate comments. Three extraction methods were used; these are designated A,B or C in Table 3.4.1 and were as follows

A: 0.25 mole of a salt of the metal were dissolved in about 300 mls of distilled water. 500 mls of 33% v/v Versatic 10 in Escaid 110 were added, and the mixture was stirred with an overhead stirrer motor and glass paddle. The mixture was heated to about 50°C and the pH was measured as in section 3.3.3. Molar NaOH solution was slowly added to the mixture to raise the pH to the level at which extraction occurs, and then to neutralise the acid formed by extraction, as in equation 3.1.1. If any insoluble hydroxides appeared they were allowed to dissolve before adding more base. Copper is extracted at a relatively low pH, so neutralisation was discontinued when it had all been extracted. For the other metals, the pH was not taken above 7, even if extraction was not complete then, to avoid

Table 3.4.1 Preparation of Metal-Versatic Solutions

Metal	Material Used	Extraction Method*	Colour of Solution	Comments
Mg	MgO	B	Colourless	
Ca	CaO	B	Colourless	
Sr	$SrCl_2 6H_2O$	A	Colourless	
Al	$Al(NO_3)_3 9H_2O$	A	Colourless	Gel formed at v.low $[Al]_{org}$. No further extraction
Ti	$Ti(SO_4)_2$ sol.	A	Colourless	V.low $[Ti]_{org}$
Cr	$Cr(OH)_3$ in $HCl+HNO_3$	A	Dark green	V.viscous-probably some $Cr(OH)_3$ in org.
Mn	$MnSO_4 4H_2O$	A	Dark brown	Mn(II) oxidised to Mn(III)during extraction
Fe	$FeCl_3 6H_2O$	C	Dark red-brown	
Co^{2+}	$CoSO_4 7H_2O$	A	Violet-blue	Pink at low loading (octahedral coord) blue at high loading (tetrahedral coord)
Co^{3+}	CoV_2		Dark greenish brown	CoV_2 oxidised with hydrogen peroxide
Ni	$NiSO_4 + H_2O$	A	Green	
Cu	$CuSO_4 5H_2O$	A	Deep blue-green	
Zn	ZnO	B	Colourless	Viscous
Cd	$CdO+H_2SO_4$	A	Colourless	Viscous

* A - neutralisation with NaOH solution

B - dissolution of oxide in Versatic solution

C - exchange extraction

loss of extractant into the raffinate, which results from its increased aqueous solubility at high pH. After extraction the phases were separated. The organic solution was then washed 3 times with distilled water to remove any impurity ions.

B: About 0.5 moles of the oxide of the metal were dissolved in 500 mls of 33% Versatic 10 in Escaid 110, and any residual oxide was filtered out, as for the preparation of calcium-Versatic, described in section 3.3.1. An excess of oxide was used to try and obtain maximum loading

C: Iron-Versatic was prepared by exchange extraction with calcium-Versatic, as described in section 3.3.1, washed continuously with 0.1M HCl, then scrubbed 3 times with distilled water.

After preparation, all of the organic solutions were passed through Whatman 1PS phase separating papers, to remove entrained water, and thus prevent slow hydrolysis of the type described by Mühl et al[27], which can occur on standing.

3.5 CHEMICAL ANALYSIS OF METAL-VERSATIC SOLUTIONS

In this work, no analysis was done in the organic phase. All organic solutions were stripped with 1:1 hydrochloric acid(about 5M) to take the metal ions into an aqueous solution, which was then chemically analysed. It was established that a single contact stripped all metal ions from the organic phase. The procedure generally adopted was to contact 5 or 10 mls of organic solution with an equal volume of acid, both volumes being measured by pipette. This gave an aqueous solution identical in metal concentration to the original organic solution.

3.5.1 EDTA Titrations

Several metals were analysed by complexometric titrations with EDTA (the disodium salt of ethylenediamine-tetra-acetic acid). Vogel gives a comprehensive discussion of this technique, and methods for analysing a large range of ions by this technique[99].

For these analyses, 2 mls of the HCl strip solution were made up to 100 mls, from which three 25 ml aliquots could be taken. These solutions were of the order of 0.01M_{metal} so the EDTA solution used was prepared to this concentration, and standardised against 1000 ppm zinc solution. Except for this detail of concentration, the standard methods given by Vogel were used to analyse the metals listed in Table 3.5.1.

There were some metals for which no suitable EDTA analytical method was available. Atomic absorption spectrophotometry was therefore used for these metals, and for all mixed solutions.

Table 3.5.1 Metals Analysed by EDTA Titrations

Metal	Indicator	Colour Change	Comments
Mg	Eriochrome Black T	Red to pure blue	Good end point
Ca	Eriochrome Black T	Wine red to blue	Substitution titration- actually observing Mg-EDTA
Co	Xylenol Orange	Red to orange yellow	Care needed near end point
Ni	Murexide	Yellow to blue violet	Poor end point
Zn	Eriochrome Black T	Wine red to blue	Good end point
Cd	Xylenol Orange	Red to yellow	Care needed near end point

3.5.2 Atomic Absorption Spectrophotometry

Atomic absorption (A.A.) spectrophotometry was widely used in this work. Aqueous solutions were obtained by stripping organic samples with 1:1 HCl. These were diluted, using a variable diluter (Hook and Tucker Instruments Ltd), to a concentration within the linear range for the element of interest, as given by Perkin-Elmer 'Analytical Methods for Atomic Absorption Spectrophotometry'[100].

Element	Wavelength nm	306 setting	Slit	Upper Limit of Linear Range	Flame Type	Relative Sensitivity
Ca	422.7	VIS 211	4	7 ppm	Reducing	1.0
Co	240.7	UV 241	3	5 ppm	Oxidising(lean blue)	1.0
Cu	324.7	UV 325	4	5 ppm	Oxidising(lean blue)	1.0
Fe	248.3	UV 248	3	5 ppm	Oxidising(lean blue)	1.0
Mg	202.6	UV 202.5	4	12 ppm	Oxidising(lean blue)	24.0
Mn	280.1	UV 280	3	6 ppm	Oxidising(lean blue)	1.9
Ni	352.5	UV 352.5	3	17.5 ppm	Oxidising(lean blue)	3.3
Zn	213.9	UV 214	4	1 ppm	Oxidising(lean blue)	turn burner thro' 90° to reduce relative sensitivity

Table 3.5.2 Standard Conditions Used for Atomic Absorption Spectrophotometry

A Perkin-Elmer double beam spectrophotometer was used. The conditions used for each element are shown in Table 3.5.2. For Mg and Mn the main line had a low limit of linearity, therefore a less sensitive line was selected, so that a realistic working range could be used. The regression programme built into a Commodore PR-100 calculator was used to relate the concentrations of the samples to those of the standards, via the measured absorbances.

Initially it was found that there was a discrepancy between the A.A. and EDTA analyses of calcium samples. This was found to be due to an error in the variable diluter, which was then calibrated by the method given in Appendix A. Good agreement between the two analytical methods was found when the diluter errors were taken into account.

The background acidity of a sample is known to affect the measured absorbance of some elements. To investigate this effect, calcium standards were prepared in water, in 0.1MHCl and in 0.5M HCl; their absorbance was found to increase in the order 0.5M HCl < H_2O < 0.1M HCl. Since the samples were highly acidic, their final acidity, and hence absorbance, would be affected by the dilution required. To minimise this source of error, 0.1M HCl was used throughout the project as the matrix for A.A. standards and samples.

Some metals can interfere with each other, so before measuring the concentrations of metals in mixed solutions, standards were prepared containing the relevant metals at comparable levels, and these were checked against single metal standards, to ensure that there was no interference. In the case of nickel, the main line, as given in the Perkin-Elmer handbook, suffered interference from any iron in solution, so a less sensitive line was used.

3.5.3 Analysis of Strontium-Versatic Solution

Strontium, stripped from the Versatic solution by 1:1 HCl, was analysed by the gravimetric precipitation of strontium sulphate. The method given by Vogel, which uses a ten-fold excess of dilute sulphuric acid, was employed[99].

3.6 SEALED TUBE SCREENING TESTS

3.6.1 Hydrolytic Stripping

The equilibrium studies were made by sealing 8 mls of organic solution with 2 mls of water in 16x150 mm medium walled rimless pyrex tubes, using an oxygen acetylene flame. Single element solutions, and two and three component mixtures were tested.

The concentrations of the metal solutions had been determined. In the two component mixtures the volumes of each were selected to give a stoichiometry of 1:2, which was based on the stoichiometry of spinels. Although some of the metal combinations did not correspond to a known spinel, the 1:2 convention was followed for consistency. The three component systems tested were Mn-Zn-Fe and Ni-Zn-Fe; in both cases the stoichiometry used was 1:1:4, which corresponds to the two commercially useful spinels discussed in section 2.3.3.

The sealed tubes were buried in a sand bath, and placed in an oven maintained at 200°C. A 0-360°C mercury thermometer was placed with its bulb at the centre of the sand bath. The tubes were left in the oven for 3 hours after the thermometer registered a temperature of 190°C, about 6 hours in total. Previous work had indicated that equilibrium is established within 3 hours at this temperature[4].

The sand bath was then removed from the oven, and after cooling, the tubes were removed. Any visible changes which had occurred were noted. The tubes were then broken open, and the contents were filtered through Whatman 542 papers. Any solid material was washed with acetone and reserved. In some cases the organic solution was also kept for analysis.

3.6.2 Identification of Precipitates by X-ray Powder Diffraction

The solid phases precipitated by hydrolytic stripping were identified by X-ray powder diffraction using a Guinier de Wolff camera of the focussing type. Samples were exposed to Co K_α radiation for $2\frac{3}{4}$ hours, with the generator operating at 30 kV, and 20 mA.

The X-ray patterns were measured with a Co K_α ruler, and identified using the JCPDS Powder Diffraction file[101].

3.6.3 Chemical Analysis of Precipitates

Some of the precipitates had very similar X-ray powder diffraction patterns. These were distinguished by chemical analysis.

0.02 g samples of the precipitate were accurately weighed, then dissolved in concentrated hydrochloric acid, and made up to 100 mls in 'A' grade volumetric flasks. These solutions were then diluted as required, and the metals in solution were analysed by atomic absorption spectrophotometry.

CHAPTER 4

RESULTS FOR THE PREPARATION AND ANALYSIS OF METAL-VERSATIC SOLUTIONS

4.1 EXCHANGE EXTRACTION OF IRON

4.1.1 Factorial Design

The five independent factors tested in the factorial design, and their levels, are shown in Table 4.1.1. The dependent variable, S, is defined as

$$S = \frac{\text{total no of moles of Ca}}{\text{total no of moles of Fe}}$$

$$= \frac{[Ca]_{org} \times \text{vol. org}}{[Fe]_{aq} \times \text{vol. aq}}$$

$$= \frac{C}{D.E} \qquad 4.1.1$$

S took four values, 3.38, 2.25, 1.50 and 1.00.

Table 4.1.1 Variables Studied in Factorial Design

Factor	Variable	+	-	Units measured
A	temperature	60	20	^{o}C
B	pH	1.5	1.0	pH units
C	$[Ca]_{org}$	.586	.391	M
D	$[Fe]_{aq}$	.260	.173	M
E	aq:org volume ratio	3:2	1:1	volume ratio

Table 4.1.2 Exchange Extraction of Iron: Factorial Design, Yates' Algorithm and Effects

Exptl Order	Test no	Treatment Code	S	Response	1	2	3	4	5	Divisor	Estimate	Identification
13	1	(1)	2.25	1	2	4	8	14	22	32	0.6875	Average
26	2	a	2.25	1	2	4	6	8	0	16	0	A
19	3	b	2.25	1	2	2	6	0	6	16	0.375	B
12	4	ab	2.25	1	2	4	2	0	0	16	0	AB
30	5	c	3.38	1	0	2	0	2	6	16	0.375	C
6	6	ac	3.38	1	2	4	0	4	0	16	0	AC
16	7	bc	3.38	1	2	0	0	0	-2	16	-0.125	BC
31	8	abc	3.38	1	2	2	0	0	0	16	0	ABC
22	9	d	1.50	0	0	0	0	2	-6	16	-0.375	D
15	10	ad	1.50	0	2	0	2	4	0	16	0	AD
9	11	bd	1.50	1	2	0	2	0	2	16	0.125	BD
28	12	abd	1.50	1	2	0	2	0	0	16	0	ABD
14	13	cd	2.25	1	0	0	0	-2	2	16	0.125	CD
29	14	acd	2.25	1	0	0	0	0	0	16	0	ACD
20	15	bcd	2.25	1	0	0	0	0	2	16	0.125	BCD
7	16	abcd	2.25	1	2	0	0	0	0	16	0	ABCD
23	17	e	1.50	0	0	0	0	-2	-6	16	-0.375	E
5	18	ae	1.50	0	0	0	2	-4	0	16	0	AE
4	19	be	1.50	1	0	2	2	0	2	16	0.125	BE
25	20	abe	1.50	1	0	0	2	0	0	16	0	ABE
17	21	ce	2.25	1	0	2	0	2	2	16	0.125	CE
24	22	ace	2.25	1	0	0	0	0	0	16	0	ACE
2	23	bce	2.25	1	0	0	0	0	2	16	0.125	BCE
3	24	abce	2.25	1	0	2	0	0	0	16	0	ABCE
8	25	de	1.00	0	0	0	0	2	-2	16	-0.125	DE
32	26	ade	1.00	0	0	0	-2	0	0	16	0	ADE
18	27	bde	1.00	0	0	0	-2	0	-2	16	-0.125	BDE
1	28	abde	1.00	0	0	0	2	0	0	16	0	ABDE
27	29	cde	1.50	0	0	0	0	-2	-2	16	-0.125	CDE
10	30	acde	1.50	0	0	0	0	4	0	16	0	ACDE
11	31	bcde	1.50	1	0	0	0	0	6	16	0.375	BCDE
21	32	abcde	1.50	1	0	0	0	0	0	16	0	ABCDE

The results of the factorial design are shown in Table 4.1.2. Successful loading is denoted by a '1' in the response column and unsuccessful loading by a '0'. The value of S is also shown in the table. The response was given a numerical value, so that the effects of the factors and their interactions could be estimated. Yates' algorithm, described by Box, Hunter and Hunter[102] and Davies[103] was used to calculate the effects and interactions. The five columns of Yates' algorithm are shown in Table 4.1.2, with the estimates of the effects, together with the identification of the effect represented by each estimate.

In this case, before considering these estimates, the values of S and the associated responses in Table 4.1.2 should be studied. It is clear that in all cases where S is greater than the stoichiometric level of 1.5, the extraction was successful. In all cases where S was below 1.5, the extraction was unsuccessful. For the treatments where S was at the stoichiometric level of 1.5, loading was successful at the higher pH level, and unsuccessful at the lower level. This indicates that factor B, pH, is significant, and that C,D and E are significant in a complex way.

Table 4.1.2 shows that factor A, temperature, has zero effect, as expected from the above observations, and that all higher order interactions involving A are also zero. B can be seen to have an effect of +0.375; the positive sign is consistent with the observation that for the treatments where S was at stoichiometry, loading was only successful at the upper level of pH. Factors C, D and E all have effects of magnitude 0.375, their sign depending upon how the different levels of the variable affect S, through equation 4.1.1.

The second and third order interactions involving B, C, D and E all take the value ± 0.125, while the fourth order interaction BCDE is 0.375, the same magnitude as the first order effects. Because of the significance of the dependent variable S, these interactions were expected to be large.

When analysing unreplicated factorial designs, it is common practice to assume that higher order interactions are

negligible. This assumption is based on the smoothness and similarity of response functions. The values of the interactions are then used as indicators of the experimental error, so that the significance of the other effects can be evaluated, usually by the t-test[98,102,103]. This procedure would clearly be erroneous in this case, which demonstrates that caution should be exercised when using interactions as estimates of error.

In this design the high order interactions are exaggerated because the response is determined by S, which is a function of C, D and E. The presence of only three numerical values for estimates of the effects, and the regularity of these estimates, suggests that none of the responses noted was erroneous.

This factorial design shows that to achieve successful loading, the absolute concentrations of the aqueous and organic phases are unimportant, as long as the overall stoichiometry is at 1.5 or above. In practice the higher value of aqueous to organic volume ratio was employed, because it reduced the viscosity of the mixture, and hence facilitated vigorous shaking. Since variable B, pH, had a positive effect, the upper value, that of unacidified ferric chloride solution, was used. The observation that between 20° and 60°C, temperature had no effect on loading, indicated that although it was not necessary to heat the solutions before contacting, there would be no detrimental effect on loading if warm, freshly prepared calcium-Versatic was used.

4.1.2 Staged Washing of Iron-Versatic Solutions

The results of the washing tests are presented in Table 4.1.3. Water was ineffective in removing residual calcium from the organic solution. Five contacts with HCl at a pH of 1.5 reduced the calcium in solution to a low level, but also stripped out some of the iron. Although the HCl at a pH of 3 did not strip out significant quantities of iron with 5 contacts, it also left the residual calcium at rather a high level, because there were insufficient hydrogen ions in solution to replace the calcium in the organic phase.

	Washing Procedure						Results		
Test No	Reagent	Initial pH	Temp °C	No of Contacts	then Reagent	No of Contacts	Chloride	$[Fe]_{org}$ g/l	$[Ca]_{org}$ g/l
1	H_2O	5	20	5	—	—	not detected	20.7	0.97
2	H_2O	5	45	5	—	—	not detected	20.7	0.95
3	HCl	3	50	5	H_2O	2	trace	20.1	~0.15
4	HCl	1.5	50	5	H_2O	2	not detected	14.5	0.028
5	H_2SO_4	1.5	50	5	H_2O	3	not detected	16.5 poor phase	0.065 separation
6	sodium Ac/ acetic acid buffer	3.72	20	1	no separation so no further tests				

Table 4.1.3 Results of Staged Washing Tests on Iron-Versatic Solution containing 20.7g/l Fe^{3+} & 3-4g/l Ca^{2+}

The test made with H_2SO_4 at a pH of 1.5 was similar to that with HCl at the same pH, in that iron was stripped from the organic. The residual calcium was higher, however, and the formation of insoluble calcium sulphate slowed down the separation of the two phases.

For this application, the inherent problem with a staged washing procedure is that if the pH of the wash solution is low, it will initially strip some iron from the Versatic solution, but if the pH is higher, a little Ca^{2+} will be removed from the organic on contact, then the pH will rise to a level at which no further extraction occurs.

It was for this reason that a buffer of pH 3.72 was tested, because by maintaining this pH all of the calcium should be removed from the organic phase without stripping the iron. Unfortunately, the buffer stabilised the organic-aqueous emulsion, probably because of an affinity between the acetic acid in the aqueous buffer, and the Versatic 10 in the organic phase. Tanaka and Nūnomi found that in the presence of acetate buffer, copper will incorporate acetate into the species formed during solvent extraction, i.e. $(CuRAc.HR)_2$ [46], and it is possible that iron behaves similarly here. As separation was impossible, this washing test was abandoned.

4.1.3 Continuous Washing of Iron-Versatic

The continuous washing procedure proved to be very much more effective than the staged contacts. Although the system took about 15 minutes to reach a steady pH of about 3.2, the procedure gave consistently low calcium levels, regardless of the initial composition of the iron-Versatic. No iron was stripped from the organic solution, because the pH was never taken below 3.0. Although the staged washing tests indicated that two contacts with distilled water were adequate, three were used to ensure the absence of chloride.

In conclusion, the stagewise washing would only be effective if the concentration of residual calcium was accurately

known. Also, the slow kinetics of removal of calcium, exhibited in the continuous washing tests, indicate that a series of short contacts will not be as effective as a continuous washing operation. Consequently, the continuous procedure was used throughout this work.

4.2 PREPARATION OF METAL-VERSATIC SOLUTIONS

Although the extraction of most metals was straightforward, the unusual behaviour exhibited by a few metals will be discussed.

Aluminium could only be loaded to very low levels, because it formed a gel in the organic phase. This was clearly similar to the macromolecules described by Leger et al[19], although there was no evidence of the physical properties of this gel changing over a 2 year period, which suggests that the Versatic gel does not break up into smaller molecules, with a change in structure, in the way that laurate gels do. Versatic is clearly different from capric acid, which is reported to form hexameric complexes[51]. Once formed, the gel was very stable, chemically as well as physically: attempts to strip out the Al with sulphuric or hydrochloric acid were unsuccessful. This was presumed to be because H^+ ions could not enter the organic phase, while the Al^{3+} ions were locked in the gel, and could not approach an interface at which stripping could occur. As stripping was impossible, the concentration of aluminium in the gel had to be estimated.

An aqueous solution of chromium(III) was prepared by dissolving $Cr(OH)_3$ in a mixture of nitric and hydrochloric acids. Neutralisation caused rapid precipitation of hydroxide, which seemed to be extracted into the organic phase. The organic solution became very viscous, but unlike the aluminium solution, it was not a gel. It was not possible to strip this organic solution with HCl, which indicated that the chromium was present, not as mobile ions, but as some massive species, probably hydroxide solvated by carboxylic acid molecules.

Titanium could only be loaded to a low concentration, because alkali additions caused irreversible precipitation of TiO_2

in the aqueous phase, even in the presence of hydrogen peroxide which had been added to complex the Ti(IV) ions.

Initially an attempt was made to prepare cadmium-Versatic by the method used for zinc-Versatic, that is, from the oxide. CdO proved to be insoluble in the organic solution, so was dissolved in dilute sulphuric acid. The cadmium was then extracted into the Versatic solution by neutralisation with NaOH solution.

When loading manganese, the manganese(II) in the aqueous solution was oxidised on extraction, with a colour change from pale pink to dark brown. The oxidation state in the organic solution is probably +3. Mn(III) forms a basic carboxylate ion, $[Mn_3O(CH_3COO)_6]^+$ with the structure shown in Figure 2.3. It is likely that the Mn(III) ion is coordinated in a similar configuration by Versatic ions, which stabilise Mn(III) relative to Mn(II). The opposite is true in aqueous solution, and stripping of the organic with 1:1 HCl is accompanied by reduction back to Mn(II).

Extraction from cobaltous sulphate solution yielded an organic solution with a pink colour at low concentrations. This gradually became violet-blue as the cobalt concentration increased, indicating that tetrahedrally coordinated Co(II) ions (blue) were predominating over the octahedrally coordinated ions(pink). The Co(II) in the Versatic solution was readily oxidised to Co(III) by hydrogen peroxide, and the resultant solution was quite stable, unlike most aqueous solutions of Co(III). The stabilisation is probably due to Versatic ligands, another example of the complexing ability of the acid.

Treatment of Ni(II) Versatic with hydrogen peroxide gave no colour change, which indicated that Ni(III) is not as readily formed in carboxylate solution as Co(III).

4.3 CHEMICAL ANALYSIS OF METAL-VERSATIC SOLUTIONS

4.3.1 EDTA Titrations

The titrations performed using Eriochrome Black T metal indicator, i.e. magnesium, calcium and zinc, gave very reliable and reproducible results, because the indicator has a sharp, well defined endpoint. The EDTA solution was standardised against zinc standard for this reason. When titrating cobalt and cadmium, using Xylenol Orange as the indicator, the colour change was not instantaneous, and when it did occur, was a gradual change from red to orange-yellow. It was therefore necessary to perform a rough titration, then to stop subsequent titrations two or three mls before this endpoint, and slowly add EDTA solution dropwise, swilling the flask continuously, to ensure even mixing.

For the nickel analysis, where Murexide was used as the indicator, the colour change from yellow to violet was quite distinctive, but slow to develop. Great care therefore had to be taken near the endpoint, to obtain reproducible results.

4.3.2 Atomic Absorption Spectrophotometry

Although atomic absorption spectrophotometry is not usually as accurate as volumetric analysis, the double beam instrument used generally gave an experimental scatter of less than 1%, which was quite acceptable for this application. For mixed solutions, such as those generated by the dissolution of precipitates, A.A. was the only practicable analytical technique. For single solutions A.A. had the advantage of being much faster than volumetric methods.

4.3.3 Concentration of Metal-Versatic Solutions

The results of the analysis of the metal-Versatic solutions are presented in Table 4.3.1. The concentrations of the aluminium, titanium and chromium solutions had to be estimated, as mentioned in section 4.2.

Table 4.3.1 Concentration of Metal in 1.749 M Versatic Acid Solutions

Metal	Concentration (molar)	Theoretical stoichiometric concentration	Method of Analysis
Mg(II)	0.76	0.87	EDTA
Ca(II)	0.70	0.87	EDTA
Sr(II)	0.187	0.87	grav. pptn of $SrSO_4$
Al(III)	(<0.1)	0.58	estimated
Ti(IV)	(v.low)	0.44	estimated
Cr(III)	(<0.25)	0.58	estimated
Mn(III)	0.273	0.58	A.A.
Fe(III)	0.329	0.58	A.A.
Co(II)	0.504	0.87	EDTA
Co(III)	0.252	0.58	EDTA
Ni(II)	0.366	0.87	EDTA
Cu(II)	0.516	0.87	A.A.
Zn(II)	0.945	0.87	EDTA
Cd(II)	0.764	0.87	EDTA

From Table 4.3.1 it can be seen that the highest loadings were achieved with magnesium, calcium, zinc and cadmium. The zinc-Versatic solution, at 0.945M, is above the stoichiometric concentration achievable with a monobasic acid at a concentration of 1.749M. This suggests that some hydroxide ions are associated with the zinc in the organic phase, to satisfy its valency. The magnesium and calcium solutions were not loaded to their maximum capacity, because the high viscosity of the saturated solutions rendered them unfilterable. This viscosity is probably due to polymerisation of partially hydrolysed species. The high loading is in marked contrast to the transition metals, which are well below stoichiometry at maximum loading. This is consistent with the literature, which reports that Fe,Ni,Co and Cu form complexes containing solvating carboxylic acid ligands, as well as carboxylate ions.

CHAPTER 5

RESULTS FROM SEALED TUBE SCREENING TESTS

5.1 IDENTIFICATION OF PRECIPITATES BY X-RAY POWDER DIFFRACTION

The lines of the powder diffraction patterns of the phases precipitated by hydrolytic stripping, were measured with a Co K_α ruler. The intensity of the lines was estimated visually, in relation to the most intense lines. The patterns were then identified with the JCPDS powder diffraction file[101].

Many of the diffraction patterns were faint, showing only the most intense lines of the complete pattern. In some cases there was also pronounced broadening of the lines. This could be due to imperfections in the crystallites, or to their not being well crystalline. However, broadening also occurs when the particle size is below 1000Å, as discussed by Gay[104], and subsequent electron microscopy indicated that the crystallite size of some of the samples was only about 160-200Å.

For some samples, very few diffraction lines could be detected, so only tentative identification was possible. Fortunately, this problem was only encountered when small quantities of precipitate formed, so these mixtures, and their hydrolysis products, are unlikely to be of future commercial importance.

The diffraction patterns for all of the ferrites formed by iron, with other metals, were very similar, as are all of the listed patterns for ferrites. The experimentally determined patterns were therefore compared only with the listed patterns containing the relevant metals. In the case of Mn-Zn-Fe, there was no pattern listed for manganese zinc ferrite, and the pattern was found to correspond more closely to zinc ferrite than to manganese ferrite.

Some of the material precipitated from mixtures containing aluminium gave well defined patterns which could not be identified using the Inorganic powder file. These precipitates could well be organic compounds, since the Al-Versatic solution is a gel,

containing carboxylate bridges which could be sufficiently stable to remain associated with the aluminium during hydrolysis.

The measured diffraction patterns of the samples are given in Appendix B, alongside the JCPDS patterns for the phases identified.

5.2 HYDROLYTIC STRIPPING OF METAL CARBOXYLATES

5.2.1 Solutions Containing a Single Metal

The results from the sealed tube tests on single metal solutions are shown in Table 5.2.1. These results are consistent, where applicable, with the results obtained by Thorsen and Monhemius [4]. Only iron-Versatic gave complete precipitation in 3 hours. Fairly large quantities of solid were precipitated from solutions loaded with copper and nickel, but stripping was obviously not complete, since the organic solutions were still coloured. Although Thorsen and Monhemius obtained rapid, complete precipitation of copper at 200°C, it is now recognised that the rate of precipitation is not reproducible in the absence of seed. It may therefore be assumed that the copper system had not reached equilibrium within 3 hours.

5.2.2 Solutions Containing Two Metals

The results from the sealed tube tests on Versatic solutions of two metals are shown in Table 5.2.2. The compositions of the solutions were such that metals A and B, as denoted in the table, were in the molar ratio 1:2. For titanium and aluminium, which were known to be at very low concentrations, 4 mls of the Ti or Al solution were used with 4 mls of the other metal solution.

The table gives the identity of any solid phase formed, as determined by X-ray powder diffraction. This technique does not detect coprecipitation where one metal ion substitutes for another in a crystal lattice, unless the substitution is accompanied by a pronounced change in the lattice parameters, or the substituting ion

Table 5.2.1 Hydrolytic Stripping of Single Metal Carboxylates*

Metal ion	Extent of Precipitation	Nature of Precipitate	Observations
Mg(II)	incomplete	$Mg(OH)_2$	
Ca(II)	slight	unidentified	
Sr(II)	slight	unidentified	
Al(III)	none	———	
Ti(IV)	slight	unidentified	
Cr(III)	none	———	polymerisation of organic with associated viscosity increase
Mn(III)	incomplete	$\gamma\ Mn_2O_3$	$\overline{Mn}^{3+} \rightarrow \overline{Mn}^{2+}$ CO_2 formed
Fe(III)	complete	$\alpha\ Fe_2O_3$	
Co(II)	none	———	
Co(III)	none	———	$\overline{Co}^{3+} \rightarrow \overline{Co}^{2+}$ CO_2 formed
Ni(II)	incomplete	$Ni(OH)_2$	
Cu(II)	incomplete	$Cu_2O + CuO$	CO_2 formed
Zn(II)	none	———	
Cd(II)	slight	unidentified	

* 8 mls of metal-Versatic solution sealed with 2 mls water. Held at 190° - 200°C for 3 hours

has an atomic scattering factor markedly different from that of the original ion. Neither of these conditions is likely in this study, where most of the metals have similar ionic radii, and are of similar atomic number. This type of coprecipitation was detected either by a change in the colour of the organic solution after stripping, as in the case of nickel and cobalt, or by chemical analysis of the precipitates, as in the case of some mixtures containing iron. Where substitution has occurred, the phase shown in Table 5.2.2 is that with

Table 5.2.2 Hydrolytic Stripping of Mixed Carboxylates: Two Metals*

METAL A \ METAL B	Mg^{2+}	Al^{3+}	Cr^{3+}	$Mn^{3+}\rightarrow Mn^{2+}$	Fe^{3+}	$Co^{3+}\rightarrow Co^{2+}$	Ni^{2+}	Cu^{2+}
Mg^{2+}	$Mg(OH)_2$ ip	? cp	np	slight	γFe_2O_3 +Mg m ip	np	$Ni(OH)_2$ ip	Cu_2O ip
Ca^{2+}	$Mg(OH)_2$ + ? ip	γ AlOOH +? cp	np	$MnCO_3$ + $CaCO_3$ ip	αFe_2O_3 ip	slight	$Ni(OH)_2$ ip	Cu_2O + $CaCO_3$ ip
Sr^{2+}	? ip	γAlOOH ip	np	slight	αFe_2O_3 ip	slight	$Ni(OH)_2$ ip	Cu_2O + $SrCO_3$ cp
Al^{3+}	—	np	—	slight	αFe_2O_3 ip	—	—	—
Ti^{4+}	np	slight	np	np	αFe_2O_3 + α FeOOH cp	np	$Ni(OH)_2$ ip	Cu_2O cp
Cr^{3+}	amorph-ous ppt ip	slight	polymer isation	slight	αFe_2O_3 ip	slight	$Ni(OH)_2$ ip	Cu_2O ip
$Mn^{3+}\downarrow Mn^{2+}$	$MgCO_3$ + $MnCO_3$ ip	γAlOOH+ $MnCO_3$ ip	np	γMn_2O_3 ip	γFe_2O_3 +Mn m ip	slight	$Ni(OH)_2$ ip	Cu_2O + $MnCO_3$ ip
Fe^{3+}	$MgFe_2O_4$ m ip	αFe_2O_3 ip	αFe_2O_3 ip	γFe_2O_3 + Mn m ip	αFe_2O_3 cp	$CoFe_2O_4$ m ip	$NiFe_2O_4$ + Ni m cp	Cu_2O ip
Co^{2+}	organic Co cmpd ip	? ip	np	np	$CoFe_2O_4$ m cp	slight	$Ni(OH)_2$ + Co ip	Cu_2O ip
$Co^{3+}\downarrow Co^{2+}$	slight	? ip	np	np	$CoFe_2O_4$ m cp	np	$Ni(OH)_2$ + Co ip	Cu_2O ip
Ni^{2+}	$Ni(OH)_2$ ip	? cp	amorph-ous ppt ip	ip	$NiFe_2O_4$ m cp	slight	$Ni(OH)_2$ cp	Cu_2O ip
Cu^{2+}	Cu_2O ip	Cu_2O ip	Cu_2O ip	$MnCO_3$ +Cu_2O ip	αFe_2O_3 +Cu_2O cp	Cu_2O ip	$Ni(OH)_2$ +Cu_2O ip	Cu_2O + CuO ip
Zn^{2+}	slight	slight	np	slight	αFe_2O_3 ip	np	$Ni(OH)_2$ ip	Cu_2O ip
Cd^{2+}	slight	γAlOOH +$CdCO_3$ ip	np	$MnCO_3$ +$CdCO_3$ ip	αFe_2O_3 ip	$CdCO_3$ ip	$Ni(OH)_2$ ip	Cu_2O +$CdCO_3$ ip

* 8 mls of organic solution sealed with 2 mls water
Held at 190 -200°C for 3 hours

Metals A and B in stoichiometric ratio 1:2

Key: np - no precipitation
m - magnetic precipitate
slight - slight precipitation
ip - incomplete precipitation
cp - complete precipitation

the X-ray powder diffraction pattern corresponding most closely to that measured for the precipitate.

The table also indicates the extent of precipitation. The term 'no precipitation' is self-explanatory, and 'slight precipitation' indicates that the amount of solid formed was insufficient for X-ray analysis. Where limited precipitation occurred, or only one component of a mixture precipitated, albeit in large quantities, the term 'incomplete precipitation' is applied. 'Complete precipitation' indicates the formation of large amounts of solid, with virtually no metal ions left in the organic solution.

For some mixtures the solids precipitated could not be identified by their X-ray patterns; these are indicated by a question mark.

The results are discussed in detail in section 5.4

5.2.3 Solutions Containing Three Metals

The three component mixtures tested were Ni-Zn-Fe, and Mn-Zn-Fe. These gave light and dark brown, magnetic precipitates respectively. The X-ray powder diffraction pattern of the former corresponded closely to that of nickel zinc ferrite $(Ni,Zn)Fe_2O_4$, whereas that of the latter corresponded to the pattern of zinc ferrite, $ZnFe_2O_4$, with slight additions.

5.3 CHEMICAL ANALYSIS OF SPINEL FERRITES

Because of the similarity of the X-ray patterns of all the ferrites, precipitates showing a ferrite pattern were analysed chemically to identify their composition. Accurately weighed samples of the precipitates were dissolved, and the metal contents were analysed by atomic absorption spectrophotometry. An attempt was made to determine the weight of oxygen in each sample by mass balance, but it soon became evident that the values obtained were far higher than expected. The error in the mass balance is largely due to the presence

of organic material, entrained in, or adsorbed on the precipitated oxides. There was insufficient material to estimate the amount of entrained impurity associated with each sample, so the analysis was limited to determining the bulk ratios of the metals in the precipitates.

The error in the determination of the metal ratios is estimated to be $\pm$ 3%. It should be noted that the main errors were not associated with the analysis of the precipitates, but in preparing the initial organic mixtures, before hydrolytic stripping. The errors included;

(1) The organic solutions were viscous, and wetted glass, causing difficulties in the preparation of mixtures of accurately known composition.

(2) The single metal organic solutions were analysed only once, following preparation. Many such solutions have been observed to age in some way on standing. Sometimes the ageing is restricted to polymerisation, which affects the kinetics of stripping, as was observed for Ni-Versatic at a later stage in this work. Since cobalt and nickel Versatic solutions which had been prepared three years previously gave results similar to those for fresh solutions when tested in the screening experiments, it appears that polymerisation does not affect the position of equilibrium reached in hydrolytic stripping. For other metals, however, the ageing process is associated with slow hydrolysis, and precipitation of gelatinous material from the organic over a period of weeks. This behaviour, exhibited by solutions of iron, calcium and zinc, would lead to a slow decrease in concentration.

5.4 DISCUSSION OF RESULTS

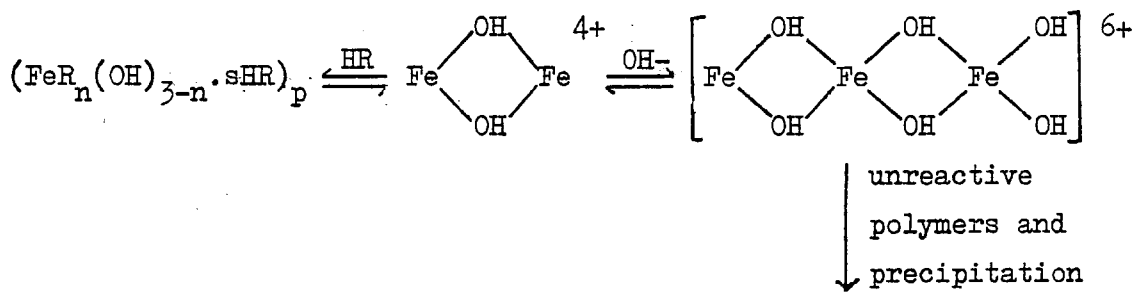
5.4.1 Solutions Containing a Single Metal

At 190°-200°C, iron, nickel and copper Versatic solutions in contact with water were extensively hydrolysed, and precipitated large quantities of αFe_2O_3, $Ni(OH)_2$ and Cu_2O respectively. At room temperature, however, the extraction of iron, nickel and copper ions into a carboxylate solution is more favourable than hydrolysis. Some of the factors which account for this apparent reversal in behaviour

will be considered with reference to iron, since the aqueous phase hydrolysis of this metal has been outlined in section 2.2.

Although iron was loaded by exchange extraction in this work, loading can be achieved by direct neutralisation. In the latter case, though, it is essential that there is vigorous mixing, and that alkali is added very slowly to the aqueous ferric solution, otherwise there is irreversible precipitation of iron hydroxide. This suggests that there is a delicate equilibrium between the ferric anion complexes in the aqueous solution, and either ferric carboxylate complexes in the organic phase, or extensively hydrolysed species in the aqueous phase. Since extraction occurs if neutralisation is very slow, the formation of ferric carboxylate complexes is clearly thermodynamically more favourable, but this process must be a slow one, since hydrolysis is evidently kinetically favourable when the pH is raised rapidly. Extraction probably becomes impossible when the hydrolysis process has proceeded to the formation of the large, unreactive polymers described in section 2.2.2. During the rapid pH changes which lead to accidental precipitation of hydroxide instead of extraction, the polymers are more likely to develop by cross-linking, to give gel colloids[59], than by oxolation to give crystalline oxides or hydroxides[76].

During extraction, some hydrolysis of iron seems to occur before carboxylate complexes are formed, since hydroxyl ions appear to be present in these. Stefanakis, for example, found that the complexes had the composition $(FeR_n(OH)_{3-n}.sHR)_p$, where n=1 to 2[49]. Carboxylate formation must,then, occur instead of further hydrolysis, which is exemplified here by the polymerisation of $Fe(OH)_2^{4+}$ described by Dousma and de Bruyn[76], although slightly different species may be involved, according to conditions. The equilibria can therefore be envisaged as:



Such a situation can be considered to be an extension of the idea of different anions influencing the development of the hydrolysed species. In this case, however, the interaction of carboxylate ions with the ferric complexes takes these into the organic phase, in which further hydrolysis cannot occur at room temperature.

At 190-200°C, however, the activity of water in the organic phase is much higher, because of its increased vapour pressure, and the hydrolysis constant of iron(III) is considerably higher than at room temperature. Hydrolysis therefore proceeds in the organic phase in a manner similar to the way in which it proceeds in an aqueous solution where there are strongly complexing anions, i.e. by progressive displacement of carboxyl ions by hydroxyl ions, polymerisation and oxolation, to give hematite, which is the stable hydrolysis product at this temperature. Thus the hydrolytic stripping of iron is not a reversal of extraction, since it does not return ferric ions to an aqueous solution. Extraction by carboxylic acids and hydrolytic stripping are essentially intermediate stages in hydrolysis, which by virtue of involving a second, immiscible phase, allow better separation from other ions, and closer control over the nature of the product than can be achieved in aqueous phase hydrolysis

The hydrolytic stripping of nickel-Versatic was obviously very similar. Stripping does not go to completion for nickel, however, which is probably due to the fact that the hydrolysis constant for nickel is lower than that for iron.

The stripping of copper(II)- Versatic was accompanied by reduction of the Cu(II) to Cu(I). The reason for this is not clear, but is probably associated with a change in coordination or electronic structure caused by replacing the carboxyl ions and carboxylic acid ligands by hydroxyl ions and water. When the sealed tubes containing copper-Versatic were broken after heating, the internal pressures were well above atmospheric, and carbon dioxide was detected. The reduction of Cu(II) therefore appears to occur in conjunction with oxidation of the carboxylic acid, with CO_2 as one of the oxidation products. As the X-ray powder diffraction patterns in Appendix B show, a significantly higher proportion of CuO was formed in a duplicate run done at 180°C, which suggests that there is less

reduction at the lower temperature.

Only a small quantity of $Mg(OH)_2$ was precipitated. Since the magnesium-Versatic had been prepared by direct dissolution of oxide in the organic solution, precipitation is a reversal of loading for this metal, and could be expected to be limited, resulting only from the difference between the hydrolysis constants for magnesium at 20° and 200°C. As expected, the precipitated $Mg(OH)_2$ was observed to redissolve slowly on standing in the Versatic solution at room temperature.

The other alkaline earth metals, together with zinc and cadmium, gave little or no precipitation. This indicates that hydrolysis is not significant for these metals, even at high temperature, probably because they have the same charge as Mg(II), but larger ionic radii.

Titanium-Versatic only precipitated a small quantity of material because the titanium concentration in the organic solution was very low. The absence of precipitation in the case of aluminium and chromium was probably due to the presence of stable complexes in the organic phase. The marked increase in viscosity of the chromium Versatic was almost certainly caused by polymerisation of the species present.

Although Co(III) and Mn(III) are stable in the Versatic/Escaid solution at room temperature, as previously discussed, both were reduced to the divalent state during hydrolytic stripping. This is not likely to be due to temperature alone. Since the trivalent state is thought to be stabilised largely by carboxylate ions and solvating acid, the displacement of these by hydroxyl ions and water would be expected to result in reduction to the divalent state, which is more stable in aqueous solution. As with the copper solution, carbon dioxide was formed. The solutions were not oxidised on cooling in the tubes, but on exposure to air both reverted to the trivalent state, although Co(II) solutions which had not been previously oxidised were stable in air. The small quantity of γMn_2O_3 precipitated from the manganese-Versatic solution was probably formed before all of the Mn(III) was reduced.

5.4.2 Solutions Containing Two and Three Metals

Mixed metal carboxylate complexes, of a form similar to the Ni:3Fe complex mentioned by Kholkin et al[40], are probably formed when the Versatic solutions of different metals are mixed. Assuming this to be so, the behaviour of mixtures during hydrolytic stripping must be determined by the way in which these complexes behave. If their structure, and the coordination of the ions is such that the polymerisation and oxolation occurring during hydrolysis can form nuclei of a stable mixed oxide, that oxide may well be precipitated. Since the hydrolysis constants of different ions vary widely, however, it is also feasible that one type of ion in the complex is more extensively hydrolysed than the other. If the bonding in the mixed complexes is weak, these complexes are then likely to break up, and a single metal oxide or hydroxide may be precipitated.

Since the mixed oxides have a fairly complex structure, they will not be nucleated unless the polymeric species which develop from the mixed complexes have a fairly long range order. As the order in most single oxides is of a shorter range, the formation of these is presumed to be kinetically favourable, even when a mixed oxide is thermodynamically more stable than a mixture of single oxides.

The only mixed oxides which formed during hydrolytic stripping were magnetic ferrites. In the solutions which precipitated ferrites, the magnetic moments of the ions in the mixed complexes may be oriented in some way, giving the complexes a net magnetic moment which is likely to provide an attractive force between the complexes; when they interact to form polymers their magnetic moments would be oriented in an ordered fashion in the polymers. This would provide a long range order which could not arise from random interactions between complexes. The experimental evidence suggests that the polymers formed in mixtures containing iron have sufficient long range order to nucleate primary solid particles, which may then agglomerate and precipitate in the manner outlined by Dousma and de Bruyn[79]. The nucleation of non-magnetic mixed oxides appears to be kinetically unfavourable under the conditions of hydrolytic stripping, since spinels such as $MgAl_2O_4$, the manganites and cobaltites did not appear from solutions containing the relevant ions.

Although magnetic spinel ferrites were precipitated from some mixtures containing iron, they did not form in the presence of all spinel formers, nor did they always have the composition of the stoichiometric ferrite.

The results of the chemical analyses are shown in Table 5.4.1, which gives the metal ratios in the precipitates and the probable composition of the material. The deviations from stoichiometry could be due to the presence of other phases in the precipitates, but the X-ray patterns showed no evidence of this, even when the deviations were pronounced. For example, the Ni:Fe ratio in the oxide precipitated from the (2Ni + Fe) Versatic solution was 1:0.516, but the X-ray diffraction pattern of this material corresponded closely to that of $NiFe_2O_4$. Moreover, there were no additional lines, although $Ni(OH)_2$ would be expected to show up in a mixture containing only about one percent, having exceedingly intense lines for d spacings of 4.605Å and 2.334Å. As it is unlikely that Ni(II) substitutes for Fe(III) in the spinel, the excess nickel must be present as an amorphous phase, or as ions adsorbed onto the surface of the very fine ferrite particles. Results obtained in Part II of this work support the latter suggestion.

The material precipitated from the (2Co(III) + Fe) mixture contained cobalt in excess of the level in $CoFe_2O_4$. The precipitate could contain Co(III), and have the defect stucture of maghemite, or it could be cobalt(II) ferrite with excess cobalt adsorbed on the surface of the particles.

When the starting composition of the organic solution corresponded, within experimental error, to the stoichiometry of the spinel ferrites, i.e. M(II) + 2Fe(III), only cobalt, nickel and nickel-zinc solutions precipitated ferrites which were of approximately stoichiometric composition.

The magnesium, manganese and manganese-zinc mixtures precipitated ferrites which were markedly deficient in the divalent metal. These precipitates are solid solutions of the stoichiometric ferrite in maghemite, γFe_2O_3. The spinels precipitated from manganese iron mixtures contained very little Mn, even when this was present in

Table 5.4.1 Chemical Analysis of Precipitates from Hydrolytic Stripping

Composition of Organic Solution	X-ray Powder Diffraction Pattern of Precipitate	Metal Ratios in Precipitate	Probable Composition of Precipitates
Mn + 2Fe	γ Fe_2O_3	Mn + 18.0Fe	$Mn_{0.14}Fe_{2.57}O_4$
Mn + 2Fe	γ Fe_2O_3	Mn + 21.5Fe	$Mn_{0.12}Fe_{2.59}O_4$
2Mn + Fe	γ Fe_2O_3	Mn + 13.05Fe	$Mn_{0.19}Fe_{2.54}O_4$
Mg + 2Fe	$MgFe_2O_4$	Mg + 9.93Fe	$Mg_{0.25}Fe_{2.5}O_4$
Co + 2Fe	$CoFe_2O_4$	Co + 2.17Fe	$Co_{0.94}Fe_{2.04}O_4$
Co + 2Fe	$CoFe_2O_4$	Co + 2.19Fe	$Co_{0.93}Fe_{2.04}O_4$
2Co + Fe	$CoFe_2O_4$	Co + 1.67Fe	$CoFe_2O_4$ + ads Co or $Co^{3+}Fe_{1.67}O_4$
Ni + 2Fe	$NiFe_2O_4$	Ni + 2.34Fe	$Ni_{0.89}Fe_{2.08}O_4$
Ni + 2Fe	$NiFe_2O_4$	Ni + 2.28Fe	$Ni_{0.90}Fe_{2.06}O_4$
2Ni + Fe	$NiFe_2O_4$	Ni + 0.516Fe	$NiFe_2O_4$ + ads Ni
Mn+Zn+4Fe	$ZnFe_2O_4$ + addns	Mn+6.25Zn+41Fe	$(Mn_{.06}Zn_{.36})Fe_{2.39}O_4$
Mn+Zn+4Fe	$ZnFe_2O_4$ + addns	Mn+5.96Zn+51Fe	$(Mn_{.05}Zn_{.28})Fe_{2.45}O_4$
Ni+Zn+4Fe	$(Ni,Zn)Fe_2O_4$	Ni+Zn+4.28Fe	$(Ni_{.48}Zn_{.48})Fe_{2.03}O_4$
Ni+Zn+4Fe	$(Ni,Zn)Fe_2O_4$	Ni+.96Zn+4.29Fe	$(Ni_{.48}Zn_{.46})Fe_{2.04}O_4$

excess in solution, and the X-ray patterns were closer to that of maghemite than to that of manganese ferrite. This deviation from stoichiometry could be due to a disruption of the structure of the metal-carboxylate complexes occurring when the carboxylic acid is oxidised during reduction of Mn(III) to Mn(II). The deviation could also be a steric effect: the cation distribution in manganese ferrite is $Mn_{0.8}Fe_{0.2}[Mn_{0.2}Fe_{1.8}]O_4$. If manganese cannot enter the sites which become the tetrahedral A sites in the spinel lattice, because of its coordination in the organic complexes, it will only be present on octahedral B sites, and the cation balance in the spinel will be maintained by additional Fe(III) and holes. The compositions of the ferrites obtained experimentally correspond quite closely to such a situation.

The magnesium deficiency in the magnesium ferrites probably results from the limited hydrolysis of this cation. As with manganese, however, even the small quantity which is present in the precipitate has been effective in altering the development of the polynuclear complexes, so that the cubic spinel lattice formed in preference to the trigonal hematite lattice.

Copper ferrite was not precipitated from mixtures containing copper and iron, although it does exist. This was probably because after reduction to Cu(I), the copper could not enter positions in the lattice suitable for divalent ions.

Zinc and cadmium were also ineffective in forming their ferrites, although the magnetic nickel-zinc and manganese-zinc ferrites were formed. This suggests that the single ferrites did not appear because they are not magnetic, which supports the earlier suggestion that magnetic interactions have an important role in the nucleation of mixed oxides. Other possible reasons for the absence of zinc and cadmium ferrites are that these metals are only slightly hydrolysed, or that there was a steric resistance to Zn and Cd entering tetrahedral sites; however, these explanations cannot account for the formation of mixed ferrites containing zinc.

Some mention should be made of the mixed carboxylates which did not contain iron. Copper(I) oxide was always precipitated

from mixtures containing copper. Mixed oxides would be particularly unlikely in copper systems, because when the Cu(II) was reduced to Cu(I), oxidation of closely associated carboxylic acid would break up the structure of the mixed carboxylate complexes, releasing separate metal ions, hydrolysed to different extents according to their chemical nature. Although not extensively hydrolysed, Ca, Sr, Cd and Mn(II) precipitated as carbonates from copper mixtures, because of the high carbon dioxide partial pressure.

Nickel hydroxide was formed by all mixtures in which nickel was in excess, except in the case of the (2Ni +Fe) mixture. It was not always precipitated when nickel was the minority cation, which indicates that the hydroxide will only nucleate when nickel is above a certain concentration. When mixed with nickel, copper precipitated as copper oxide, but cobalt precipitated by substitution in the $Ni(OH)_2$.

Although Al-Versatic precipitated no material when hydrolytically stripped alone, mixtures with Ca, Sr, Mn and Cd precipitated γ AlOOH, and mixtures with Co(II), Co(III) and Ni precipitated material which could not be identified, but was presumed to be organic. The reason for these observations could be that the gel structure of the aluminium Versatic prevents water from approaching Al to hydrolyse it, whereas in mixtures the gel breaks down to some extent, and Al may be hydrolysed.

Magnesium-calcium Versatic precipitated magnesium hydroxide, while magnesium-manganese mixtures gave the carbonates of both metals.

Some carbonates were precipitated from mixtures containing manganese or Co(III), because of the carbon dioxide formed by oxidation of the Versatic. Otherwise these metals had no significant effect.

Cr, Ti and Zn Versatic in binary mixtures had no significant effect. In the case of Cr and Ti, this was probably because of the low concentrations of free ions in their organic solutions.

The sealed tube tests established that spinel ferrites were the only mixed oxides precipitated by the metals tested during hydrolytic stripping. The iron-nickel system was selected for further study, to investigate the factors which affect the precipitation of nickel ferrite. Of the ferrites which had formed, nickel ferrite was of most interest because the stoichiometric ferrite had been precipitated, and being magnetically soft, this was representative of the soft ferrites which are commercially important.

PART II

THE HYDROLYTIC STRIPPING OF IRON-NICKEL CARBOXYLATE SOLUTIONS

CHAPTER 6

EXPERIMENTAL PROCEDURE

6.1 INTRODUCTION

The sealed tube screening tests made in Part I had shown that hydrolytic stripping of a 33% solution of Versatic 10 in Escaid 110, loaded with iron and nickel, caused precipitation of nickel ferrite, $NiFe_2O_4$, within a period of 3 hours at 190-200°C.

The purpose of the second part of the project was to study the kinetics of this reaction, with a view to understanding the precipitation process. An initial study was made, using sealed tube tests in two highly fractionated experimental designs, to assess the importance of a number of experimental variables. Kinetic tests were then done to determine the effect of the significant variables on the rate of hydrolytic stripping.

Some organic samples from the kinetic runs were examined by high temperature infared spectrophotometry, to determine the concentrations of free carboxylic acid, and to obtain information about the type of ligand bonding in the metal-Versatic species. Some organic solutions were also examined by thin layer chromatography. Surface area analysis and electron microscopy were used to study some of the nickel ferrite precipitates. The infared, surface area and electron microscopy techniques are outlined in later chapters.

6.2 SCREENING TESTS

As in Part I, pyrex tubes were filled with organic solutions and water, then sealed. The composition of the organic solution used for each run was determined by the design matrices. Tubes which accommodate 20 mls of organic solution were used for these tests, to ensure that there would be sufficient precipitate formed for chemical analysis.

The sealed tubes were heated to the required temperature in a water filled 3.5 l autoclave, which was held at temperature for the required time, then cooled. An autoclave was used instead of a heated sand bath, as in Part I, because it afforded closer control over the temperature. After cooling, the tubes were broken and their contents were filtered. The precipitates and organic solutions were analysed for Fe and Ni by the A.A. method described in sections 3.5 and 3.6.

6.3 KINETIC STUDIES: APPARATUS AND MATERIALS

A 300 ml capacity stainless steel autoclave was used for the kinetic studies. This was mounted in a rig which incorporated most of the ancillary equipment for measurement and control of the experimental conditions, and for sampling of the autoclave contents. Figures 6.1 and 6.2 show the apparatus; the details of the ancillary equipment are given in the keys to these figures. A special feature of the autoclave was the heated and pressurised reservoir. This is necessary for accurate kinetic measurements, because it allows the reagents to be heated separately, then mixed at the beginning of a kinetic experiment. For these studies, the water was heated in the reservoir, then injected into the autoclave containing the organic solution.

The materials used for the preparation of the iron and nickel Versatic solutions were the same as those used in Part I. Several types of solid material were tested in preliminary runs as seeds for the precipitation of nickel ferrite. These are listed in Table 6.3.1.

KEY TO FIGURE 6.1

1. Chart recorder (autoclave thermocouple)
2. Nitrogen cylinder
3. Nitrogen pressure regulator
4. Line pressure gauge
5. Line vent valve
6. Autoclave vent valve
7. Autoclave gas inlet valve
8. Reservoir gas inlet valve
9. Autoclave pressure gauge
10. Water injection valve
11. Sampling valve
12. Autoclave water injection/sampling valve
13. Sample tube
14. Eurotherm temperature register/controller
15. Vacuum line
16. Ammeter (for autoclave heater)
17. Main electrical switch
18. Vacuum pump switch
19. Stirrer speed control
20. Reservoir heater switch
21. Vacuum pump
22. Potentiometer (for reservoir thermocouple)

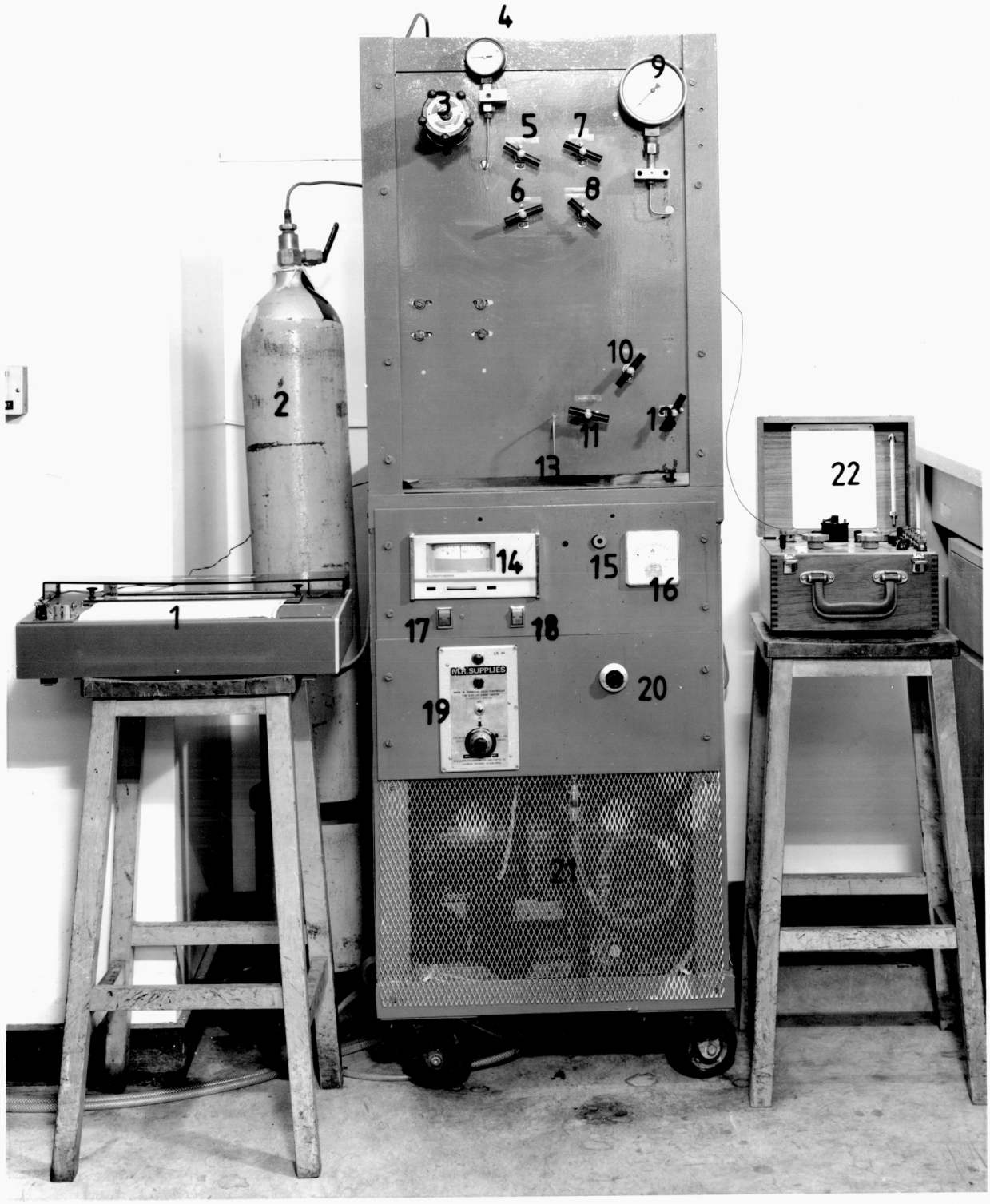


Figure 6.1 Front View of Experimental Apparatus

KEY TO FIGURE 6.2

23. Reservoir thermocouple well
24. Heated reservoir
25. Nitrogen inlet
26. Stirrer
27. Stirrer motor
28. Stirrer belt
29. Trap for vented liquid
30. Sample cooler
31. Tubes for cooling water
32. Sample filter
33. Thermocouple connector

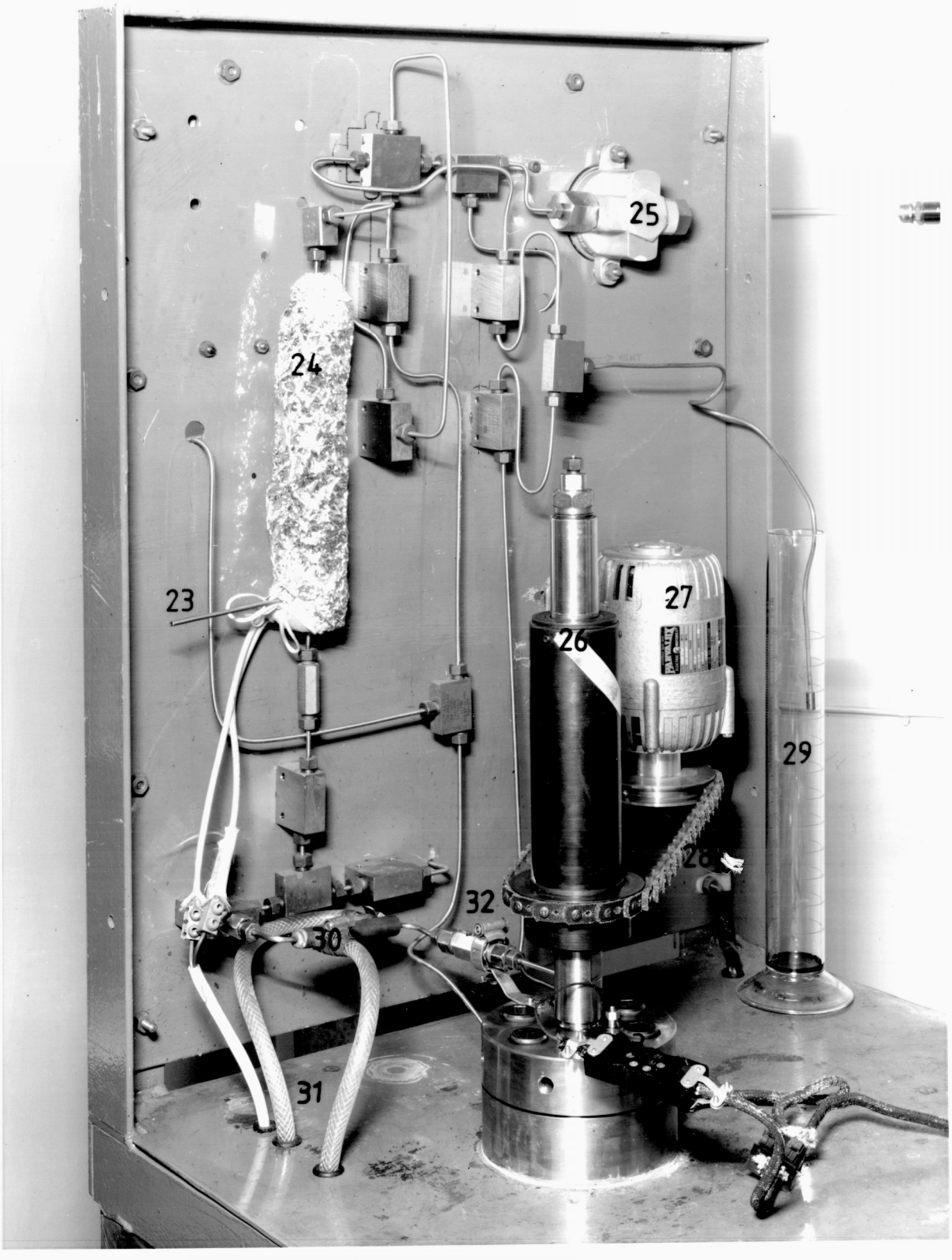


Figure 6.2 Rear View of Experimental Apparatus

Table 6.3.1. Materials Tested as Seeds for Precipitation of Nickel Ferrite

Material	Supplier and Quality, or Preparation Method
Al_2O_3	BDH : for chromatographic adsorption analysis, Brockmann activity II
SiO_2	Crystalline
α Fe_2O_3	BDH : Precipitated ferric oxide, 85% hematite.
Fe_3O_4	H & W : Magnetic iron oxide
Activated carbon	Irish Ceca Ltd : 'Acticarbone AHC'
Colloidal graphite	'Oildag' : Graphite in oil
$Ni(OH)_2$	Precipitated from nickel sulphate soln by NaOH soln
$NiFe_2O_4$	Precipitated from nickel-iron Versatic by hydrolytic stripping
$NiFe_2O_4$(I)	Mixture of Fe_2O_3 & $NiCO_3$, sintered at 1050°C, 72 hours
$NiFe_2O_4$(II)	Mixture of $Fe_2(CO_3)_3$, coprecipitated. Sintered at 1050°C, 72 hours

Nickel ferrite, precipitated by hydrolytic stripping, was selected to seed the main kinetic runs. About 300 g of ferrite were prepared by stripping a total of 12 l of nickel-iron Versatic at 200°C for 2.5 hours. The precipitate was filtered, dispersed in acetone, filtered again and dried. Traces of residual Versatic solution caused the nickel ferrite to form a hard filter cake. This was ground and sized. The size analysis is presented in Table 6.3.2.

Table 6.3.2 Size Analysis of Nickel Ferrite Used to Seed Main Kinetic Runs

Size Range, μm	Wt of $NiFe_2O_4$(g)	Percentage
+125	11.7476	4.04
-125 + 90	219.3788	75.39
- 90 + 63	44.4724	15.28
- 63 + 53	14.5671	5.00
- 53	0.8351	0.29
	291.001 g	100.00

6.4 KINETIC STUDIES: ROUTINE PROCEDURE

As discussed in section 8.5, preliminary kinetic runs indicated that the age of the iron and nickel Versatic solutions, and of the calcium Versatic solution used to prepare the iron Versatic, all had a significant effect on the initial rate of hydrolytic stripping. To ensure reproducibility, therefore, all organic solutions were prepared on the day that the kinetic run was made. Some modification of the preparation procedures described in Part I was needed, to reduce the total time of each run to a practicable level. Each kinetic run comprised three sections:

(1) Preparation of iron and nickel Versatic solutions, analysis, and preparation of mixed organic solution of the required composition.
(2) Charging the autoclave, heating, and hydrolytic stripping, taking samples to follow the reaction rate.
(3) Analysis of the samples.

6.4.1 Preparation of Versatic Solutions

Stock solutions of 25%, 33%, 45% and 50% v/v Versatic 10 in Escaid 110 were prepared, and stored for use. The volumes of iron-Versatic and nickel-Versatic prepared for each run were determined by the final organic solution concentration required; for example, for a final mixed solution concentration of 0.2M Fe and 0.1M Ni, 160 mls of approximately 0.32M iron-Versatic and 90 mls of 0.32M nickel-Versatic were prepared.

Calcium-Versatic : The required volume of Versatic/Escaid solution was heated to 50°C. While stirring continuously, calcium oxide, in the proportion 50 g CaO/litre Versatic solution, was gradually sieved into the organic solution in approximately 0.5g portions, taking care to ensure that each portion was well dispersed before adding the next. The calcium oxide dissolved rapidly when added in this manner, whereas if it was added rapidly, it agglomerated into lumps which only dissolved after two or three hours. After stirring for a further 15 mins. after the final addition of oxide, the calcium-Versatic solution was filtered under vacuum through Whatman 541 paper.

Iron-Versatic : Ferric chloride, in the proportion 92 g $FeCl_3 6H_2O$/litre calcium-Versatic solution, was dissolved in a volume of water equal to, or slightly in excess of the volume of calcium-Versatic. The ferric solution was placed in a 500 ml separating funnel with the filtered calcium-Versatic solution, then the stoppered funnel was shaken vigorously for two minutes, during which time dark brown iron-Versatic formed by exchange extraction with the calcium-Versatic. The organic phase separated rapidly from the clear, colourless raffinate, which was removed. The iron-Versatic was then transferred to a 1000 ml beaker containing 100 mls of water. The phases were mixed with a magnetic stirrer, then 0.1M HCl was slowly added, to scrub out all residual calcium, while the pH was continually measured. The pH was never allowed to fall below 3.0. When a steady pH of 3.2 was reached, the phases were separated. The iron-Versatic solution was washed three times with distilled water, then was filtered through glass fibre papers. The organic solution was then passed through phase separating paper. Filtration through glass fibre paper was necessary to break up any crud, since this tended to block the phase separating paper and hinder the flow of iron-Versatic through the paper.

Nickel-Versatic : Nickel sulphate, in the proportion 90 g $NiSO_4 6H_2O$/ litre Versatic solution, was dissolved in water in a 1000 ml beaker, then Versatic solution was added. 1M NaOH solution was slowly mixed in, and the pH was continually measured. When a steady pH of 7 was reached, after 20-30 minutes, the mixture was transferred to a separating funnel, and the raffinate was removed. The green nickel-Versatic solution was washed three times with water, then passed through phase separating paper.

Samples of the iron and nickel Versatic solutions were analysed by stripping with 1:1 HCl, then analysing the metal chloride solutions by A.A. as described in section 3.5.2. An Oxford Macro Set transfer pipette (5 ml max) was used to measure both the organic solutions and the stripping acid. This instrument considerably reduced the error which had been associated with measuring the organic solution volumes, when a conventional glass pipette was used. In the automatic pipette, volumes are delivered by difference, so are not affected by the viscosity and surface tension of the fluid. Each solution was analysed in duplicate; the two results generally differed by about 1%.

When the concentrations of the iron and nickel Versatic solutions were known, 200 mls of mixed solution of the required composition were prepared, using the iron and nickel solutions, and stock Versatic solution of the appropriate concentration.

In previous work, iron-Versatic solutions were analysed by U.V. spectrophotometry[15]. This was more suitable as an analytical method than A.A., because it could be done directly on the organic phase, and required less dilute samples. The nickel-Versatic U.V. absorption spectrum was measured, to find whether a U.V. technique would be suitable for this work. The nickel-Versatic showed an absorption peak at 405 nm, which was the wavelength of an absorption shoulder of the iron-Versatic spectrum. Thus, although U.V. analysis could be used for iron and nickel solutions separately, it could not be used for mixtures, as the two metals could not be distinguished. For consistency, A.A. was selected for analysing both the single metal solutions and mixtures.

6.4.2 Hydrolytic Stripping Runs

Care was taken to ensure that the autoclave was clean and completely dry before each run. The autoclave was charged with the mixed Versatic solution, and any seed material to be used. All valves were closed, and the autoclave lid was fastened down. The autoclave was then flushed with nitrogen. The required amount of water was injected into the reservoir, then the stirrer motor was switched on. The autoclave and reservoir were heated to the required temperature. The autoclave thermocouple was connected to a chart recorder, and to a Eurotherm temperature register-controller. The reservoir thermocouple was connected to a potentiometer, and the heater was controlled manually.

When the autoclave and reservoir had reached the required temperature, a 3 ml sample was withdrawn from the autoclave. The water in the reservoir was then injected into the autoclave, and a stop-clock was started to time the run. The autoclave temperature was found to fall by $5^{\circ}C$ when the water was injected, but recovered within $1\frac{1}{2}$ minutes. After this, the recorded temperature fluctuated by no more than $\pm$ $0.5^{\circ}C$ from the required value.

Samples were withdrawn from the autoclave at appropriate intervals throughout the run, flushing back the sample line with nitrogen between samples. The samples were centrifuged to separate the organic solution from water and any precipitated nickel ferrite. 10 - 12 samples were generally taken during the course of a run.

After the last sample had been withdrawn, the autoclave heater, stirrer motor and chart recorder were switched off. When the autoclave had cooled to room temperature, the autoclave and gas lines were vented, then the autoclave was opened. The contents were emptied, using a vacuum pump, and the autoclave and sample lines were thoroughly cleaned with acetone. If the next run was to be unseeded, the autoclave was then cleaned with 20 g/l oxalic acid solution at $90^{\circ}C$ for 1 hour, to dissolve any nickel ferrite plated on the impeller, baffle or walls of the vessel. All parts were then rinsed with water, and carefully dried.

6.4.3 Analysis of Samples

Using the automatic pipette, 2 mls of organic solution were withdrawn from each sample after centrifuging, and contacted with 2 mls of 1:1 HCl to strip out all metal ions. The aqueous solutions were then diluted and analysed by A.A. spectrophotometry.

Portions of the t=0 organic samples were reserved for infrared spectrophotometry, which was done to measure the concentration of free Versatic acid. Samples of precipitate were reserved for X-ray powder diffraction, if it seemed likely that a phase other than $NiFe_2O_4$ could have formed, and for electron microscopy and surface area analysis.

CHAPTER 7

SCREENING OF VARIABLES

7.1 INTRODUCTION

There were a large number of factors which might have affected the precipitation of nickel ferrite by the hydrolytic stripping of nickel-iron Versatic solutions. Sealed tube screening tests were carried out to assess the importance of some of these factors. Three different responses were measured; the percentage of iron and percentage of nickel precipitated within the test period, and the Fe:Ni ratio in any precipitate. Although sealed tube tests yield less information than kinetic tests which are sampled throughout the test period, any factor which significantly affected the kinetics of precipitation was expected to affect at least one of the three responses. Sealed tube experiments were used because they are quicker and simpler to perform than kinetic experiments.

7.2 PLACKETT-BURMAN DESIGN

The variables temperature, Versatic concentration, iron concentration, iron to nickel ratio, age of iron solution and age of nickel solution were investigated in an eight experiment Plackett-Burman design.

Plackett-Burman designs are highly fractionated factorial designs which allow the main effects of up to n-1 variables to be estimated in n runs. Each variable is studied at two levels, which are coded + and - in the design matrices proposed by Plackett and Burman (105). The designs do not take into account any interaction effects between the variables, and as in all factorial designs, assume that each variable behaves linearly between the high and low levels. To obtain an estimate of the experimental error, one or more of the n-1 variables in the design matrix is assigned to a dummy variable, which does not correspond to a real change in the experimental conditions. The effects of the dummies are then used to assess the significance of the effects of the real variables.

Run No	VARIABLES							RESPONSES		
	A Temp °C	B [V] % v/v	C $[Fe]_{org}$ M	D $[Fe]/[Ni]_{org}$ M ratio	E Age Fe soln	F Dummy	G Age Ni soln	% Fe^{3+} pptd	% Ni^{2+} pptd	Fe/Ni in ppt
1	+ 200	+ 50%	+ 0.12	- 1	+ old	- low	- fresh	73%	30%	1.28
2	+ 200	+ 50%	- 0.06	+ 2	- fresh	- low	+ old	97%	90%	2.36
3	+ 200	- 33%	+ 0.12	- 1	- fresh	+ high	+ old	99%	78%	1.35
4	- 170	+ 50%	- 0.06	- 1	+ old	+ high	+ old	7%	3%	-
5	+ 200	- 33%	- 0.06	+ 2	+ old	+ high	- fresh	88%	71%	2.30
6	- 170	- 33%	+ 0.12	+ 2	+ old	- low	+ old	8%	0.3%	-
7	- 170	+ 50%	+ 0.12	+ 2	- fresh	+ high	- fresh	19%	17%	2.26
8	- 170	- 33%	- 0.06	- 1	- fresh	- low	- fresh	8%	17%	0.29
Effect on % Fe^{3+} pptd	78.75	-1.75	-0.25	6.25	-11.75	6.75	5.75			
t-ratio	11.67	-0.26	-0.04	0.93	-1.74	1.0	0.85			
Significance	S	NS	NS	NS	NS	NS	NS			
Effect on % Ni^{2+} pptd	57.93	-6.58	-13.93	12.58	-24.43	7.93	9.08			
t-ratio	7.31	-0.83	-1.76	1.59	-3.08	1.0	1.15			
Significance	S	NS	NS	NS	NS*	NS	NS			
Effect on Fe/Ni ratio	0.55	0.65	-0.02	1.33	0.23	0.66	0.32			
t-ratio	0.83	0.98	-0.03	2.02	0.35	1.00	0.48			
Significance	NS	NS	NS	NS	NS	NS	NS			

* = significant at 80%

S = significant at 90%

NS = not significant

6.31 double-sided t distribution for $\nu = 1$

Table 7.2.1 Results from Plackett-Burman Design

The levels of the factors are reported in Table 7.2.1, together with the responses - percentage iron precipitated, percentage nickel precipitated and iron to nickel ratio in the precipitate - for each run. The design matrix, also included in the table, was used to calculate the effect of each factor, defined as the difference between the average response for the runs where the factor is set at the high (+) level, and the average response at the low (-) level, i.e.

$$E_i = \frac{R \text{ at}(+)}{\text{no at}(+)} - \frac{R \text{ at}(-)}{\text{no at}(-)}$$

where E_i = effect of factor i and R = response

The effects of the variables on all three responses are given in Table 7.2.1, together with the analysis of effects. The t-ratio for each factor was calculated as the ratio of the effect of the factor to the effect of the dummy. A significance level of 90% was selected here, i.e. an effect was only considered to be significant if the probability of it being unequal to the effect of the dummy was greater than 90%. There was only one degree of freedom in the estimate of error, since the design contained only one dummy. The critical t-value for one degree of freedom and 90% probability was obtained from the double-sided t-distribution tabulated by Davies[103]: $t_{90\%} = 6.31$.

It can be seen from Table 7.2.1 that the t-ratio exceeded 6.31 for the effect of temperature on percentage iron precipitation and percentage nickel precipitation. This factor is therefore significant. All other variables appear to be not significant at the 90% level. This could be because none of these variables are significant, but it is more likely to be due to the inaccuracies of such a highly fractionated design.

In fractionated designs, the main effects of variables are confounded with higher order effects, that is, the column in the design matrix for each factor is identical to the columns for several interactions. The value calculated for the effect of each factor is, therefore, actually the combined effect of the factor and of these interactions. The main effect can therefore not be distinguished from

Table 7.2.2 Confounding within the 8 Experiment Plackett-Burman Design

Main Effect	Confounded Two Factor Interactions
A Temperature	(-BF) + (-CD) + (-EG)
B V	(-AF) + (-CG) + (-DE)
C [Fe]	(-AD) + (-BG) + (-EF)
D [Fe]/[Ni]	(-AC) + (-BE) + (-FG)
E Age Fe soln	(-AG) + (-BD) + (-CF)
F Dummy	(-AB) + (-CE) + (-DG)
G Age Ni soln	(-AE) + (-BC) + (-DF)

the effects of the associated, or confounded interactions. Table 7.2.2 lists the two factor interactions which are confounded with each main effect in the Plackett-Burman design. Each main effect is also confounded with higher degree interactions. The high level of confounding can have two results:

(1) If large interactions are confounded with a rather small main effect, that effect can be erroneously designated as significant.

(2) The effect of the dummy, which is used as an estimate of the experimental error, also includes the effects of those interactions confounded with the dummy. These can lead to a high estimate of error. Effects which are actually significant may appear to be not significant when compared with this large estimate of error. This is almost certainly true for this design. For each response considered in Table 7.2.1 there is at least one factor for which the t-ratio is less than 1, which suggests that the effect of the dummy includes the effects of real interactions in addition to the experimental error.

7.3 RESOLUTION IV FRACTIONATED FACTORIAL DESIGN

In the Plackett-Burman design, each main effect was confouned with three two-factor interactions, as well as with higher interactions. This defines the Plackett-Burman design as having resolution III. Box,

Hunter and Hunter discuss the concept and implications of design resolution in detail[102]; a thorough discussion is beyond the scope of this project. In general, a design of resolution R is one in which no p-factor effect is confounded with any other effect containing less than R-p factors.

Other workers have found Plackett-Burman designs to be rather inconclusive[12,56], so a design of resolution IV was selected for the second set of screening tests. In this, main order effects were confounded only with three-factor interactions, and two-factor interactions were confounded with each other. Although, as demonstrated in section 4.1.1, three-factor interactions may be appreciable, in most smooth response functions they are smaller than two-factor interactions, so the results of a design of resolution IV should be less ambiguous than those of a Plackett-Burman design of resolution III.

The design selected allowed up to 8 variables to be investigated in 16 runs. The variables studied were: the nature of the diluent, aliphatic (Escaid 110) or aromatic (Solvesso), the [Fe]/[Ni] ratio, concentration of Versatic, concentration of iron, volume of water, temperature, time at temperature, and a dummy.

The levels of these variables are shown in Table 7.3.1, together with the design matrix. The three responses used before are reported, and the effect of each factor on each response was calculated using the design matrix, as described for the Plackett-Burman design. The effects were analysed as before, using the effect of the dummy as the estimate of experimental error. The calculated t-ratios were compared with the critical $t_{90\%}$ of 6.31 for one degree of freedom and a double-sided t-distribution. Temperature was the only factor to have a significant effect at 90%, although the iron-nickel ratio had a significant effect on the iron to nickel ratio in the precipitate at the 80% level.

Table 7.3.1 shows that for all three responses in this design, there were factors with effects much lower than the effect of the dummy. To assess the significance of the factors without reference to the dummy, the effects of the confounded 2-factor interactions were

Run No	VARIABLES								RESPONSES		
	A Diluent	B $[Fe]/[Ni]_{org}$ M ratio	C Time hrs	D V % v/v	E Temp °C	F $[Fe]_{org}$ M	G Vol H_2O mls	H Dummy	% Fe^{3+} pptd	% Ni^{2+} pptd	Fe/Ni in ppt
1	- Solvesso	- 1	- 3	+ 50%	+ 170	+ 0.12	- 2	+ high	6.0%	15.1%	0.48
2	+ Escaid	- 1	- 3	- 33%	- 200	+ 0.12	+ 5	+ high	98.7%	77.5%	1.20
3	- Solvesso	+ 2	- 3	- 33%	+ 170	- 0.06	+ 5	+ high	25.3%	25.3%	1.97
4	+ Escaid	+ 2	- 3	+ 50%	- 200	- 0.06	- 2	+ high	97.2%	91.0%	2.00
5	- Solvesso	- 1	+ 6	+ 50%	- 200	- 0.06	+ 5	+ high	98.8%	59.5%	1.43
6	+ Escaid	- 1	+ 6	- 33%	+ 170	- 0.06	- 2	+ high	10.8%	8.0%	0.33
7	- Solvesso	+ 2	+ 6	- 33%	- 200	+ 0.12	- 2	+ high	99.9%	99.0%	1.95
8	+ Escaid	+ 2	+ 6	+ 50%	+ 170	+ 0.12	+ 5	+ high	1.8%	0.0%	0.47
9	+ Escaid	+ 2	+ 6	- 33%	- 200	- 0.06	+ 5	- low	99.9%	96.1%	1.93
10	- Solvesso	+ 2	+ 6	+ 50%	+ 170	- 0.06	- 2	- low	0.0%	0.0%	-
11	+ Escaid	- 1	+ 6	+ 50%	- 200	+ 0.12	- 2	- low	98.8%	65.2%	1.40
12	- Solvesso	- 1	+ 6	- 33%	+ 170	+ 0.12	+ 5	- low	62.4%	51.5%	1.15
13	+ Escaid	+ 2	- 3	- 33%	+ 170	+ 0.12	- 2	- low	69.2%	66.0%	2.21
14	- Solvesso	+ 2	- 3	+ 50%	- 200	+ 0.12	+ 5	- low	99.9%	97.8%	1.90
15	+ Escaid	- 1	- 3	+ 50%	+ 170	- 0.06	+ 5	- low	1.8%	7.3%	0.29
16	- Solvesso	- 1	- 3	- 33%	- 200	- 0.06	- 2	- low	99.2%	72.1%	1.25
Effect on % Fe^{3+} pptd	-1.66	2.09	-3.11	-20.14	-76.89	12.96	0.94	-11.59			
t-ratio	0.14	-0.18	0.27	1.74	6.64	-1.12	-0.08	1.00			
Significance	NS	NS	NS	NS	S	NS	NS				
Effect on % Ni^{2+} pptd	-1.15	14.88	-9.10	-19.95	-60.63	14.11	-0.18	-10.08			
t-ratio	0.11	-1.48	0.90	1.98	6.01	-1.40	0.02	1.00			
Significance	NS	NS	NS	NS	NS*	NS	NS				
Effect on Fe/Ni	-0.22	0.83	-0.18	-0.36	-0.65	-0.03	-0.08	-0.22			
t-ratio	1.00	-3.80	0.82	1.65	2.98	0.14	0.37	1.00			
Significance	NS	NS*	NS	NS	NS	NS	NS				

* = significant at 80%
S = significant at 90%
NS = not significant at 90%

Table 7.3.1 Resolution IV, Fractionated Factorial Design - Responses, Main Effects and Design Matrix

Run No	INTERACTIONS							RESPONSES		
	AB=CG =DH=EF	AC=EH =BG=DF	AD=BH =CF=EG	AE=CH =BF=DG	AF=GH =CD=BE	AG=BC =FH=DE	AH=BD =CE=FG	% Fe pptd	% Ni pptd	Fe/Ni in ppt
1	+	+	-	-	-	+	-	6.0	15.1	0.48
2	-	-	-	-	+	+	+	98.7	77.5	1.20
3	-	+	+	-	+	-	-	25.3	25.3	1.97
4	+	-	+	-	-	-	+	97.2	91.0	2.00
5	+	-	-	+	+	-	-	98.8	59.5	1.43
6	-	+	-	+	-	-	+	10.8	8.0	0.33
7	-	-	+	+	-	+	-	99.9	99.0	1.95
8	+	+	+	+	+	+	+	1.8	0.0	0.47
9	+	+	-	-	-	+	-	99.9	96.1	1.93
10	-	-	-	-	+	+	+	0.0	0.0	-
11	-	+	+	-	+	-	-	98.8	65.2	1.40
12	+	-	+	-	-	-	+	62.4	51.5	1.15
13	+	-	-	+	+	-	-	69.2	66.0	2.21
14	-	+	-	+	-	-	+	99.9	97.8	1.90
15	-	-	+	+	-	+	-	1.8	7.3	0.29
16	+	+	+	+	+	+	+	99.2	72.1	1.25
Effect on %Fe pptd	12.41	-10.79	0.39	-0.86	1.74	-19.39	-3.71			
t-ratio	-1.07	0.93	-0.03	0.07	-0.15	1.67	0.32			
Signif.	NS	NS	NS	NS	NS	NS	NS			
Effect on %Ni pptd	8.90	-9.03	-1.08	-1.50	-12.53	-12.15	-4.45			
t-ratio	-0.88	0.90	0.11	0.15	1.24	1.21	0.44			
Signif.	NS	NS	NS	NS	NS	NS	NS			
Effect on Fe/Ni, ppt	0.07	-0.25	-0.04	-0.22	0.16	-0.47	-0.27			
t-ratio	-0.32	1.14	0.18	1.00	-0.73	2.14	1.23			
Signif.	NS	NS	NS	NS	NS	NS	NS			

NS = not significant at 90%

Table 7.3.2 Resolution IV, Fractionated Factorial Design - Two-Factor Effects

calculated, as shown in Table 7.3.2. A normal probability plot was drawn for the effects and interactions. The use of these plots is described by Box, Hunter and Hunter[102]. The vertical scale of the plots is non-linear, and is selected so that a normal distribution plots as a straight line.

When the experimentally observed effects of a design are plotted in ascending order on a normal probability axis, all effects which are due to experimental error lie on a straight line through the origin, if the experimental errors are independent and normally distributed. Real effects, however, lie off the straight line, and can therefore be distinguished as being significant.

The probability plot of the effect of variables on the percentage of iron precipitated is shown in Figure 7.1. It is clear that the main effects -temperature, concentration of Versatic and concentration of iron - lie well off the line, and are therefore significant. The confounded interactions - AG=BC=FH=DE, AC=EH=BG=DF and AB=CG=DH=EF - also appear to be significant. From the main effects, the interactions in these groups which are most likely to be significant are DE, EH and EF. It is also clear that the dummy is significant, which suggests that the three-factor interactions confounded with the dummy are rather high. This result explains why the t-test indicated that only temperature was significant: a significant effect was being used as the estimate of error.

The normal probability plots of the effects on the responses percentage of nickel precipitated and iron to nickel ratio in the product, were inconclusive, because there was no obvious straight line through the origin. These plots are therefore not shown. Since none of the effects appeared to belong to a single, normally distributed population, few could be singled out as being significant. Temperature had a significant effect on the percentage of nickel precipitated, and the iron to nickel ratio in the organic solution had a significant effect on the iron to nickel ratio in the precipitate.

The nature of the diluent, and the volume of water had no significant effect on any of the responses.

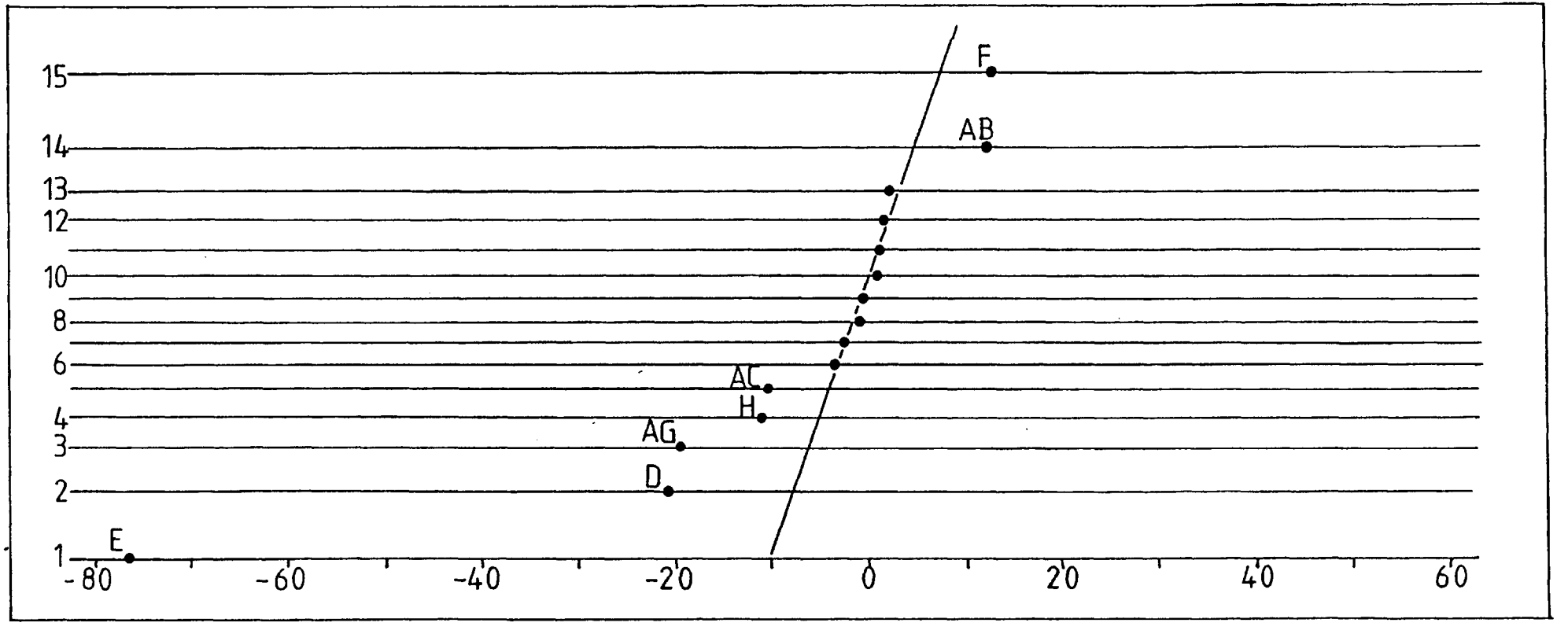


Figure 7.1 Normal Probability Plot of Effects on the Response: Percentage of Iron Precipitated

7.4 SELECTION OF VARIABLES FOR KINETIC STUDIES

The results of the two screening experiments were used to plan the kinetic studies. Temperature, Versatic concentration, iron concentration and iron to nickel ratio were selected for further study. Although the age of the iron-Versatic solution appeared to be significant, this variable was not studied. As the nature of the diluent appeared to be unimportant, Escaid 110 was used in all the kinetic runs. Although the water volume was not significant when in a large excess, the effect of water volume at lower levels was measured in the kinetic runs. It was also necessary to investigate the effect of stirring speed, and of seed material in the kinetic runs. These factors could not have been studied easily in the sealed tube experiments.

CHAPTER 8

KINETIC TESTS

8.1 INTRODUCTION

Most of the variables selected for further study were investigated using a conventional sequential approach, altering one factor at a time, after determining suitable levels at which to hold the other factors, and continually assessing the results when planning further runs. The iron to nickel ratio, and Versatic concentration were studied in a factorial design later in the experimental programme.

Factorial designs were considered to be inappropriate at the beginning of the experimental programme for two reasons:

(1) Several variables required investigation. There was insufficient time to study all of these in a full factorial design, and the two screening tests had demonstrated the uncertainties which can arise when a fractionated factorial design is used.

(2) Very little was known about the system. Had a factorial design been used, the upper and lower levels for each factor would have been selected arbitrarily. This is not good practice, since the region delineated may yield little information.

The data from a 2^n factorial design can be used to formulate an empirical model describing the measured behaviour in terms of the main factors and interactions. However, such a model is only valid for the region studied, and assumes that the effect of each variable is linear within the range selected, so should only be obtained after ascertaining that the variables have a roughly linear effect, and that the region is likely to be of practical interest.

The 'one variable at a time' approach cannot give an empirical model, but the variables can be studied at several levels, which allows a response curve to be drawn for each. These curves can be extrapolated to give some indication of the behaviour outside of the range studied.

8.2 MEASUREMENT OF INITIAL REACTION RATES

Curves of iron concentration against time, and nickel concentration against time were plotted for each run from the analysis of the organic samples. In most runs the initial concentration of iron was double that of nickel, and this concentration ratio was constant throughout the hydrolytic stripping process, indicating that stoichiometric $NiFe_2O_4$ was being precipitated. The iron reaction rate was therefore double the nickel reaction rate, and either could have been used to characterise the response. When the initial iron to nickel ratio was not 2, the behaviour was not as simple, so it was necessary to express the reaction rate in terms of both the iron and nickel rates. This was done by relating the iron and nickel rates to the rate of precipitation of nickel ferrite. X-ray powder diffraction analysis showed that ferrite was the only phase formed. The concentration-time curves showed that the ferrite had the composition $NiFe_2O_4$ when the iron to nickel ratio in the Versatic solution was 2 or less, and a varying composition, intermediate between γFe_2O_3 and $NiFe_2O_4$, when the iron to nickel ratio exceeded 2. The simplified hydrolytic stripping reaction was therefore a combination of equations 8.2.1 and 8.2.2.

$$2\overline{FeV_3} + \overline{NiV_2} + 4H_2O = NiFe_2O_4 + 8\overline{HV} \qquad 8.2.1$$

$$2.67\overline{FeV_3} + 4H_2O = 1.33\gamma Fe_2O_3 + 8\overline{HV} \qquad 8.2.2$$

Each mole of nickel reacts with a mole of water, and is associated with, and equivalent to 1 mole of O^{2-} ions in the precipitated spinel, while each mole of iron is equivalent to 1.5 moles of O^{2-} ions in the spinel. These equivalences were used to calculate the 'oxygen equivalent' of the iron and nickel in each organic sample, defined by:

$$O.E. = [Ni] + 3/2[Fe] \qquad 8.2.3$$

Differentiating, it is clear that the rate of change of the oxygen equivalent is the sum of the rates of reaction of the iron and nickel.

$$\frac{d(O.E.)}{dt} = \frac{d[Ni]}{dt} + \frac{d[Fe]}{dt} \qquad 8.2.4$$

Since the rate of change of the oxygen equivalent of the metal in solution is equal to the rate of precipitation of oxide, this rate is a valid measure of the reaction rate.

The iron and nickel concentration-time data for each run were combined as in equation 8.2.3 to give 'oxygen-equivalent'-time data. A third degree polynomial was fitted to the O.E.-time data, to give an expression of the form:

$$[O.E.]_t = [O.E.]_o - \alpha_1 t + \alpha_2 t^2 - \alpha_3 t^3 \qquad 8.2.5$$

where $[O.E.]_t$ and $[O.E.]_o$ are the O.E. concentrations at t, and t=0 respectively. Differentiating 8.2.5 gives

$$\frac{d[O.E.]}{dt} = -\alpha_1 + 2\alpha_2 t - 3\alpha_3 t^2 \qquad 8.2.6$$

therefore the initial rate of depletion of iron and nickel is $-\alpha_1$. The initial rate of precipitation of ferrite is α_1. This value is used throughout this work to characterise the overall rate.

The Minitab statistical computer package[106] was used to analyse all the experimental data. An example of the output from the polynomial fitting routine for the data from run R52 is shown in Table 8.2.1. The regression equation, in which X1,X2 and X3 correspond to t, t^2 and t^3, is shown, together with the coefficients $[O.E]_o$, α_1, α_2 and α_3 and their standard deviations and t-ratios. The squared correlation coefficient between the data and the fitted curve, R-squared, is also shown. The overall goodness of fit was assessed from these statistical data. For most runs the t-ratio for α_1 was greater than 10, i.e. the coefficient was 10 times greater than the standard deviation associated with it, and the squared correlation coefficient was higher than 99%.

The multiple regression analysis used for polynomial fitting also gave the predicted values, and the residuals, i.e. the difference between the measured and predicted values for each sample. The residuals were plotted against the predicted values, to ensure that they were randomly distributed, and the predicted values were plotted against the measured values; a 45° line indicated a good fit.

Table 8.2.1 Computer Output of Polynomial Fitting Routine

Data stored in columns, ci.
c6 = 0.E. c1 = t c8 = t^2 c9 = t^3
Regression command generates residuals and predicted values, puts these into c11 and c12

```
? regr c6 3 c1,c8,c9,c11,c12

NOTE - THE FOLLOWING VARIABLES ARE HIGHLY
CORRELATED WITH OTHER PREDICTOR VARIABLES
C9

THE REGRESSION EQUATION IS
Y =     .388 - .0112 X1 + .0001 X2
    - .0000 X3

                                        ST. DEV.     T-RATIO =
        COLUMN      COEFFICIENT         OF COEF.     COEF/S.D.
        --           0.388047           0.001784       217.51
X1      C1          -0.0111570          0.0002676      -41.69
X2      C8          0.000126975         0.000009889     12.84
X3      C9         -6.10385E-07         9.547815E-08    -6.39

THE ST. DEV. OF Y ABOUT REGRESSION LINE IS
S = 0.002318
WITH (  10- 4) =    6 DEGREES OF FREEDOM

R-SQUARED =100.0 PERCENT
R-SQUARED =100.0 PERCENT, ADJUSTED FOR D.F.

ANALYSIS OF VARIANCE

 DUE TO      DF          SS          MS=SS/DF
REGRESSION    3     0.1351467       0.0450489
RESIDUAL      6     0.0000322       0.0000054
TOTAL         9     0.1351790

FURTHER ANALYSIS OF VARIANCE
SS EXPLAINED BY EACH VARIABLE WHEN ENTERED IN THE ORDER GIVEN

 DUE TO      DF          SS
REGRESSION    3     0.1351467
C1            1     0.1270966
C8            1     0.0078306
C9            1     0.0002196

            X1           Y      PRED. Y     ST.DEV.
ROW         C1          C6       VALUE      PRED. Y    RESIDUAL     ST.RES.
 10       70.0    0.019927    0.019875    0.002295    0.000052       0.16 X

X DENOTES AN OBS. WHOSE X VALUE GIVES IT LARGE INFLUENCE.

DURBIN-WATSON STATISTIC = 2.41
```

These graphical techniques revealed any points where the fitted curve deviated from the experimental data. Since the initial rate was the parameter required, it was important to check that the fitted curve corresponded closely to the experimental data at the beginning of each run.

For the runs where the iron to nickel ratio was 2, the plots of log concentration against time were roughly linear, indicating first order kinetic behaviour. The gradients of the log plots were not used as a measure of the rate constant, however, because the residuals were usually not randomly distributed, and were rather high at time zero. Furthermore, this relationship did not apply to those runs where the iron to nickel ratio was not 2, and it was necessary to characterise all the runs in the same way, so that valid comparisons of the rate could be made.

Although the coefficients α_3 were very small, generally about 10^{-7}, it was necessary to fit a third degree polynomial to get a satisfactory distribution of residuals for most runs. No further improvement in fit was observed with fourth and fifth degree polynomials.

The data for all the kinetic runs are listed in Appendix C.

8.3 UNSEEDED RUNS

Runs R3, R4 and R13 were unseeded. The runs were made at 170°C, with initial concentrations of 0.2M Fe, 0.1M Ni in 33% Versatic 10 in Escaid 110, using 200 mls of organic solution, 10 mls of water, and stirring at 1000rpm. The iron and nickel concentration curves are shown in Figure 8.1. Note that different scales are used for the iron and nickel concentrations, so that they lie on the same curve when present in the stoichiometric ratio of 2. Runs R3 and R4 were made in an autoclave without a heated reservoir, so the water was heated in contact with the organic solution. Time zero was taken as the time at which the temperature reached 170°C, but samples were withdrawn before this, so that any reaction at lower temperatures could be observed. Run R13 was made in the autoclave with the heated reservoir, where

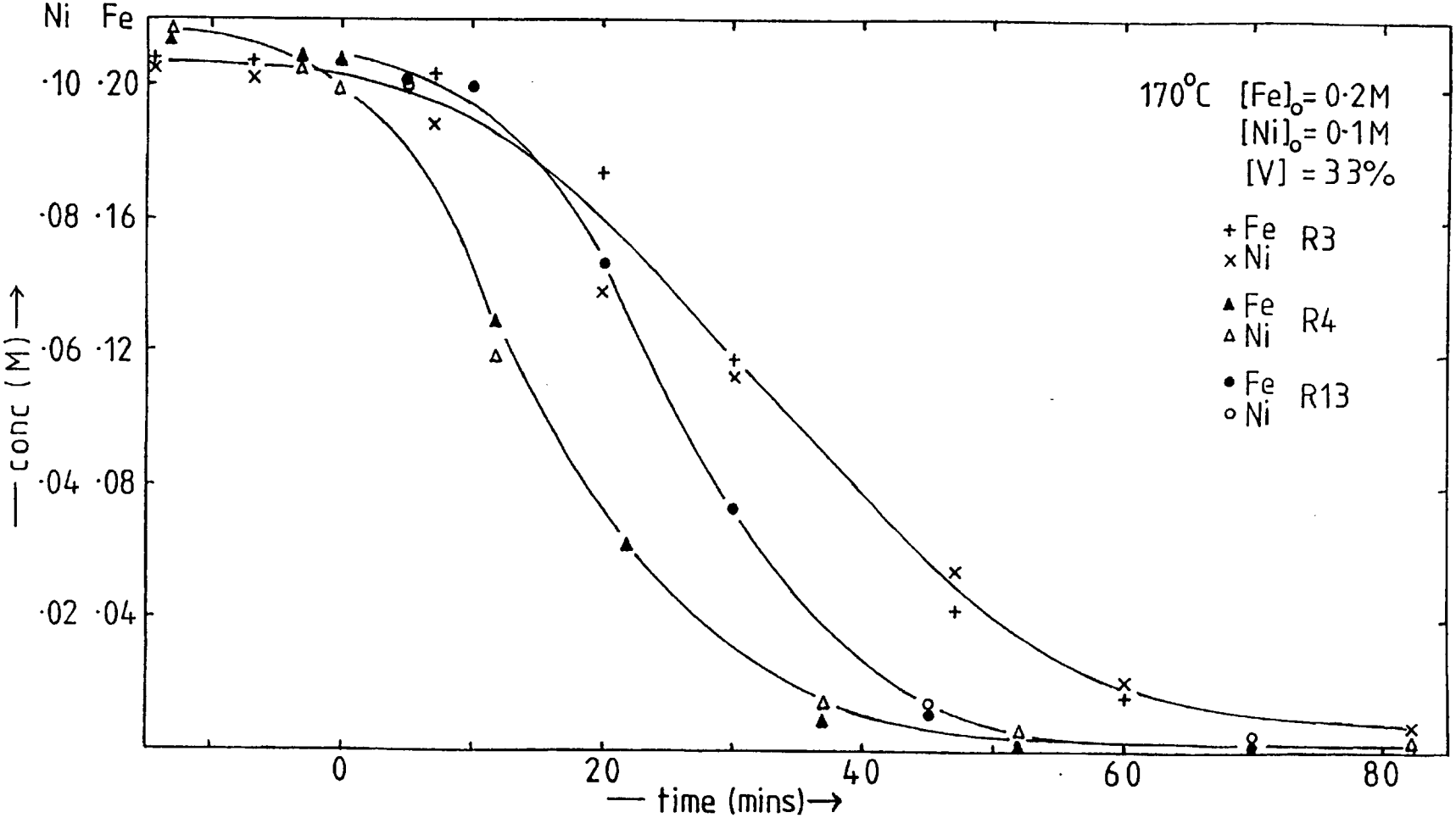


Figure 8.1 Unseeded Runs

Table 8.3.1 Initial Rates of Unseeded Runs

$T = 170^{o}C$ $[Fe]_o = 0.2M$ $[Ni]_o = 0.1M$ $[V] = 33\%$

Run	Initial Rate($M\ min^{-1}$)	t-ratio(rate)	R^2 %
R3	.0037	-3.46	97.8
R4	.0103	-4.91	94.9
R13	.0105	-3.02	96.6

time zero corresponded to the injection of water into the autoclave.

It is evident from Figure 8.1 that there is poor reproducibility in the unseeded runs. The initial rates, as determined by polynomial fitting, are presented above, in Table 8.3.1, together with the t-ratio for the rate, and the squared correlation coefficient for the curve. Both statistical parameters are unacceptably low, because the fitted curves did not show the induction period which was observed in all three runs. The residuals were therefore very large at the beginning of the runs, so the values obtained for the initial rate had little real meaning.

The induction period corresponded in physical terms to the homogeneous nucleation of ferrite particles. The faster rate, observed after nucleation had occurred, corresponded to growth of ferrite nuclei by heterogeneous precipitation. Since this section of the curve appeared to be more reproducible, and would be more amenable to polynomial curve fitting, it was decided to limit the experimental programme to conditions of heterogeneous precipitation.

8.4 EFFECT OF DIFFERENT SEED MATERIALS

To achieve heterogeneous precipitation, a material which acted as a seed for ferrite precipitation would have to be present during hydrolytic stripping. Nickel ferrite was not commercially

Table 8.4.1 Effect of Different Seed Materials on Rates of Precipitation

$T = 170^{\circ}C$ $[Fe]_o = 0.2M$ $[Ni]_o = 0.1M$ $[V] = 33\%$

Run	Seed Material	Qualitative Effect Relative to Unseeded Run, R4
R5	Al_2O_3, 5g	similar to R4
R6	Colloidal graphite in oil, 5 mls	similar to R4
R7	Activated carbon, 3.5g	considerably slower
R8	Hematite, 5g	considerably slower
R9	Nickel hydroxide, 4g	initially similar to R4, then dissolution of $Ni(OH)_2$
R10	$NiFe_2O_4$(pptd), 4.69g	rapid, no induction period
R11	Magnetite, 4.7g	similar to R4
R12	Silica, 5g	very slow, with long induction period
R14	$NiFe_2O_4$(I)sintered, 4g	very slow
R15	$NiFe_2O_4$,sintered & etched in HCl, 4g	slow, but no induction period
R16	$NiFe_2O_4$(II)sintered,4.3g	very slow, with long induction period

available, so a variety of materials which have a high surface area, and are active as seeds for some processes, were tested to find which, if any, would be suitable as seed for nickel ferrite precipitation.

The materials were tested under the same conditions as those used for the unseeded runs, i.e. $170^{\circ}C$, 0.2M Fe, 0.1M Ni and 33% Versatic. Most of the curves showed induction periods, so no attempt was made to measure the initial rate by polynomial fitting. The effects are described qualitatively, in relation to an unseeded run R4, in Table 8.4.1.

The concentration-time curves for runs R7, R12 and R16 are shown in Figure 8.2. These runs were seeded with activated carbon, silica and sintered nickel ferrite respectively. In each case the measured rate was slower than the rate in the unseeded run, R4, which is shown for comparison. The most probable explanation for this is that nickel ferrite could not precipitate heterogeneously on the surface of these materials, but when nuclei of ferrite were formed by homogeneous precipitation, these were adsorbed onto the surface of the 'seed' material, so their growth by heterogeneous precipitation was inhibited.

When alumina, colloidal graphite and magnetite were present, the observed rates were very similar to the rate in unseeded runs. This suggests that although these materials did not initiate heterogeneous precipitation, they did not interfere with the growth of any nuclei which formed.

Figure 8.3 shows the concentration-time curves for runs R8 and R9 which were made with hematite and nickel hydroxide. These were tested because although neither hematite nor nickel hydroxide are homogeneously precipitated from a mixed iron-nickel Versatic solution, it was possible that these phases might form by heterogeneous precipitation. In R8, where hematite was present, the iron in the first sample was 0.177M, which is lower than the starting concentration of 0.2M. This suggests that a little iron precipitated during the heating period, possibly as hematite. At 170°C, however, the iron and nickel curves followed each other, albeit more slowly than in the unseeded runs, suggesting that only $NiFe_2O_4$ was precipitating at this temperature. In R9, where nickel hydroxide was present, the nickel concentration in the first sample was higher than the starting concentration. The iron and nickel concentrations initially fell at a rate similar to that for the unseeded runs. In the later stages, the nickel concentration increased steadily. This behaviour indicates that two processes were occurring; homogeneously nucleated precipitation of nickel ferrite, and steady dissolution of nickel hydroxide.

The fact that hematite and nickel hydroxide were not precipitated, even in the presence of these materials, provides

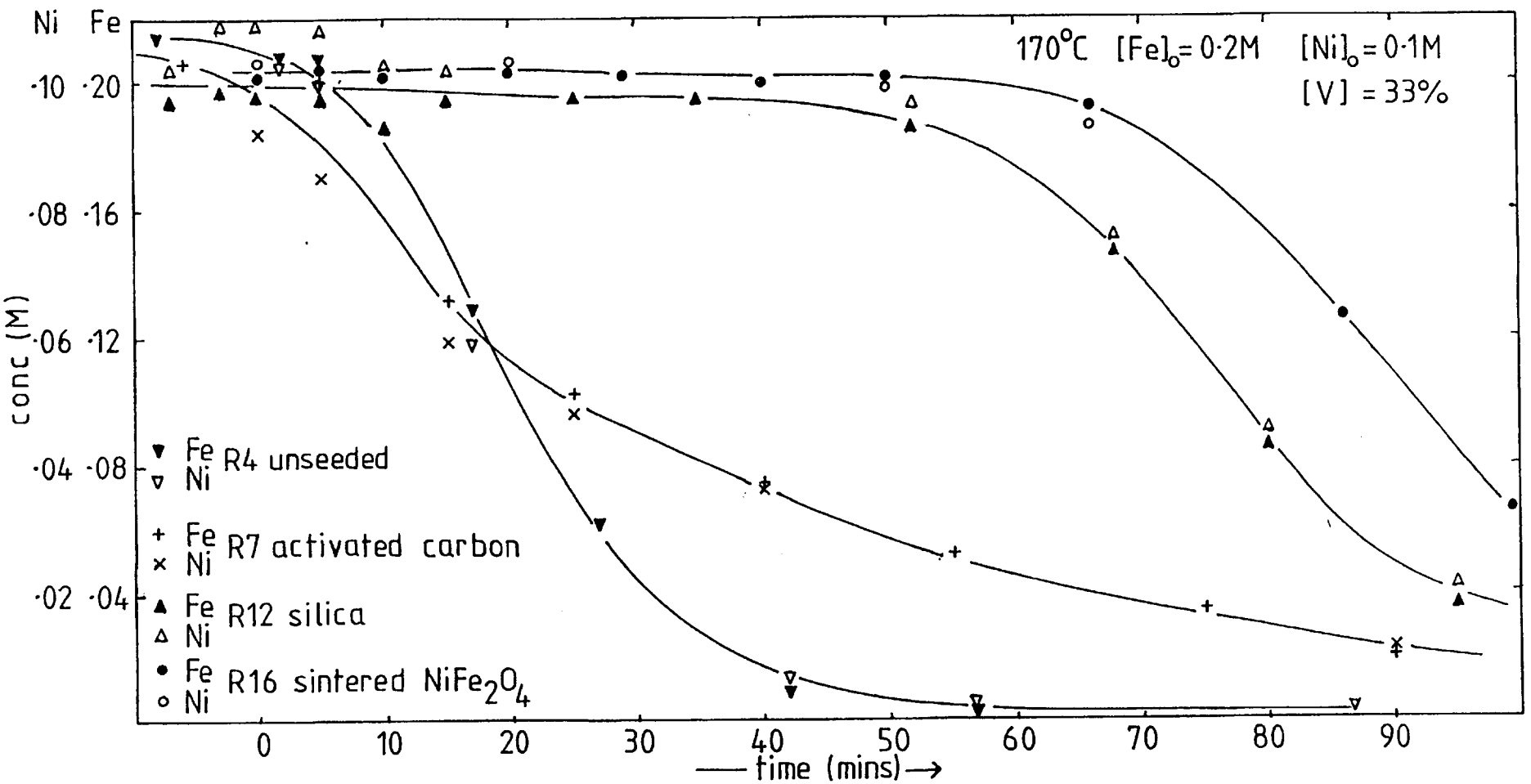


Figure 8.2 Effect of Activated Carbon, Silica and Sintered Nickel Ferrite on Precipitation Rate

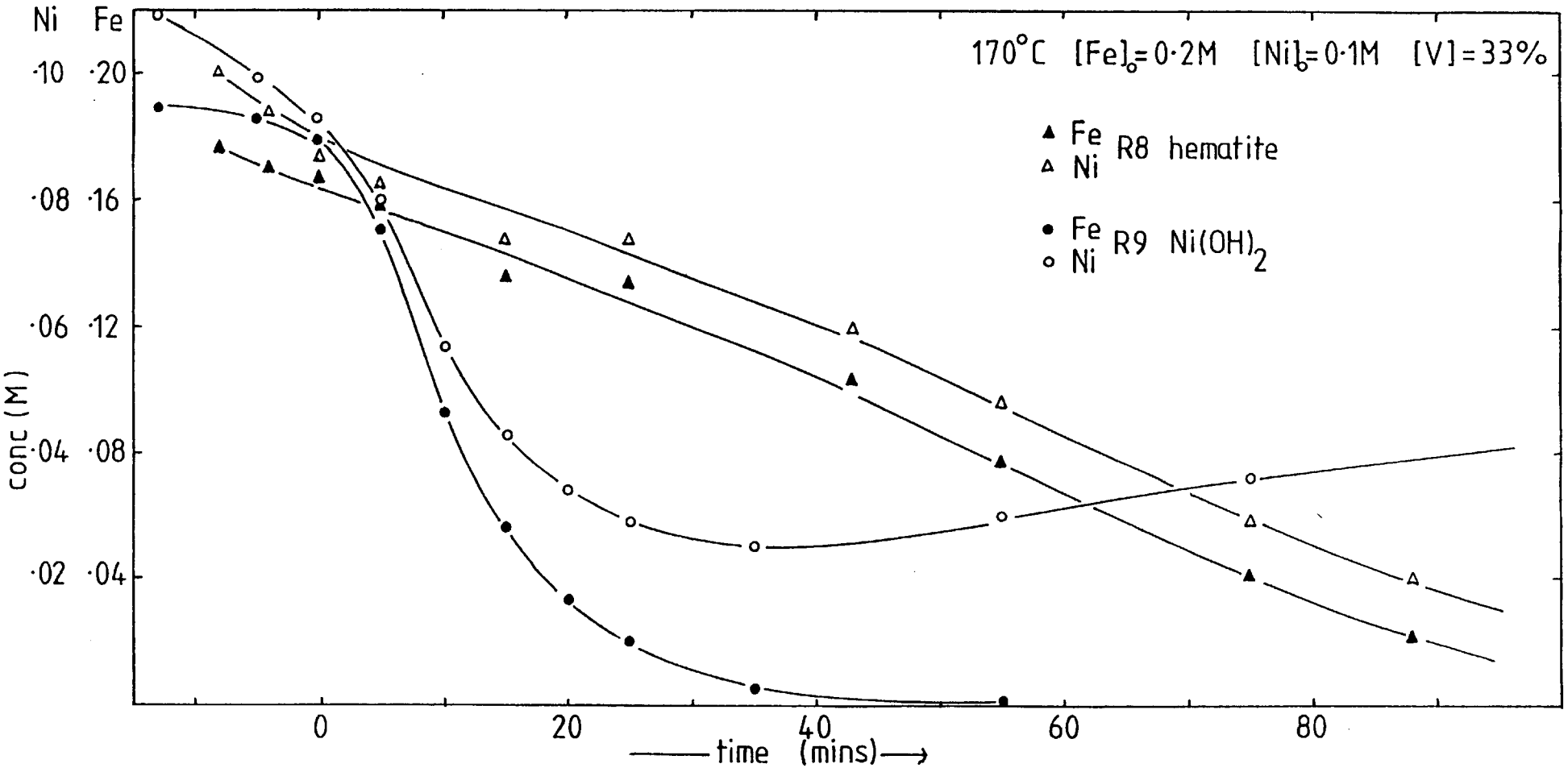


Figure 8.3 Effect of Seeding with Hematite and Nickel Hydroxide

further evidence of the existence of mixed iron-nickel Versatic complexes, as postulated in section 5.4.2. The iron and nickel were both at concentrations which would have given heterogeneous precipitation at 170°C in the absence of the other metal[4]. It must therefore be assumed that the metals are present in the organic phase as complexes, in which the behavior of each metal is modified by the other.

Figure 8.4 compares the concentration-time curve of the unseeded run R4 with the curve for R10, which was seeded with nickel ferrite previously precipitated by hydrolytic stripping. In R 10 precipitation started before the temperature reached 170°C (t = 0), then proceeded rapidly. The absence of an induction period meant that the concentration-time curve could be closely fitted by a polynomial, to obtain a meaningful value for the initial rate. Precipitation was almost certainly occurring by a heterogeneous mechanism when seeded with precipitated nickel ferrite. This was verified later when the effect of seed area was studied.

Since, of the materials tested, precipitated nickel ferrite was the only suitable seed, it was selected for use in all subsequent runs. Enough ferrite was prepared for use in all runs, to ensure consistent seed quality.

8.5 EFFECT OF THE AGE OF METAL-VERSATIC SOLUTIONS

The results of the Plackett-Burman design reported in section 7.1 suggested that the age of the iron-Versatic solution has a significant effect on the precipitation of nickel ferrite, but that the age of the nickel-Versatic solution is not important. In the first few kinetic runs seeded with nickel ferrite, therefore, the iron solution used was prepared just before the run, but the calcium-Versatic from which it was prepared, and the nickel solution were of various age.

It became evident from these runs that the age of the calcium and nickel solutions exerts an important influence. The initial rates of runs R17, R18, R19 and R20, in which the organic solutions

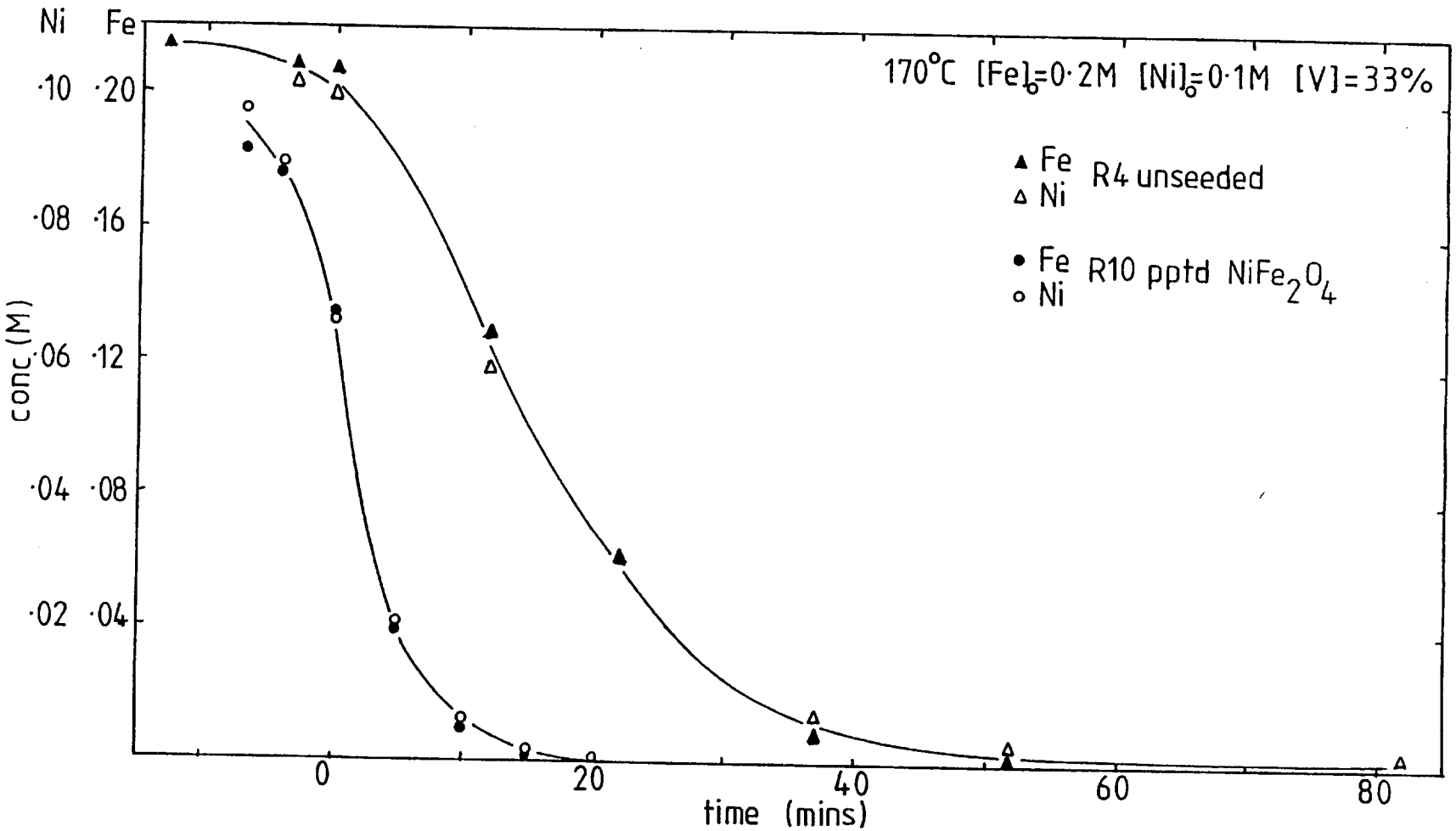


Figure 8.4 Effect of Precipitated Nickel Ferrite on Rate

Table 8.5.1 Effect of the Age of Metal-Versatic Solutions on Rate

$T = 170^{\circ}C$ $[Fe]_o = 0.2M$ $[Ni]_o = 0.1M$ $[V] = 33\%$ 100% seed

Run	Age of Ca-Versatic	Age of Fe-Versatic	Age of Ni-Versatic	Initial Rate ($M\ min^{-1}$)
R17	4 days	fresh	1 day	.0133
R18	1 day	fresh	2 days	.0202
R19	fresh	fresh	4 days	.0181
R20	fresh	fresh	fresh	.0401
R26	fresh	fresh	fresh	.0437
R27	fresh	fresh	fresh	.0427

were of different ages, are shown in Table 8.5.1, together with runs R26 and R27, which were repeats of R20 and are included to show the observed experimental scatter, which is only a few percent. The experimental conditions for these runs were $170^{\circ}C$, 0.2M Fe, 0.1M Ni, 33% Versatic solution, 4.69g $NiFe_2O_4$ seed and 1000rpm. The level of seed corresponds to the weight of nickel ferrite which would be precipitated by completely stripping 200 mls of Versatic solution loaded with 0.2M Fe and 0.1M Ni. This weight of seed is referred to as 100% seed throughout this work.

The difference between run R20 and runs R17, R18 and R19 is more than 50% and is obviously not due to experimental error. The reasons for such effects were not investigated further. The ageing of the nickel-Versatic is probably due to the formation of polymers in which the nickel is less reactive towards water, and less able to form mixed complexes when mixed with iron-Versatic solutions. The large influence of the age of the precursor calcium-Versatic solution on the rate suggests that a polymeric structure develops within the calcium-Versatic solution, and that this structure influences the structure of the iron-Versatic complexes formed by exchange extraction. In this respect the Versatic solution appears to behave more like a

solid ion exchanger than a liquid-liquid extractant.

After run R19, all organic solutions were prepared on the same day as the run, to minimise any effects due to age.

8.6 EFFECT OF WATER VOLUME AND STIRRING SPEED

In all of the previous runs, 10 mls of water and a stirring speed of 1000 rpm had been used. The effects of water volume and seed were investigated in a short series of runs, although these variables were not expected to have a significant effect on the rate of precipitation.

These runs were conducted at 160°C, with 0.2M Fe, 0.1M Ni, 33% Versatic and 100% seed. The reults are given below in Table 8.6.1, together with the results from two later runs made with 10 mls of water at 1000 rpm, and show that the volume of water has no effect on

Table 8.6.1 Effect of Water Volume and Stirring Speed on Rate

$T = 160^{\circ}C \quad [Fe]_o = 0.2M \quad [Ni]_o = 0.1M \quad [V] = 33\% \quad 100\%$ seed

Run	Water Volume mls	Stirring Speed rpm	Initial Rate M min^{-1}
R21	5	1000	.0237
R22	15	1000	.0232
R23	15	1000	.0230
R24	5	1000	.0219
R25	10	1600	.0271
R39	10	1000	.0234
R51	10	1000	.0300

the precipitation rate. All three levels tested were well in excess of the stoichiometric requirement of 1.44 mls of water, needed to precipitate all of the metal from the organic solution. A volume of 10 mls was used in all subsequent runs.

Comparison of runs R25, R39 and R51 indicates that the stirring speed has no significant effect on the rate when increased from 1000 rpm to 1600 rpm. Since there were mechanical problems due to vibration of the rig at the higher speed, a speed of 1000 rpm was used for all further runs.

8.7 EFFECT OF TEMPERATURE ON INITIAL RATE

The effect of temperature on the rate of precipitation of nickel ferrite was investigated between 140° and 180°C. The experimental conditions used were 0.2M Fe, 0.1M Ni, 33% Versatic solution and 100% seed.

Typical rate plots are shown in Figure 8.5, for runs R36, R39 and R34, made at 180°, 160° and 145°C respectively, and indicate that the rate is very sensitive to temperature. Table 8.7.1 gives the results of all the runs made in this series, together with the result of R51, which was the run in the factorial design having experimental conditions equivalent to those used here. 1/T and ln(initial rate) were calculated for each run, and were used to compile the Arrhenius plot shown in Figure 8.6.

The gradient of the plot was determined by linear regression analysis, using the Minitab package. This gave:

$$\ln k = 30.841 - 14.9579 \frac{1}{T} \times 1000 \qquad 8.7.1$$

Where k is the initial rate. The t-ratio for the gradient was -16.7, and the squared correlation coefficient 96.5%, with a random distribution of residuals.

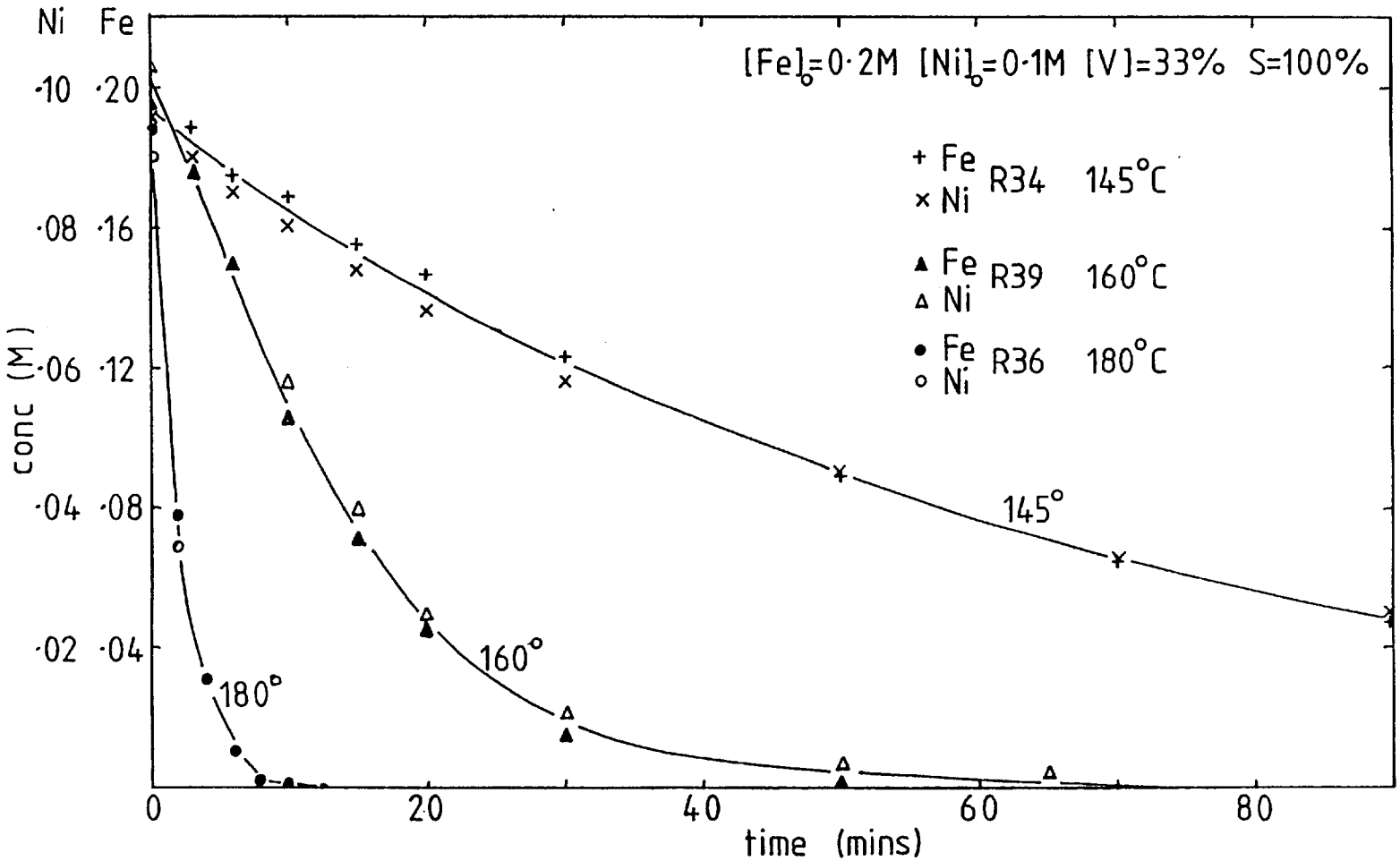


Figure 8.5 Effect of Temperature on Rate of Hydrolytic Stripping

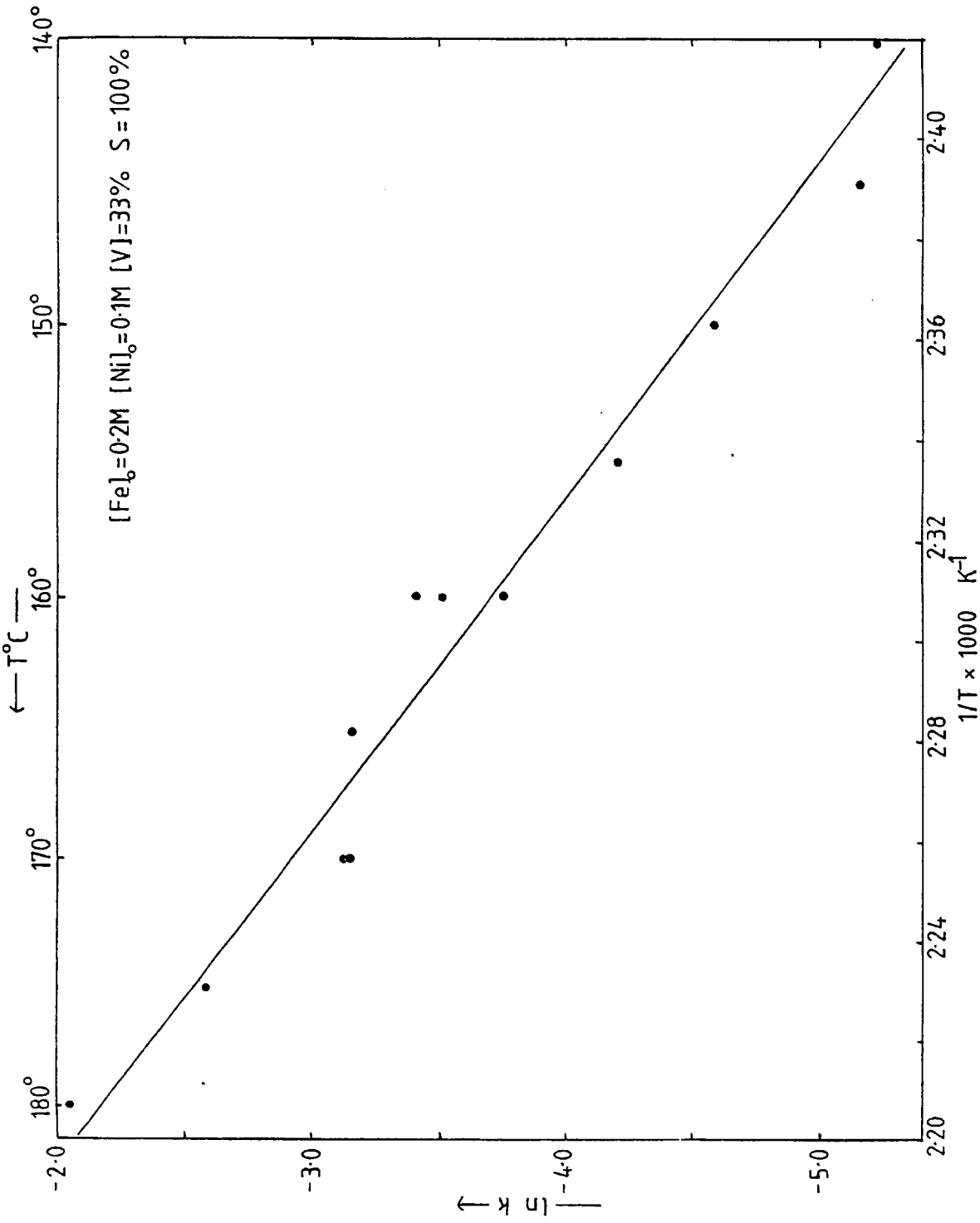


Figure 8.6 Arrhenius Plot

Table 8.7.1 Effect of Temperature on Initial Rate of Precipitation

$[Fe]_o$ = 0.2M $[Ni]_o$ = 0.1M [V] = 33% 100% seed

Run	Temperature °C	$\frac{1}{T}$ x 1000	Initial Rate $M\ min^{-1}$	ln(initial rate)
R26	170°	2.257	.0437	-3.131
R27	170°	2.257	.0427	-3.153
R28	165°	2.282	.0427	-3.154
R29	160°	2.309	.0335	-3.397
R39	160°	2.309	.0234	-3.756
R51	160°	2.309	.0300	-3.507
R30	155°	2.336	.0149	-4.206
R31	150°	2.363	.0103	-4.580
R34	145°	2.391	.0057	-5.160
R33	140°	2.420	.0054	-5.221
R35	175°	2.231	.0749	-2.591
R36	180°	2.207	.1289	-2.053

The Arrhenius plot is based on the Arrhenius equation

$$k = A \exp\left(\frac{-E_a}{RT}\right) \qquad 8.7.2$$

where A is a constant, E_a the activation energy of the process and R the gas constant. From 8.7.2

$$\ln k = \ln A - \frac{E_a}{R}.\frac{1}{T} \qquad 8.7.3$$

From 8.7.1 and 8.7.3:

$$\frac{E_a}{R}.\frac{1}{T} = 14.9579 \times 1000.\frac{1}{T} \qquad 8.7.4$$

$$\therefore \quad \underline{E_a = 124.37\ kJ\ mol^{-1}}$$

This comparatively high activation energy shows the heterogeneous precipitation reaction to be under chemical control (as a general 'rule of thumb', activation energies over 60 kJ mol^{-1} indicate chemical control). There is no indication of a change in gradient in Figure 8.6, which suggests that the process occurs by the same mechanism throughout the temperature range studied. This temperature range could not be extended for the experimental conditions used, because, as is evident from Figure 8.5, at a temperature above 180°C the rate would be too rapid to follow by sampling, while at a temperature below 140°C the reaction would be too slow to follow in a practicable time period.

From the concentration-time plots for different temperatures, 160°C was selected as the fixed temperature for all subsequent runs. The rate at 160°C was intermediate under the experimental conditions used in this series of runs. It was therefore unlikely that altering any of the variables would affect the rate, either positively or negatively, to such an extent that the rate would become unmeasurable.

8.8 EFFECT OF NICKEL FERRITE SEED ON INITIAL RATE

The effect of the level of nickel ferrite seed was studied at 160°C, with 0.2M Fe, 0.1M Ni and 33% Versatic solution. The results are presented in Table 8.8.1.

The initial rates are plotted against seed level in Figure 8.7. The relationship is clearly linear, but the intercept is not zero. Linear regression analysis of the data gave the gradient of Figure 8.7 as .0003M $min^{-1}(\%\ seed)^{-1}$, with zero rate at 9.7% seed.

The linear response shows that the rate controlling process occurs on the surface of the nickel ferrite seed. Although some hydrolysis may occur in the bulk of the solution, it is evidently insufficient to cause homogeneous nucleation of ferrite particles, since such nucleation would result in a non-linear relationship between seed and rate. It is therefore probable that most of the hydrolysis occurs on the seed surface. However, the linear response can give no indication of the surface process which is rate controlling.

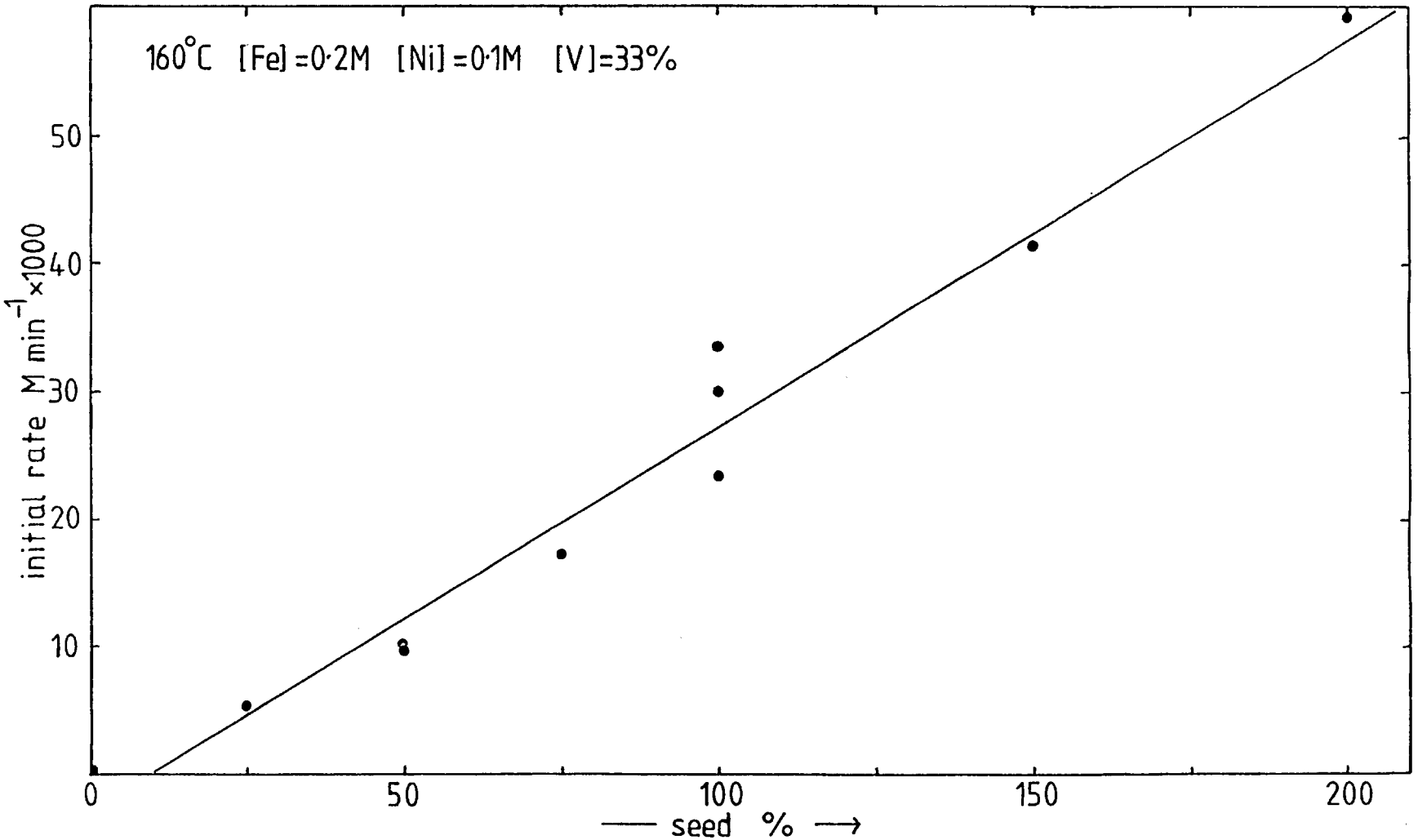


Figure 8.7 Effect of Seed Level on Initial Rate

Table 8.8.1 Effect of Nickel Ferrite Seed Level on Initial Rate

160°C Fe_o = 0.2M Ni_o = 0.1M V = 33% 100% seed = 4.69g

Run	Seed Level	Initial Rate $M\ min^{-1}$
R37	200%	.0592
R38	150%	.0415
R39	100%	.0234
R29	100%	.0335
R51	100%	.0300
R40	75%	.0172
R41	50%	.0101
R42	50%	.0098
R44	25%	.0053
R43	0%	0

The predicted rate of zero at 9.7% seed was interpreted as being due to poisoning of the area corresponding to that percentage. A gelatinous, yellow-green, nickel rich precipitate was formed in small quantities during all unseeded runs, although there was no measurable change in iron or nickel concentration during these runs. This phase could not be identified by X-ray powder diffraction analysis, but could have been an organo-metallic compound formed by an impurity in the Versatic 10 or Escaid. If this is so, it was probably formed in all runs, but was not detected when there was seed present, because it was adsorbed onto the seed. This could have 'poisoned' a fixed number of active surface sites, giving the observed behaviour.

8.9 EFFECT OF IRON, NICKEL AND VERSATIC CONCENTRATION: FACTORIAL DESIGN

A 2^3 factorial design was used to investigate the effect of iron, nickel and Versatic concentration at 160°C with 100% seed. The levels chosen for these variables are shown below in Table 8.9.1. The iron and nickel levels were selected to give a stoichiometric iron to nickel ratio of 2 when both factors were at either the high or the low level, and to give both iron-rich and nickel-rich deviations from stoichiometry when the factors were at different levels. 33% Versatic was selected as one level of Versatic concentration, so that the region studied would overlap the experimental conditions used in the earlier runs. Since 33% Versatic was nearly fully loaded at the high levels of iron and nickel, it was convenient to use a higher Versatic concentration as the second level. 50% was selected. The runs were all written in standard order, then performed in random order.

The concentration-time curves for the half of the design with Versatic concentration at 50% are shown in Figure 8.8 (a) and (b). As before, the iron and nickel concentration scales are different, so that the iron and nickel concentrations lie on a single curve when in the stoichiometric ratio of 2. The curves for the other half of the design were similar, but with faster rates.

Table 8.9.1 Levels of the Variables Studied in Factorial Design

Symbol	Factor	Low(-) level	High(+) level	Units Measured
F	Iron concentration	0.1	0.2	M
N	Nickel concentration	0.05	0.1	M
V	Versatic concentration	33%	50%	% v/v in Escaid

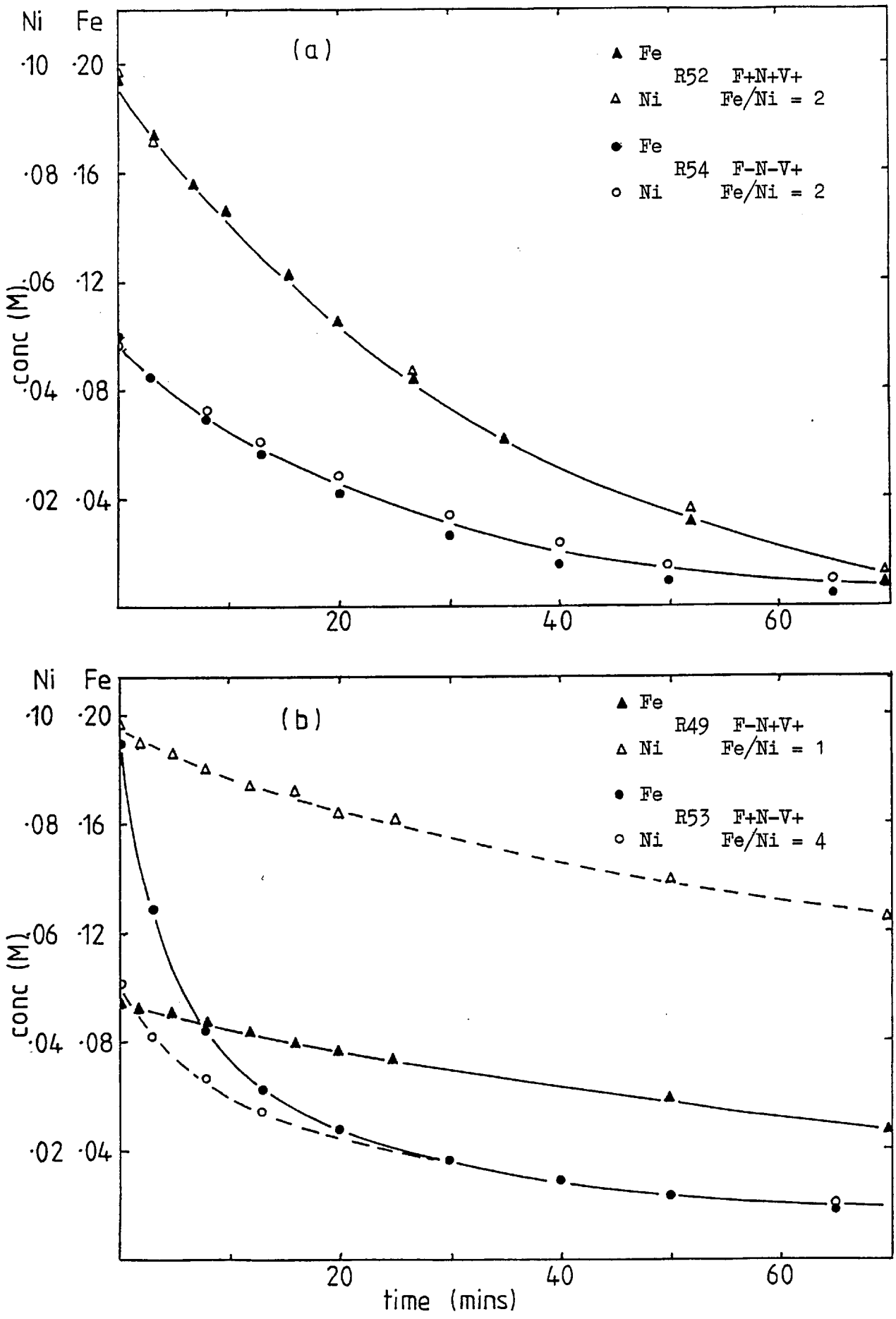


Figure 8.8 Factorial Design: Concentration-Time Curves for [V] = 50% Varying $[Fe]_o$ and $[Ni]_o$

The curves in Figure 8.8(a) are for the runs R52 and R54 where the iron to nickel ratio was 2. These curves are similar in form to those presented earlier for seeded runs. The curves in 8.8(b) are for the runs which were not stoichiometric in iron to nickel ratio. Where this ratio was 4, in run R53, the iron concentration (solid curve) decreased more rapidly than the nickel concentration (broken curve) until the iron to nickel ratio fell to 2, after 20 minutes. Thereafter the two curves were coincident. Initially the phase precipitating must have been a solid solution of nickel ferrite and maghemite. The proportion of nickel in this mixture increased as the iron concentration in the organic decreased, until after 20 minutes the composition of the precipitate corresponded closely to that of nickel ferrite.

Where the iron to nickel ratio was 1, in run R49, the nickel curve is roughly parallel with the iron curve throughout the run, indicating that nickel ferrite was precipitated, and that this was stoichiometric, with no excess nickel. The rate was much slower than the rate of the run R54, with 0.1M Fe and 0.05M Ni. Since the simplified hydrolytic stripping equation is:

$$2\overline{FeV_3} + \overline{NiV_2} + 4H_2O = NiFe_2O_4 + 8\overline{HV} \qquad 8.9.1$$

the rate would be expected to increase with an increase in the concentration of the reactants, and decrease only with an increase in the concentration of the products. Under these conditions, however, an increase in the concentration of nickel, one of the reactants, reduces the rate, which suggests that equation 8.9.1 is very much an oversimplification of the real situation.

The combined initial rate (d/dt(0.E.)) for each run is shown in Table 8.9.2, together with Yates' algorithm, which was used to calculate the estimates of the effects and interactions, as in section 4.1.1. The rates given are positive, that is, they refer to the rate of precipitation, not to the rate of change of concentration, which is a negative quantity. Therefore an effect is positive when the effect increases the rate of precipitation, and negative when the effect decreases the rate of precipitation.

Run No	Exptl Order	Test No	Design Matrix Variables F	N	V	Yates' Algorithm Initial Rate M min^{-1}	1	2	3	Divisor	Estimate of Effects	Identification of Effects
R50	3	1	-	-	-	.0153	.0441	.0867	.1253	8	.0157	Mean
R47	1	2	+	-	-	.0288	.0426	.0386	.0497	4	.0124	F
R48	7	3	-	+	-	.0126	.0247	.0309	-.0123	4	-.0031	N
R51	4	4	+	+	-	.0300	.0139	.0188	.0021	4	.0005	FN
R54	8	5	-	-	+	.0072	.0135	-.0015	-.0481	4	-.0120	V
R53	6	6	+	-	+	.0175	.0174	-.0108	-.0121	4	-.0030	FV
R49	2	7	-	+	+	.0027	.0103	.0039	-.0093	4	-.0023	NV
R52	5	8	+	+	+	.0112	.0085	-.0018	-.0057	4	-.0014	FNV

Table 8.9.2 Factorial Design: Initial Rates, Yates' Algorithm and Effects

The concentration-time curves shown in Figure 8.8 (a) and (b) showed three distinctly different types of behaviour. Each effect shown in Table 8.9.2 is estimated in the Yates' algorithm, using the rates of all eight runs, according to the signs in the design matrix. The effect of iron, E_F, for example, is given by:

$$E_F = \frac{-R_1 + R_2 - R_3 + R_4 - R_5 + R_6 - R_7 + R_8}{4} \qquad 8.9.2$$

which can be rewritten as:

$$E_F = \underbrace{\frac{R_2 + R_4 + R_6 + R_8}{4}}_{\text{average effect at high level of F}} - \underbrace{\frac{R_1 + R_3 + R_5 + R_7}{4}}_{\text{average effect at low level of F}}$$

Thus the numerical value obtained for each effect is the average effect for three different types of behaviour, so has little real physical meaning. The concentration-time curves give far more indication of the physical and chemical processes occurring for the three different iron to nickel ratios. Because of this, no formal significance tests were applied to the effects. The three-factor interaction FNV, and the two-factor interaction FN were both substantially lower than the other effects, so were considered to give some indication of the magnitude of the experimental error.

Iron concentration had a large, positive effect on the rate, and Versatic concentration had a similarly large negative effect. Nickel concentration, however, has an overall negative effect, albeit of a smaller magnitude than the other two main effects. The main effects are represented in Figure 8.9 (a), (b) and (c), in which the initial rates of all runs are plotted in pairs at both levels of Versatic, iron and nickel concentration respectively. Versatic concentration has a negative effect, and iron a positive effect in all cases, as might be expected, since Versatic is a product of the reaction, and iron is one of the reactants. Nickel has a smaller, negative effect for three pairs of rates, and a slight positive effect for one pair, which may be due only to experimental error. The negative effect on the pair F-V+ was observed in Figure 8.8

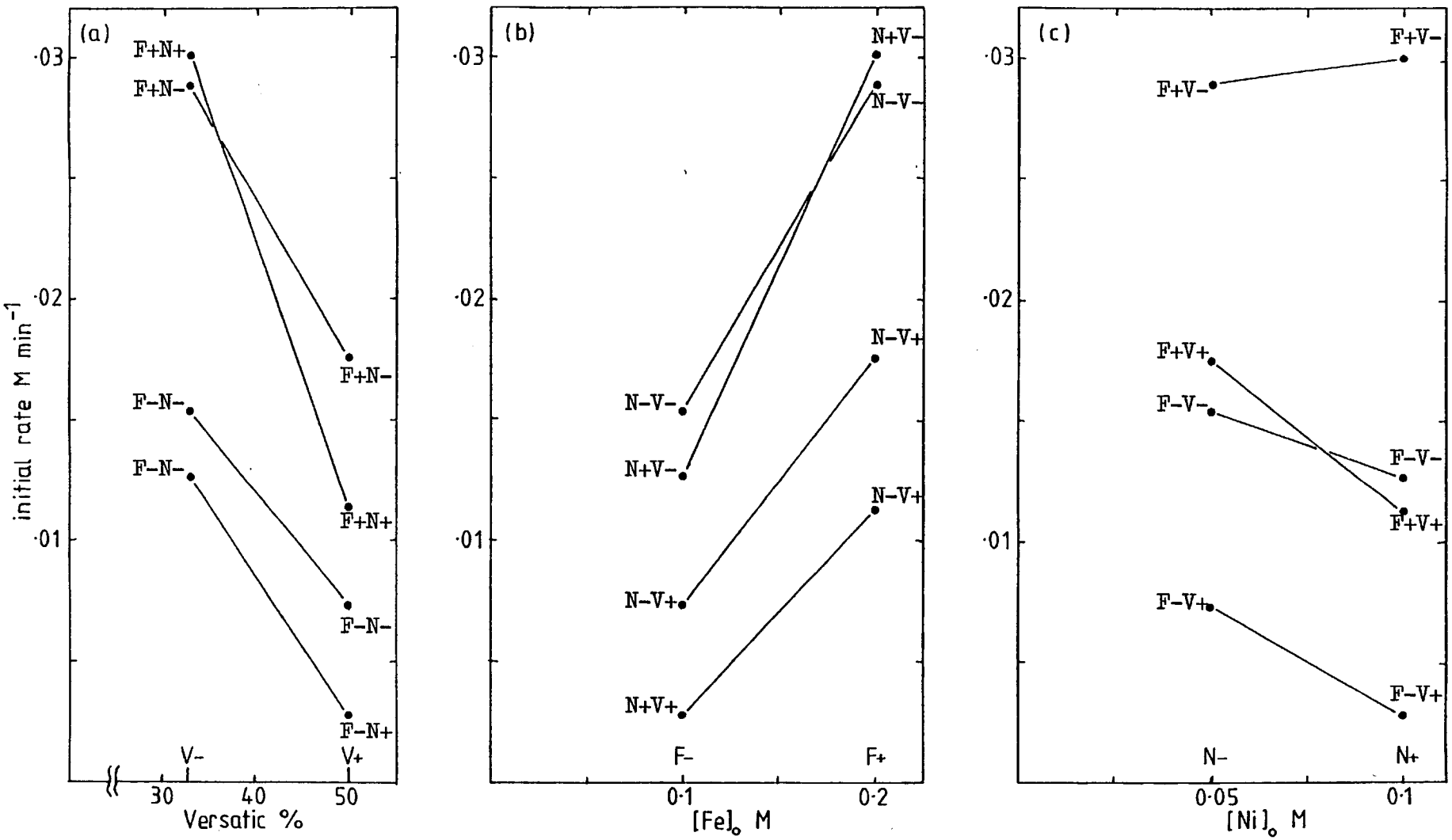


Figure 8.9 Effect of (a) Versatic, (b) Iron and (c) Nickel on Initial Rate

when going from R54 to R49. The negative effect on the pair F+V+ indicates that there is also a reduction in rate going from R53 to R52 in Figure 8.8, which is less obvious.

The lines in Figure 8.9 (a), (b) and (c) are not all parallel in each plot, which indicates that there are significant interactions. From Table 8.9.2 these are FV and NV.

8.10 ORGANIC INJECTION RUNS

To obtain some idea of the stability of the iron-nickel complexes present in the Versatic solutions, two runs were made in which organic solutions were injected with the water from the heated reservoir into the autoclave. If the complexes are very stable, the observed rate would be characteristic of the solution composition before injection, whereas if the complexes are labile, the rate would immediately be characteristic of the composition after mixing.

Two runs were made; R55, in which Versatic acid was injected into the autoclave to raise the concentration from 33% to 45% Versatic,

Table 8.10.1 Injection Runs: Compositions Before and During Runs, and Initial Rates

Experiment	Run No	Organic Volume and Composition Before Injection	Organic Composition During Run	Initial Rate M min^{-1}
Versatic injection	R55	165 mls, .242M Fe .121M Ni, 33% V	.2M Fe .1M Ni 45% V	.0139
	R51		.2M Fe .1M Ni 33% V	.0300
	R52		.2M Fe .1M Ni 50% V	.0112
Fe Versatic injection	R57	155 mls, .128M Ni 33% V	.1M Fe .1M Ni 33% V	.0081
	R48		.1M Fe .1M Ni 33% V	.0126

and R57 in which iron-Versatic was injected into nickel-Versatic solution. The compositions before and after injection are shown in Table 8.10.1, together with the initial rates. For comparison, the rates for runs R51, R52 and R48 are given.

The autoclave used had a common tube for injection and sampling, so the first sample withdrawn from each injection run was erroneous, because contaminated by traces of the injected organic solution left in the sample line. In addition, these first samples could only be taken after 1 minute, since at time zero the two organic solutions were not mixed. These two considerations meant that the initial rates for these runs, as derived by polynomial regression, were not an accurate measure of the overall behaviour. The concentration-time curves for the runs were therefore drawn, so that the behaviour throughout the runs could be compared. The curves for runs R55, R51 and R52 are shown in Figure 8.10 (a) and those for runs R57 and R48 are shown in Figure 8.10 (b).

From 8.10 (a) it is clear that the rate of R55, where Versatic was injected to give a final Versatic concentration of 45%, was intermediate between the rates of R51 and R52, made with 33% and 50% Versatic respectively, and closer to the latter.

From Figure 8.10 (b) it is clear that, within experimental error, the rate of R57 (solid line), where iron-Versatic was injected into nickel-Versatic to give a mixed solution containing 0.1M of each metal, was the same as the rate during R48 (broken line), which had the same metal concentration.

Both injection runs indicated that any mixed complexes present in the organic solutions are labile, and that the composition of the organic solution during the heating up period had little influence on the behaviour if this composition was altered immediately prior to reaction.

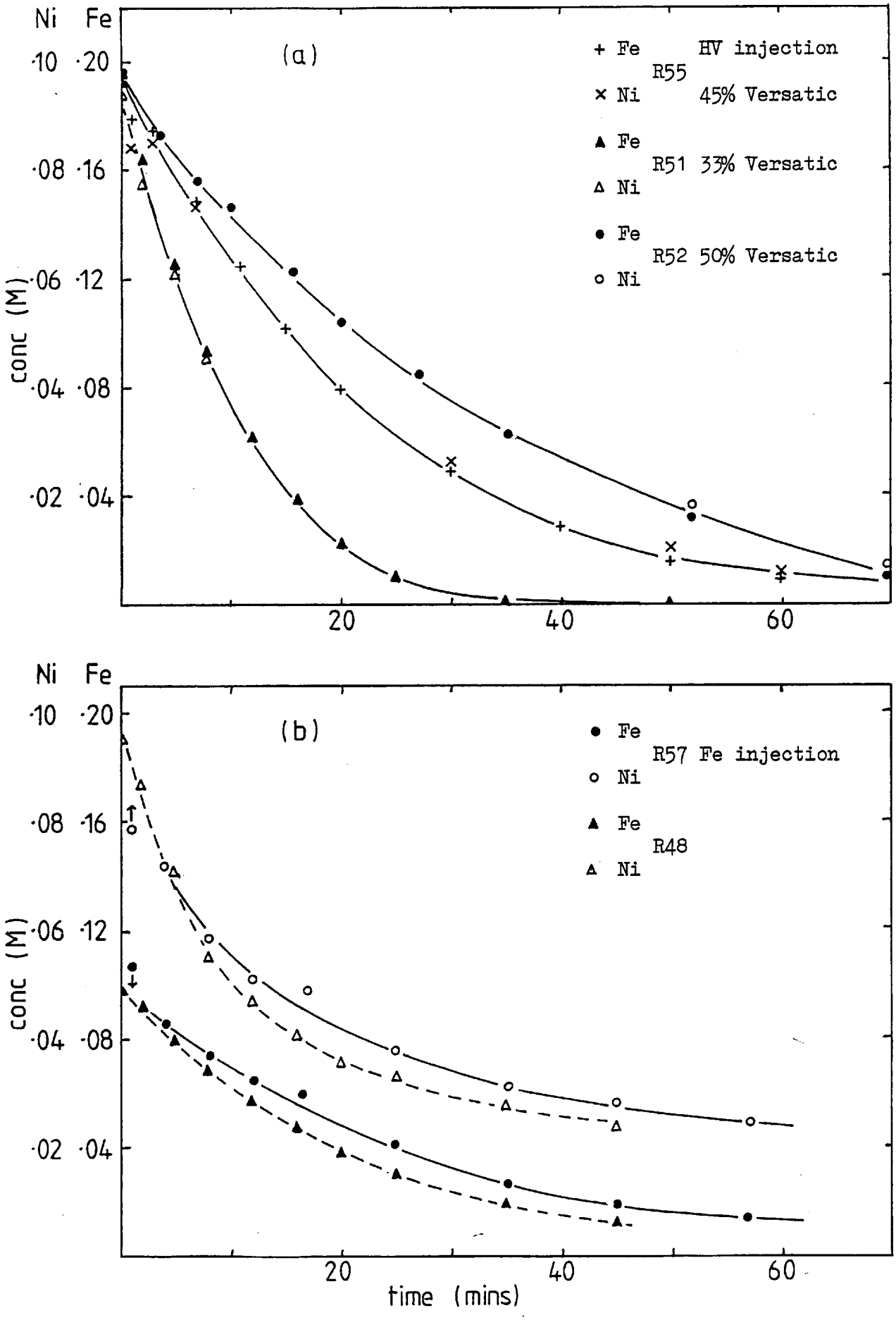


Figure 8.10 Injection Runs (a)Injection of Versatic Acid
(b)Injection of Iron Versatic Solution

8.11 EFFECT OF VERSATIC CONCENTRATION ON INITIAL RATE

The factorial design gave the effect of Versatic concentration at two levels, 33% and 50%. Run R55, in which Versatic acid was injected into the autoclave, appeared to give an indication of the rate at 45% Versatic. Three more runs were made to measure the initial rate at 45% Versatic and 25% Versatic. These runs were made at 160°C with 100% seed. The metal concentrations used were; runs R56 and R46 - 0.1M Fe, 0.05M Ni, and run R45 - 0.2M Fe and 0.1M Ni. The initial rates are given in Table 8.11.1. These rates are shown with the rates of earlier runs in Figure 8.11 (a) and (b), which indicates the effect of Versatic (a) for an initial concentration of 0.2M Fe and 0.1M Ni and (b) for an initial concentration of 0.1M Fe and 0.05M Ni. The rate falls rapidly as the total Versatic concentration increases. Although a convenient experimental variable, the Versatic concentration is not a kinetic variable, since it includes free Versatic acid, Versatic anions and solvated Versatic acid. The response to this variable was therefore not investigated further. The free acid was measured by infrared spectrophotometry, and the effect of this variable on rate is considered in Chapter 9.

Table 8.11.1 Effect of Versatic at 25% and 45%

Run	[V]%	$[Fe]_o$ M	$[Ni]_o$ M	Initial Rate, M min^{-1}
R56	45%	0.1	0.05	.0109
R45	25%	0.2	0.1	.0678
R46	25%	0.1	0.05	.0285

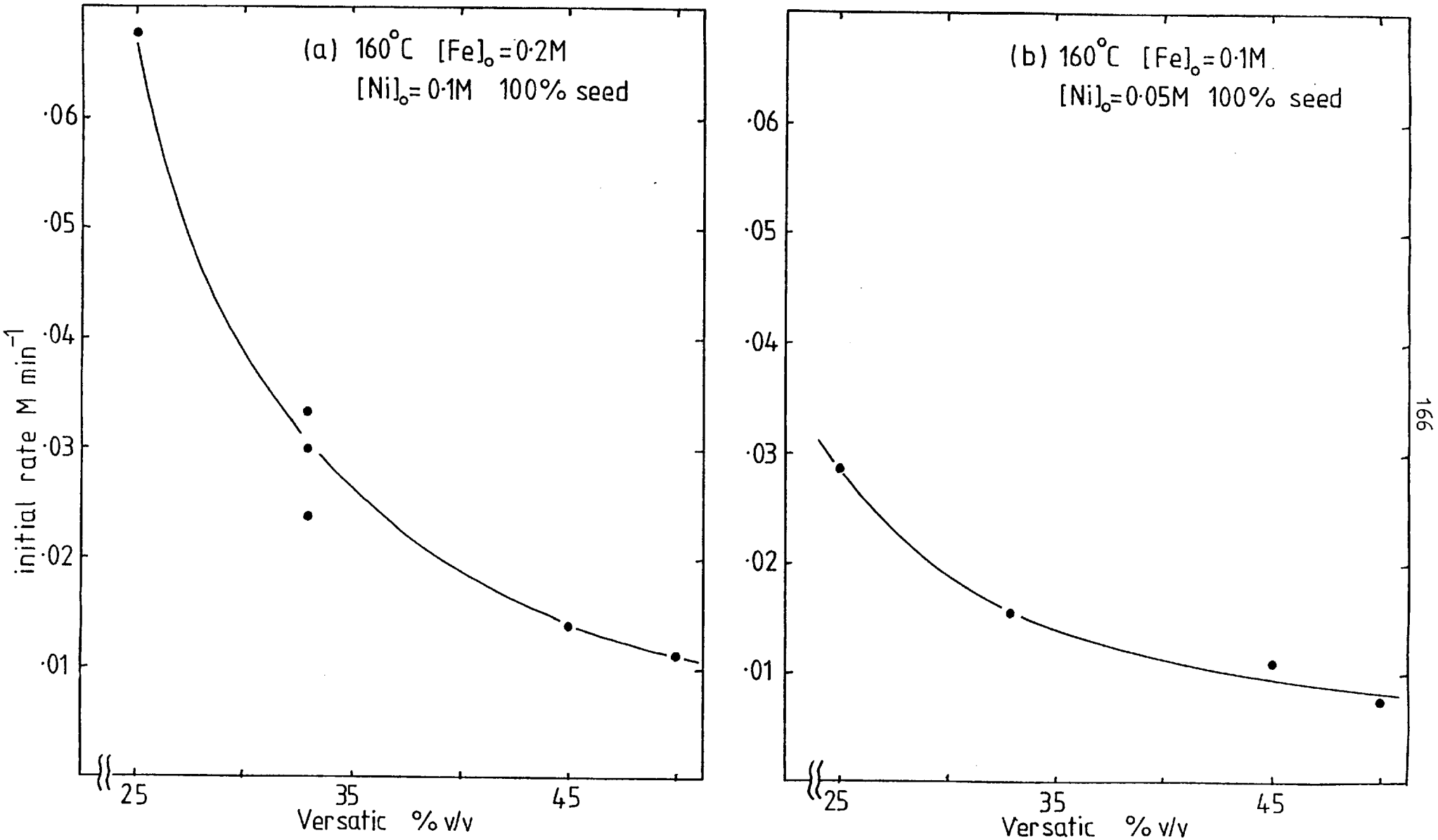


Figure 8.11 Effect of Versatic Concentration on Initial Rate

CHAPTER 9

INFRA-RED SPECTROPHOTOMETRY

9.1 INTRODUCTION

Infrared spectrophotometry was used primarily to measure the concentration of free Versatic acid in samples of the organic solutions used in the kinetic runs. The technique was also expected to reveal information on the composition of the metal-Versatic complexes in the solutions.

A Perkin-Elmer 577 double beam grating infrared spectrophotometer was used. This instrument can only give accurate measurements in the high frequency region of the infrared spectrum ($4000-650cm^{-1}$). The absorption peaks in this region result from the vibrations or bending of bonds within organic molecules, ions or ligands. The carboxylate anion can coordinate a metal in a variety of modes. These modes have different carbonyl stretching frequencies, so can be distinguished, therefore the secondary effects of coordination can be detected. The absorptions resulting from the vibrations of metal ligand bonds would be more useful in elucidating the structure of metal-Versatic complexes. Because of the high relative mass of transition metal ions, however, these absorptions lie in the low frequency (far infrared) region ($650-50cm^{-1}$)[107] which could not be measured on the instrument available.

The free Versatic acid is mainly present in the organic solutions as monomers and dimers. The dimer has a planar, hydrogen-bonded structure, with a centre of symmetry. There are two carbonyl (C=O) stretching modes, symmetric and antisymmetric. However, a deformation mode is only IR active if it results in a change in dipole moment, and because of the centre of symmetry in the dimer, only the antisymmetric stretch causes such a change. This antisymmetric stretch gives a strong absorption band in the range $1740-1680cm^{-1}$. This peak, which occurs at $1700cm^{-1}$ for Versatic 10, was used in this work to measure the concentration of dimer. The frequencies of the absorption bands commonly observed for carboxyl dimers and monomers are summarised in Tables 9.1.1 and 9.1.2 respectively. Since the

Table 9.1.1 Carboxyl Dimer Spectral Regions[108]

Deformation	Band(cm^{-1})
OH stretch	ca 3000 very broad
Overtones and combinations	2700 - 2500
C=O stretch	1740 - 1680
OH deformation in plane	1440 - 1395
C-O stretch	1315 - 1280
OH deformation out of plane	960 - 875

Table 9.1.2 Carboxyl Monomer Spectral Regions[108]

Deformation	Band(cm^{-1})
OH stretch	3580 - 3500
C=O stretch	1800 - 1740
OH deformation	1380 - 1280
C-O stretch	1190 - 1075

carboxyl group in the monomer is not restricted to a single plane by hydrogen bonding, there are not separate in-plane and out of plane OH deformations, as shown by the dimer. There is only one carbonyl stretch, and this occurs at a higher frequency than that of the dimer, because the carbonyl bond is not strongly hydrogen bonded, and is therefore stronger. The monomer carbonyl band, occurring at $1750cm^{-1}$ for Versatic 10, was used to measure monomer concentration.

Figure 9.1 shows the infrared spectrum of a 2.5% solution of Versatic acid at 25° and 165°C. At 25°C the absorption peak at $1750cm^{-1}$ is very weak, which indicates that there is very little monomer present, but at 165°C the monomer and dimer peaks have a similar optical density. At 165°C, the narrow OH stretch of the monomer is seen at $3540cm^{-1}$.

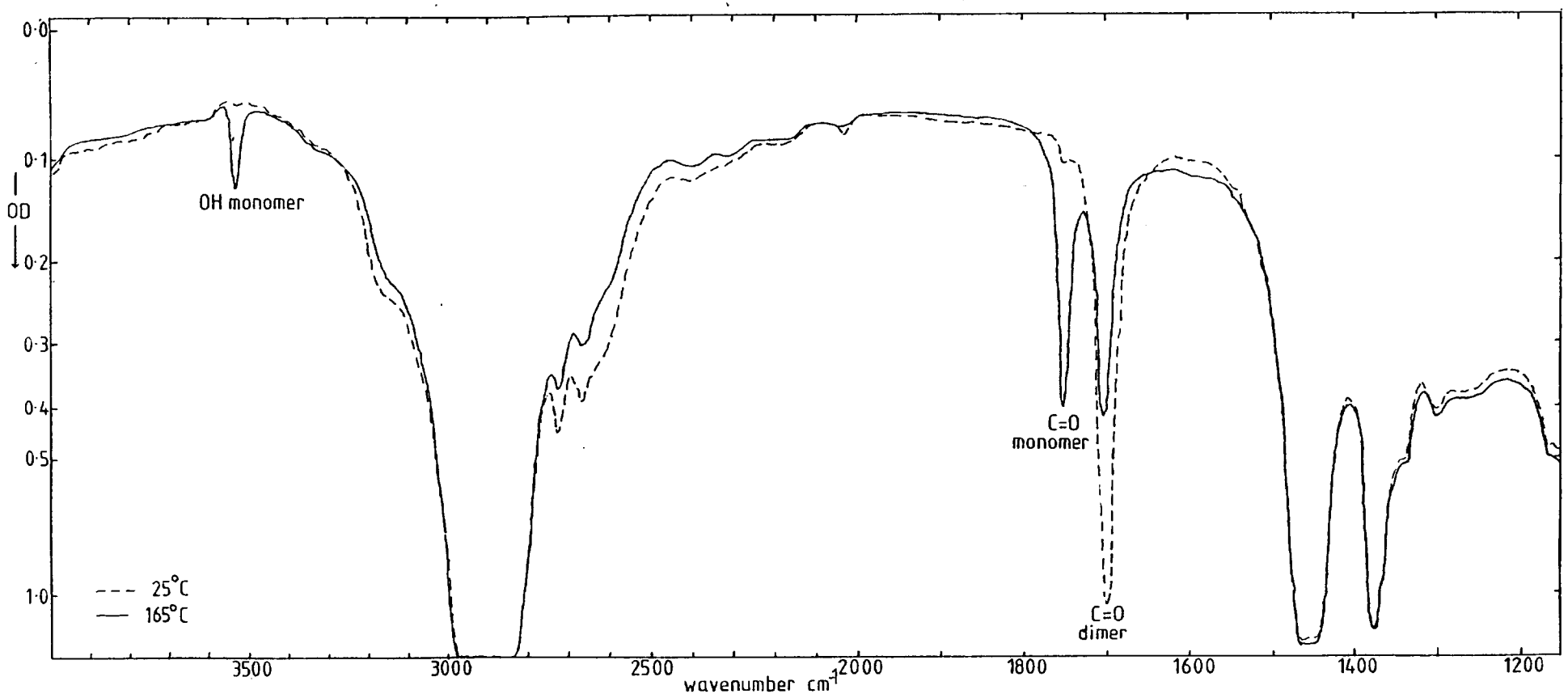
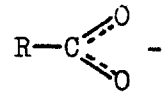


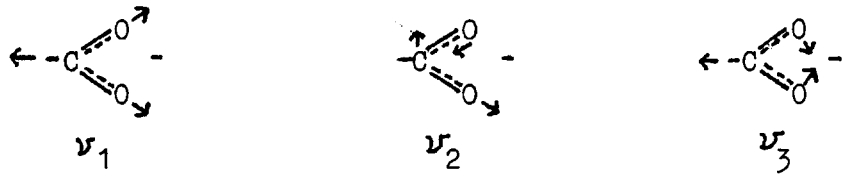
Figure 9.1 Infrared Spectrum of a 2.5% Solution of Versatic 10 at 25° and 165°C

Versatic acid solvating a metal complex is more strongly hydrogen bonded than is the dimer. The carbonyl bond is therefore further weakened, and absorbs at a lower frequency than in the dimer. Crabtree and Rice reported a frequency of $1675cm^{-1}$ for Versatic acid solvating Co(II) complexes[109].

Carboxylic acids have C=O and C-O bonds, which absorb at different frequencies as shown in Tables 9.1.1 and 9.1.2. When a carboxylate anion forms from the acid, these bonds are replaced by two equivalent carbon-oxygen bonds, with an intermediate force constant, denoted by



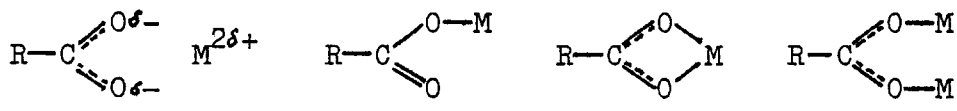
Three fundamental vibrations are expected for the O-C-O system[109]



ν_1 ν_2 ν_3

The strong antisymmetric stretch ν_2 occurs at $1650-1540cm^{-1}$, and the weaker symmetric stretch ν_1 occurs between $1450-1380cm^{-1}$. ν_3 is a predominantly bending deformation and absorbs at a lower frequency, below the carbonyl range.

The carboxylate anion may be bonded to a metal in any of the following ways[109,110]:



I II III IV

Structure I comprises free ions, and is unlikely to occur in Versatic/ Escaid solutions which have a low dielectric constant. Structures II, III and IV are monodentate complexing, bidentate chelating and bidentate bridging, respectively.

The difference between the frequencies of the antisymmetric and symmetric stretching modes of the carboxylate anion (i.e. structure I), $\nu_2-\nu_1$ or $\Delta\nu$, is commonly regarded as being indicative of the dentative properties of the anion. The larger the value of $\Delta\nu$, the more dissimilar are the two C-O bonds, and therefore the more like structure II is the bonding[109]. The dissimilarity of the C-O bonds results from an increase in the strength of the M-O bond[110]. When the bonding is principally of type II, there is only one absorption in the carbonyl frequency. The other stretching frequency is much lower. In this structure, it is more meaningful to regard the two deformations as the C=O and C-O stretch, than as the antisymmetric and symmetric modes.

Because of the high relative mass of the metal, the carbonyl frequency of a monodentate complexing group is lower than that of the corresponding acid. However, it is larger by about $100cm^{-1}$ than the antisymmetric stretching mode of structure IV.

The bidentate chelating and bridging structures (III and IV) have the same symmetry as the free anion, structure I, and will therefore have both symmetric and antisymmetric stretching modes. The two C-O bonds in these structures are equivalent, regardless of the strength of the M-O bonds, therefore changes in the metal have no predictable effect on $\Delta\nu$. The O-C-O system has a more dense electron cloud in structure III than in structure IV, therefore the former has a higher bond order and frequency.

Crabtree and Rice used derivative infrared spectroscopy to study Co(II) Versatic complexes[109]. Since this technique gives the second derivative of the conventional plot of absorption vs frequency, weak bands and points of inflection can be resolved more easily than on conventional plots. The studies involved observing the spectra of cobalt-Versatic extracts, and the effects of dilution, and of the addition of free acid on the spectra.

The undiluted cobalt-Versatic extract showed a maximum absorption at $1580cm^{-1}$, with lesser vibrations up to $1610cm^{-1}$, and a band at $1480cm^{-1}$ which was ascribed to bidentate complexing. The lesser vibrations and the bidentate band disappeared on dilution.

Addition of free acid to cobalt-Versatic complexes introduced a new band at 1595-1602cm^{-1}, at the expense of the 1580cm^{-1} peak. A band which appeared at 1425cm^{-1} was thought to be due to bidentate carboxylate complexing[109].

Stefanakis observed bands for iron-Versatic analagous to the 1595, 1580 and 1425cm^{-1} bands reported by Crabtree and Rice for cobalt-Versatic. Bands at 1600, 1575 and 1415cm^{-1} were tentatively assigned to monodentate complexing, bidentate chelating and bidentate bridging respectively[48].

It was concluded from both studies that the metal-Versatic complexes contained carboxylate anions in different modes of bonding.

9.2 MEASUREMENT OF FREE VERSATIC ACID IN ORGANIC SOLUTIONS

In each of the kinetic runs, the overall Versatic concentration was known. This known concentration was the total of the free Versatic acid, and of Versatic anions and solvating acid in complexes of the form $(M(OH)_mV_{n-m}.sHV.qH_2O)_x$. When considering kinetic data, the concentration of free acid is of interest, but there is no straightforward method for determining this. Titration, for example, would measure the solvating acid in addition to the free acid. When dealing with runs made at elevated temperatures, a further consideration is that the composition of metal complexes was shown by Van der Zeeuw to change with temperature[41], therefore the concentration of free acid in a given solution is likely to be temperature dependent.

Infared spectrophotometry has proved to be a suitable technique for estimating the free acid, although there is a rather high experimental error associated with the technique[12,48]. Spectra can be recorded at the temperature at which the kinetic runs were made, to measure the equilibrium concentration of free acid which was present at the beginning of each run.

9.2.1 Determination of the Monomer and Dimer Extinction Coefficients

A heated optical cell with CaF_2 windows (Specac-Analytic Accessories Ltd) was used for all spectrophotometric measurements. The temperature of the cell was measured and controlled by a thermocouple connected to a Eurotherm temperature controller. The path length of the heated cell, nominally 0.1mm, was measured using interference fringes at temperatures from 20°-170°C. Within this range the path length increased from 0.103 to 0.108mm. For experimental purposes the variation was regarded as negligible, and the path length was taken to be 0.108mm between 130° and 165°C.

The infrared traces were recorded on paper directly calibrated in optical density (O.D) on the vertical scale. The O.D of each peak was taken as the difference between the optical densities at the peak maximum, and at the baseline.

At elevated temperatures, free acid is present as both monomers and dimers, as shown in Figure 9.1. The monomer and dimer carbonyl peaks at 1750 and 1700cm^{-1} were therefore both measured for all quantitative work. It was assumed that further polymerisation of the free acid was negligible.

A series of standards containing from 0.4 to 4.0% Versatic in Escaid was prepared. The dimer peak had previously been shown to obey Beers Law at 25°C at optical densities up to 0.96[12]. It was not necessary to verify this behaviour, since room temperature measurements were not required for the purpose of this project. Each standard was run at three elevated temperatures; 130°, 150° and 165°C. In addition, the 2.0 and 2.5% standards were run at 25°C to observe the room temperature spectrum of the acid. The optical densities of the monomer and dimer peaks, denoted as OD_{HV} and $OD_{(HV)_2}$ respectively, were measured at each temperature, for each standard. These data are presented in Tables 9.2.1 and 9.2.2. The total concentration of Versatic in each standard is denoted by C_V. It is evident that for each standard, OD_{HV} increased, and $OD_{(HV)_2}$ decreased with increasing temperature, which indicates that dissociation is temperature dependent.

Table 9.2.1 OD_{HV} versus C_V in the range 25-165°C

C_V		OD_{HV}		
% v/v	M(25°C)	25°	130°	150°	165°
0.4	0.0210		0.042	0.051	0.049
0.8	0.0420		0.066	0.077	0.083
1.0	0.0525		0.118	0.152	0.165
1.6	0.0840		0.161	0.198	0.231
2.0	0.1050	0.020	0.190	0.233	0.267
2.5	0.1312	0.021	0.220	0.281	0.315
3.0	0.1574		0.244	0.298	0.343
3.5	0.1837		0.262	0.329	0.376
4.0	0.2099		0.285	0.356	0.413

Table 9.2.2 $OD_{(HV)_2}$ versus C_V in the range 25-165°C

C_V		$OD_{(HV)_2}$		
% v/v	M(25°C)	25°	130°	150°	165°
0.4	0.0210		0.023	0.014	0.007
0.8	0.0420		0.057	0.036	0.027
1.0	0.0525		0.181	0.122	0.099
1.6	0.0840		0.315	0.240	0.181
2.0	0.1050	0.733	0.375	0.304	0.246
2.5	0.1312	1.000	0.491	0.390	0.319
3.0	0.1574		0.590	0.482	0.400
3.5	0.1837		0.685	0.550	0.457
4.0	0.2099		0.801	0.663	0.581

Assuming that the free acid exists only in the monomeric and dimeric forms, the mass balance

$$C_V = [HV] + 2[(HV)_2] \qquad 9.1$$

applies to each standard. If Beers Law is assumed to apply to both monomer and dimer, from 9.1

$$C_V = \frac{1}{l.\varepsilon_{HV}} .OD_{HV} + \frac{2}{l.\varepsilon_{(HV)_2}} .OD_{(HV)_2} \qquad 9.2$$

where ε_{HV} and $\varepsilon_{(HV)_2}$ are the extinction coefficients of the monomer and dimer, and l is the path length of the cell.

For each standard, of known C_V, there were three sets of OD_{HV} and $OD_{(HV)_2}$ measurements, which could be correlated to find the extinction coefficients. Regression analysis of the data in Tables 9.2.1 and 9.2.2 was made. The data obtained at 25°C were omitted because they were outside of the temperature range of interest, and exerted a large influence on the regression equation. The equation derived from all high temperature data was

$$C_V = 0.26467\ OD_{HV} + 0.16296\ OD_{(HV)_2} \qquad 9.3$$

From equation 9.2, using a value of 0.108mm for the cell length, $\varepsilon_{HV} = 3.498 \times 10^4$ OD units mol^{-1} m^{-1}, and $\varepsilon_{(HV)_2} = 11.364 \times 10^4$ OD units mol^{-1} m^{-1}.

The predicted values of C_V, i.e. $\hat{C}_V$ are plotted against the actual values in Figure 9.2(a), and give a reasonable 45° line, which indicates that Beers Law is applicable over the range studied. The residuals are plotted against $\hat{C}_V$ in Figure 9.2(b) and indicate that the experimental error associated with this technique is about 10%. Although the residuals are not randomly distributed, they were considered to be satisfactory in view of the large error.

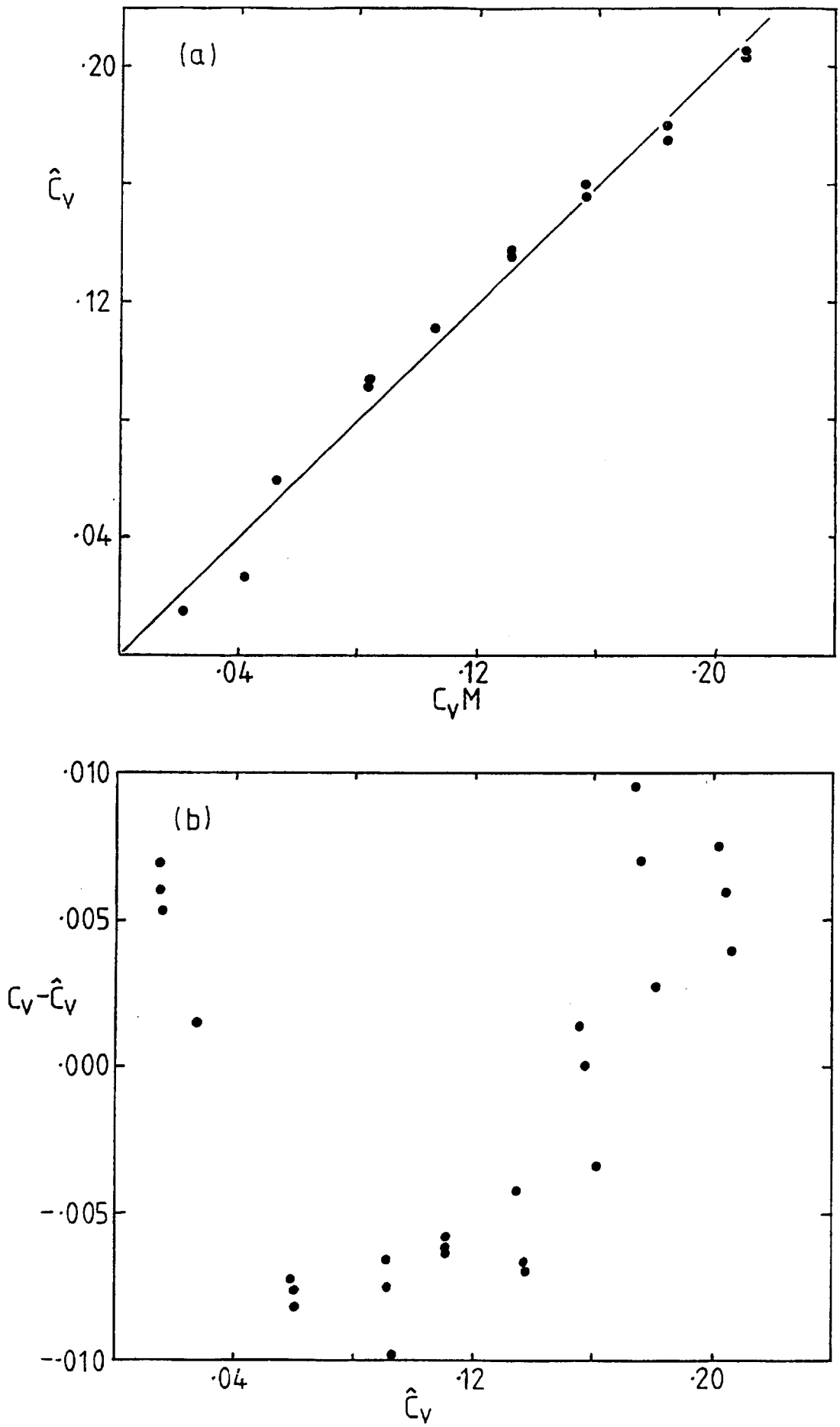


Figure 9.2 (a) Predicted $\hat{C}_V$ versus actual C_V
(b) Plot of residuals versus predicted $\hat{C}_V$

9.2.2 Determination of the Dimer Dissociation Constant

The dissociation of the dimer to the monomer can be represented as

$$(HV)_2 = 2HV \qquad K_{diss} = \frac{\{HV\}^2}{\{(HV)_2\}} \qquad 9.4$$

Simplifying, by replacing thermodynamic activities by analytical concentrations, and applying Beers Law to 9.4 gives

$$K_{diss} = \frac{OD_{HV}^{\ 2}}{OD_{(HV)_2}} \cdot \frac{\varepsilon_{(HV)_2}}{1.\varepsilon_{HV}^{\ 2}} \qquad 9.5$$

Let $r = OD_{HV}^{\ 2}/OD_{(HV)_2}$, which is the experimentally determined part of 9.5. Then

$$\ln K_{diss} = \ln r + \ln\left[\frac{\varepsilon_{(HV)_2}}{1.\varepsilon_{HV}^{\ 2}}\right] \qquad 9.6$$

Because of the relation $\Delta G = -RT \ln K$, a plot of ln r against 1/T should give a straight line, which can be used to find K_{diss}.

The values of ln r calculated for each Versatic standard are given in Table 9.2.3, together with the corresponding value of 1/T. The cell temperature fluctuated by a few degrees during each scan; the value shown in Table 9.2.3 is the temperature noted when the wavelength scan had reached 1750-1700cm^{-1}.

Plots of ln r against 1/T were made for each value of C_V. These verified that the gradient of each plot was independent of the concentration. All the data were then used in a linear regression analysis, which gave the relationship as

$$\ln r = 12.4098 - 5970.4\ (1/T) \qquad 9.7$$

The squared correlation coefficient for this line was 97.0%. The ln r against 1/T plot is shown in Figure 9.3.

C_V(M)	Nom 130°C T°C	$1/Tx10^3$ K^{-1}	ln r	Nom 150°C T°C	$1/Tx10^3$ K^{-1}	ln r	Nom 165°C T°C	$1/Tx10^3$ K^{-1}	ln r
0.0210	130.5	2.477	-2.568	150.5	2.360	-1.683	165	2.282	-1.070
0.0420	130	2.481	-2.572	150	2.363	-1.804	165	2.282	-1.366
0.0525	126	2.505	-2.565	150.5	2.360	-1.664	165	2.282	-1.291
0.0840	129	2.487	-2.498	150	2.363	-1.812	165	2.282	-1.221
0.1050	130	2.481	-2.341	149	2.369	-1.723	165	2.282	-1.239
0.1312	131	2.474	-2.317	150	2.363	-1.597	165	2.282	-1.168
0.1574	130	2.481	-2.294	150	2.363	-1.692	165	2.282	-1.224
0.1837	130	2.481	-2.300	150	2.363	-1.626	166	2.277	-1.173
0.2099	130	2.481	-2.289	150	2.363	-1.655	164	2.288	-1.226

Table 9.2.3 ln r values for nominal temperatures 130°, 150° and 165°C

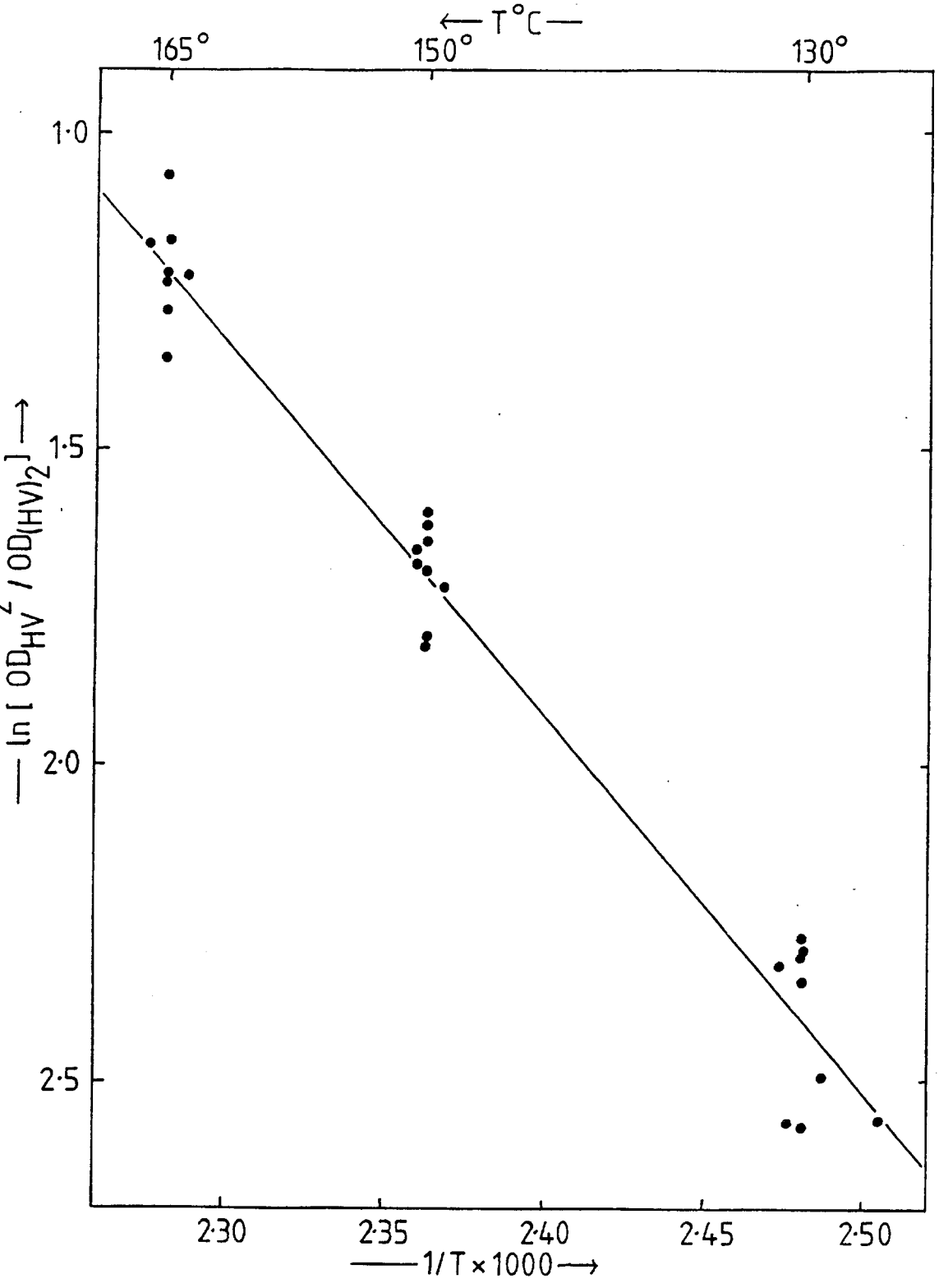


Figure 9.3 Determination of Dissociation Constant: ln r against 1/T

Table 9.2.4 Calculated Dissociation Constants for Various Temperatures

$T^{\circ}C$	K_{diss}(moles)
130°	0.0780
150°	0.1571
160°	0.2176
165°	0.2547

From equations 9.6 and 9.7

$$\ln K_{diss} = \ln r + \ln \left[\frac{\varepsilon_{(HV)_2}}{1.\varepsilon_{HV}^{2}} \right]$$

$$= 12.4098 - 5970.4. \frac{1}{T} + \ln \left[\frac{11.364 \times 10^{4}}{.108 \times 10^{-3} (3.498 \times 10^{4})^{2}} \right]$$

$$\ln K_{diss} = 12.2589 - 5970.4(1/T) \qquad 9.8$$

Equation 9.8 confirms the experimental observation that dissociation increases markedly with increasing temperature. The dissociation constants calculated for 130°, 150°, 160° and 165°C are shown in Table 9.2.4 above.

9.2.3 Effect of Dilution on Free Versatic in Iron-Nickel Solutions

The organic samples to be analysed by infrared spectrophotometry required dilution, to bring the measured optical densities into the linear range. Crabtree and Rice observed that when cobalt-Versatic extracts were diluted, solvated Versatic was released as free Versatic acid[109]. This effect was therefore studied, so that an accurate estimate of the free acid in undiluted samples could be obtained from measurements made on the diluted samples.

Three solutions with 0.2M Fe and 0.1M Ni were examined at 160°C at several dilutions. The measured monomer and dimer optical densities are reported in Table 9.2.5, together with $[HV]_f'$, the concentration of free Versatic, and K_{diss}, the dissociation constant, which was calculated from the optical densities. In Figure 9.4 the $[HV]_f'$ values are plotted against dilution for the three solutions, and it is evident that the measured free acid concentration increases with increasing dilution. This increase is assumed to result from de-solvation.

Three parallel lines were fitted to the experimental points; these had a gradient of 0.0145. The free acid, $[HV]_f$, in an undiluted sample (D=1) could therefore be obtained from the free acid measured in a solution at dilution D, by

$$[HV]_f = [HV]_f' - .0145(D - 1) \qquad 9.9$$

When fitting straight, parallel lines to the experimental points in Figure 9.4, it was implicitly assumed that desolvation is a function only of dilution, and is independent of free acid concentration. This is unlikely to be strictly true. However, no attempt was made to include free acid in the term for de-solvation, because the resulting expression could not have been used to correct the experimental results for samples with unknown free acid.

When fitting lines to the points in Figure 9.4, most weight was given to the points for relatively low dilutions. As dilution increases, the available solvated Versatic acid will decrease, so desolvation is only likely to have a linear effect over a narrow range. There is some indication of a decrease in the gradient of the lines for 25% and 50% Versatic at high dilution. However, all three lines in Figure 9.4 appeared to be linear up to a dilution of 10, which was the highest dilution used for the organic samples.

The dissociation constants calculated from the optical densities are shown in Table 9.2.5, and were below the theoretical value of 0.2176 at 160°C, calculated from equation 9.8. The deviation from the theoretical value appeared to increase with decreasing total

Table 9.2.5 Effect of Dilution on Concentration and Dissociation Constant of Free Versatic Acid at 160°C

Sample	Dilution D	OD_{HV}	$OD_{(HV)_2}$	$[HV]_f'(M)$*	K_{diss}^+
0.2M Fe	4	.252	.360	.501	.1517
0.1M Ni	5	.209	.264	.492	.1423
25%v/v[V]	6.667	.187	.201	.548	.1496
(1.312M)	10	.144	.120	.577	.1486
	20	.083	.037	.560	.1601
0.2M Fe	5.125	.333	.535	.899	.1782
0.1M Ni	6.667	.291	.400	.948	.1821
33%v/v[V]	10	.238	.253	1.042	.1925
(1.749M)	20	.146	.107	1.122	.1713
0.2M Fe	6.667	.443	.790	1.640	.2136
0.1M Ni	10	.350	.525	1.782	.2007
50%v/v[V]	13.33	.307	.360	1.866	.2251
(2.624M)	20	.224	.224	1.916	.1926
	40	.143	.085	2.068	.2069

*$[HV]_f' = D(0.26467\ OD_{HV} + 0.16296\ OD_{(HV)_2})$

+ $K_{diss} = \dfrac{OD_{HV}^2}{OD_{(HV)_2}} \cdot \dfrac{\varepsilon_{(HV)_2}}{1.\varepsilon_{HV}^2}$

K_{diss} = 0.2176 for 160°C from equation 9.8

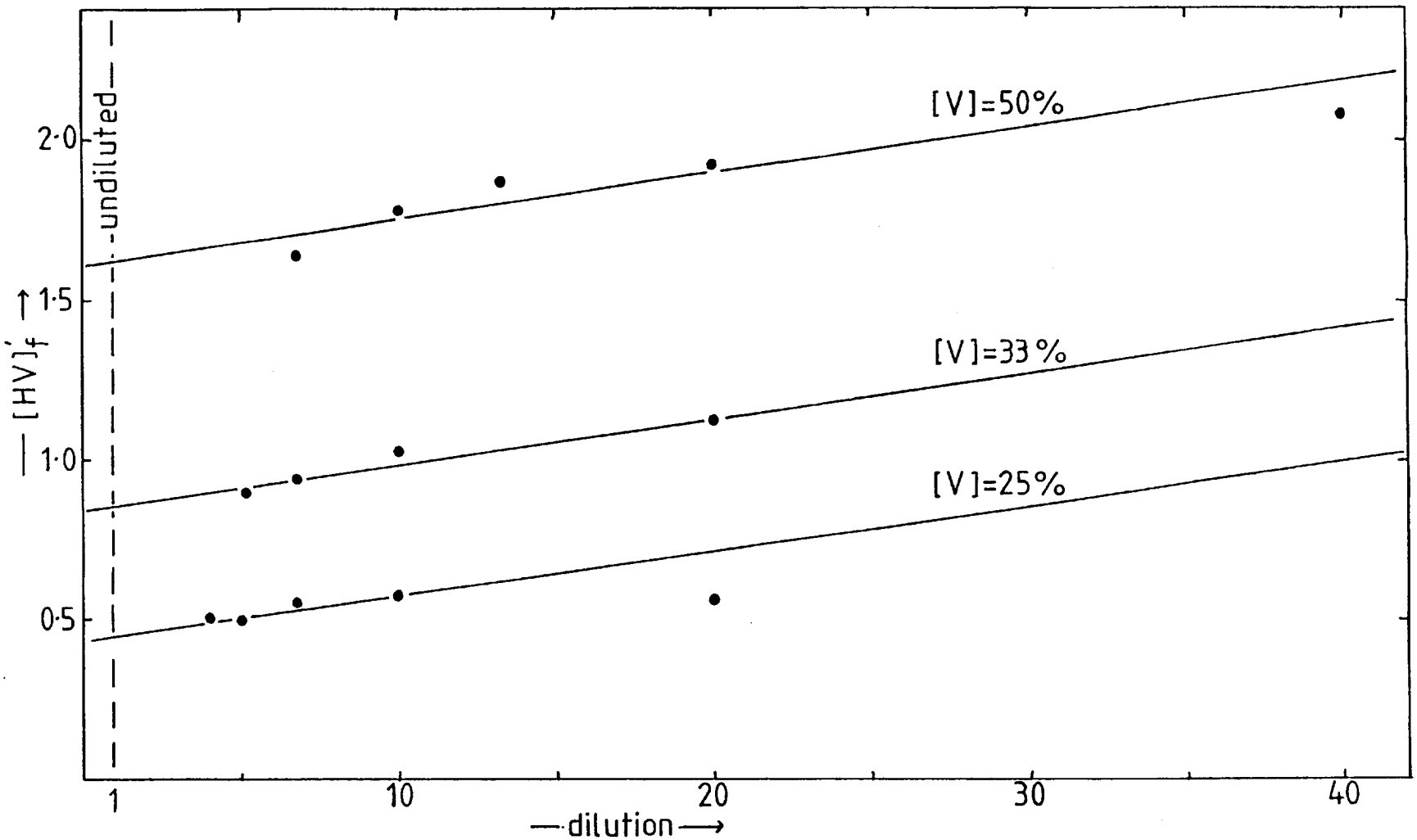


Figure 9.4 Effect of Dilution on Concentration of Free Versatic Acid

Versatic concentration. The reason for the deviation could be associated with the fact that the theoretical dissociation constant, as given in equation 9.8, is not a thermodynamic constant, because it was derived from concentrations, not activities. It can therefore only be expected to be valid for solutions in which the activity coefficients of the monomer and dimer are similar to those in the standards used to determine the constant. It is possible that the presence of metal ions in solution alters the activity coefficients of the free acid species in such a way as to suppress the dissociation of dimers to monomers. The dissociation constant would then be expected to be lowest for the samples with the lowest [V]/M.

It is also possible that the change in dissociation constant is due to experimental error, which appeared to be about 10% for the overall predicted concentration. A factor which could contribute to additional error when measuring the monomer and dimer peaks in metal loaded solutions is the presence of a peak at $1610cm^{-1}$, which might enlarge the dimer peak at $1700cm^{-1}$, and therefore reduce the apparent dissociation constant.

9.2.4 Examination of Organic Samples from Kinetic Runs

The infrared spectra of several organic samples taken from kinetic runs were recorded at $160^{\circ}C$, the temperature at which the runs had been made. Samples were selected to cover the range of iron, nickel and total Versatic concentrations which had been investigated in the kinetic experiments. For most of the runs, only the sample taken at the beginning of the run was examined, so that the initial free acid could be determined and correlated with the initial rate. For three runs, however, samples taken during the course of the run were examined, so that the free acid could be correlated with the metal concentration down to very low concentrations.

The measured optical densities of the monomer and dimer peaks for each sample are presented in Table 9.2.6. The dissociation constant for each sample was calculated, and there is scatter, albeit lower than the deviation observed in section 9.2.3, either side of the theoretical value. This suggests that the discrepancies are due

Run no	t(mins)	Solution [Fe] M	[Ni] M	$[V]_{tot}$ M	Diluted Samples Diln D	OD_{HV}	$OD_{(HV)_2}$	Calculated Values $[HV]_f$*	M_t(M)"	$(V/M_t)^x_{cmp}$	K_{diss}
R45	0	0.198	0.097	1.312	10	0.144	0.120	0.446	.788	1.099	0.1486
R46	0	0.095	0.047	1.312	6.667	0.294	0.350	0.817	.379	1.307	0.2124
R51	0	0.193	0.094	1.7492	10	0.238	0.253	0.912	.767	1.092	0.1925
R50	0	0.097	0.047	1.7492	10	0.309	0.353	1.263	.385	1.264	0.2326
R52	0	0.195	0.098	2.624	10	0.370	0.483	1.636	.781	1.265	0.2437
R54	0	0.100	0.048	2.624	10	0.431	0.635	2.045	.396	1.462	0.2516
R55	1	0.179	0.084	2.3616	10	0.356	0.532	1.679	.705	0.969	0.2049
R56	0	0.100	0.046	2.3616	10	0.371	0.501	1.668	.392	1.770	0.2363
R56	7.5	0.061	0.031	2.3616	10	0.408	0.570	1.878	.245	1.973	0.2511
R48	0	0.098	0.095	1.7492	10	0.272	0.296	1.072	.484	1.400	0.2149
R49	0	0.095	0.099	2.624	10	0.402	0.600	1.911	.483	1.476	0.2316
R47	0	0.184	0.049	1.7492	10	0.268	0.267	1.014	.650	1.131	0.2313
R53	0	0.190	0.051	2.624	10	0.387	0.538	1.771	.672	1.270	0.2394
R24	0	0.188	0.093	1.7492	10	0.215	0.227	0.809	.750	1.254	0.1751
R24	17.5	0.060	0.030	1.7492	10	0.318	0.376	1.324	.240	1.772	0.2313
R24	56	0.005	0.003	1.7492	10	0.354	0.466	1.566	.021	8.733	0.2313
Fe Versatic		0.38	-	1.7492	10	0.228	0.220	0.832	1.14	0.805	0.2032
Ni Versatic		-	0.34	1.7492	10	0.180	0.154	0.597	.680	1.695	0.1809
R57	1	0.107	0.079	1.7492	10	0.271	0.325	1.116	.479	1.321	0.1943
R57	17.5	0.060	0.049	1.7492	10	0.310	0.409	1.357	.278	1.413	0.2021
R57	35	0.027	0.031	1.7492	10	0.332	0.433	1.454	.143	2.066	0.2189
R57	75	0.008	0.023	1.7492	10	0.341	0.470	1.538	.070	3.019	0.2128

*$[HV]_f = D(.26467\ OD_{HV} + .16296\ OD_{(HV)_2}) - .0145(D-1)$ "$M_t = 3[Fe] + 2[Ni]$

x$[V/M_t]_{cmp} = ([V]_{total} - [HV]_f)/M_t$

Table 9.2.6 Organic Samples from Kinetic Runs: Optical Densities, Free Acid and Average Complex Composition

Table 9.2.7 Free Acid Concentration and Initial Rate of Selected Kinetic Runs

Run No	(nominal conc) $[Fe]_o$ M	$[Ni]_o$ M	$[HV]_f$ M	$1/[HV]_f$	Initial Rate M min^{-1}
R45	0.2	0.1	0.446	2.242	.0678
R46	0.1	0.05	0.817	1.224	.0285
R51	0.2	0.1	0.912	1.096	.0300
R50	0.1	0.05	1.263	0.792	.0153
R52	0.2	0.1	1.636	0.611	.0112
R54	0.1	0.05	2.045	0.489	.0072
R56	0.1	0.05	1.668	0.600	.0109
R48	0.1	0.1	1.072	0.933	.0126
R49	0.1	0.1	1.911	0.523	.0027
R47	0.2	0.05	1.014	0.986	.0288
R53	0.2	0.05	1.771	0.565	.0175
R57	0.1	0.1	1.116	0.896	.0081

to experimental error only, and not to a change in activity coefficients as suggested in the previous section. The concentration of free acid was calculated by the relation

$$[HV]_f = D(.26467\ OD_{HV} + .16296\ OD_{(HV)_2}) - .0145(D-1) \quad 9.10$$

which was obtained from equations 9.3 and 9.9.

The initial free acid concentrations and initial rates of the kinetic runs are shown in Table 9.2.7 above, and the data are plotted in Figures 9.5 and 9.6.

In Figure 9.5 the experimental points for the runs where the iron to nickel ratio was 2 all appear to lie on a single curve. This is in marked contrast to Figure 8.11, where the rates for these runs were plotted against total Versatic concentration, and gave distinctly different curves for the two concentration levels. Figure 9.6 indicates that when iron and nickel are in a stoichiometric ratio, the initial rate is independent of metal concentration and linearly

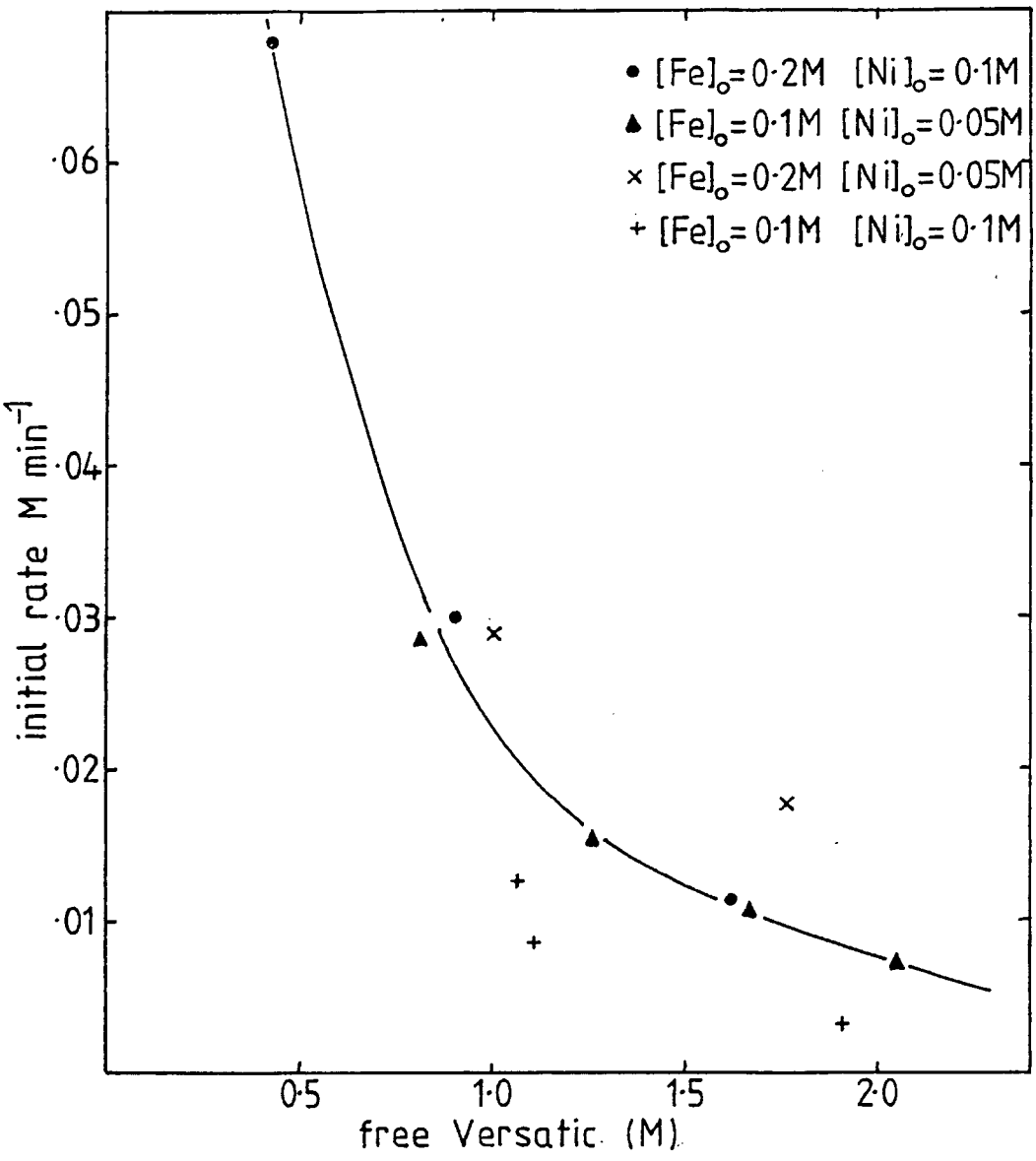


Figure 9.5 Initial Rate against Free Versatic Concentration for Kinetic Runs

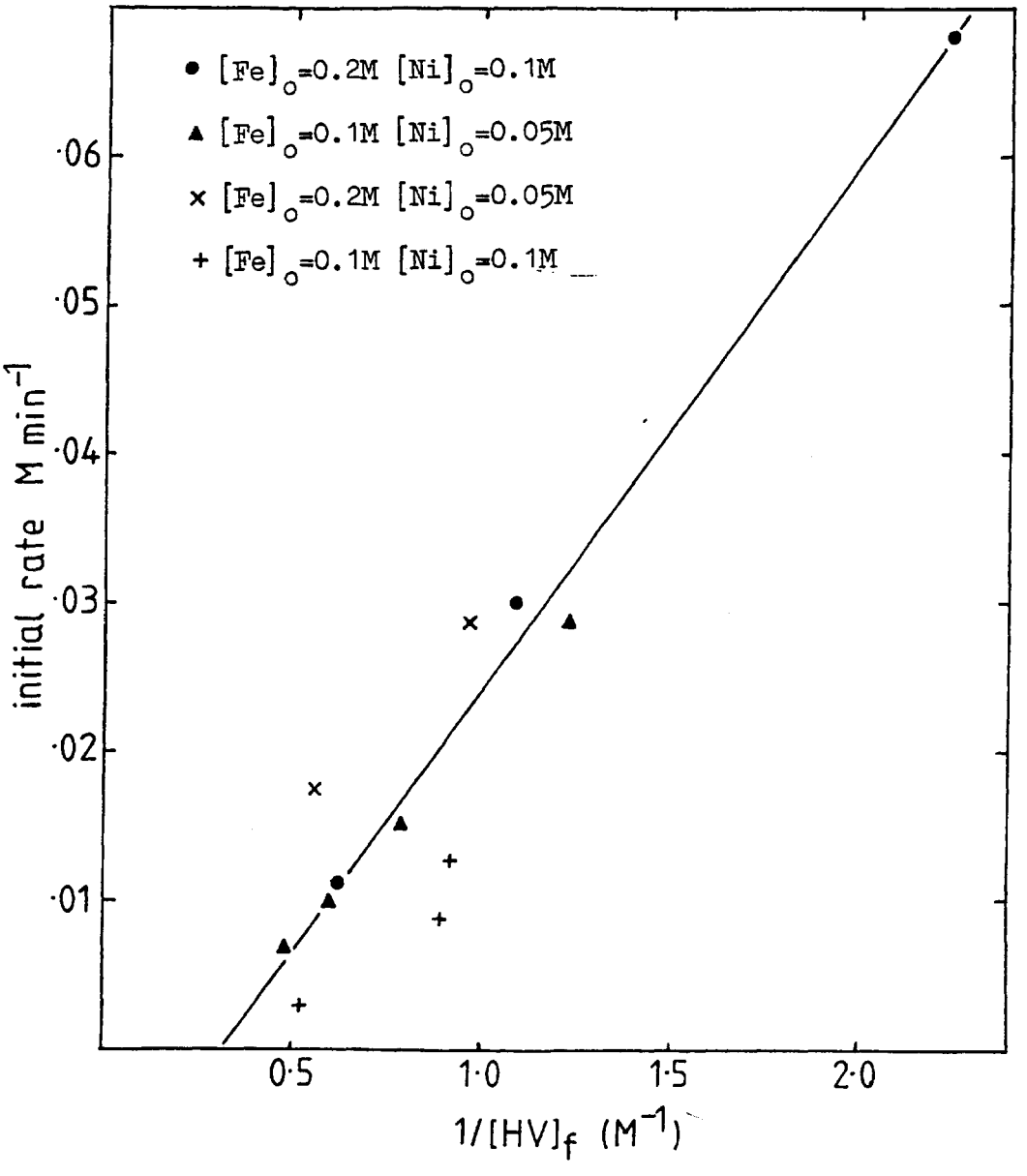


Figure 9.6 Initial rate against $1/[HV]_f$ for Kinetic Runs

dependent on $1/[HV]_f$. This suggests that the rate determining step in precipitation of nickel ferrite is desorption of free Versatic acid from the seed surface. However, there were large errors in the infrared measurements used to estimate the free acid, as demonstrated by the magnitude of the residuals in Figure 9.2(b), and by the scatter of the calculated dissociation constants ($\pm$ 20-25% of the theoretical value). Therefore it would be useful to examine more samples, taken both from runs made at 160°C using 100% seed, and from runs made at other temperatures, seed levels and metal concentrations, to verify that the initial rates are independent of metal concentration for a wide range of experimental conditions.

In Figures 9.5 and 9.6, the experimental points for the two runs where the iron to nickel ratio was 4 lie above the lines for stoichiometric concentrations. The points for the runs where the ratio was 1 lie below the lines. This is in agreement with the qualitative results obtained in the factorial design, which indicated that the iron to nickel ratio in the organic solution determined the behaviour during hydrolytic stripping.

9.3 COMPOSITION OF MIXED-METAL VERSATIC COMPLEXES

Each of the organic solutions examined in the previous section is likely to contain a range of mixed complexes, with iron to nickel ratio corresponding approximately to the ratio in the bulk composition, and with varying solvation, hydrolysis, hydration and polymerisation numbers. Although the composition of individual complexes could not be determined by infrared spectrophotometry, the average composition was determined from the metal concentration of each solution, and the difference between the total and free Versatic. To take into account the different valencies of iron(III) and nickel (II), the quantity M_t, defined by

$$M_t = 3[Fe] + 2[Ni] \qquad 9.11$$

was evaluated for each solution. It should be noted that $M_t = 2xO.E$ where O.E is the 'oxygen equivalent' used to combine iron and nickel concentrations in the kinetic runs, before polynomial fitting. The

average composition of the complexes in each solution was then calculated as

$$(V/M_t)_{cmp} = (V_{total} - [HV]_f)/M_t \qquad 9.12$$

This gives the average number of Versatic groups, either anions or solvating acid, associated with each cation charge in the complexes in solution. This parameter is shown in Table 9.2.6 for each of the solutions studied. It can be seen that this ratio is greater than 1 for all but two of the solutions listed, which indicates that there is solvating acid in most complexes, in addition to the Versatic anions necessary to satisfy the valency of the cations. The metal complexes probably contain some OH^-, however, and the concentration of this in the solutions was not determined. The relative proportions of Versatic anion and solvating acid in the complexes could therefore not be found.

The results from Table 9.2.6 are shown in Figure 9.7 and define a narrow band of possible complex compositions for a given metal concentration. The Versatic associated with each metal charge in the organic complexes decreases rapidly as the total metal concentration increases from zero. The Versatic to metal ratio in the complexes does not appear to be affected by the iron to nickel ratio in the solution.

The decrease in associated Versatic with increasing total metal concentration could be due to an increase in the number of OH^- ions in the complexes, but is probably largely due to solvated acid, which is assumed to be in equilibrium with the free acid. At low metal concentrations there is a high concentration of free acid, hence there can be high levels of solvated acid associated with the metal in the complexes. As the metal concentration increases, the free acid of a given solution decreases, so de-solvation occurs. A steady Versatic to metal ratio of 1.1 - 1.3 appears to be reached at high metal concentrations. For solutions with iron to nickel ratio of 2, this corresponds to complex compositions $(Fe_2Ni(OH)_mV_{8-m}.sHV.qH_2O)_x$ where s = 1+m or 2+m, for example $(Fe_2NiV_8.2HV)_x$ and $(Fe_2Ni(OH)_2V_6.4HV)$.

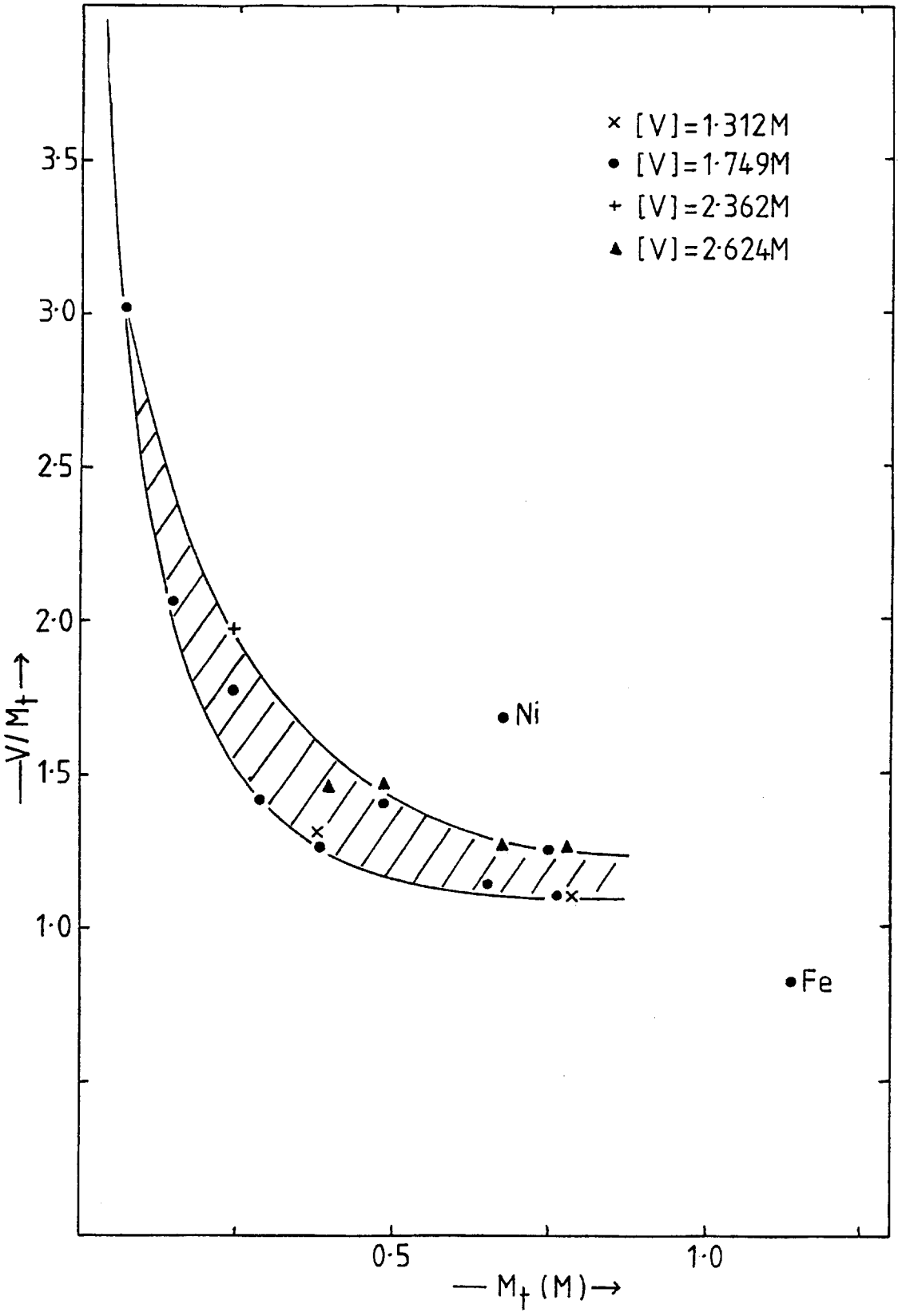


Figure 9.7 Versatic to Metal Charge Ratio in Complexes as a Function of Total Metal Charge

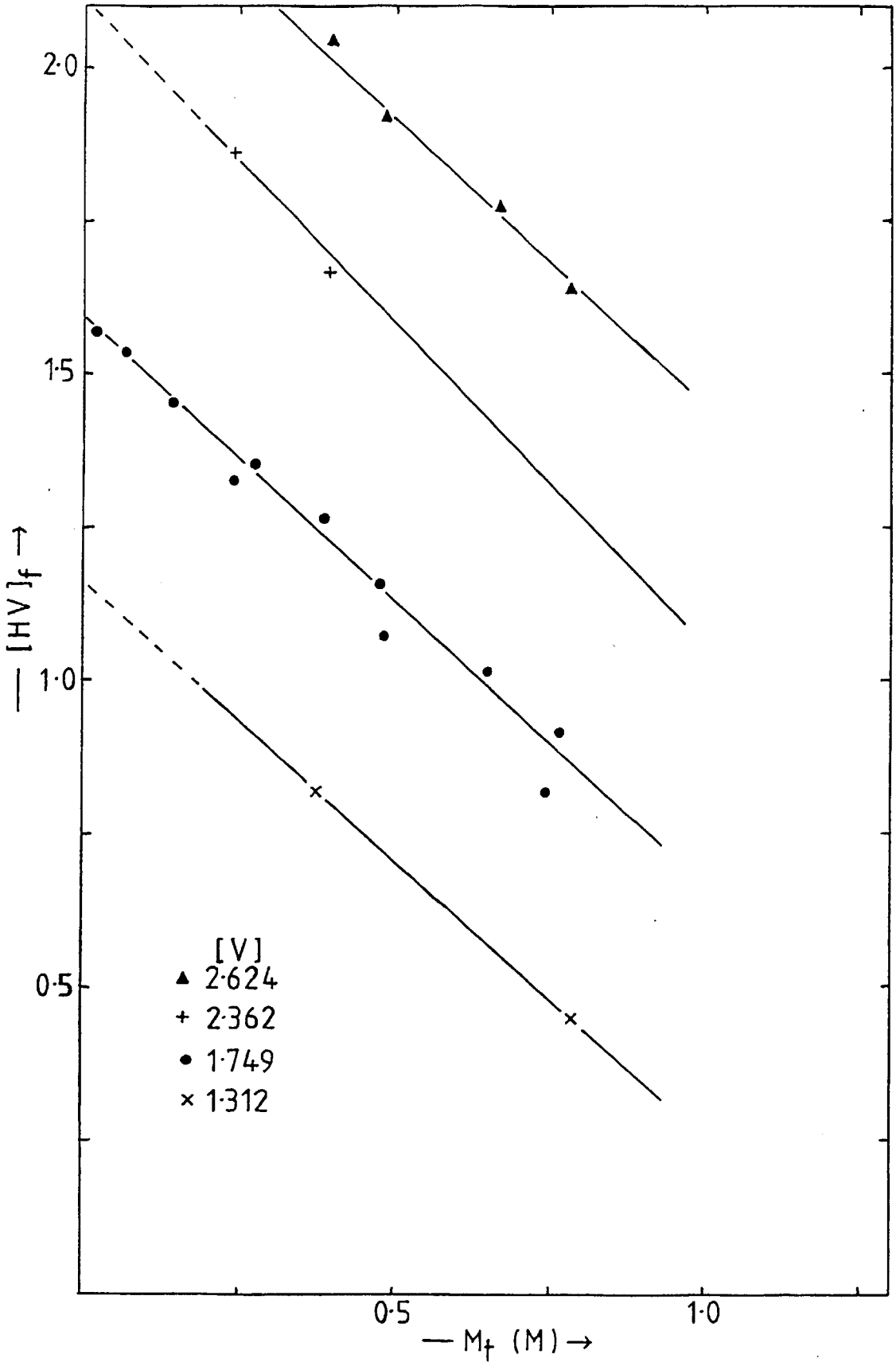


Figure 9.8 Plots of Free Versatic against Total Metal for Different Total Versatic Concentrations

Values of free Versatic concentration are plotted against the total metal concentration in Figure 9.8. These values appear to lie on four roughly parallel straight lines, which correspond to the four different total Versatic concentrations used. These have gradients of -0.91 to -1.07, which is in reasonable agreement with the value 1.1 - 1.3 for Versatic to metal ratio in the complexes at high metal concentration.

The intercept of each line at the vertical axis is approximately 0.15M below the total Versatic concentration. This is because at low metal concentrations $(V/M_t)_{cmp}$ becomes large, and the plots will become non-linear. Thus, although these curves are likely to be useful for predicting the free Versatic concentration in solutions with known metal concentrations, they are unlikely to give accurate results at low metal concentrations.

9.4 INFRARED SPECTRA OF METAL VERSATIC SOLUTIONS

The infrared spectra of iron-Versatic, nickel-Versatic and iron-nickel Versatic solutions at 25° and 160°C are shown in Figures 9.9, 9.10 and 9.11 respectively. The higher optical densities at 160°C are due to the solutions being more concentrated, and do not indicate that the extinction coefficients are temperature dependent. There is a slight shift in some of the peaks towards lower frequency at 160°C, and the free monomer peak emerges at 1750cm^{-1}; otherwise the traces are essentially similar at both temperatures.

The iron-Versatic shows an inflection at 1685cm^{-1} due to solvated Versatic acid, and main peaks at 1575 and 1418cm^{-1}. These have been tentatively assigned to bidentate chelating and bidentate bridging by Stefanakis[48].

The nickel-Versatic shows peaks at 1665 and 1590cm^{-1}. The peak at 1590cm^{-1} is probably due to monodentate coordination. The 1665cm^{-1} peak is difficult to assign, since it is rather too intense, and at too low a frequency to be due to solvating acid. Figure 9.7 suggests that there is more solvated Versatic in nickel complexes than in iron complexes, which could account for the higher optical

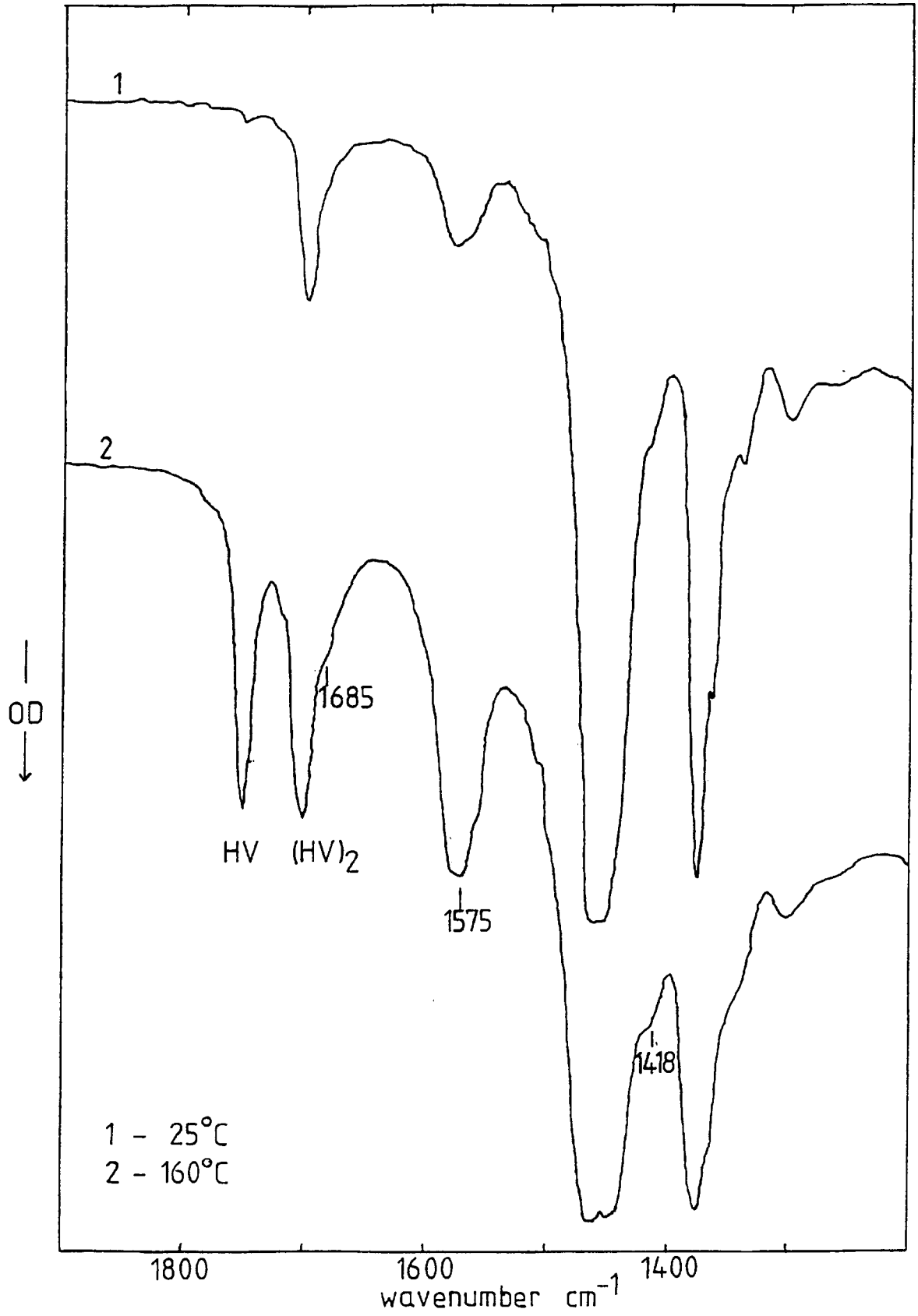


Figure 9.9 Infrared Spectrum of Iron-Versatic (carbonyl range)

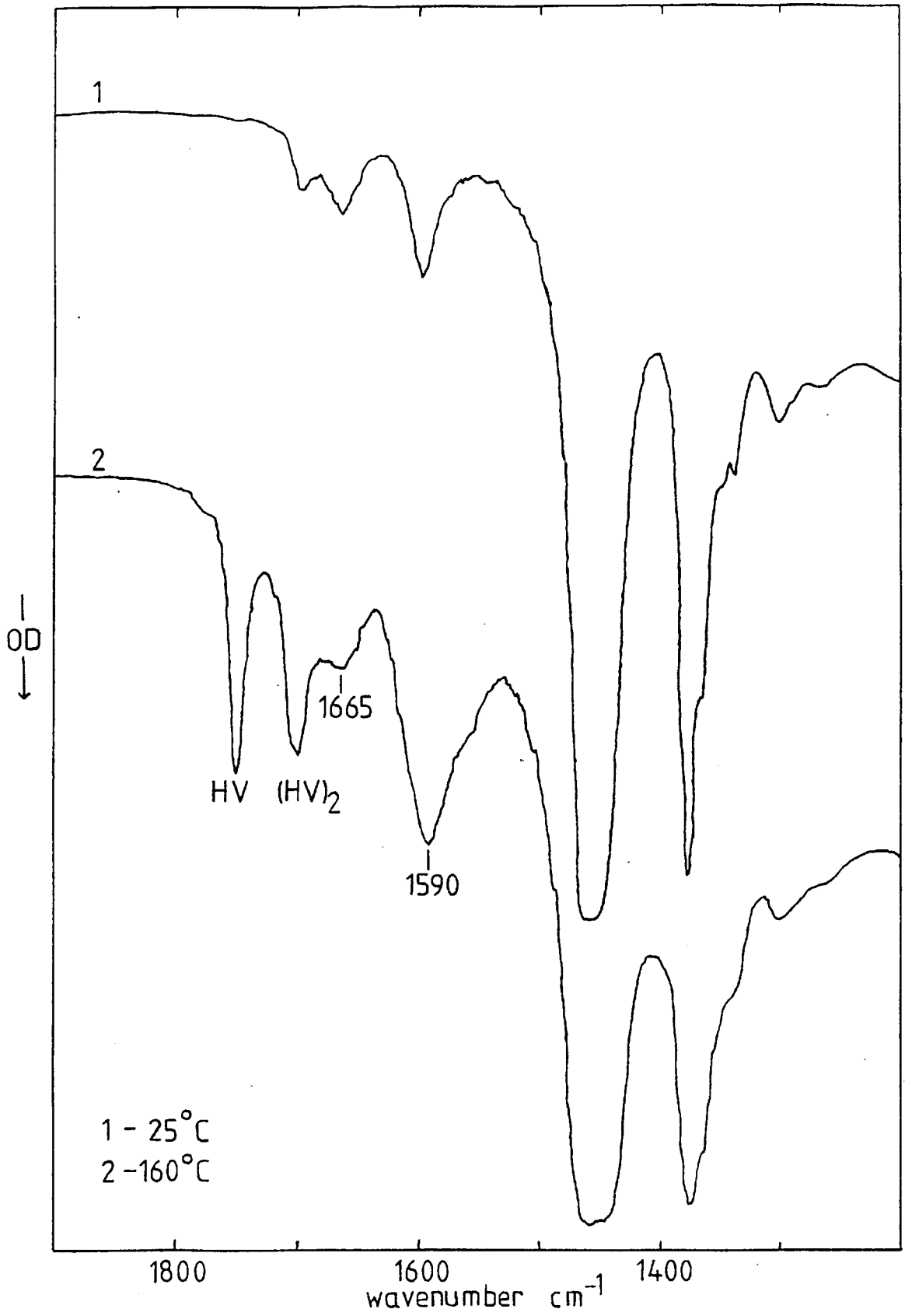


Figure 9.10 Infrared Spectrum of Nickel-Versatic (carbonyl range)

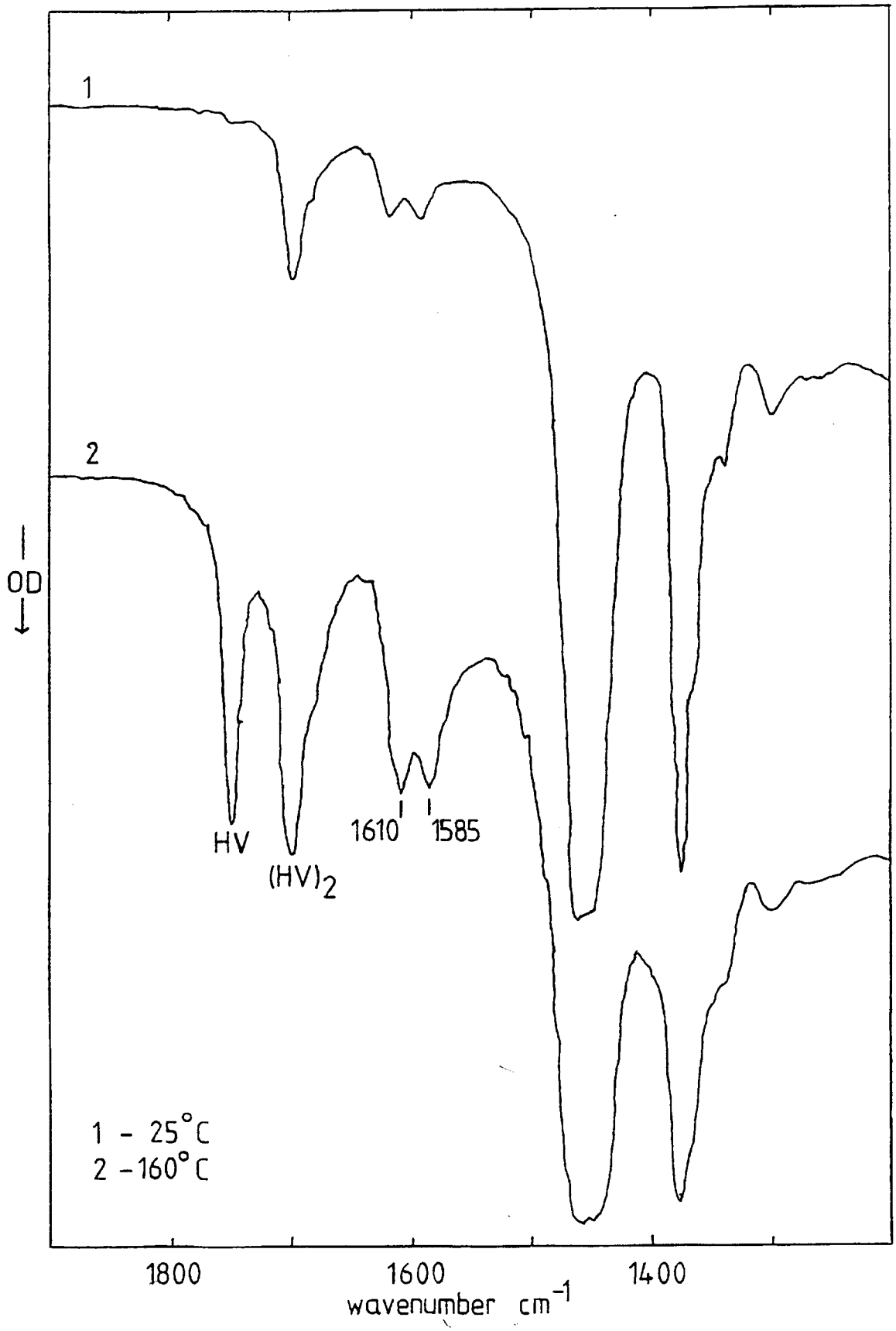


Figure 9.11 Infrared Spectrum of Iron-Nickel Versatic

density. However, if there were more solvating molecules in each nickel complex, the bonding between these molecules and the complex would be expected to be weaker than in the iron complexes. This would increase the carbonyl absorption frequency, not decrease it.

The iron-nickel Versatic complex shows none of the peaks of either iron, or nickel-Versatic; there are two main peaks at 1610 and 1585cm^{-1}. These are probably due to monodentate complexing and bidentate chelating respectively. The fact that both peaks are at a slightly higher frequency than the peaks for the same type of complexing in the single metal complexes indicates that the carbonyl bond is slightly stronger for the ligands in the mixed metal complexes, probably because coordination is weaker.

Figure 9.12 shows the traces of 10% solutions of samples containing (a)0.2M Fe, 0.05M Ni, (b)0.1M Fe, 0.05M Ni and (c)0.1M Fe, 0.1M Ni, all with 33% total Versatic. When the iron to nickel ratio is at the stoichiometric level of 2, i.e.(b), the 1610 and 1585cm^{-1} peaks have similar optical density. When iron is in excess, i.e.(a), the 1585cm^{-1} peak increases at the expense of the 1610cm^{-1} peak, suggesting that the amount of bidentate chelation increases and the amount of monodentate complexing decreases. There is no evidence of the 1575 and 1418cm^{-1} peaks which are characteristic of iron-Versatic. When nickel is in excess of the stoichiometric ratio, i.e.(c), the 1610cm^{-1} peak increases at the expense of the 1585cm^{-1} peak, which indicates that there is a preponderance of monodentate complexing. There is no evidence of the 1665 and 1590cm^{-1} peaks which are characteristic of nickel-Versatic.

It is clear from these observations that mixed iron-nickel Versatic solutions are not composed of a mixture of iron and nickel complexes, even when one of the metals is present in excess. Mixed complexes are formed. Monodentate coordination, which occurs in nickel complexes, predominates in nickel-rich mixed complexes, while bidentate chelation, which occurs in iron complexes, predominates in iron-rich mixtures. However, both types of complexing are always present, and the bond strengths of the ligands in the mixed complexes are different from the strengths of the ligands in either single metal complex.

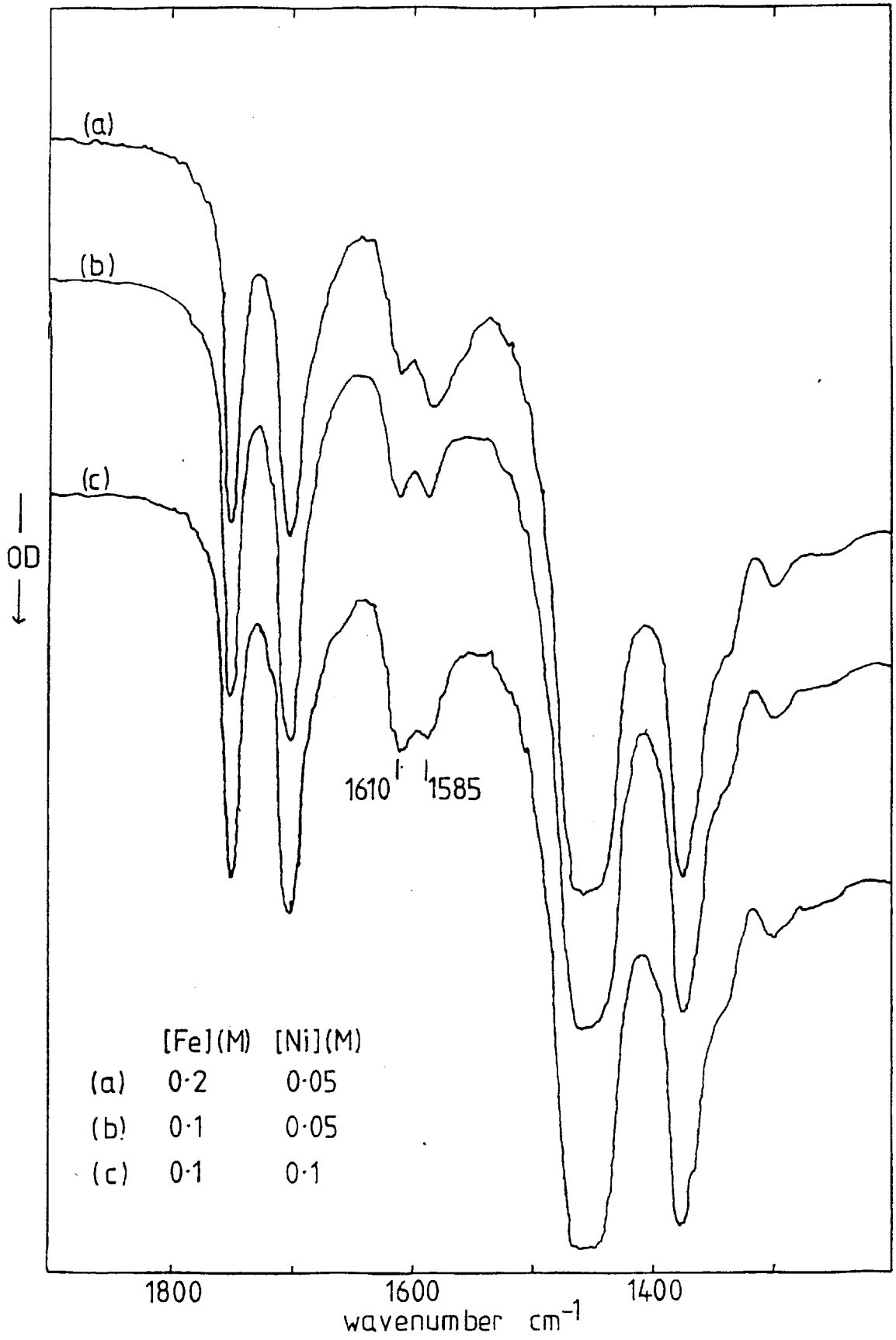


Figure 9.12 Infrared Spectra of 33% Versatic Solutions With Varying Iron and Nickel Concentrations

It was not possible to assign structures to the mixed iron-nickel complexes on the basis of the high frequency infrared measurements made, because these only yield information about the ligands in the complexes. Low frequency infrared measurements, which give information on metal-ligand bonding, and UV-visible spectroscopy, which would have given some indication of the coordination of the metals in the complexes would also be needed before a structure could be postulated.

Nevertheless, for the purpose of this project, the qualitative infrared work was valuable in that it gave direct evidence of the existence of mixed metal complexes, which have had to be assumed to exist to account for experimental results throughout the work.

CHAPTER 10

ADDITIONAL EXPERIMENTAL WORK

10.1 SURFACE AREA MEASUREMENTS

10.1.1 Experimental Method

The specific surface areas of the seed material, and of samples of nickel ferrite precipitated under various conditions, were measured using a Monosorb instrument (Quantachrome). The instrument utilises the fact that at low temperatures (liquid nitrogen), solids adsorb a monolayer of nitrogen, whereas at room temperature, adsorption is negligible.

Samples to be measured are placed in a Pyrex U-tube, through which a mixture of 70% helium + 30% nitrogen is passed. The gas is then passed through a thermal conductivity cell, which measures variations in the nitrogen partial pressure. The sample is first cooled in liquid nitrogen, to allow nitrogen to be adsorbed onto the surface from the gas stream. When equilibrium is established, the sample is rapidly brought back to room temperature, and the amount of nitrogen desorbed from the sample is measured.

The instrument is calibrated by injecting 1ml of air into the gas stream just before it enters the conductivity cell. When properly adjusted, the instrument gives a direct reading of the total surface area of the sample. To eliminate any surface contaminants, samples were heated to about 200°C in the helium/nitrogen stream for about 30 minutes before measuring the surface area.

10.1.2 Results of Surface Area Measurements

The specific surface areas of the seed material used throughout the kinetic work, and of the precipitates from the factorial design, are presented in Table 10.1.1.

For each sample, the instrument measurements had a maximum

Table 10.1.1 Surface Area of Seed, and Precipitates from Factorial Design

Run No	T°C	$[Fe]_o$ M	$[Ni]_o$ M	[V] %	Specific Surface Area of Product m^2/g 1	2
SEED MATERIAL USED IN ALL RUNS					65.45	
R50	160°	0.1	0.05	33	28.29	
R47	160°	0.2	0.05	33	17.14	39.32
R48	160°	0.1	0.1	33	32.69	43.54
R51	160°	0.2	0.1	33	26.84	
R54	160°	0.1	0.05	50	34.46	
R53	160°	0.2	0.05	50	24.01	
R49	160°	0.1	0.1	50	37.29	

scatter of ±1.5%. As the duplicated samples of material from runs R47 and R48 show, however, there was a very large discrepancy between different samples of the same material. The reason for this is that all the precipitates caked to some extent during filtration, probably mainly because of magnetic attraction between the particles. Before making area measurements the caked material was placed between papers, and a roller was passed over the top, so that the agglomerates were subjected to a vertical force, with a minimal shear component which might break up primary particles. Some of the agglomerates were very hard, and it seemed most unlikely that the rolling operation could break up the agglomerates into individual particles. The specific surface area, as measured, was therefore likely to depend only on the sample preparation, and give little indication of the area of the interface between the organic solution and the precipitate during the kinetic runs. No attempt, therefore, was made to investigate the effects of different experimental conditions on the final precipitate area.

The specific surface area measured for the seed was meaningful, because this material had been ground and sized before use, and no further treatment was given before measuring the surface area. Since the specific surface area was $65.45 m^2/g$, the 100% level of seed used in most runs had a total area of $307 m^2$.

To obtain some idea of the changes occurring during a typical kinetic run, the thickness of the ferrite layer deposited was calculated, assuming that a coherent deposit formed over the whole surface, and that there was no change in surface area with time (Appendix E). In runs where the initial iron and nickel concentrations were 0.2M and 0.1M respectively, the layer would be about 3.4 unit cells, or 28Å in thickness.

If the seed is assumed to be composed of uniform spheres, these would be of radius 85Å to account for the measured surface area (see Appendix F). If the particles were spheres, in a typical run where the seed weight doubles, the surface area would increase to $2^{\frac{2}{3}}$ or 1.59 times the original area.

In practice, it is unlikely that the deposit would be a uniform coherent deposit which would leave the surface area unchanged. If the seed surface was porous, the pores could become infilled, lowering the surface area. It is also unlikely that the seed particles grow exactly as uniform spheres, so no accurate prediction of precipitate surface area can be made.

10.2 X-RAY POWDER DIFFRACTION ANALYSIS

In runs where there was a possibility that a phase other than nickel ferrite could have precipitated, the product was analysed by X-ray powder diffraction analysis.

Runs R5 - R16 were made with a variety of materials, to test their ability to seed precipitation. The X-ray patterns of the products from these runs all showed mixtures of the 'seed' material and nickel ferrite. There was no evidence of other phases forming preferentially.

In the factorial design, three different iron to nickel ratios were used, and it was quite possible that hematite or nickel hydroxide could have formed under iron-rich or nickel-rich conditions. There was no evidence of this. The concentration-time curves showed that an iron-rich product was precipitated when the iron to nickel ratio was 4; since the precipitate showed only the spinel ferrite lines this product was assumed to be intermediate between maghemite and nickel ferrite. There was no evidence of nickel hydroxide in the product of the runs where the iron to nickel ratio was 1. Since nickel hydroxide has two very strong lines for d spacings of 4.605 and 2.334Å, this phase would have been detected at very low percentages.

The X-ray patterns for nickel ferrite were the same as those in Appendix B. The measured patterns for other materials were standard, as given in the JCPDS file[101].

10.3 ELECTRON MICROSCOPY

10.3.1 Specimen Preparation

Two electron microscopes were used to examine the ferrite precipitates, a Jeol Temscan, in which specimens can be examined in transmission and scanning modes, at high magnification (good resolution up to 100K and poorer resolution at higher magnification), and a Jeol T200 scanning microscope, which is of much lower power.

Entirely different sample preparation techniques were needed for the two microscopes. For examination in the Temscan, specimens had to be mounted on a medium transparent to the electron beam. Carbon film, supported on fine mesh copper grids about 3mm in diameter, was used. The carbon film was prepared by evaporating carbon onto a clean microscope slide conditioned with detergent, and floating the film off the slide, in water. The film was then lifted from the surface of the water onto the copper grids. Samples of the materials to be examined were dispersed in acetone, using an ultrasonic bath, then sprayed through a nebuliser onto carbon-coated grids held about 0.5m away. For transmission microscopy it was essential that the film was not heavily coated with sample. Another carbon film was then

evaporated over the specimens. This was needed to conduct away any absorbed electrons, because if samples are allowed to charge up the electron beam is distorted, which results in a poor image. The carbon film was also needed to mechanically hold the particles in place, because there are strong magnetic fields within the microscope, for focussing the beam, and any magnetic powders attracted into these fields would have distorted the image.

For examination on the T200, specimens were mounted on solid aluminium stubs. Samples of the material to be examined were dispersed in acetone, then a few drops of suspension were placed on each stub and allowed to evaporate. A carbon film was then evaporated over the specimens, to prevent charging, and to hold the powders in place.

10.3.2 Examination of Precipitates

Figures 10.1 and 10.2 were taken at 130K magnification in the transmission mode on the Temscan; therefore the darkness of features gives an indication of their thickness. Figure 10.1 shows homogeneously nucleated material precipitated at 170°C. This consists of roughly spherical clusters, about .07-.10μm in diameter. Within these clusters, some areas are clearly darker, and therefore thicker, than others. The darker areas within the clusters appear to be due to smaller particles of about .01-.02μm (or 100-200Å) diameter. The electron diffraction pattern of one of these clusters showed a series of concentric circles, each composed of a large number of spots. One of the brighter spots was identified as part of the diffraction pattern of a single ferrite particle about 200Å in diameter. The diffraction observations suggest that the small particles are crystallites, with a single crystallographic orientation, and that these crystallites are randomly oriented within the clusters. This indicates that the scheme of precipitation is very similar to that proposed by Dousma and de Bruyn, i.e. nucleation of small primary particles, agglomeration, flocculation and precipitation[79]. Each cluster appears to be surrounded by a halo; this is probably organic material adsorbed on the surface of the precipitates.

Figure 10.2 shows material heterogeneously precipitated at 140°C. The smallest particles visible are about 160Å in diameter; these are presumed to be crystallites, but there is clearly less pronounced clustering of the crystallites in this sample than in the homogeneously nucleated sample shown in figure 10.1. The size of these particles is significant, since it corresponds closely to the particle size (85Å radius) predicted in section 10.1 from the surface area of the seed material. The clarity of the image in Figure 10.2 is severely impaired by a halo around each particle, and the figure illustrates the 'bunching' of particles which was a problem encountered with all the specimens prepared for microscopic examination. Although care was taken to disperse the powders in acetone, the magnetic attraction between the particles caused them to bunch together in suspension while being sprayed onto the carbon film, or while the acetone was evaporating from the aluminium stubs. It was therefore very difficult to observe single particles.

Figures 10.3 and 10.4 were taken at 50K magnification in the scanning mode on the Temscan microscope, so only the surface morphology is revealed. Figure 10.3 shows the seed material. There is a large agglomerate of irregular clusters, which have a size distribution of .03-.10μm. This agglomerate is unlikely to have developed by 'bunching' during spraying -- it is more likely that the clusters were held together quite strongly, and were not separated during ultrasonic treatment. A few individual clusters can also be seen. Figure 10.4 shows the homogeneously precipitated material which was shown in transmission in Figure 10.1. Two chains of rounded clusters are visible. Chains were seen in several samples. They could be formed by magnetic attraction between the clusters during specimen preparation, or could indicate that the material precipitated by anisotropic flocculation, as discussed by Dousma and de Bruyn[79]. The clusters visible in Figure 10.4 are about 0.1μm in diameter. No surface detail can be seen on each cluster; this could be because the surface contamination, which gave haloes on the transmission micrographs, masks the irregularities caused by the crystallites within the clusters.

Figures 10.5 - 10.12 were obtained on the T200 microscope, and are therefore at much lower magnification than Figures 10.1 - 10.4.

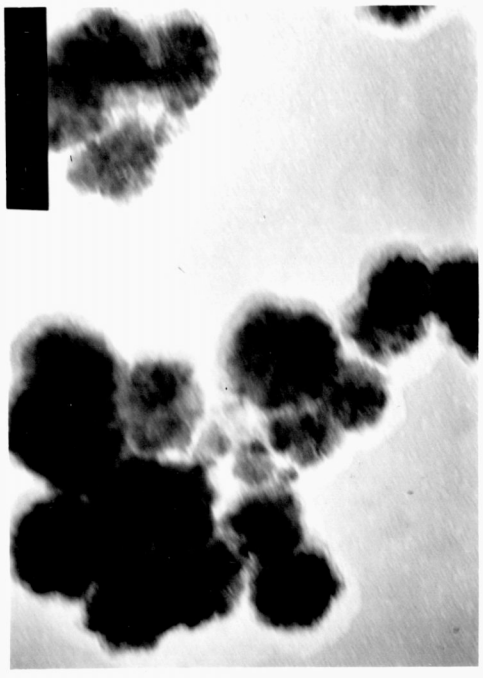


Figure 10.1 : Magn 130K

Transmission mode
T = 170°C
[Fe] = 0.2M
[Ni] = 0.1M
[V] = 33%
Unseeded

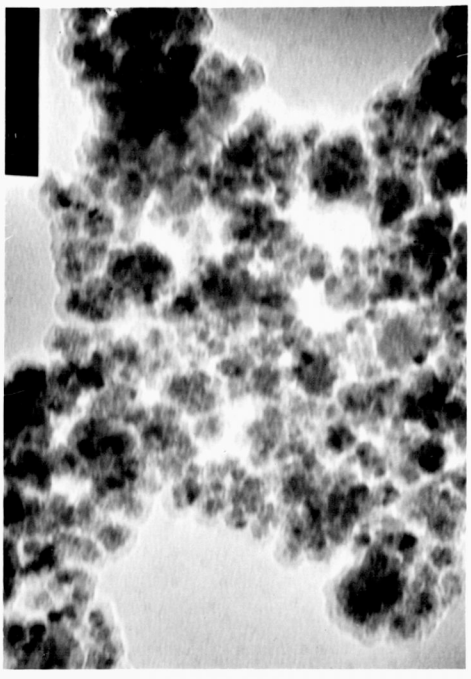


Figure 10.2 : Magn 130K

Transmission mode
T = 140°C
[Fe] = 0.2M
[Ni] = 0.1M
[V] = 33%
Seed: 4.69g $NiFe_2O_4$

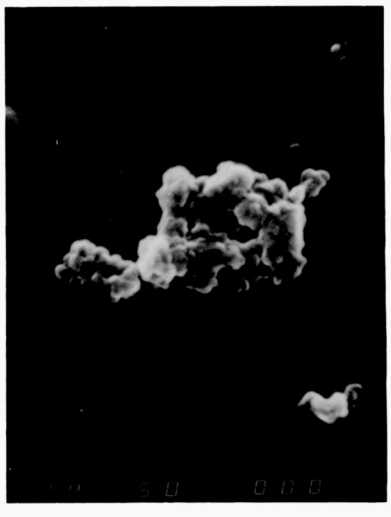


Figure 10.3 : Magn 50K

Scanning mode

Seed $NiFe_2O_4$

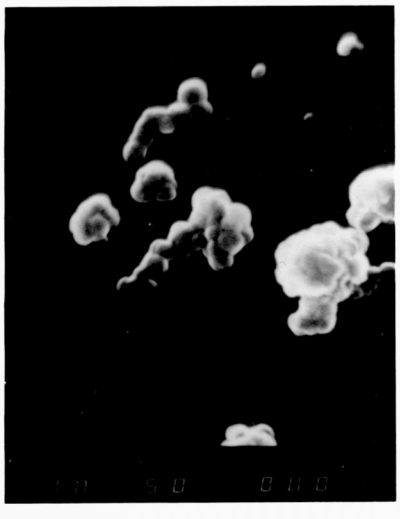


Figure 10.4 : Magn 50K

Scanning mode
T = 170°C
[Fe] = 0.2M
[Ni] = 0.1M
[V] = 33%
Unseeded

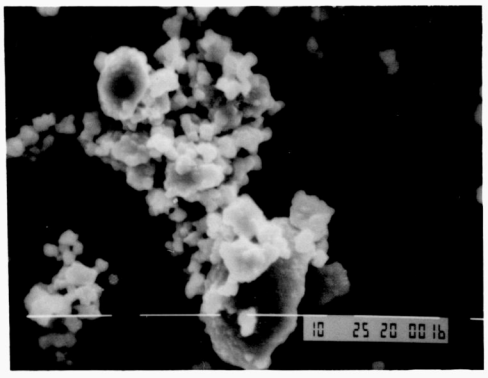


Figure 10.5 : Magn 2K

T = 170°C
[Fe] = 0.2M
[Co] = 0.1M
[V] = 33 %
$CoFe_2O_4$

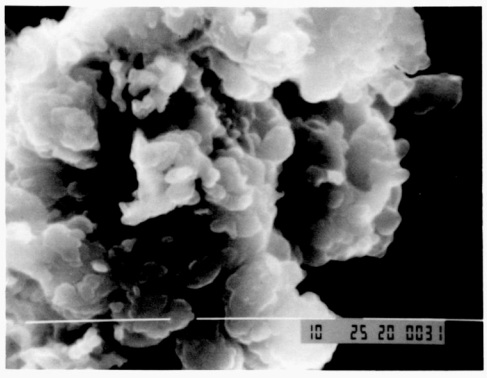


Figure 10.6 : Magn 3.5K

T = 170°C
[Fe] = 0.2M
[Ni] = 0.1M
[V] = 33 %
Unseeded

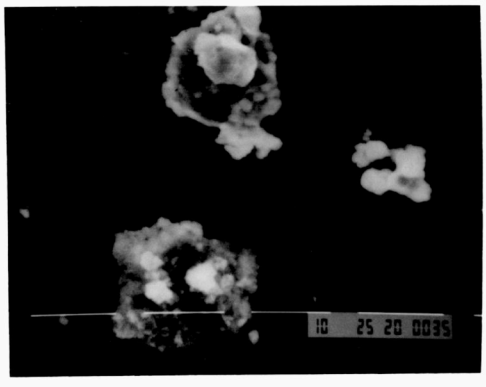


Figure 10.7 : Magn 2K

T = 170°C
[Fe] = 0.2M
[Ni] = 0.1M
[V] = 33 %
Seed: 4.69g $NiFe_2O_4$

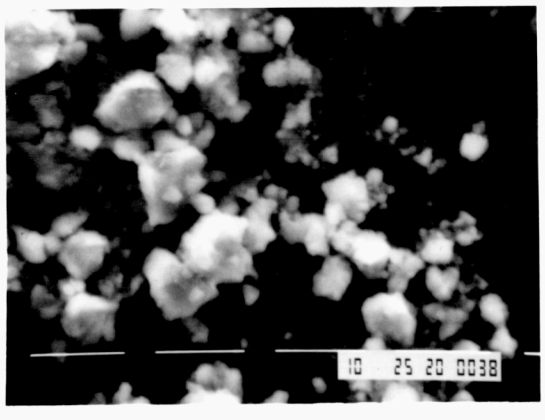


Figure 10.8 : Magn 2K

T = 140°C
[Fe] = 0.2M
[Ni] = 0.1M
[V] = 33 %
Seed: 4.69g $NiFe_2O_4$

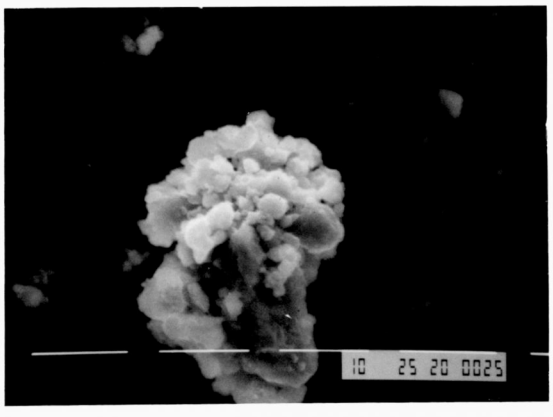


Figure 10.9 : Magn 2K

T = 160°C
[Fe] = 0.2M
[Ni] = 0.05M
[V] = 33 %
Seed: 4.69g $NiFe_2O_4$

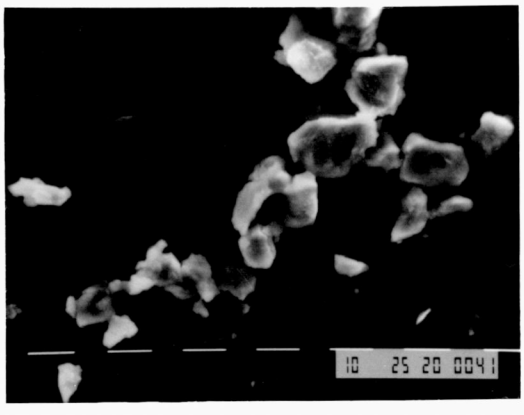


Figure 10.10 : Magn 1K

T = 160°C
[Fe] = 0.1M
[Ni] = 0.1M
[V] = 33 %
Seed: 4.69g $NiFe_2O_4$

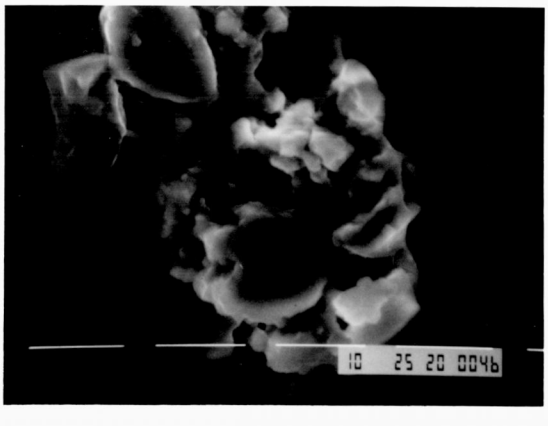


Figure 10.11 : Magn 2K

T = 160°C
[Fe] = 0.1M
[Ni] = 0.05M
[V] = 33 %
Seed: 4.69g $NiFe_2O_4$

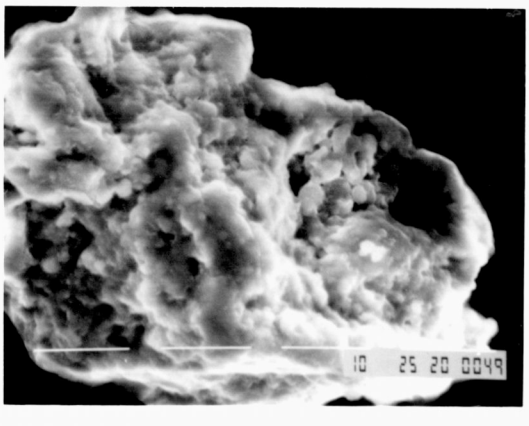


Figure 10.12 : Magn 2K

T = 160°C
[Fe] = 0.2M
[Ni] = 0.1M
[V] = 50 %
Seed: 4.69g $NiFe_2O_4$

Clusters can be detected on some of the micrographs, but the magnification is too low to reveal crystallites.

Figure 10.6 shows a very large agglomerate of the homogeneously nucleated material shown in Figures 10.1 and 10.4. This was probably formed during filtration, and was not broken up during dispersion. Some clusters of about 0.2μm can be seen in the centre of the agglomerate; very little else can be distinguished.

Figure 10.7 shows material precipitated at 170°C onto seed. Some individual clusters of 0.1μm are visible. Individual clusters, or small groups of these can be seen on the surface of the two large agglomerates, which are about 7.5μm in diameter. Figure 10.8 shows the product from a seeded run made at 140°C. The individual particles are of similar size to those seen in Figure 10.7, but very little detail is discernable on the surface of the agglomerates.

Figure 10.9 shows small particles within the range 0.2 - 1μm, together with an agglomerate which has a well defined surface morphology. The undulations on the agglomerate surface at the bottom of the figure are probably caused by individual clusters, while small agglomerates predominate at the top of the particle. Figure 10.10 shows angular agglomerates , 1 - 5μm in length. Since both angular and rounded areas are seen on the large agglomerate in Figure 10.11, the morphology of the agglomerates is probably not determined by the individual properties of the sample, but is purely random. This agglomerate and the large one shown in Figure 10.12 were unlikely to have been formed by 'bunching' of the individual particles, although this was more pronounced on the aluminium stubs than on the carbon film. These agglomerates probably formed during filtration, and are clearly very strong mechanically. This indicates that the reason for poor reproducibility for the surface area results in section 10.1 was that the results depended on the extent to which agglomerates in the material were mechanically broken down.

Figure 10.5 shows cobalt ferrite, homogeneously precipitated in run Co1 (see Appendix D). A large number of agglomerates of about 1.5μm are visible, together with two larger agglomerates. The undulations on the surface of the agglomerates indicate particles of

about 0.25μm; these are probably rounded clusters of crystallites similar to those shown in Figure 10.1.

At the magnifications used, it was not possible to observe any relationship between precipitate morphology and the experimental conditions under which precipitates were formed.

10.4 THIN LAYER CHROMATOGRAPHY OF ORGANIC SOLUTIONS

The results obtained throughout this project indicated that mixed carboxylate complexes are present in solutions containing a mixture of ions, and that these mixed complexes have a strong influence on the behaviour of such solutions. The infrared measurements reported in Chapter 9 gave evidence of the existence of these mixed complexes. Some thin layer chromatography tests were done to see whether the mixed complexes could be distinguished from single metal complexes by this means.

Small amounts of iron-Versatic solution, nickel-Versatic solution and mixed solutions with iron to nickel ratios of 4, 2 and 1 were spotted on silica-gel coated microscope slides. Four different eluting systems were used; ethyl acetate, ethanol, and 10:1 and 1:1 mixtures of ethyl acetate and ethanol, to provide solvents with a range of polarities.

The retention factors, defined as

$$RF = \frac{\text{distance moved by sample spot}}{\text{distance moved by solvent front}}$$

are reported in Table 10.4.1. In all four eluting systems, iron-Versatic left a continuous streak on the plate, with retention factor of 0 up to 0.86 in ethanol. Nickel-Versatic gave a well defined spot. The three iron-nickel Versatic solutions all showed similar behaviour for a given eluting system. In all cases the mixed solutions had a higher mean retention factor than the nickel-Versatic and did not give a long streak as the iron had done.

Table 10.4.1 Thin Layer Chromatography Results: Retention Factors

Conc of Metal in 33% Versatic Solution(M)	Ethyl Acetate	10 Ethyl Acetate + 1 Ethanol	1 Ethyl Acetate + 1 Ethanol	Ethanol
0.3M Fe 0.0M Ni	0.0 - 0.76 diffuse continuous streak	0.0 - 0.84 continuous streak	0.0 - 0.81 continuous streak	0.0 - 0.86 continuous streak
0.0M Fe 0.3M Ni	0.64	0.70	0.74	0.72
0.2M Fe 0.05M Ni	0.58 - 0.79	0.79*	0.67 - 0.92	0.80*
0.2M Fe 0.1M Ni	0.58 - 0.79	0.79*	0.67 - 0.92	0.80*
0.1M Fe 0.1M Ni	0.58 - 0.79	0.79*	0.67 - 0.92	0.80*

* denotes compact spot - mean RF shown

These observations clearly indicate that in mixed solution at room temperature, iron and nickel are present in a form different from that in single solutions.

CHAPTER 11

GENERAL DISCUSSION

The results of Part I of the experimental work, together with observations made during examination of precipitates on the Temscan electron microscope, indicated that homogeneous nucleation of spinel ferrites during hydrolytic stripping proceeds by a mechanism analagous to the hydrolysis and precipitation of iron(III) in aqueous solution. Crystallites are formed by polymerisation, which probably occurs by addition of OH^- (olation) and elimination of water (oxolation). The crystallites form clusters, which appear then to undergo anisotropic flocculation. Magnetic interactions between the species present in the organic solution were thought to be important in forming nuclei with the long range order of the spinel structure.

The purpose of the kinetic experiments was to investigate the effects of process variables on the rate of hydrolysis of iron-nickel Versatic solutions, to establish the conditions suitable for the production of nickel ferrite, and to attempt to determine the mechanism of precipitation of nickel ferrite. Since seed material was used in the kinetic runs, the study gave information only on the growth of particles by heterogeneous precipitation.

Any mechanism proposed for heterogeneous precipitation must be consistent with the following experimental observations:

(1) The precipitation rate was not affected by stirring speed, or volume of water (when well in excess of the stoichiometric requirement). This indicates that hydrolysis does not occur at the aqueous/organic interface, since the area of the interface would change with stirring speed and water volume.

(2) Furthermore, the rate was proportional to nickel ferrite seed area, which indicates that the rate controlling step of the hydrolysis reaction occurs on the surface of the seed.

(3) When a variety of materials were tested as potential nucleating agents, it was found that the reaction was not seeded by activated carbon, colloidal graphite, silica or alumina, which have very high specific surface areas, or by sintered nickel ferrite or coarse grained magnetite. The reaction was seeded by nickel ferrite

precipitated previously by hydrolytic stripping. The ineffectiveness of the materials with a high specific surface area suggests that the crystallographic structure and/or the magnetic properties of the solid surface play an important role in the mechanism of heterogeneous precipitation. The inability of sintered nickel ferrite, or coarse grained magnetite, to seed precipitation could be due to the low specific surface area of these materials, or could indicate that precipitation is localised at high energy lattice imperfections. The fine grained precipitated nickel ferrite which did seed the reaction probably contains many imperfections, whereas imperfections have probably disappeared from the sintered material.

(4) The infrared work indicated that the carboxylate groups coordinate by bidentate chelating and bridging in iron-Versatic, and by monodentate coordination in nickel-Versatic. Mixtures of iron and nickel Versatic contained carboxylate groups coordinating by both bidentate chelating and monodentate coordination, but the carbonyl stretching frequency of both types of carboxylate group was higher in mixed solutions than in single metal solutions. This indicates that the carbonyl bond is stronger in mixed solutions, and therefore that the carboxylate group - metal bonding is weaker. This provides evidence of the existence of mixed complexes in Versatic solutions containing both iron and nickel.

(5) Thin layer chromatography also gave evidence of the existence of mixed iron-nickel Versatic complexes.

(6) Magnetic spinel ferrites, MFe_2O_4, were the only mixed oxides with a crystal structure different from that of the individual metal oxides, which were formed during hydrolytic stripping of mixed carboxylate solutions. Although the magnetic mixed zinc ferrites, $(MnZn)Fe_2O_4$ and $(NiZn)Fe_2O_4$, were formed, the non-magnetic single ferrites $ZnFe_2O_4$ and $CdFe_2O_4$ did not form. This suggests that magnetic interactions are important in forming mixed oxides with longer range order than single oxides.

(7) The injection runs indicated that metal carboxylate complexes are labile, and rapidly change to adopt the bulk organic solution composition. Nevertheless, hematite and nickel hydroxide were not precipitated from Versatic solutions containing iron and nickel, even when these materials were introduced prior to hydrolysis, and iron and nickel were both at a concentration that would have

given precipitation in the absence of the other metal. This suggests that mixed complexes will not break up in solution to form iron or nickel species which can move independently of each other.

(8) When the iron to nickel ratio in the organic solution was 2, the initial rate appeared to be proportional to $1/[HV]_f$. The overall metal concentration was important only in the way it affected the free acid. This indicates that when the iron to nickel ratio is 2, desorption of Versatic acid from the seed surface is rate controlling.

(9) The factorial design revealed three distinctly different types of behaviour for iron to nickel ratios of 4, 2 and 1. When the iron to nickel ratio was 2, stoichiometric nickel ferrite was precipitated throughout the run. Where the iron to nickel ratio was 4, the initial rate of precipitation of iron was very much faster than that of nickel, indicating that iron-rich material was being formed. The material initially precipitated had an iron to nickel ratio of 5.5, which corresponds to a composition of $Ni_{0.43}Fe_{2.38}O_4$. Since the ratio is greater than the bulk ratio, iron hydrolysis must be more rapid than nickel hydrolysis under these conditions, although nickel is hydrolysed more rapidly than iron in single metal solutions[4]. Iron-rich material was precipitated until the organic solution iron to nickel ratio reached 2, after which stoichiometric $NiFe_2O_4$ was formed. When the iron to nickel ratio was 1, the precipitation rate was very slow. The iron and nickel concentration-time curves were parallel throughout (on the axes used), which indicated that stoichiometric $NiFe_2O_4$ was precipitated.

It is not possible to derive an empirical mathematical model from the experimental results to describe the rate of reaction in terms of the experimental variables, because the 'one variable at a time' approach was used in favour of factorial designs for the kinetic runs.

It would also be difficult to derive a mechanistic model from the experimental data; the reaction is known to take place at the seed surface, therefore the rate equation for any model should contain the surface concentrations of species involved in the reaction, not

bulk concentrations.

For some systems, the surface and bulk concentrations can be related by the Langmuir adsorption isotherm[111]. The Langmuir isotherm assumes that a solid surface has a fixed number of sites per unit area which can accommodate adsorbed species, and that an equilibrium is established between a bulk species, free active surface sites, and species adsorbed onto surface sites. The fraction of occupied sites can therefore be expressed in terms of the equilibrium constant for adsorption, and the bulk concentration of a given species. Theoretical expressions can also be derived to describe the situation where two or more species are competing for the same surface sites.

A reaction occurring on a surface can be considered to involve 5 consecutive steps[111]:

(1) Diffusion of reactants to the surface
(2) Adsorption of the reactants
(3) Reaction at the surface
(4) Desorption of the products
(5) Diffusion of products away from the surface

Since steps 1 and 5 are generally rapid, the rate determining step in a heterogeneous reaction usually involves steps 2, 3 or 4. If step 3 is assumed to be rate determining, steps 2 and 4, adsorption of the reactants and desorption of the products, should be at equilibrium, so the Langmuir adsorption isotherm can be used to estimate the surface concentration of the reactants. Possible mechanisms for the reaction can be proposed, then the rate equations which should result from such mechanisms under the experimental conditions used can be derived, and compared with experimentally determined rates to test the validity of the proposed mechanism.

However, it would be inappropriate to use such an approach to model the heterogeneous precipitation of nickel ferrite for the following reasons:

(1) Since the crystallography of the solid surface is important in determining its effectiveness as a seed, it is assumed that there are octahedrally and tetrahedrally coordinated surface sites. Since nickel is only present on octahedral sites in the ferrite

lattice, it is likely that nickel species can only be accommodated on octahedral surface sites. Iron, however, can probably be accommodated on both octahedral and tetrahedral sites. The species could therefore neither be considered to be competing for all the active sites, nor be considered as being adsorbed on entirely different sites. The relative proportions of octahedral and tetrahedral sites at the surface cannot be predicted, as they will be determined by the crystallographic orientation. The Langmuir isotherm can therefore not be reliably applied to estimate the concentration of adsorbed iron and nickel.

(2) The product of hydrolytic stripping is either nickel ferrite, or a solid solution of maghemite in nickel ferrite. There are therefore two possible reactions, and the overall mechanism is unlikely to be sufficiently simple to be modelled using the available data.

(3) Desorption of the Versatic acid released during hydrolysis appears to be the rate controlling step when the bulk iron to nickel ratio is 2. The Langmuir isotherm therefore cannot be used to determine the surface concentration of species, since the isotherm assumes that adsorption and desorption processes are at equilibrium, and that surface reaction is rate controlling.

(4) Since ferrite is precipitated at the surface by the reaction, there is clearly interaction between the species adsorbed on adjacent active sites. The Langmuir isotherm is based on the assumption that there is negligible interaction between adsorbed species, and therefore cannot be used to obtain the surface concentrations of reacting species.

Nevertheless, although it is not possible to derive any meaningful mathematical model of the hydrolysis reaction, a speculative discussion on a possible mechanism can be made. The concept of active surface sites, as used in the Langmuir adsorption isotherm, provides a useful basis for qualitative discussion of the experimental observations.

Several of the observations listed at the beginning of this chapter led to fairly definite conclusions, as discussed previously. These are:

(1) Heterogeneous precipitation of nickel ferrite during hydrolytic stripping is a surface reaction.

(2) The crystallography and/or magnetic properties of the solid surface

are important. The reaction was only seeded by precipitated ferrite.

(3) A Versatic solution of iron and nickel contains mixed complexes of iron, nickel and Versatic groups. There is no evidence of single metal complexes in mixed solutions.

(4) When the organic solution iron to nickel ratio is 2, the rate determining step appears to be desorption of Versatic acid from the precipitate surface.

The results of the factorial design revealed three types of behaviour for the three different iron to nickel concentration ratios used. When iron was in excess of the stoichiometric ratio of 2, the material precipitated contained a higher proportion of iron than the bulk solution, which indicates that iron is hydrolysed more rapidly than nickel under these conditions. Furthermore, the factorial design indicated that nickel has a negative effect on the precipitation rate. With the limited amount of data, there is no obvious, unambiguous explanation of the behaviour, therefore discussion of a mechanism which would result in the behaviour observed experimentally must necessarily be speculative.

The following assumptions are made:

(1) Mixed complexes only dissociate at the seed surface, therefore the ratio of iron to nickel in species reaching the surface is the same as the ratio in the bulk organic solution. This can be justified from the fact that the mixed complexes are thought to have a magnetic moment. The complexes would therefore be unlikely to break up when approaching the magnetic seed, as this would lower their magnetic moment, hence the attractive forces between the seed and complexes.

(2) There are active octahedrally and tetrahedrally coordinated sites, present in the ratio 2:1. This assumption is based on the following points (a)The only effective seed was precipitated ferrite, with the spinel structure which has octahedral and tetrahedral sites, (b)Although not all of the tetrahedral and octahedral vacancies in the oxide sub-lattice of spinel are occupied, the occupied sites are ordered, not random. Therefore the active surface sites which can accommodate adsorbed species are also likely to be ordered, as in the crystal lattice. (c)Only 8 of the 64 tetrahedral vacancies, and 16 of the 32 octahedral vacancies are occupied in the unit

cell of ferrite. It is assumed that the crystallographic orientation is such that this ratio is also valid for the surface sites.

(3) Nickel is only adsorbed on octahedral sites, whereas iron can be accommodated on octahedral and tetrahedral sites. This assumption is based on the propensity of nickel(II) to adopt octahedral coordination, and on the distribution of iron and nickel within the ferrite lattice, i.e. $Fe[NiFe]O_4$.

(4) When adsorbed species are hydrolysed, their coordination does not change.

(5) When nickel ferrite is precipitated during hydrolytic stripping, the new surface created has the same number and distribution of active sites as the original surface. This is a reasonable assumption, since the original seed is precipitated ferrite.

(6) Adsorbed iron is hydrolysed more rapidly than nickel. Although this assumption is inconsistent with the hydrolysis rates of iron and nickel in single metal Versatic solutions[4], the assumption is necessary to account for the precipitation of material with an iron to nickel ratio of about 5.5 from a solution where the ratio is 4.

The assumptions 1, 2 and 3 were used to compile Figure 11.1, which schematically shows the distribution of Fe(III) and Ni(II) species over active sites, for organic solution iron to nickel ratios of 4, 2 and 1.

(a) When the iron to nickel concentration ratio is 4, 6 of the 20, or 0.3, of the octahedral sites are occupied by Ni, and the remaining 0.7 of the octahedral sites accommodate iron. Since it has been assumed that the coordination of species does not change during or after hydrolysis, it follows that a ferrite lattice will only form when sufficient species on octahedral and tetrahedral surface sites are hydrolysed. If the iron is hydrolysed before the nickel (assumption 6), this would provide all of the tetrahedral iron, and 1.4 of the 1.67 Fe(III) ions required on octahedral sites to precipitate maghemite $Fe[Fe_{1.67}]O_4$. The lattice charge balance could then be completed by slower hydrolysis of some of the surface nickel. The resulting precipitate would be $Fe[Ni_{0.4}Fe_{1.4}]O_4$, which has an iron to nickel ratio of $\frac{1 + 1.4}{0.4} = 6$. This corresponds closely to the value of 5.5

(a) Organic solution Fe:Ni = 4:1

Product - $Ni_{0.43}Fe_{2.38}O_4$

probably $Fe[Ni_{0.43}Fe_{1.38}]O_4$

Tet	[Oct	Oct]	Tet	[Oct	Oct]
Fe	Ni	Fe	Fe	Ni	Fe
Fe	Fe	Fe	Fe	Fe	Fe
Fe	Ni	Fe	Fe	Ni	Fe
Fe	Fe	Fe	Fe	Fe	Fe
Fe	Ni	Fe	Fe	Ni	Fe

(b) Organic solution Fe:Ni = 2:1

Product - $Fe[NiFe]O_4$

Tet	[Oct	Oct]	Tet	[Oct	Oct]
Fe	Ni	Fe	Fe	Ni	Fe
Fe	Ni	Fe	Fe	Ni	Fe
Fe	Ni	Fe	Fe	Ni	Fe
Fe	Ni	Fe	Fe	Ni	Fe
Fe	Ni	Fe	Fe	Ni	Fe

(c) Organic solution Fe:Ni = 1:1

Product - $Fe[NiFe]O_4$

Tet	[Oct	Oct]	Tet	[Oct	Oct]
Fe	Ni	Fe	Fe	Ni	Ni
Fe	Ni	Ni	Fe	Ni	Fe
Fe	Ni	Fe	Fe	Ni	Ni
Fe	Ni	Ni	Fe	Ni	Fe
Fe	Ni	Fe	Fe	Ni	Ni

Figure 11.1 Schematic Distribution of Fe(III) and Ni(II) species over Active Surface Sites, for Organic Solution Iron to Nickel Ratios of 4, 2 and 1 (first model proposed)

experimentally observed. Not all of the surface nickel needs to be hydrolysed, because the charge balance can be maintained by iron(III) with lattice vacancies. Precipitation of iron-rich material would decrease the organic solution iron to nickel ratio, therefore the iron to nickel ratio in the precipitate would decrease with time accordingly.

(b) When the organic iron to nickel ratio is 2, half the octahedral sites would be occupied by iron, and half by nickel. The remaining iron would be on the tetrahedral sites. All the adsorbed nickel would have to be hydrolysed in addition to all adsorbed iron, in order to develop material with the spinel lattice. Therefore stoichiometric nickel ferrite $Fe[NiFe]O_4$ would form. In this case the rate is known to be determined by desorption of Versatic acid.

(c) When the organic solution iron to nickel ratio is 1, 15 of the 20, or 0.75 of all octahedral sites, would be occupied by nickel. This is greater than the proportion which can be accommodated in a ferrite lattice, therefore ferrite will only be formed when some of the nickel is desorbed, and replaced by complexes containing the iron needed for precipitation. The precipitate eventually formed would contain the maximum possible concentration of nickel, i.e. $Fe[NiFe]O_4$.

The experimental observations can be explained by the above model. It must be emphasised, however, that the model is based on several assumptions, and therefore only speculative. If some of the assumptions are altered, a slightly different model can be proposed. Retain assumptions 1, 2 and 5. Omit assumptions 3, 4 and 6, and replace by assumptions 7, 8 and 9 as below. This gives the folowing:

(1) The ratio of iron and nickel in species reaching the surface is the same as the ratio in the bulk solution

(2) There are active octahedral and tetrahedral surface sites, present in the ratio 2:1

(5) When nickel ferrite is precipitated during hydrolytic stripping, the new surface created has the same number and distribution of active sites as the original surface.

(7) Iron and nickel are both adsorbed on active octahedral and tetrahedral sites

(8) The coordination of iron and nickel can change during or after hydrolysis

(9) Iron on both octahedral and tetrahedral sites is hydrolysed,

(a) Organic solution Fe:Ni = 4:1

Product - $Fe_{0.8}[Ni_{0.4}Fe_{1.6}]O_4$

further rearrangement expected

Tet	[Oct	Oct]	Tet	[Oct	Oct]
Ni	Fe	Fe	Fe	Fe	Ni
Fe	Ni	Fe	Fe	Fe	Fe
Fe	Fe	Ni	Fe	Fe	Fe
Fe	Fe	Fe	Ni	Fe	Fe
Fe	Fe	Fe	Fe	Ni	Ni

(b) Organic solution Fe:Ni =2:1

Product - $Fe_{0.67}[Ni_{0.67}Fe_{1.33}]O_4$

migration of Ni from tet sites needed for formation of $NiFe_2O_4$

Tet	[Oct	Oct]	Tet	[Oct	Oct]
Ni	Fe	Fe	Ni	Fe	Fe
Fe	Ni	Fe	Fe	Ni	Fe
Fe	Fe	Ni	Fe	Fe	Ni
Ni	Fe	Fe	Ni	Fe	Fe
Fe	Ni	Fe	Fe	Ni	Fe

(c) Organic solution Fe:Ni = 1:1

Product - $Fe_{0.5}[NiFe]O_4$

more Fe needed on tet sites for formation of $NiFe_2O_4$

Tet	[Oct	Oct]	Tet	[Oct	Oct]
Ni	Fe	Ni	Fe	Ni	Fe
Fe	Ni	Fe	Ni	Fe	Ni
Ni	Fe	Ni	Fe	Ni	Fe
Fe	Ni	Fe	Ni	Fe	Ni
Ni	Fe	Ni	Fe	Ni	Fe

Figure 11.2 Schematic Distribution of Fe(III) and Ni(II) Species over Active Surface Sites, for Organic Solution Iron to Nickel Ratios of 4, 2 and 1 (second model proposed)

whereas only octahedrally coordinated nickel can be hydrolysed, and then only to make up the lattice charge balance.

Figure 11.2 shows the distribution of Fe(III) and Ni(II) species which would result from the above assumptions.
(a) Where the iron to nickel ratio is 4, iron would occupy 0.8 of both octahedral and tetrahedral sites, and nickel would occupy 0.2 of both. Hydrolysis would therefore initially produce material of composition $Fe_{0.8}[Ni_{0.4}Fe_{1.6}]O_4$. In iron-rich spinel ferrites the lattice vacancies are generally only on the octahedral sites[92]. Rearrangement would therefore be needed to give the required metal distribution on the tetrahedral and octahedral sub-lattices, but as in the first model, the overall iron to nickel ratio in the precipitate would be $\frac{0.8 + 1.6}{0.4} = 6$.

(b) When the organic iron to nickel ratio is 2, 0.67 of the octahedral and tetrahedral sites would be occupied by iron, and 0.33 of the octahedral and tetrahedral sites would be occupied by nickel. Hydrolysis would initially give $Fe_{0.67}[Ni_{0.67}Fe_{1.33}]O_4$. Nickel would have to migrate to octahedral sites to give $Fe_{0.67}[NiFe_{1.33}]O_4$, then the hydrolysed iron would have to rearrange to give $Fe[NiFe]O_4$, which is the product formed under these conditions.
(c) When the organic iron to nickel ratio is 1, 0.5 of octahedral and tetrahedral sites would accommodate both iron and nickel. The solid initially precipitated would then be $Fe_{0.5}[NiFe]O_4$. More iron would be needed to produce ferrite with the correct charge balance, therefore the rate would be expected to be lower than for (a) and (b).

The second model is probably less satisfactory than the first, because it requires rearrangement of the initial product to give the structures reported in the literature for the phases which formed under the different conditions. Nevertheless, the second model does illustrate the fact that the experimental results can be interpreted in more than one way.

CHAPTER 12

CONCLUSIONS AND SUGGESTIONS FOR FURTHER WORK

12.1 CONCLUSIONS FROM EXPERIMENTAL WORK

12.1.1 Part I: Preparation of Metal-Versatic Solutions and Hydrolysis of Single and Mixed Solutions in Sealed Tubes

(1) Iron-Versatic solution can be prepared by exchange extraction with calcium-Versatic solution if the ratio S, $\frac{\text{total number of moles Ca}}{\text{total number of moles Fe}}$ is greater than or equal to 1.5. Between 20° and 60°C, temperature does not affect exchange extraction.
Residual calcium is removed from the organic solution most effectively by continuous washing with dilute HCl.

(2) Calcium, zinc and magnesium Versatic solutions were prepared by dissolving the appropriate oxide in Versatic acid. Solutions of most other metals investigated in this work were prepared by solvent extraction from aqueous solutions of their salts.
Aluminium-Versatic formed a stable gel at low concentrations of aluminium. The gel was thought to contain carboxylate bridges between partially hydrolysed aluminium ions.
Manganese(II) was oxidised by air during extraction, probably to Mn(III). Cobalt(II) Versatic was oxidised by hydrogen peroxide to Co(III), which was stable in air at room temperature.

(3) When heated to 200°C in sealed tubes with water, iron, copper and nickel Versatic solutions precipitated large quantities of αFe_2O_3, Cu_2O and $Ni(OH)_2$ respectively, by hydrolytic stripping. Magnesium-Versatic precipitated some $Mg(OH)_2$ which redissolved on standing at room temperature. Manganese(III) and cobalt(III) in Versatic solution were reduced to the divalent state. This reduction resulted in the production of carbon dioxide by oxidation of the Versatic acid.

(4) In general, mixed carboxylate solutions behaved as mixtures of their components during hydrolytic stripping. Carbonates of magnesium, calcium, strontium, manganese and cadmium were precipitated from some cobalt, manganese and copper solutions by the carbon dioxide generated during reduction.

(5) Magnetic spinel ferrites, MFe_2O_4, were the only mixed oxides with a crystal structure different from that of the individual metal oxides which were formed during hydrolytic stripping of mixed carboxylate solutions. Although the magnetic mixed zinc ferrites $(MnZn)Fe_2O_4$ and $(NiZn)Fe_2O_4$ were precipitated during hydrolytic stripping, the non-magnetic zinc and cadmium ferrites did not form.

The magnetic moment of mixed carboxylate complexes was thought to play an important role in the formation of hydrolysed polymeric species with the long range order needed to nucleate mixed oxides.

12.1.2 Part II: Hydrolytic Stripping of Iron-Nickel Versatic Solutions

(1) To assess the significance of several variables, sealed tube tests were made using two fractionated factorial designs. These were rather inconclusive because the dummy variable, which was used as an estimate of the experimental error, was confounded with significant interactions. In both designs, only temperature was significant at the 90% level, as determined by the t-test. When a normal probability plot was used to estimate the significance of the main effects and confounded second order interactions in the ResolutionIV design, temperature, iron concentration and Versatic concentration, together with the dummy and three sets of confounded two-factor interactions, all had a significant effect on the percentage of iron precipitated.

(2) Kinetic studies were made to investigate systematically the effect of experimental variables on the initial reaction rate. The initial rate was obtained by fitting a polynomial to the concentration-time data obtained throughout each run.

Unseeded runs were not studied, because they were not reproducible, and had a variable induction period, which resulted in a concentration-time curve which was not amenable to curve fitting.

(3) Several materials were tested as potential nucleating agents. Precipitation during hydrolytic stripping was not nucleated by activated carbon, colloidal graphite, silica or alumina, which have very high specific surface areas, or by sintered nickel ferrite or coarse grained magnetite. In the presence of nickel ferrite precipitated in a previous stripping run, heterogeneous precipitation occurred immediately, with no induction period.

Precipitated nickel ferrite was used as seed for the kinetic studies, since the concentration-time curves of these runs could be described by third degree polynomials with low residuals near $t = 0$.

(4) Hematite and nickel hydroxide did not precipitate from mixed iron-nickel Versatic solution, even when these materials had been added previously. This suggests that the iron and nickel are associated as mixed complexes in the organic solution, and cannot react independently.

(5) The age of organic solutions was found to affect substantially the rate of precipitation of nickel ferrite. It is thought that polymeric carboxylate complexes form on standing and that these react with water rather slowly. The age of the calcium-Versatic used to prepare iron-Versatic by exchange extraction affects the kinetics of precipitation of nickel ferrite.

(6) The rate of precipitation increased rapidly with increasing temperature. Between 140° and 180°C, heterogeneous precipitation appeared to proceed by a single mechanism. The activation energy for the process was +124.4kJ mol^{-1}.

(7) The stirring speed, and volume of water (when well in excess of the stoichiometric requirement) did not affect the rate of precipitation.

(8) The rate was proportional to the nickel ferrite seed area, which indicated that the rate controlling step of the hydrolysis reaction occurred on the surface of the seed. It is likely that a small area of the seed surface was poisoned by a nickel-rich material which could have been formed by an impurity in Versatic 10 or Escaid 110.

(9) The factorial design revealed three distinctly different types of behaviour for iron to nickel ratios of 4, 2 and 1. Where the iron to nickel ratio was 2, stoichiometric nickel ferrite was precipitated throughout the course of the run. When the iron to nickel ratio was 4, the initial rate of precipitation of iron was very much faster than that of nickel. The iron to nickel ratio of the material initially precipitated was about 5.5. Iron-rich material continued to be precipitated until the iron to nickel ratio in the organic solution reached 2. Thereafter, stoichiometric nickel ferrite was precipitated. When the iron to nickel ratio was 1, the precipitation rate was very low, and stoichiometric

nickel ferrite was precipitated.

X-ray powder diffraction analysis gave no evidence of hematite or nickel hydroxide in the material precipitated from the iron-rich or nickel-rich solutions.

(10) The factorial design indicated that iron concentration had a strong positive effect on the precipitation rate, and Versatic concentration a strong negative effect. Nickel concentration had a smaller negative effect, and there were significant interactions

(11) The precipitation rates in both injection runs were characteristic of the bulk concentration after mixing, which indicated that the metal carboxylate complexes are labile, and rapidly change to adopt the bulk composition.

(12) The concentration of total Versatic in the organic solution was found to have a strong influence on the rate of precipitation. The initial rate decreased rapidly with increasing total Versatic, in a non-linear fashion.

12.1.3 Infrared Spectrophotometry

(1) The concentration of free Versatic acid in the organic phase at elevated temperatures was measured using infrared spectrophotometry. The carboxylic acid is present as both monomeric and dimeric forms. The optical densities of the C=O bands of both monomer and dimer (1750 and 1700 cm^{-1} respectively) were measured in standard solutions at 130°, 150° and 165°C. The extinction coefficients of the monomer and dimer were found to be 3.498×10^4 and 11.368×10^4 OD units $mol^{-1} m^{-1}$ respectively.

(2) The dissociation constant for the dimer was found to be

$$\ln K_{diss} = 12.2589 - 5970.4(1/T) \qquad 12.1$$

There was an experimental error of ±20-25% associated with this value.

(3) At 160°C, the free acid in undiluted samples, $[HV]_f$ was found to be related to the free acid, $[HV]_f^!$, at dilution D, by the approximate relationship:

$$[HV]_f = [HV]_f^! - .0145(D-1) \qquad 12.2$$

(4) The free acid in organic samples taken from the kinetic runs was determined at 160°C: the ratio of Versatic to metal charge in the complexes, $(V/M_t)_{cmp}$, was found to decrease sharply with increasing concentration of metal. At metal charge concentrations greater than 0.5M, $(V/M_t)_{cmp}$ was between 1.5 and 1.0. The free Versatic appeared to derease linearly with increasing total metal concentration.

(5) Where the iron to nickel ratio was 2, the initial rate appeared to be inversely proportional to the concentration of free acid: the overall metal concentration was important only in the way it affected the free acid.

(6) Iron-Versatic complexes appeared to contain carboxylate groups coordinating by bidentate chelating and bridging, whereas the carboxylate groups in nickel-Versatic complexes seemed to coordinate by monodentate coordination. Mixtures containing iron and nickel Versatic showed bands corresponding to both types of coordination. The band frequencies were higher for the mixed metal solutions than for the single metal solutions, which suggests that coordination is weaker in the mixed complexes. Thus the IR spectra gave direct evidence of the existence of mixed carboxylate complexes at 160°C.

12.1.4 Additional Experimental Work

(1) The surface area measurements indicated that the nickel ferrite seed material had a specific surface area of 65.45 m^2g^{-1}. If the material was composed of uniform spheres, this would correspond to a particle radius of 85Å.

(2) It was not possible to obtain reproducible surface area measurements for the material precipitated during the kinetic runs, because when the precipitate was filtered from the organic solution, hard filter cakes formed. Estimates were made of the changes occurring in runs where complete precipitation doubled the weight of seed present. Assuming uniform spheres, the area would increase by $2^{\frac{2}{3}} = 1.59$ times. Assuming uniform deposition, and no change in surface area, a layer 28Å or 3.4 unit cells would be deposited.

(3) Electron microscopy indicated that the precipitates comprised chains of clusters, each of diameter .07 - .1μm, containing

randomly oriented crystallites of about 50-100Å radius. This observation agrees with the precipitation scheme proposed by Dousma and de Bruyn[79].

(4) Thin layer chromatography gave direct evidence of the existence of mixed iron-nickel Versatic complexes at room temperature.

12.2 SUGGESTIONS FOR FURTHER WORK

This work has shown that magnetic ferrites can be precipitated from metal carboxylate solutions by hydrolytic stripping. The kinetic experiments have given some indication of the effect of process variables on the rate of precipitation of nickel ferrite. Although an attempt has been made to interpret the results in terms of possible mechanisms, a variety of assumptions have had to be introduced. Further work could be done to establish a possible mechanism with greater certainty.

(1) The magnetic susceptibility of single and mixed metal Versatic solutions could be measured. This would show if those mixtures which precipitated ferrites have a higher susceptibility than mixtures which did not precipitate mixed oxides. This would indicate whether magnetic interactions are important in nucleating mixed oxides.

(2) Homogeneous precipitation could be studied kinetically. It is probable that the induction times observed for 33% Versatic solutions at iron and nickel concentrations of 0.2M and 0.1M at 170°C, could be reduced or eliminated at higher temperatures or metal concentrations, or lower Versatic concentrations. This would facilitate curve fitting. Reproducible results would probably be obtained if fresh organic solutions were used, as for heterogeneous precipitation.

(3) Fairly conclusive evidence of the existence of mixed Versatic complexes was obtained in this work. Far infrared spectrophotometry (i.e. at 650-50 cm^{-1}) might reveal information on the nature of the metal-ligand bonds within the complexes.

(4) Further experimental and infrared work could be done to establish whether the rate of precipitation is indeed inversely proportional to the free Versatic concentration, for organic solutions with an iron to nickel ratio of 2. The relationship between rate and

Versatic concentration could also be studied for non-stoichiometric organic solutions.

(5) Since the behaviour of iron-nickel solutions was markedly affected by the iron to nickel ratio, it would be useful to study the kinetics of solutions with a variety of iron to nickel ratios.

(6) More kinetic runs could be made, using factorial designs, to establish an empirical model for the hydrolysis reaction.

(7) The effect of ageing on organic solutions could be studied with infrared spectrophotometry, and possibly injection runs and thin layer chromatography, to establish whether polymerisation is responsible for the slower rates shown by aged organic solutions.

The physical properties of the precipitated ferrites have not been studied in this project, but will have to be investigated to establish whether commercial grade ferrites could be viably produced by hydrolytic stripping. Initial work should include:

(1) The precipitation of mixed nickel-zinc and manganese-zinc ferrites. These are the commercially important ferrites, and it is important that material having the required composition can be prepared. Although non-stoichiometric manganese-zinc ferrite was formed during stripping of a solution containing Mn(III), Zn(II) and Fe(III), stoichiometric $(Mn,Zn)Fe_2O_4$ might precipitate if Mn(II) were used. Mn(II) Versatic could probably be prepared by solvent extraction under nitrogen.

(2) The magnetic properties of the precipitated ferrites should be measured.

(3) If ferrites are to be produced by hydrolytic stripping, organic entrained in the precipitate would be a significant process cost. Some method to reduce such losses would have to be developed.

(4) Soft ferrites are generally used as fabricated components. The compacting and sintering properties should be investigated, although they are expected to be satisfactory.

APPENDIX A

CALIBRATION OF VARIABLE DILUTER

To use the variable diluter, one of 7 possible sample volumes, from 0.02 - 1.0mls is selected, then the exact diluent volume needed to achieve the required volume is selected, using a variable dial. The selected sample volume is then withdrawn from the solution of interest, and delivered with the preselected volume of diluent, to give the diluted solution. Thus, for a sample volume of S, and a diluent volume D, the diluted sample has a concentration S/(S+D) times that of its original concentration.

Assume that each value of S is associated with an error σ_i, and that there is a single 'dead space' error of δ associated with D. Then the concentration of the diluted sample, C, is given by:

$$C = \frac{S_i + \sigma_i}{S_i + \sigma_i + D + \delta} \qquad A.1$$

Thus $$S_i + \sigma_i + D + \delta = \frac{S_i + \sigma_i}{C} \qquad A.2$$

Therefore $$D = \frac{S_i + \sigma_i}{C} - (S_i + \sigma_i + \delta) \qquad A.3$$

For each S_i, C can be measured as a function of D on an A.A. against standards prepared with A grade volumetric apparatus.

Then a plot of D against 1/C should be a straight line of gradient $(S_i + \sigma_i)$, with intercept $-(S_i + \sigma_i + \delta)$, so that the unknowns σ_i and δ can be determined.

The technique was used for all sample volumes; good straight lines were obtained, and the values of δ obtained for each line were in good agreement, and at around 0.02mls were regarded as low enough to be due to experimental error, rather than to any real effect.

For convenience, these errors were used to compile a table showing the actual dilution given when each sample volume, S_i, was used with a diluent volume of 10-$S_i$mls; the error was about $\pm$1-2% for all but the lowest two sample volumes, which were avoided because of the large associated errors.

APPENDIX B

X-RAY POWDER DIFFRACTION PATTERNS

X-RAY POWDER DIFFRACTION PATTERNS FOR PRECIPITATES FROM SINGLE-METAL VERSATIC SOLUTIONS

$Mg(OH)_2$ JCPDS 7-239		Precipitate from Magnesium-Versatic	
d(Å)	I/I_1	d(Å)	I/I_1
4.77	90	4.77	V.S
2.725	6	2.72	w
2.365	100	2.36	V.S
1.794	55	1.785	V.S
1.573	35	1.567	V.S
1.494	18	1.487	S
1.373	16		
1.363	2	$Mg(OH)_2$	

$Ni(OH)_2$ JCPDS 14-117		Precipitate from Nickel-Versatic	
d(Å)	I/I_1	d(Å)	I/I_1
4.605	100	4.60	V.S
2.707	45	2.70	S
2.334	100	2.33	V.S
2.302	2	2.295	v.w
1.754	35	1.754	V.S
1.563	25	1.560	S
1.535	<1	1.530	v.w
1.480	16	1.475	S
1.354	4	$Ni(OH)_2$	

γMn_2O_3 JCPDS 18-803		Precipitate from Manganese-Versatic	
d(Å)	I/I_1	d(Å)	I/I_1
4.92	70	4.95	v.w
		3.65	v.w
3.08	90	3.08	M
2.88	20	2.85	M
2.76	90	2.755	M
2.49	100	2.48	S
		2.38	v.w
2.36	30	2.36	v.w
		2.17	M
2.04	60	2.04	M
		2.00	M
1.83	10		
1.79	30	1.79	w
1.70	20		
1.64	10		
1.57	30	1.57	w
1.54	80	1.54	M
1.44	30		
1.38	10	γMn_2O_3 + ?	

all lines difficult to measure because of fluorescence on pattern

αFe_2O_3 JCPDS 24-072		Precipitate from Iron-Versatic		αFe_2O_3 JCPDS 13-534	
d(Å)	I/I_1	d(Å)	I/I_1	d(Å)	I/I_1
3.686	33	3.67	S	3.66	25
2.703	100	2.69	V.S	2.69	100
2.519	70	2.52	V.S	2.51	50
2.295	2	2.28	v.w	2.285	2
2.208	17	2.20	S	2.201	30
2.080	2	2.07	v.w	2.070	2
1.8428	31	1.84	V.S	1.838	40
1.6966	36	1.69	V.S	1.690	60
1.6013	8	1.595	w	1.596	16
1.4873	22	1.483	M	1.484	35
1.4543	21	1.450	S	1.452	35
1.3514	2	αFe_2O_3			

V.S - very strong S - strong M.S - moderately strong M - medium w - weak v.w - very weak
h.v - hardly visible

X-RAY POWDER DIFFRACTION PATTERNS FOR PRECIPITATES FROM SINGLE-METAL VERSATIC SOLUTIONS

Cu_2O JCPDS 5-0667		Precipitate from Cu-Versatic(200°C)		Precipitate from Cu-Versatic(180°C)		CuO JCPDS 5-0661	
d(Å)	I/I_1	d(Å)	I/I_1	d(Å)	I/I_1	d(Å)	I/I_1
3.020	9	3.02	M	3.02	h.v		
		2.74	w	2.74	h.v	2.751	12
						2.530	49
		2.52	S	2.52	V.S	2.523	100
2.465	100	2.455	V.S	2.455	v.w		
		2.32	S	2.32	V.S	2.33	96
						2.312	30
2.135	37	2.125	V.S	2.13	v.w		
		1.95	h.v	1.95	h.v	1.959	3
		1.858	M.S	1.858	M.S	1.866	25
		1.77	h.v			1.778	2
1.743	1	1.735	v.w				
		1.703	v.w	1.70	h.v	1.714	8
		1.575	M	1.575	M	1.581	14
1.510	27	1.500	V.S	1.500	M.S	1.505	20
		1.412	w			1.418	12
		1.403	w	1.403	w	1.410	15
		1.370	w	1.375	w	1.375	19
		Cu_2O + CuO		CuO + Cu_2O			

X-RAY POWDER DIFFRACTION PATTERNS FOR PRECIPITATES FROM MIXED VERSATIC SOLUTIONS: A + 2Mg

$Mg(OH)_2$ JCPDS 7-239		Precipitate from (Ca+2Mg) Versatic		Precipitate from (Sr+2Mg) Versatic	
d(Å)	I/I_1	d(Å)	I/I_1	d(Å)	I/I_1
4.77	90	4.755	w		
		3.22	h.v	3.22	h.v
		3.15	h.v	3.15	h.v
		3.02	v.w	3.03	h.v
		2.96	v.w		
2.725	6	2.72	w		
2.365	100	2.36	V.S		
1.794	55	1.79	M		
1.573	35	1.565	V.S		
1.494	18	1.485	M		
		$Mg(OH)_2$ + ?		?	
		note that relative intensities of some lines differ from those of listed pattern			

$MgCO_3$ JCPDS 8-479		Precipitate from (Mn+2Mg) Versatic		$MnCO_3$ JCPDS 7-268	
d(Å)	I/I_1	d(Å)	I/I_1	d(Å)	I/I_1
				3.66	35
		2.82	w	2.84	100
2.742	100	2.760	S		
2.503	18				
				2.39	20
2.318	4	2.32	h.v		
				2.172	25
2.102	45	2.120	M.S		
				2.000	25
1.939	12	1.945	v.w		
				1.829	12
1.769	4			1.770	30
				1.763	35
1.700	35	1.71	M		
				1.556	2
				1.533	14
1.510	4	$MgCO_3$ (with slightly expanded lattice) + traces of $MnCO_3$			
1.488	6				

X-RAY POWDER DIFFRACTION PATTERNS FOR PRECIPITATES FROM MIXED VERSATIC SOLUTIONS: A + 2Mg

$MgFe_2O_4$:l.temp JCPDS 17-464		Precipitate from (Fe+2Mg) Versatic	
d(Å)	I/I_1	d(Å)	I/I_1
4.84	4		
2.96	40		
2.525	100	2.52	M(diffuse)
2.418	2		
2.094	25		
1.709	14		
1.612	30		
1.481	35	1.475	M(diffuse)
1.324	6		

probably $MgFe_2O_4$- very small particle size or not well crystalline, so only strongest lines visible

$Ni(OH)_2$ JCPDS 4-117		Precipitate from (Ni+2Mg) Versatic	
d(Å)	I/I_1	d(Å)	I/I_1
4.805	100	4.62	S
2.707	45	2.70	M.S
2.334	100	2.34	V.S
2.302	2		
1.754	35	1.755	M
1.563	25	1.560	M.S
1.535	1		
1.480	16	1.475	M
1.354	4		

$Ni(OH)_2$-note that relative intensities differ from listed pattern

Cu_2O JCPDS 5-0667		Precipitate from (Cu+2Mg) Versatic	
d(Å)	I/I_1	d(Å)	I/I_1
3.020	9	3.02	w
2.465	100	2.46	V.S
2.135	37	2.13	S
1.743	1	1.735	v.w
1.510	27	1.502	S
		Cu_2O	

Precipitate from (Co+2Mg Versatic	
d(Å)	I/I_1
11.8	S

only one line- this deep blue powdery precipitate was soluble in acetone, so is prob. an organic compound

X-RAY POWDER DIFFRACTION PATTERNS FOR PRECIPITATES FROM MIXED VERSATIC SOLUTIONS: A + Al

γ AlOOH JCPDS 21-1307		Precipitate from (Ca+Al) Versatic		Precipitate from (Sr+Al) Versatic		Precipitate from (Mn+Al) Versatic	
d(Å)	I/I_1	d(Å)	I/I_1	d(Å)	I/I_1	d(Å)	I/I_1
6.11	100	6.10	S	6.10	S	6.10	S
						3.40	S
3.164	65	3.17	M	3.17	w	3.17	v.w
		3.02	M.S	3.02	w	3.02	v.w
						2.70	S
						2.40	M
2.346	55	2.345	S	2.345	w	2.345	w
		2.28	w	2.28	h.v	2.28	h.v
		2.085	v.w			2.18	h.v
1.980	6						
		1.905	w				
1.860	30	1.870	w				
1.850	25	1.85	S	1.85	v.w	1.85	h.v
1.770	6					1.77	M
1.662	14	1.655	h.v			1.66	w
		1.595	h.v			1.65	v.w
1.527	6	1.52	h.v	1.52	h.v	1.52	h.v
1.453	16	1.45	w	1.45	h.v	1.45	h.v
1.434	10	1.43	w	1.43	h.v	1.43	h.v
		γAlOOH + ?		γAlOOH +?		γAlOOH + ?	

X-RAY POWDER DIFFRACTION PATTERNS FOR PRECIPITATES FROM MIXED VERSATIC SOLUTIONS: A + Al

αFe_2O_3 JCPDS 13-534		Precipitate from (Fe+Al) Versatic	
d(Å)	I/I_1	d(Å)	I/I_1
3.66	25	3.67	M
2.69	100	2.68	V.S
2.51	50	2.505	S
2.285	2		
2.201	30	2.19	M.S
2.070	2		
1.838	40	1.83	M.S
1.690	60	1.68	S
1.634	4		
1.596	16	1.585	w
1.484	35	1.475	M.S
1.452	35	1.44	M.S
		αFe_2O_3	

Precipitate from (Mg+Al) Versatic	
d(Å)	I/I_1
2.56	w diffuse
1.51	w diffuse
?	

γAlOOH JCPDS 21-1307		Precipitate from (Cd+Al) Versatic		$CdCO_3$ JCPDS 8-456	
d(Å)	I/I_1	d(Å)	I/I_1	d(Å)	I/I_1
6.11	100	6.2	M		
		3.80	M.S	3.78	100
3.164	65	3.15	v.w		
		2.95	S	2.95	100
				2.72	4
		2.47	M	2.46	35
2.346	55	2.345	w	2.245	8
		2.070	v.w	2.066	25
1.980	6				
		1.895	v.w	1.890	14
1.860	30	1.855	w		
1.850	25			1.838	25
		1.82	w	1.823	35
1.770	6				
1.662	14				
		1.58	v.w	1.582	16
1.527	6			1.522	4
		1.50	h.v	1.500	12
1.453	16	1.46	h.v	1.473	6
1.434	10	1.44	h.v	1.423	8
		γAlOOH + $CdCO_3$			

Cu_2O JCPDS 5-0667		Precipitate from (Cu+Al) Versatic	
d(Å)	I/I_1	d(Å)	I/I_1
3.020	9	3.02	M
2.465	100	2.465	V.S
2.135	37	2.135	S
1.743	1	1.74	v.w
1.510	27	1.504	S
		Cu_2O	

Precipitate from $(Co^{2+}$+Al) Versatic		Precipitate from $(Co^{3+}$+Al) Versatic		Precipitate from (Ni+Al) Versatic	
d(Å)	I/I_1	d(Å)	I/I_1	d(Å)	I/I_1
7.5	M	7.7	M	9.5	M
6.9	w	7.1	w	7.8	v.w
2.645	w	2.64	w	6.8	w
2.58	S	2.585	S	2.60	M.S
		2.37	v.w	1.505	M
2.27	v.w	2.28	v.w	all very	
1.525	S	1.525	S	diffuse	
1.495	M.S	1.495	M		
?		?		?	

X-RAY POWDER DIFFRACTION PATTERNS FOR PRECIPITATES FROM MIXED VERSATIC SOLUTIONS: A + 2Cr

α Fe_2O_3 JCPDS 13-534		Precipitate from (Fe+2Cr) Versatic	
d(Å)	I/I_1	d(Å)	I/I_1
3.66	25	3.67	v.w
2.69	100	2.70	S
2.51	50	2.52	M.S
2.285	2		
2.201	30	2.20	w
1.838	40	1.835	M
1.690	60	1.690	M.S
1.634	4		
1.596	16	1.595	h.v
1.484	35	1.482	w
1.452	35	1.45	w
		αFe_2O_3	

Cu_2O JCPDS 5-0667		Precipitate from (Cu+2Cr) Versatic	
d(Å)	I/I_1	d(Å)	I/I_1
3.02	9	3.01	M
2.465	100	2.46	V.S
2.135	37	2.130	S
1.743	1	1.735	v.w
1.510	27	1.505	S
		Cu_2O	

X-RAY POWDER DIFFRACTION PATTERNS FOR PRECIPITATES FROM MIXED VERSATIC SOLUTION: A + $2Mn^{3+}$

$CaCO_3$ Vaterite JCPDS 24-30		$CaCO_3$ Calcite JCPDS 24-27		Precipitate from ($Ca+2Mn^{3+}$) Versatic		$MnCO_3$ JCPDS 7-268		γFe_2O_3 JCPDS 4-0755		Precipitate from ($Fe+2Mn^{3+}$) Versatic	
d(Å)	I/I_1	d(Å)	I/I_1	d(Å)	I/I_1	d(Å)	I/I_1	d(Å)	I/I_1	d(Å)	I/I_1
4.245	5							5.90	2		
		3.852	29					4.82	5		
				3.70	M	3.66	35	4.18	1		
3.577	51							3.73	5		
3.296	100							3.41	2		
		3.030	100	3.06	h.v			2.95	34	2.95	v.w
		2.834	2	2.90	V.S	2.84	100	2.78	19		
2.735	62			2.75	M.S			2.52	100	2.52	S
				2.70	h.v			2.41	1		
		2.495	7	2.475	S			2.32	6		
				2.41	v.w	2.39	20	2.23	0.5	2.23	M
		2.284	18					2.08	24	2.08	v.w
2.219	2							1.87	0.5		
				2.20	w	2.172	25	1.70	12		
2.122	3							1.61	33	1.60	h.v
		2.094	27					1.55	0.5		
2.065	31							1.53	1		
				2.02	S	2.000	25	1.48	53	1.48	M.S
		1.9261	4					1.43	1		
		1.9071	17							γFe_2O_3	
		1.8726	34								
1.8569	9										
1.8253	20					1.829	12				
1.7883	2			1.79	v.w						
						1.770	30				
						1.763	35				
1.6481	7	1.6259	2								
		1.6040	15								
		1.5821	2			1.556	2				
Mixture of $MnCO_3$, Vaterite and Calcite				1.535	v.w	1.533	14				

X-RAY POWDER DIFFRACTION PATTERNS FOR PRECIPITATES FROM MIXED VERSATIC SOLUTIONS: A + $2Mn^{3+}$

Cu_2O JCPDS 5-0667		Precipitate from $(Cu+2Mn^{3+})$Versatic		$MnCO_3$ JCPDS 7-268		$MnCO_3$ JCPDS 7-268		Precipitate from $(Cd+2Mn^{3+})$Versatic		$CdCO_3$ JCPDS 8-456	
d(Å)	I/I_1	d(Å)	I/I_1	d(Å)	I/I_1	d(Å)	I/I_1	d(Å)	I/I_1	d(Å)	I/I_1
		3.67	v.w	3.66	35			3.75	S	3.78	80
3.020	9	3.02	M			3.66	35	3.70	M.S		
		2.85	w	2.84	100			2.975	V.S	2.95	100
2.465	100	2.47	V.S			2.84	100	2.88	V.S		
		2.39	h.v	2.39	20					2.72	4
		2.18	v.w	2.172	25			2.44	M	2.46	35
2.135	37	2.13	S			2.39	20	2.415	M		
		2.00	v.w	2.000	25			2.225	h.v	2.245	8
				1.829	12	2.172	25	2.19	v.w		
		1.765	v.w	1.770	30			2.045	M	2.066	25
		1.760	v.w	1.763	35	2.000	25	2.02	w		
1.743	1	1.74	w					1.875	v.w	1.89	14
				1.556	2			1.850	v.w	1.838	25
				1.533	14	1.829	12	1.82	v.w	1.825	35
1.510	27	1.505	S					1.805	w		
				1.452	2	1.770	30	1.78	w		
				1.423	1	1.763	35				
		$Cu_2O + MnCO_3$		1.379	10					1.582	16
						1.556	2	1.564	w		
								1.550	w		
						1.533	14				
										1.522	4
								1.48	w	1.473	6
						1.452	2	1.463	v.w		
						1.423	1			1.423	8
								$CdCO_3 + MnCO_3$			

X-RAY POWDER DIFFRACTION PATTERNS FOR PRECIPITATES FROM MIXED VERSATIC SOLUTIONS: A + 2Fe

αFe_2O_3 JCPDS 24-72		Precipitate from (Ca+2Fe) Versatic		Precipitate from (Sr+2Fe) Versatic		Precipitate from (Al+Fe) Versatic	
d(Å)	I/I_1	d(Å)	I/I_1	d(Å)	I/I_1	d(Å)	I/I_1
3.686	33	3.70	w	3.70	w	3.68	w
2.703	100	2.70	V.S	2.70	V.S	2.69	V.S
2.519	70	2.515	V.S	2.52	S	2.51	S
2.295	2						
2.208	7	2.205	M	2.205	M	2.20	M
2.080	2						
1.8428	31	1.840	M	1.840	M.S	1.835	M
1.6966	36	1.695	S	1.690	S	1.685	S
1.6013	8	1.595	h.v	1.598	w	1.59	v.w
1.4873	22	1.485	M	1.483	M	1.48	M
1.4543	21	1.450	M.S	1.450	M	1.45	M
1.3514	2						
		αFe_2O_3		αFe_2O_3		αFe_2O_3	

X-RAY POWDER DIFFRACTION PATTERNS FOR PRECIPITATES FROM MIXED VERSATIC SOLUTIONS: A + 2Fe

$MgFe_2O_4$ l.temp JCPDS 17-464		Precipitate from (Mg+2Fe) Versatic		γFe_2O_3 JCPDS 4-0755	
d(Å)	I/I_1	d(Å)	I/I_1	d(Å)	I/I_1
				5.90	2
4.84	4			4.82	5
				4.18	1
				3.73	5
				3.41	2
2.96	40	2.95	M	2.95	34
				2.78	19
2.525	100	2.51	V.S	2.52	100
2.418	2			2.41	1
				2.32	6
		2.24	v.w	2.23	.5
2.094	25	2.08	v.w	2.08	24
				1.87	.5
1.709	14	1.70	h.v	1.70	12
1.612	30	1.60	v.w	1.61	33
				1.55	.5
				1.53	1
1.481	35	1.472	V.S	1.48	53
				1.43	1
		γFe_2O_3 or $MgFe_2O_4$			

$MnFe_2O_4$ JCPDS 10-319		Precipitate from (Mn+2Fe) Versatic		γFe_2O_3 JCPDS 4-0755	
d(Å)	I/I_1	d(Å)	I/I_1	d(Å)	I/I_1
				5.90	2
4.906	20				
				4.82	5
				4.18	1
				3.73	5
				3.41	2
3.005	35				
		2.95	v.w	2.95	34
				2.78	19
2.563	100				
		2.54	v.w		
		2.51	V.S	2.52	100
2.450	12			2.41	1
				2.32	6
		2.23	w	2.23	.5
2.124	25				
		2.08	h.v	2.08	24
				1.87	.5
1.7342	20				
				1.70	12
1.6355	35				
		1.60	v.w	1.61	33
				1.55	.5
				1.53	1
1.5031	1				
		1.473	M.S	1.48	53
1.4376	4			1.43	1
		γFe_2O_3			

Cu_2O JCPDS 5-0667		Precipitate from (Cu+2Fe) Versatic		αFe_2O_3 JCPDS 13-534	
d(Å)	I/I_1	d(Å)	I/I_1	d(Å)	I/I_1
		3.68	w	3.66	25
3.02	9	3.02	v.w		
		2.695	S	2.69	100
		2.51	M.S	2.51	50
2.465	100	2.46	V.S		
				2.285	2
		2.20	M	2.201	30
2.135	37	2.13	S		
				2.070	2
		1.835	M	1.838	40
1.743	1				
		1.685	S	1.690	60
				1.634	4
		1.595	v.w	1.596	16
1.510	27	1.502	M		
		1.480	M	1.484	35
		1.447	M.S	1.452	35
		$Cu_2O + \alpha Fe_2O_3$			

αFe_2O_3 JCPDS 24-72		Precipitate from (Zn+2Fe)Versatic		Precipitate from (Cd+2Fe)Versatic	
d(Å)	I/I_1	d(Å)	I/I_1	d(Å)	I/I_1
3.686	33	3.70	M	3.68	M
2.703	100	2.70	V.S	2.70	V.S
2.519	70	2.52	S	2.52	S
2.295	2				
2.208	17	2.21	M.S	2.205	M
2.080	2			2.09	h.v
1.8428	31	1.840	M.S	1.835	M
1.6966	56	1.695	S	1.685	M.S
1.6013	8	1.600	w	1.59	v.w
1.4873	22	1.485	M.S	1.480	w
1.4543	21	1.455	S	1.449	M.S
1.3514	2			1.442	v.w
		αFe_2O_3		αFe_2O_3	

X-RAY POWDER DIFFRACTION PATTERNS FOR PRECIPITATES FROM MIXED VERSATIC SOLUTIONS: A + 2Fe

αFe_2O_3 JCPDS 13-534		Precipitate from (Ti+2Fe) Versatic		α FeOOH JCPDS 17-536	
d(Å)	I/I$_1$	d(Å)	I/I$_1$	d(Å)	I/I$_1$
		4.955	w	4.98	10
		4.18	S	4.18	100
3.66	25	3.68	S		
		3.37	v.w	3.38	10
		2.955	v.w		
2.69	100	2.695	V.S	2.69	30
		2.595	w	2.58	8
2.51	50	2.510	V.S	2.52	4
		2.480	w	2.490	16
		2.445	M.S	2.452	25
2.285	2				
		2.245	w	2.252	10
2.201	30	2.200	M.S	2.192	20
		2.175	M		
		2.090	h.v		
2.070	2	2.070	h.v		
		2.000	h.v	2.009	2
		1.915	v.w	1.920	6
1.838	40	1.835	S		
		1.79	w	1.799	8
		1.765	h.v	1.770	2
		1.71	M	1.721	20
1.690	60	1.685	S	1.694	10
		1.65	h.v	1.661	4
1.634	4				
		1.605	v.w	1.606	6
1.596	16	1.59	M		
		1.55	M	1.564	16
		1.501	w	1.509	10
1.484	35	1.480	S		
				1.467	4
1.452	35	1.445	S	1.453	10
		1.425	h.v	1.418	2
		1.385	h.v	1.392	8
				1.357	8

α FeOOH + αFe_2O_3

$CoFe_2O_4$ JCPDS 3-0864		Precipitate from (Co^{2+}+2Fe)Versatic		Precipitate from (Co^{3+}+2Fe)Versatic	
d(Å)	I/I$_1$	d(Å)	I/I$_1$	d(Å)	I/I$_1$
4.86	6	4.80	h.v	4.80	v.w
2.97	20	2.96	M	2.96	M.S
2.53	100	2.53	V.S	2.525	V.S
2.41	6			2.42	h.v
2.08	20	2.095	M	2.095	M
1.70	16	1.71	w	1.71	w
1.61	40	1.61	M.S	1.61	M.S
1.48	64	1.48	S	1.48	S
1.42	2				

$CoFe_2O_4$ $CoFe_2O_4$

αFe_2O_3 JCPDS 24-72		Precipitate from (Cr+2Fe) Versatic	
d(Å)	I/I$_1$	d(Å)	I/I$_1$
3.686	33	3.70	M
2.703	100	2.70	V.S
2.519	70	2.52	S
2.295	2		
2.208	17	2.205	M.S
2.080	2		
1.8428	31	1.840	M.S
1.6966	36	1.695	S
1.6013	8	1.600	w
1.4873	22	1.485	M
1.4543	21	1.450	M.S
1.3514	2		

αFe_2O_3

$NiFe_2O_4$ JCPDS 10-325		Precipitate from (Ni+2Fe) Versatic	
d(Å)	I/I$_1$	d(Å)	I/I$_1$
4.82	20	4.80	w
2.948	30	2.945	w
2.513	100	2.52	V.S
2.408	8		
2.085	25	2.08	M
1.9125	4		
1.7025	8	1.69	w
1.6051	30	1.600	M.S
1.4760	40	1.470	S
1.4100	2		

$NiFe_2O_4$

X-RAY POWDER DIFFRACTION PATTERNS FOR PRECIPITATES FROM MIXED VERSATIC SOLUTIONS: A + $2Co^{3+}$

$CoFe_2O_4$ JCPDS 3-0864		Precipitate from $(Fe+2Co^{3+})$Versatic		Cu_2O JCPDS 5-0667		Precipitate from $(Cu+2Co^{3+})$Versatic		$CdCO_3$ JCPDS 8-456		Precipitate from $(Cd+2Co^{3+})$Versatic	
d(Å)	I/I_1	d(Å)	I/I_1	d(Å)	I/I_1	d(Å)	I/I_1	d(Å)	I/I_1	d(Å)	I/I_1
4.86	6	4.80	v.w	3.020	9	3.01	w	3.78	80	3.75	S
2.97	20	2.96	M	2.465	100	2.47	V.S	2.95	100	2.925	V.S
2.53	100	2.525	V.S	2.135	37	2.135	S	2.72	4	2.68	h.v
2.41	6	2.41	h.v	1.743	1	1.740	v.w	2.46	35	2.455	M.S
2.08	20	2.09	M	1.510	27	1.505	S	2.245	8	2.22	w
1.70	16	1.707	v.w					2.066	25	2.05	M
1.61	40	1.607	M.S			Cu_2O		1.890	14	1.875	w
1.48	64	1.475	S					1.838	25	1.830	M
1.42	2							1.825	35	1.810	M.S
		$CoFe_2O_4$						1.582	16	1.57	M.S
								1.522	4		
								1.500	12	1.50	v.w
								1.473	6	1.485	M
										1.455	v.w
								1.423	8	1.411	w
										1.395	h.v
								1.357	2		
										$CdCO_3$	

d spacings lower than standard

X-RAY POWDER DIFFRACTION PATTERNS FOR PRECIPITATES FROM MIXED VERSATIC SOLUTIONS: A + 2Ni

$Ni(OH)_2$ JCPDS 14-117		Precipitate from (Mg+2Ni)Versatic		Precipitate from (Ca+2Ni)Versatic		Precipitate from (Sr+2Ni)Versatic		Precipitate from (Ti+Ni) Versatic		Precipitate from (Cr+2Ni)Versatic	
d(Å)	I/I_1	d(Å)	I/I_1	d(Å)	I/I_1	d(Å)	I/I_1	d(Å)	I/I_1	d(Å)	I/I_1
4.605	100	4.605	V.S	4.605	V.S	4.605	V.S	4.605	V.S	4.60	S
2.707	45	2.71	S	2.71	S	2.71	S	2.71	S	2.70	M.S
2.334	100	2.34	V.S	2.34	V.S	2.34	V.S	2.34	V.S	2.33	S
2.302	2			2.30	h.v	2.30	h.v				
1.754	35	1.755	M.S	1.755	M.S	1.755	M.S	1.755	M.S	1.75	M.S
1.563	25	1.560	M.S	1.560	M.S	1.560	M.S	1.560	M.S	1.555	M.S
1.535	1			1.530	h.v	1.530	h.v	1.530	h.v		
1.480	16	1.475	M	1.475	M	1.475	M	1.475	M	1.475	M
1.354	4	1.350	w	1.350	w	1.350	w	1.350	w		
1.335	8	1.338	w	1.338	w	1.338	w	1.338	w	small proportion	
		$Ni(OH)_2$		$Ni(OH)_2$		$Ni(OH)_2$		$Ni(OH)_2$		of $Ni(OH)_2$ in	
										amorphous material	

X-RAY POWDER DIFFRACTION PATTERNS FOR PRECIPITATES FROM MIXED VERSATIC SOLUTIONS: A + 2Ni

$Ni(OH)_2$ JCPDS 14-117		Precipitate from (Mn+2Ni)Versatic		Precipitate from (Co^{2+}+2Ni)Versatic		Precipitate from (Co^{3+}+2Ni)Versatic		Precipitate from (Zn+2Ni)Versatic		Precipitate from (Cd+2Ni)Versatic	
d(Å)	I/I_1	d(Å)	I/I_1	d(Å)	I/I_1	d(Å)	I/I_1	d(Å)	I/I_1	d(Å)	I/I_1
4.605	100	4.61	V.S	4.61	V.S	4.60	V.S d	4.60	V.S	4.60	V.S
2.707	45	2.70	S	2.70	S	2.70	S	2.70	S	2.70	S
2.334	100	2.330	V.S	2.330	V.S	2.325	V.S d	2.330	V.S	2.330	V.S
2.302	2			2.300	h.v			2.30	h.v		
1.754	35	1.750	M.S	1.750	M.S	1.750	M d	1.75	S	1.75	M.S
1.563	25	1.560	M.S	1.560	M.S	1.560	M.S	1.560	M.S	1.560	M.S
1.535	1	1.535	h.v	1.535	h.v			1.535	h.v		
1.480	16	1.478	M	1.478	M	1.475	M d	1.475	M	1.475	M
1.354	14	$Ni(OH)_2$		$Ni(OH)_2$ (+ some Co)		$Ni(OH)_2$ d=very broad diffuse line		$Ni(OH)_2$		$Ni(OH)_2$	

$NiFe_2O_4$ JCPDS 10-325		Precipitate from (Fe+2Ni) Versatic	
d(Å)	I/I_1	d(Å)	I/I_1
4.82	20	4.80	w
2.948	30	2.95	M
2.513	100	2.51	V.S
2.408	8	2.40	v.w
2.085	25	2.085	M.S
1.9125	4		
1.7025	8	1.695	v.w
1.6051	30	1.60	M.S
1.4760	40	1.470	S
1.4100	2		
		$NiFe_2O_4$	

$Ni(OH)_2$ JCPDS 14-117		Precipitate from (Cu+2Ni) Versatic		Cu_2O JCPDS 5-0667	
d(Å)	I/I_1	d(Å)	I/I_1	d(Å)	I/I_1
4.605	100	4.60	S d		
				3.020	9
2.707	45	2.70	S		
		2.46	S	2.465	100
2.334	100	2.325	V.S d		
2.302	2				
		2.130	w	2.135	37
1.754	35	1.75	M d		
				1.743	1
1.563	25	1.555	M.S		
1.535	1				
		1.503	w	1.510	27
1.480	16	1.475	w d		
1.354	4				
		$Ni(OH)_2$ (some lines v. diffuse) + Cu_2O			

X-RAY POWDER DIFFRACTION PATTERNS FOR PRECIPITATES FROM MIXED VERSATIC SOLUTIONS: A + 2Cu

Cu_2O JCPDS 5-0667		Precipitate from (Mg+2Cu) Versatic		Precipitate from (Ti+2Cu) Versatic		Precipitate from (Cr+2Cu) Versatic		Precipitate from (Fe+2Cu) Versatic	
d(Å)	I/I_1	d(Å)	I/I_1	d(Å)	I/I_1	d(Å)	I/I_1	d(Å)	I/I_1
3.020	9	3.01	w	3.01	w	3.01	w	3.01	w
2.465	100	2.46	V.S	2.455	V.S	2.455	V.S	2.455	V.S
2.135	37	2.125	S	2.125	S	2.125	S	2.125	S
1.743	1	1.735	v.w	1.735	v.w	1.735	v.w	1.735	v.w
1.510	27	1.503	S	1.502	S	1.502	S	1.502	S
		Cu_2O		Cu_2O		Cu_2O		Cu_2O	

X-RAY POWDER DIFFRACTION PATTERNS FOR PRECIPITATES FROM MIXED VERSATIC SOLUTIONS: A + 2Cu

Cu_2O JCPDS 5-0667		Precipitate from $(Co^{2+}+2Cu)$ Versatic		Precipitate from $(Co^{3+}+2Cu)$ Versatic		Precipitate from (Ni+2Cu) Versatic		Precipitate from (Zn+2Cu) Versatic	
d(Å)	I/I_1	d(Å)	I/I_1	d(Å)	I/I_1	d(Å)	I/I_1	d(Å)	I/I_1
3.02	9	3.01	w	3.01	w	3.01	w	3.01	w
2.465	100	2.46	V.S	2.46	V.S	2.46	V.S	2.46	V.S
2.135	37	2.13	S	2.13	S	2.13	S	2.13	S
1.743	1	1.74	v.w	1.74	v.w	1.74	v.w	1.74	v.w
1.510	27	1.503	S	1.503	S	1.503	S	1.503	S
		Cu_2O		Cu_2O		Cu_2O		Cu_2O	

Cu_2O JCPDS 5-0667		Precipitate from (Ca+2Cu) Versatic		$CaCO_3$ calcite JCPDS 24-27		$CaCO_3$ vaterite JCPDS 24-30	
d(Å)	I/I_1	d(Å)	I/I_1	d(Å)	I/I_1	d(Å)	I/I_1
						4.245	5
		3.82	v.w	3.852	29		
		3.56	v.w			3.577	51
		3.29	v.w			3.296	100
3.020	9	3.02	M.S	3.03	100		
				2.834	2		
		2.730	v.w			2.735	62
		2.53	v.w	2.495	7		
2.465	100	2.46	V.S				
		2.32	v.w	2.284	18		
		2.28	v.w				
						2.219	2
2.135	37	2.130	S			2.122	3
		2.090	w	2.094	27		
		2.065	v.w			2.065	31
		1.92	h.v	1.9261	4		
		1.91	w	1.9071	17		
		1.87	w	1.8726	34		
						1.8569	9
		1.820	h.v			1.8253	20
						1.7883	2
1.743	1	1.740	v.w				
		1.645	h.v			1.6481	7
		1.620	h.v	1.6259	2		
		1.600	v.w	1.6040	15		
				1.5821	2		
		1.52	h.v	1.5247	3		
1.510	27	1.503	S	1.5061	2		
		1.433	h.v	1.4405	5		
				1.4168	3		
		$Cu_2O + CaCO_3$					

X-RAY POWDER DIFFRACTION PATTERNS FOR PRECIPITATES FROM MIXED VERSATIC SOLUTIONS: A + 2Cu

Cu_2O JCPDS 5-0667		Precipitate from (Sr+2Cu) Versatic		$SrCO_3$ JCPDS 5-0148	
d(Å)	I/I_1	d(Å)	I/I_1	d(Å)	I/I_1
				4.367	14
				4.207	6
		3.55	M.S	3.535	100
		3.45	M.S	3.450	70
3.02	9	3.01	M	3.014	22
				2.859	5
		2.845	w	2.838	20
		2.60	v.w	2.596	12
		2.555	w	2.554	23
		2.485	M	2.481	34
2.465	100	2.460	V.S	2.458	40
				2.4511	33
				2.2646	5
		2.18	w	2.1831	16
2.135	37	2.13	S		
				2.1035	7
		2.050	M	2.0526	50
		1.980	w	1.9860	26
		1.945	w	1.9489	21
		1.900	M	1.9053	35
				1.8514	3
		1.825	M	1.8253	31
		1.815	v.w	1.8134	16
				1.8023	4
		1.76	h.v	1.7685	7
1.743	1	1.74	h.v		
		1.72	h.v	1.7253	5
		1.660	h.v	1.6684	3
		1.615	h.v	1.6286	4
		1.600	v.w	1.6080	13
				1.5981	3
		1.56	w	1.5676	13
		1.54	v.w	1.5447	11
1.510	27	1.505	S	1.5072	3
		1.470	h.v	1.4782	6
				1.4596	4
		1.450	h.v	1.4551	9
				1.4293	6
		1.425	v.w	1.4246	7
				1.4120	5
				1.4024	4
		Cu_2O + $SrCO_3$			

Cu_2O JCPDS 5-0667		Precipitate from (Mn+2Cu) Versatic		$MnCO_3$ JCPDS 7-268	
d(Å)	I/I_1	d(Å)	I/I_1	d(Å)	I/I_1
		3.65	v.w	3.66	35
3.020	9	3.01	M.S		
		2.845	M	2.84	100
2.465	100	2.45	V.S		
		2.39	h.v	2.39	20
		2.17	h.v	2.172	25
2.135	37	2.125	S		
		2.00	h.v	2.000	25
				1.829	12
		1.768	h.v	1.770	30
		1.760	v.w	1.763	35
1.743	1	1.737	w		
				1.556	2
				1.533	14
1.510	27	1.502	S		
				1.452	2
		Cu_2O + $MnCO_3$		1.423	1
				1.379	10

Cu_2O JCPDS 5-0667		Precipitate from (Cd+2Cu) Versatic		$CdCO_3$ JCPDS 8-456	
d(Å)	I/I_1	d(Å)	I/I_1	d(Å)	I/I_1
		3.77	M.S	3.78	80
3.02	9	3.00	w		
		2.94	S	2.95	100
		2.70	v.w	2.72	4
2.465	100	2.45	V.S	2.46	35
		2.235	v.w	2.245	8
2.135	37	2.125	S		
		2.06	M.S	2.066	25
		1.88	M	1.890	14
		1.835	M	1.838	25
		1.820	M.S	1.825	35
1.743	1	1.735	v.w		
		1.576	M	1.582	16
		1.515	w	1.522	4
1.510	27	1.502	S		
		1.495	w	1.500	12
		1.468	w	1.473	6
		1.415	M	1.423	8
				1.357	2
		Cu_2O + $CdCO_3$			

X-RAY POWDER DIFFRACTION PATTERNS FOR PRECIPITATES FROM MIXED VERSATIC SOLUTIONS: A + Zn + 4Fe

$(Ni,Zn)Fe_2O_4$ JCPDS 8-234		Precipitate from (Ni+Zn+4Fe) Versatic	
d(Å)	I/I_1	d(Å)	I/I_1
4.85	14		
2.966	45	2.97	M.S
2.699	4		
2.533	100	2.535	V.S
2.423	6		
2.100	25	2.095	M
1.715	10	1.71	w
1.617	25	1.61	M.S
1.485	35	1.48	S
1.417	2		
		$(Ni,Zn)Fe_2O_4$	

$MnFe_2O_4$ JCPDS 10-319		Precipitate from (Mn+Zn+4Fe) Versatic		$ZnFe_2O_4$ JCPDS 22-1012	
d(Å)	I/I_1	d(Å)	I/I_1	d(Å)	I/I_1
4.906	20			4.87	7
3.005	35				
		2.96	M.S	2.984	35
2.563	100				
		2.54	V.S	2.543	100
2.450	12				
		2.25	w	2.436	6
2.124	25				
		2.09	v.w	2.109	17
				1.937	1
1.7342	20				
		1.72	v.w	1.723	12
1.6355	35				
		1.62	M.S	1.624	30
1.5031	40	1.503	v.w		
		1.483	S	1.491	35
		1.467	v.w		
1.4376	4				
				1.4270	1
		Mainly $ZnFe_2O_4$			

APPENDIX C

RESULTS FROM KINETIC RUNS

Results presented as follows:

Run number, conditions; temperature, ^{o}C,

Fe - nominal initial iron concentration, M

Ni - nominal initial nickel concentration, M

V - total Versatic concentration, %v/v

S - seed level or type of seed

Kinetic Data, presented as iron, nikel and oxygen equivalent (O.E) concentrations of samples taken at time t minutes.

Below the data, the rate equation fitted to the O.E - time data is presented, in the form

$$O.E = \alpha_0 + \alpha_1 t + \alpha_2 t^2 + \text{sm.terms}$$

the rate at time zero is α_1, therefore t_{α_1}, the t-ratio for α_1 is presented , with R^2, the squared correlation coefficient.

R3 170^{o} Fe0.2 Ni0.1 V33 S=0

tmin	Fe M	Ni M	O.E M
-15	.208	.103	.415
- 7	.207	.101	.411
0	.201	.101	.402
7	.203	.094	.399
20	.174	.069	.330
30	.117	.056	.232
47	.051	.027	.103
60	.015	.010	.032
82	.002	.003	.006
105	.000	.002	.002
120	.000	.000	.000

$O.E = .396 - .0037t + .0001t^2 + sm$

$t_{\alpha_1} = -3.46$ $R^2 = 97.8\%$

R4 170^{o} Fe0.2 Ni0.1 V33 S=0

tmin	Fe M	Ni M	O.E M
-13	.214	.108	.428
- 3	.209	.102	.416
0	.208	.100	.412
12	.129	.059	.253
22	.062	.031	.125
37	.009	.007	.021
52	.001	.003	.005
82	.000	.002	.003
117	.000	.002	.002

$O.E = .346 - .0103t + sm$

$t_{\alpha_1} = -4.91$ $R^2 = 94.9\%$

R5 170^{o} Fe0.2 Ni0.1 V33 S=Al_2O_3

tmin	Fe M	Ni M	O.E M
-15	.205	.099	.407
- 5	.207	.093	.405
0	.204	.089	.395
5	.185	.081	.359
10	.147	.068	.288
17	.115	.054	.226
25	.078	.038	.155
35	.035	.020	.073
52	.011	.008	.024
67	.005	.004	.011
81	.002	.002	.006
94	.002	.002	.004

R6 170^{o} Fe0.2 Ni0.1 V33 S= colloidal graphite

tmin	Fe M	Ni M	O.E M
- 9	.183	.078	.352
- 3	.184	.090	.365
0	.188	.090	.371
4	.184	.082	.359
11	.141	.061	.273
23	.060	.027	.117
40	.006	.005	.015
54	.001	.003	.004
73	.000	.002	.003
91	.000	.002	.003

$O.E = .339 - .0075t + sm$

$t_{\alpha_1} = -3.07$ $R^2 = 95.2\%$

R7 170^{o} Fe0.2 Ni0.1 V33 S= activated carbon

tmin	Fe M	Ni M	O.E M
- 6	.206	.103	.413
0	.205	.092	.399
5	.200	.085	.385
15	.132	.059	.256
25	.103	.048	.203
40	.074	.036	.147
55	.052	.026	.105
75	.035	.017	.069
90	.019	.011	.040
103	.013	.008	.028
110	.009	.006	.020
120	.006	.004	.013

R8 170^{o} Fe0.2 Ni0.1 V33 s= hematite

tmin	Fe M	Ni M	O.E M
- 8	.177	.100	.365
- 4	.170	.094	.348
0	.168	.087	.339
5	.158	.083	.321
15	.136	.074	.279
26	.135	.074	.277
43	.104	.060	.216
55	.078	.048	.165
75	.041	.029	.091
88	.021	.020	.051
103	.008	.014	.026
120	.002	.012	.015

R9 170° Fe0.2 Ni0.1 V33 S= $Ni(OH)_2$

t min	Fe M	Ni M	O.E M
-13	.189	.113	.398
- 5	.186	.099	.378
0	.179	.093	.361
5	.150	.080	.305
10	.093	.057	.197
15	.057	.043	.128
20	.033	.034	.083
25	.020	.029	.058
35	.005	.025	.032
55	.001	.030	.031
75	.001	.036	.036
101	.000	.041	.042

R10 170°Fe0.2 Ni0.1 V33 S= ppt $NiFe_2O_4$

t min	Fe M	Ni M	O.E M
- 7	.183	.098	.373
- 4	.176	.090	.354
0	.134	.066	.267
5	.039	.021	.080
10	.009	.006	.020
15	.001	.002	.003
20	.000	.001	.002
30	.000	.001	.001
45	.000	.001	.001
65	.000	.001	.001

R11 170°Fe0.2 Ni0.1 V33 S= Fe_3O_4

t min	Fe M	Ni M	O.E M
- 7	.194	.098	.389
- 4	.194	.101	.393
0	.193	.099	.388
5	.181	.087	.358
10	.141	.066	.278
15	.089	.045	.178
23	.050	.026	.101
30	.025	.016	.054
52	.003	.003	.008
75	.001	.001	.002

R12 170°Fe0.2 Ni0.1 V33 S= SiO_2

t min	Fe M	Ni M	O.E M
- 7	.194	.102	.394
- 3	.198	.110	.406
0	.197	.111	.406
5	.196	.108	.402
10	.186	.103	.382
15	.195	.102	.395
25	.194	.097	.387
35	.193	.096	.387
52	.185	.097	.374
68	.146	.076	.295
80	.086	.045	.174
95	.035	.021	.073

R13 170°Fe0.2 Ni0.1 V33 S=0

t min	Fe M	Ni M	O.E M
0	.201	.104	.406
5	.201	.099	.400
10	.199	.100	.398
20	.146	.074	.294
30	.073	.036	.147
45	.010	.007	.022
60	.001	.002	.003
70	.000	.002	.002
86	.000	.002	.002
100	.000	.002	.002

O.E = .448 -.0105t + sm

t_{α_1} = -3.02 R^2= 96.6%

R14 170°Fe0.2 Ni0.1 V33 S= sintered $NiFe_2O_4$ (1)

t min	Fe M	Ni M	O.E M
0	.198	.104	.401
5	.201	.100	.402
10	.203	.098	.403
15	.194	.100	.391
25	.181	.096	.368
35	.199	.095	.393
50	.197	.097	.392
71	.190	.092	.377
85	.165	.079	.328
111	.092	.046	.184

R15 170°Fe0.2 Ni0.1 V33 S= sintered etched $NiFe_2O_4$(1)

t min	Fe M	Ni M	O.E M
0	.186	.098	.377
5	.179	.085	.353
10	.176	.082	.346
15	.167	.078	.328
25	.150	.068	.293
35	.116	.055	.228
50	.059	.030	.118
70	.016	.010	.033
87	.004	.004	.010
105	.001	.003	.004

O.E = .375 -.0020t +.0001t^2

t_{α_1} = -2.0 R^2= 99.5%

R16 170°Fe0.2 Ni0.1 V33 S= sintered $NiFe_2O_4$(2)

t min	Fe M	Ni M	O.E M
0	.200	.103	.403
5	.201	.102	.404
10	.201	.102	.404
20	.203	.103	.408
29	.202	.100	.403
40	.199	.099	.397
50	.200	.098	.399
66	.192	.092	.381
86	.136	.064	.268
100	.067	.032	.132

R17 170°Fe0.2 Ni0.1 V33 S=100% ppt $NiFe_2O_2$

t min	Fe M	Ni M	O.E M
0	.208	.109	.420
3.5	.155	.081	.313
6.5	.141	.072	.284
11.5	.118	.062	.239
16.5	.112	.057	.225
24.5	.101	.055	.206
32.5	.088	.048	.179
41	.074	.044	.154
56.5	.063	.038	.133
80	.054	.032	.113

O.E =.380 -.0133t +.0003t^2

t_{α_1} = -4.94 R^2= 94.8%

R18 170°Fe0.2 Ni0.1 V33 S=100%

t min	Fe M	Ni M	O.E M
0	.200	.101	.402
5.75	.106	.051	.210
10.5	.073	.037	.145
15	.060	.029	.119
20	.042	.024	.086
25	.033	.019	.069
31	.024	.015	.051
38	.020	.011	.041
60	.006	.004	.013
92	.001	.001	.002

$O.E = .354 - .0202t + .0004t^2$

$t_{\alpha_1} = -6.43$ $R^2 = 94.3\%$

R19 170°Fe0.2 Ni0.1 V33 S=100%

t min	Fe M	Ni M	O.E M
0	.195	.101	.393
7.5	.100	.051	.201
12.5	.075	.039	.151
17.5	.060	.031	.122
21	.047	.027	.097
26.5	.038	.023	.080
41	.021	.014	.046
59	.011	.007	.024
74	.004	.004	.010
96	.002	.002	.005

$O.E = .357 - .0181t + .0003t^2$

$t_{\alpha_1} = -7.41$ $R^2 = 96.0\%$

R20 170°Fe0.2 Ni0.1 V33 S=100%

t min	Fe M	Ni M	O.E M
0	.200	.099	.399
1	.168	.079	.330
5	.098	.048	.195
10	.057	.031	.116
15	.044	.025	.091
20	.035	.019	.072
26	.026	.014	.053
42	.011	.007	.024

$O.E = .379 - .0401t + .0016t^2$

$t_{\alpha_1} = -8.94$ $R^2 = 98.7\%$

R21 160°Fe0.2 Ni0.1 V33 S=100% w=5mls

t min	Fe M	Ni M	O.E M
0	.193	.093	.382
2	.157	.075	.311
5	.127	.060	.251
8	.105	.051	.209
12	.084	.042	.168
16	.069	.035	.138
20	.059	.030	.119
25	.049	.025	.099
35	.035	.018	.071
51	.020	.011	.040

$O.E = .366 - .0237t + .0007t^2$

$t_{\alpha_1} = -12.73$ $R^2 = 99.2\%$

R22 160°Fe0.2 Ni 0.1 V33 S=100% w=10mls

t min	Fe M	Ni M	O.E M
0	.190	.093	.378
2	.157	.077	.313
5	.128	.061	.254
8	.105	.051	.209
12	.081	.041	.164
16	.065	.033	.131
20	.053	.027	.107
25	.039	.020	.080
35	.022	.012	.046
50	.007	.005	.015

$O.E = .364 - .0232t + .0006t^2$

$t_{\alpha_1} = -15.06$ $R^2 = 99.6\%$

R23 160°Fe0.2 Ni0.1 V33 S=100% w=15mls

t min	Fe M	Ni M	O.E M
0	.194	.094	.384
2.5	.159	.076	.314
5	.131	.062	.258
7.5	.112	.053	.220
12.5	.082	.039	.161
18	.057	.029	.115
24	.038	.020	.078
30	.026	.014	.053
40	.013	.007	.026
55	.003	.002	.007

$O.E = .371 - .0230t + .0005t^2$

$t_{\alpha_1} = -15.87$ $R^2 = 99.6\%$

R24 160° Fe0.2 Ni0.1 V33 S=100% w=5mls

t min	Fe M	Ni M	O.E M
0	.188	.093	.374
2.5	.152	.072	.300
5	.133	.060	.260
7.5	.112	.053	.221
17.5	.060	.030	.120
23	.040	.021	.082
30	.027	.015	.056
40	.017	.009	.034
56	.005	.003	.011

$O.E = .362 - .0219t + .0005t^2$

$t_{\alpha_1} = -15.98$ $R^2 = 99.7\%$

R25 160° Fe0.2 Ni0.1 V33 S=100% 1600 rpm

t min	Fe M	Ni M	O.E M
0	.189	.094	.378
2.5	.151	.073	.300
5	.125	.059	.247
7.5	.101	.048	.200
11	.073	.036	.145
15	.051	.026	.103
20	.031	.017	.064
25	.018	.010	.036
35	.005	.004	.011
50	.001	.001	.003

$O.E = .369 - .0271t + .0007t^2$

$t_{\alpha_1} = -27.59$ $R^2 = 99.9\%$

R26 170°Fe0.2 Ni0.1 V33 S=100%

t min	Fe M	Ni M	O.E M
0	.205	.102	.409
1	.175	.084	.347
2.5	.140	.066	.276
5	.089	.041	.175
10	.032	.017	.066
15	.013	.007	.027
20	.003	.003	.008
25	.001	.002	.004
35	.000	.001	.001
50	.000	.001	.001

$O.E = .385 - .0437 + .0015t^2$

$t_{\alpha_1} = -12.07$ $R^2 = 98.7\%$

R27 170°Fe0.2 Ni0.1 V33 S=100%

t min	Fe M	Ni M	O.E M
0	.195	.095	.397
3	.116	.055	.229
6	.074	.035	.146
10	.045	.022	.090
17	.022	.012	.045
25	.009	.005	.019
30	.005	.003	.011
40	.001	.001	.003

$O.E = .365 - .0427t + .0017t^2$

$t_{\alpha_1} = -7.99$ $R^2 = 98.2\%$

R28 165°Fe0.2 Ni0.1 V33 S=100%

t min	Fe M	Ni M	O.E M
0	.201	.101	.403
1	.182	.088	.361
3	.148	.070	.292
6	.102	.047	.200
10	.054	.026	.107
15	.018	.011	.038
21	.004	.003	.010
44	.000	.001	.001

$O.E = .404 - .0427t + .0015t^2$

$t_{\alpha_1} = -57.34$ $R^2 = 100\%$

R29 160°Fe0.2 Ni0.1 V33 S=100%

t min	Fe M	Ni M	O.E M
0	.205	.103	.411
2	.171	.082	.338
4	.136	.065	.270
8	.099	.046	.194
12	.069	.033	.137
16	.044	.024	.089
23	.023	.014	.049
30	.012	.008	.026
41	.004	.004	.010

$O.E = .402 - .0335t + .0010t^2$

$t_{\alpha_1} = -18.96$ $R^2 = 99.8\%$

R30 155°Fe0.2 Ni0.1 V33 S=100%

t min	Fe M	Ni M	O.E M
0	.198	.102	.399
3	.180	.091	.361
6	.165	.082	.330
10	.139	.070	.279
15	.106	.057	.216
20.3	.083	.045	.170
30	.053	.029	.107
45	.024	.014	.049
67	.006	.005	.015
90	.001	.002	.004

$O.E = .404 - .0149t + .0002t^2$

$t_{\alpha_1} = -30.73$ $R^2 = 99.9\%$

R31 150°Fe0.2 Ni0.1 V33 S=100%

t min F	Fe M	Ni M	O.E M
0	.200	.106	.407
3	.190	.096	.380
6	.178	.089	.356
10	.164	.080	.326
15	.144	.071	.287
20	.112	.061	.229
30	.085	.046	.174
50	.045	.025	.092
70	.021	.013	.045
90	.009	.007	.020

$O.E = .412 - .0103t + .0001t^2$

$t_{\alpha_1} = -14.98$ $R^2 = 99.8\%$

R32 145°Fe0.2 Ni0.1 V33 S=100%

t min	Fe M	Ni M	O.E M
0	.204	.098	.404
3	.183	.087	.362
6	.167	.078	.329
10	.151	.070	.296
15	.132	.061	.258
20	.112	.052	.220
30	.085	.044	.171
50	.059	.030	.118
70	.044	.022	.088
90	.032	.016	.064

$O.E = .399 - .0117t + .0002t^2$

$t_{\alpha_1} = -31.51$ $R^2 = 99.9\%$

R33 140°Fe0.2 Ni0.1 V33 S=100%

t min	Fe M	Ni M	O.E M
0	.200	.102	.402
3	.196	.095	.389
6	.189	.090	.374
10	.177	.088	.353
15	.168	.082	.333
20	.159	.079	.318
30	.133	.072	.272
50	.111	.060	.227
70	.095	.050	.192
90	.081	.043	.165

$O.E = .404 - .0054t + .0000t^2$

$t_{\alpha_1} = -17.14$ $R^2 = 99.9\%$

R34 145°Fe0.2 Ni0.1 V33 S=100%

t min	Fe M	Ni M	O.E M
0	.194	.096	.386
3	.189	.090	.374
6	.175	.085	.348
10	.169	.080	.333
15	.155	.074	.307
20	.147	.068	.289
30	.123	.058	.243
50	.088	.045	.178
70	.064	.033	.129
90	.047	.025	.095

$O.E = .387 - .0057t + .0000t^2$

$t_{\alpha_1} = -18.91$ $R^2 = 99.9\%$

R35 175°Fe0.2 Ni0.1 V33 S=100%

t min	Fe M	Ni M	O.E M
0	.191	.094	.381
2	.119	.055	.233
4	.074	.034	.144
7	.036	.018	.072
11	.010	.006	.021
15	.001	.001	.003
19	.000	.001	.001
23	.000	.000	.001

$O.E = .374 - .0749t + .0052t^2$

$t_{\alpha_1} = -13.76$ $R^2 = 99.7\%$

R36 180°Fe0.2 Ni0.1 V33 S=100%

t min	Fe M	Ni M	O.E M
0	.189	.090	.373
2	.078	.034	.152
4	.031	.015	.062
6	.010	.006	.021
8	.002	.002	.005
10	.000	.001	.001
12	.000	.001	.001

$O.E = .367 - .128t + .0150t^2$

$t_{\alpha_1} = -14.27$ $R^2 = 99.6\%$

R37 160°Fe0.2 Ni0.1 V33 S=200%

t min	Fe M	Ni M	O.E M
0	.196	.093	.387
2.5	.135	.061	.263
5	.081	.038	.159
7.5	.046	.022	.091
10	.025	.013	.050
15	.006	.004	.013
20	.001	.002	.004
25	.001	.001	.002
35	.001	.001	.002
50	.000	.001	.001

$O.E = .389 - .0592t + .0030t^2$

$t_{\alpha_1} = -46.61$ $R^2 = 100\%$

R38 160°Fe0.2 Ni0.1 V33 S=150%

t min	Fe M	Ni M	O.E M
0	.192	.094	.381
2.5	.136	.065	.269
5	.096	.044	.188
7.5	.064	.032	.129
11	.038	.020	.077
15	.018	.011	.038
20	.006	.004	.013
25	.002	.002	.005
32	.001	.001	.002
40	.000	.001	.002

$O.E = .369 - .0415t + .0015t^2$

$t_{\alpha_1} = -20.04$ $R^2 = 99.6\%$

R39 160°Fe0.2 Ni0.1 V33 S=100%

t min	Fe M	Ni M	O.E M
0	.196	.103	.397
3	.175	.087	.349
6	.150	.076	.301
10	.105	.058	.216
15	.070	.040	.145
20	.044	.025	.091
30	.014	.010	.030
50	.001	.003	.005
65	.000	.002	.002

$O.E = .410 - .0234t + .0004t^2$

$t_{\alpha_1} = -18.26$ $R^2 = 99.7\%$

R40 160°Fe0.2 Ni0.1 V33 S=75%

t min	Fe M	Ni M	O.E M
0	.190	.089	.374
3	.160	.073	.313
8	.122	.057	.239
14	.094	.045	.186
21	.071	.034	.141
29	.056	.026	.110
36	.044	.021	.087
43	.034	.017	.068
50	.025	.014	.052
60	.017	.010	.035

$O.E = .366 - .0172t + .0004t^2$

$t_{\alpha_1} = -16.15$ $R^2 = 99.7\%$

R41 160°Fe0.2 Ni0.1 V33 S=50%

t min	Fe M	Ni M	O.E M
0	.197	.094	.389
5	.168	.079	.330
10	.145	.066	.283
15	.127	.058	.249
20	.114	.054	.224
30.5	.093	.043	.183
40	.078	.036	.153
55	.057	.028	.113
70	.040	.020	.080
90	.024	.013	.049

$O.E = .380 - .0101t + .0001t^2$

$t_{\alpha_1} = -13.42$ $R^2 = 99.6\%$

R42 160°Fe0.2 Ni0.1 V33 S=50%

t min	Fe M	Ni M	O.E M
0	.204	.108	.414
3	.196	.099	.394
7	.185	.093	.371
12	.163	.081	.326
20	.123	.066	.250
30	.095	.051	.194
40	.068	.037	.139
55	.044	.025	.091
70	.028	.017	.060
90	.015	.010	.033

$O.E = .424 - .0098t + .0001t^2$

$t_{\alpha_1} = -13.28$ $R^2 = 99.8\%$

R43 160°Fe0.2 Ni0.1 V33 S=0

t min	Fe M	Ni M	O.E M
0	.209	.108	.422
3	.207	.105	.416
8	.211	.105	.422
13	.206	.103	.412
20	.207	.105	.416
30	.204	.104	.411
45	.208	.104	.416
60	.207	.102	.413
76	.206	.103	.412
95	.206	.104	.414
116	.209	.102	.416

Rate = 0

R44 160°Fe0.2 Ni0.1 V33 S=25%

t min	Fe M	Ni M	O.E M
0	.198	.097	.395
5	.186	.087	.366
10	.176	.082	.346
15	.164	.077	.323
20	.159	.074	.312
40	.137	.065	.269
50	.128	.059	.251
72	.110	.050	.215
85	.099	.046	.195

$O.E = .392 - .0053t + .0001t^2$

$t_{\alpha_1} = -14.33$ $R^2 = 99.8\%$

R45 160°Fe0.2 Ni0.1 V25 S=100%			
t min	Fe M	Ni M	O.E M
0	.198	.097	.395
2	.124	.059	.244
4	.078	.036	.152
7	.041	.019	.080
10	.019	.009	.038
13	.012	.005	.024
16	.007	.003	.014
19	.006	.003	.012
22	.005	.003	.011
25	.005	.002	.009

$O.E = .379 - .0678t + .0041t^2$

$t_{\alpha_1} = -14.47$ $R^2 = 99.2\%$

R46 160°Fe0.1 Ni0.05 V25 S=100%			
t min	Fe M	Ni M	O.E M
0	.095	.047	.190
2	.068	.033	.136
4	.047	.024	.094
7	.026	.013	.052
10	.013	.007	.025
13	.005	.003	.011
16	.002	.001	.004
19	.001	.001	.002
22	.000	.001	.001
25	.000	.000	.001

$O.E = .189 - .0285t + .0015t^2$

$t_{\alpha_1} = -53.47$ $R^2 = 100\%$

R47 160°Fe0.2 Ni0.05 V33 S=100%			
t min	Fe M	Ni M	O.E M
0	.184	.049	.324
3	.105	.033	.191
6	.063	.025	.119
10	.040	.018	.078
12.5	.031	.015	.061
15	.026	.013	.051
17.5	.022	.011	.044
20	.019	.010	.038
37	.007	.004	.015
50	.003	.002	.007

$O.E = .290 - .0288t + .0010t^2$

$t_{\alpha_1} = -7.49$ $R^2 = 95.6\%$

R48 160°Fe0.1 Ni0.1 V33 S=100%			
t min	Fe M	Ni M	O.E M
0	.098	.095	.242
2	.092	.087	.225
5	.079	.071	.190
8	.068	.055	.157
12	.057	.047	.133
16	.047	.041	.112
20	.038	.036	.093
25	.030	.033	.079
35	.019	.028	.056
45	.012	.024	.042

$O.E = .245 - .0126t + .0003t^2$

$t_{\alpha_1} = -20.98$ $R^2 = 99.8\%$

R49 160°Fe0.1 Ni0.1 V50 S=100%			
t min	Fe M	Ni M	O.E M
0	.095	.099	.242
2	.094	.095	.237
5	.091	.093	.229
8	.087	.090	.221
12	.084	.087	.213
16	.080	.086	.206
20	.077	.082	.197
25	.074	.081	.192
50	.059	.070	.159
70	.047	.063	.134

$O.E = .242 - .0027t + .0000t^2$

$t_{\alpha_1} = -29.45$ $R^2 = 100\%$

R50 160°Fe0.1 Ni0.05 V33 S=100%			
t min	Fe M	Ni M	O.E M
0	.097	.047	.192
3.5	.072	.034	.142
8	.047	.023	.093
14	.023	.013	.048
20	.010	.007	.022
30	.002	.002	.005
35	.001	.001	.003
40	.001	.001	.002
45	.000	.001	.002

$O.E = .191 - .0153t + .0004t^2$

$t_{\alpha_1} = -77.16$ $R^2 = 100\%$

R51 160°Fe0.2 Ni0.1 V33 S=100%			
t min	Fe M	Ni M	O.E M
0	.193	.094	.384
2	.162	.077	.320
5	.126	.060	.248
8	.093	.045	.185
12	.061	.030	.122
16	.038	.020	.077
20	.022	.012	.045
25	.010	.006	.021
35	.002	.002	.005
50	.000	.001	.001

$O.E = .380 - .0300t + .0008t^2$

$t_{\alpha_1} = -70.46$ $R^2 = 100\%$

R52 160°Fe0.2 Ni0.1 V50 S=100%			
t min	Fe M	Ni M	O.E M
0	.195	.098	.390
3.5	.174	.086	.347
7	.156	.079	.314
10	.146	.072	.291
15.5	.122	.061	.244
20	.104	.053	.210
27	.084	.043	.169
35	.062	.032	.126
52	.031	.018	.065
70	.009	.007	.020

$O.E = .388 - .0112t + .0001t^2$

$t_{\alpha_1} = -41.69$ $R^2 = 100\%$

R53 160°Fe0.2 Ni0.05 V50 S=100%			
t min	Fe M	Ni M	O.E M
0	.190	.051	.336
3	.129	.041	.234
8	.084	.033	.159
13	.062	.027	.121
20	.048	.023	.096
30	.036	.018	.072
40	.029	.015	.058
50	.022	.012	.040
65	.017	.010	.035
75	.013	.008	.028

$O.E = .302 - .0175t + .0004t^2$

$t_{\alpha_1} = -6.65$ $R^2 = 96.1\%$

R54 160°Fe0.1 Ni0.05 V50 S=100%

t min	Fe M	Ni M	O.E M
0	.100	.048	.198
3	.084	.042	.167
8	.069	.036	.140
13	.057	.030	.116
20	.042	.024	.086
30	.026	.017	.056
40	.016	.012	.035
50	.009	.008	.022
65	.004	.006	.011
75	.002	.004	.008

$O.E = .194 - .0072t + .0001t^2$

$t_{\alpha_1} = -22.66$ $R^2 = 99.9\%$

R55 160°Fe0.2 Ni0.1 V45 S=100%

t min	Fe M	Ni M	O.E M
1	.179	.084	.353
3	.174	.085	.347
7	.148	.073	.294
11	.124	.062	.248
15	.102	.051	.204
20	.079	.040	.158
30	.049	.026	.099
40	.028	.015	.058
50	.015	.010	.033
60	.008	.006	.018

$O.E = .378 - .0139t + .0002t^2$

$t_{\alpha_1} = -13.62$ $R^2 = 99.8\%$

R56 160° Fe0.1 Ni0.05 V45 S=100%

t min	Fe M	Ni M	O.E M
0	.100	.046	.196
2.5	.084	.040	.166
5	.072	.036	.144
7.5	.061	.031	.122
11	.049	.026	.100
15	.038	.021	.078
20	.029	.017	.060
27.5	.019	.011	.039
37.5	.009	.007	.021
50	.003	.004	.009

$O.E = .193 - .0109t + .0002t^2$

$t_{\alpha_1} = -29.5$ $R^2 = 99.9\%$

R57 160°Fe0.1 Ni0.1 V33 S=100%

t min	Fe M	Ni M	O.E M
1	.107	.079	.240
4	.086	.072	.201
8	.074	.058	.169
12	.065	.051	.148
17	.060	.049	.139
25	.042	.038	.101
35	.027	.031	.072
45	.019	.028	.056
57	.012	.024	.042
75	.008	.023	.035

$O.E = .237 - .0081t + .0001t^2$

$t_{\alpha_1} = -8.14$ $R^2 = 99.0\%$

Co1 170°Fe0.2 Co0.1 V33 S=0

t min	Fe M	Co M	O.E M
0	.205	.089	.397
5	.195	.086	.378
13	.166	.077	.325
20	.146	.071	.291
30	.111	.057	.223
40	.084	.044	.170
50	.060	.031	.121
65	.034	.019	.069
80	.016	.011	.034
113	.011	.004	.021

$O.E = .404 - .0063t + .0000t^2$

$t_{\alpha_1} = -13.68$ $R^2 = 99.9\%$

Co2 170°Fe0.2 Co0.1 V33 S=Fe_3O_4

t min	Fe M	Co M	O.E M
0	.210	.084	.399
5	.086	.039	.168
10	.035	.023	.076
17	.016	.011	.035
24	.006	.006	.014
34	.001	.005	.007

$O.E = .392 - .0524t + .0024t^2$

$t_{\alpha_1} = -9.16$ $R^2 = 99.3\%$

Co3 170°Fe0.2 Co0.1 V33 S=0

t min	Fe M	Co M	O.E M
0	.211	.091	.407
5	.205	.091	.399
10	.205	.092	.399
20	.203	.092	.396
30	.198	.091	.388
47	.198	.091	.387
65	.192	.090	.378
80	.189	.090	.373
100	.183	.089	.363
120	.174	.087	.348

$O.E = .405 - .0007t + .0000t^2$

$t_{\alpha_1} = -4.62$ $R^2 = 99.2\%$

Co4 170°Fe0.2 Co0.1 V33 S=$CoFe_2O_4$

t min	Fe M	Co M	O.E M
0	.207	.093	.403
5	.200	.089	.390
10	.201	.088	.390
20	.188	.084	.366
32	.176	.080	.344
45	.161	.075	.316
65	.142	.066	.279
105	.110	.050	.214
128	.084	.042	.167

$O.E = .404 - .0020t + .0000t^2$

$t_{\alpha_1} = -7.28$ $R^2 = 99.8\%$

Co5 170°Fe0.2 Co0.1 V33 S=Fe_3O_4

t min	Fe M	Co M	O.E M
0	.210	.089	.404
5	.209	.089	.402
12.5	.208	.087	.399
25	.202	.081	.384
45	.187	.077	.356
84	.114	.058	.228
100	.024	.017	.052
110	.014	.013	.034
126	.017	.012	.038
142	.015	.012	.034

APPENDIX D

PRECIPITATION OF COBALT FERRITE

Five kinetic runs, Co1, Co2, Co3, Co4 and Co5 were made on iron cobalt mixtures, using the experimental procedure described in section 6.4.2. The experimental conditions used were 170°C, 0.2M Fe and 0.1M Co in 33% Versatic in Escaid. The objective of these runs was to investigate the feasibility of using hydrolytic stripping to deposit an even layer of cobalt ferrite onto acicular particles of magnetite, Fe_3O_4, used in the manufacture of recording tapes.

The 'oxygen equivalent' concentration-time curves for runs Co3, Co4 and Co5 are shown in Figure D. Run Co3 was unseeded, and had a very slow rate, roughly comparable to the rate of precipitation of nickel ferrite in the absence of seed at 170°C. Run Co4 was seeded with homogeneously precipitated cobalt ferrite. The precipitation rate was far slower than the rate of the nickel system under similar conditions. However, these runs were made before it was recognised that the age of all the organic solutions had a significant effect on the rate of precipitation, so the calcium-Versatic used to prepare the iron-Versatic was several days old, and the cobalt-Versatic solution was 18 months old. Much faster rates would probably result from using fresh solutions.

Run Co5 was seeded with the acicular magnetite. There appeared to be an induction period of about 15 minutes before precipitation started. The organic solutions used for this run were also old, and faster rates would probably be obtained if fresh solutions were used.

Cobalt ferrite only improves the performance of magnetite in recording tape if it is coated as a thin, even layer. The material prepared did not conform to this specification, because cobalt did not remain at the surface, but diffused into the magnetite lattice. Therefore no further work was done on cobalt-iron mixtures.

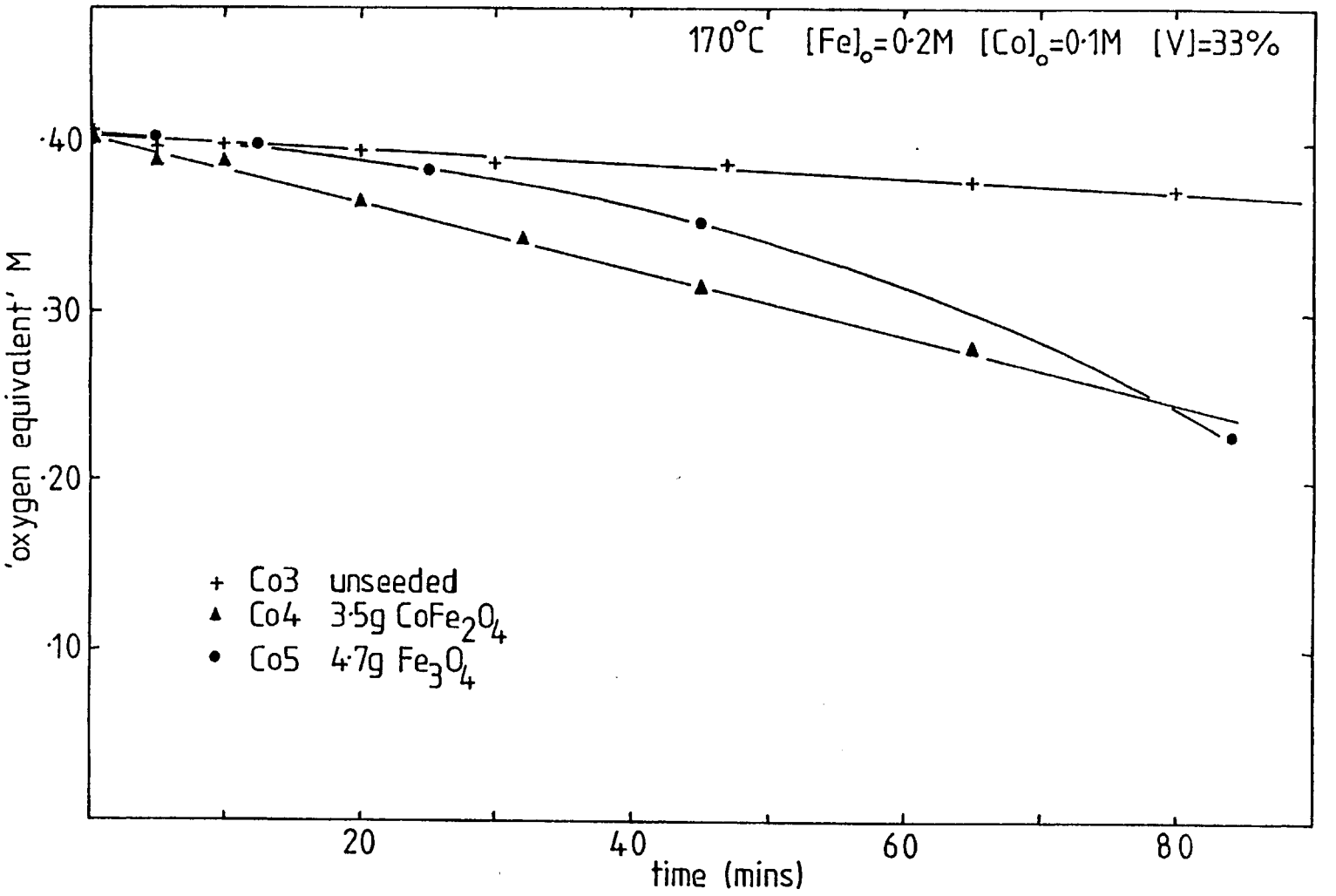


Figure D Precipitation of Cobalt Ferrite Under Different Seeding Conditions

APPENDIX E

ESTIMATE OF THICKNESS OF FERRITE LAYER PRECIPITATED DURING SEEDED KINETIC RUN

Nickel Ferrite: unit cell $Ni_8Fe_{16}O_{32}$

$$a = 8.325\text{Å}$$

$$a^2 = 69.31\times10^{-20}\,m^2$$

Surface area of 4.69g seed = $307\,m^2$

At surface there are $\dfrac{307}{69.31\times10^{-20}} = 4.43\times10^{20}$ unit cells of ferrite

Assume that there is no change in surface area during a run, and that a coherent, uniform layer is deposited.
In runs where there are 200mls of organic solution, with 0.2M Fe and 0.1M Ni, complete hydrolysis precipitates

$$0.2 \times 0.2 \times 6.022\times10^{23} = 2.4\times10^{22} \text{ ions Fe}$$

$$\text{and } 0.1 \times 0.2 \times 6.022\times10^{23} = 1.2\times10^{22} \text{ ions Ni}$$

Therefore deposit $\dfrac{1.2\times10^{22}}{8} = 1.5\times10^{21}$ unit cells $Ni_8Fe_{16}O_{32}$

Thickness of deposit $= \dfrac{1.5\times10^{21}}{4.43\times10^{20}} = 3.39$ unit cells

$= 28.22\text{Å}$

APPENDIX F

ESTIMATE OF THE RADIUS OF SEED PARTICLES

Density of Nickel Ferrite

$Ni_8Fe_{16}O_{32}$: MWt = 1875.23g

Volume of unit cell = $(8.325 \times 10^{-10})^3 = 5.77 \times 10^{-28} m^3$

Volume of 1 mole $Ni_8Fe_{16}O_{32} = 5.77 \times 10^{-28} \times 6.022 \times 10^{23}$

Therefore density $= \dfrac{1875.23}{5.77 \times 10^{-28} \times 6.022 \times 10^{23}} = 5.40 \times 10^6 g/m^3$

Assume that seed is composed of spheres, radius r

4.69g seed has volume $\dfrac{4.69}{5.40 \times 10^6} = 8.69 \times 10^{-7} m^3$

$$n \frac{4}{3} \pi r^3 = 8.69 \times 10^{-7}$$

$$n\, 4 \pi r^2 = 307 \qquad \text{from surface area data}$$

Therefore $r = \dfrac{3 \times 8.69 \times 10^{-7}}{307}$

$= \underline{8.49 \times 10^{-9} m}$

If the seed is composed of uniform spheres, these have a radius of 85Å

REFERENCES

1. BURKIN, A.R., RICHARDSON, F.D.
Powder Metall. 10 (1967) p 33

2. BURKIN, A.R., BURGESS, J.E.A.
'Production of metal powders by reduction of loaded extractants with hydrogen' Proc. Int. Symp. Solv. Extraction in Metal. Processes, Antwerp, May 1972 pp 49-52

3. BURKIN, A.R., BURGESS, J.E.A.
'Production of high purity metal powders by direct pressure reduction of loaded extractants' Proc. First Ann. Meeting Can. Hydrometallurgists 1977 pp 51-58

4. THORSEN, G., MONHEMIUS, A.J.
'Precipitation of metal oxides from loaded carboxylic acid extractants by hydrolytic stripping' TMS Paper A-79-12, A.I.M.E Annual Meeting, New Orleans(1979)

5. KIRK-OTHMER
'Encyclopedia of Chemical Technology' 2nd Ed. (1965) John Wiley-Interscience Vol 6, pp 265-281

6. MONHEMIUS, A.J., THORSEN, G.
'The application of hydrolytic stripping to the iron problem in hydrometallurgy' I.S.E.C. '80. Vol 3 pp 80-91 Liege, Belgium (1980)

7. CRAIGEN, W.J.S., RITCEY, G.M., LUCAS, B.H.
'By-product iron - discard or recover' C.I.M. Bulletin 68 Apr (1975) pp 70-83

8. GORDON, A.R
'Improved use of raw material, human and energy resources in the extraction of zinc' Advances in Extractive Metallurgy I.M.M. London (1977) pp 155-160

9. PAMMENTER, R.V., HAIGH, C.J.
'Improved metal recovery with the low contaminant Jarosite process' Extraction Metallurgy '81 I.M.M. London(1981) pp141-148

10. THORNHILL, P.G., WIGSTOL, E., VAN WEERT, G.
'The Falconbridge Matte Leach process' J. Metals 23 (7) July (1971) pp 13-18

11. COOK, L.F., SZMOKALUK, W.W.
'Refining of cobalt and nickel sulphate solutions by solvent extraction using D2EHPA' Proc. Int'l Solvent Extraction Conf. The Hague (1971) p 451

12. TEIXEIRA, L.A.C.
'Kinetics of precipitation of ferric oxide from a carboxylic acid extractant' Ph.D. thesis, Imperial College, London (1982)

13. THORSEN, G., SVENDSEN, H.F., GRISLINGÅS, A.
'The integrated organic leaching solvent extraction operation in hydrometallurgy' Proc. NATO Advanced Research Institute on Hydrometallurgical Process Fundamentals, Cambridge (1982)

14. MÜHL, P., GLOE, K., SARADSHOW, M., GINDIN, L.M., KHOLKIN, A.I., IVANOVA, S.N.
'The preparation of high purity iron compounds by solvent extraction with aliphatic monocarboxylic acids' Hydrometallurgy 1 (1975) pp 113-121

15. DOYLE, F.M.
'The hydrolytic stripping of iron-loaded liquid cation exchangers at 100°C' M.Sc. Report Imperial College, London (1979)

16. THORSEN, G., MONHEMIUS, A.J.
U.S. Patent 4,282,189

17. FINAR, I.L.
'Organic Chemistry' Vol 1, 6th Ed, pp233-245 Longman (1976)

18. FLETT, D.S., JAYCOCK, M.J.
'Extraction of metals by carboxylic acids', Ion-Exchange and Solvent Extraction Vol 3, Ed Marinsky, J.A., Marcus, Y. pp 1-50 Marcel Dekker Inc (1973)

19. LEGER, A.E., HAINES, R.L., HUBLEY, C.E, HYDE, J.C., SHEFFER, J.
'The structure of aluminium di- and tri-soaps' Canad. J. Chem. 35 (1957) pp 799-816

20. FLETCHER, A.W., WILSON, J.C.
'Naphthenic acid as a liquid-liquid extraction reagent for metals' Trans. I.M.M. 70 1960/61 pp 355-366

21. FLETCHER, A.W., FLETT, D.S., WILSON, J.C.
'Solvent extraction of ferric iron by a carboxylic acid' Trans. I.M.M. 73 (1964) pp 765-777

22. GINDIN, L.M., BOBIKOV, P.I., KOUBA, E.F., BUGAEVA, A.V.
'Separation of metals by exchange extraction with aliphatic acids in alkali' Russ. J. Inorg. Chem. 5 no 8 (1960) pp 906-910

23. GINDIN,L.M., BOBIKOV, P.I., KOUBA, E.F., BUGAEVA, A.V.
Russ. J. Inorg. Chem. 6 no 12 (1961) pp 1412-1416

24. GINDIN, L.M., BOBIKOV, P.I., KOUBA, E.F., BUGAEVA, A.V.
Russ. J. Inorg. Chem. 5 no 10 (1960) pp 1146-1149

25. SPITZER, E.L.T.M., RADDER, J., MUYS, H.M.
'Extraction tests on aqueous metal sulphate solutions using 'Versatic'9' Trans. I.M.M. C75 (1966) pp 265-266

26. MIKHAILICHENKO, A.I., KLIMENKO, M.A., BULGAKOVA, V.B.
'Extraction of the alkaline earth elements and magnesium by aliphatic monocarboxylic acids' Russ. J. Inorg. Chem. 17 (3) (1972) pp 400-403

27. MÜHL, P., GINDIN, L.M., KHOLKIN, A.I., GLOE, K.,LUBOSHNIKOVA, K.S.
'Investigations on the mechanism of Fe(III) extraction by n-caprylic acid' Proc. Int. Solv. Extr. Conf. 1974 Vol 2 S1717-1728

28. MÜHL, P., GLOE, K., FISCHER, C., ZIEGEBALG, S., HOFFMANN, H.
'The application of liquid-liquid extraction for the separation of iron during the production of alumina' Hydrometall. 5 (1980) pp 161-178

29. VAN DER ZEEUW, A.J.
'Purification of zinc calcine leach solutions by exchange extraction with the zinc salt of 'Versatic' acid' Hydrometall. 2 (1976/77) pp 275-284

30. WOOD, J.A., RYCROFT, C.P.
Colloid Polymer Science 253 (1975) pp 311-314

31. FLETCHER, A.W., FLETT, D.S.
'Carboxylic acids as reagents for the solvent extraction of metals' Proc. Int. Conf. Solv. Extr. of Metals, Harwell, (1965) (ed. Jenkins, I., McKay, H.A.C.) MacMillan, London(1966) p 359

32. ASHBROOK, A.W.
'A review of the use of carboxylic acids as extractants for the separation of metals in commercial liquid-liquid extraction operations' Miner. Sci. Engng 5 no 3, July (1973) pp 169-180

33. RICE, N.M.
'Recent developments and potential uses for carboxylic acid extractants - a review' Hydrometall. 3 (1978) pp 111-133

34. FLETT, D.S.
'Solvent extraction in extractive metallurgy' Miner. Sci. Engng. 2 (3) (1970) p 17

35. FLETT, D.S.
'A survey of reagents used for solvent extraction in extractive metallurgy' Proc. Int. Symp. Solv. Extr. in Metal. Processes, Antwerp (1972) pp 19-26

36. FLETT, D.S.
'A selectivity reversal in solvent extraction' Nature 200 (1963) pp 465-466

37. HAFFENDEN, W.J., LAWSON, G.J.
'Effect of ammonium salts on the sovent extraction of metal ions with liquid cation exchangers' Advances in Extractive Metallurgy I.M.M. (1967) London pp 678-685

38. LAWSON, G.J., PRIDDEN, B.J.
'Extraction of copper, nickel and cobalt with Versatic acid from ammonia solution' Proc. Int. Solv. Extr. Conf. (1974) pp 711-723

39. MÜHL, P., GLOE, K., SCHOLZE, H., KHOLKIN, A.I., GINDIN, L.M., LUBOSHNIKOVA, K.S.
Talanta 26 (1979) pp 227-231

40. KHOLKIN, A.I., GLOE, K., LUBOSHNIKOVA, K.S., MÜHL, P., GINDIN, L.M., KLUGE, V.
'On the coextraction of nickel and iron in the systems with monocarboxylic acids' Izv. Sib. Ord. Akad. Nauk. S.S.S.R. Ser. Khim. Nauk. (1981) 3 pp 113-117 Chem Abstr. No 95:139502v

41. VAN DER ZEEUW, A.J.
'Metals extraction with carboxylic acids,I. Composition of complexes with nickel, cobalt(II) and iron(III)' Hydrometall. 4 (1979) pp 21-37

42. VAN DER ZEEUW, A.J.
'Metals extraction with carboxylic acid, II. Effect of temperature on the extraction of Cu, Ni, Co(II), Zn, Fe(III) and Co(III). Hydrometall. 4 (1979) pp 39-50

43. GRADON, D.P.
'The absorption spectra of complex salts - IV. Cupric alkanoates' J. Inorg. Nucl. Chem. 17 (1961) p 222

44. TANAKA, M., NAKASUKA, N., SASANE, S.
'Extraction of nickel with capric acid' J. Inorg. Nucl. Chem. 31 (1969) pp 2591-2597

45. HAFFENDEN, W.J., LAWSON, G.J.
'The solvent extraction of Cu(II) with pivalic acid'
J. Inorg. Nucl. Chem. 29 (1967) pp1133-1137

46. TANAKA, M., NÜNOMI, T.
'Extraction of copper(II) with capric acid dissolved in benzene'
J. Inorg. Nucl. Chem. 27 (1965) pp431-437

47. JAYCOCK, M.J., JONES, A.D., ROBINSON, C.
J. Inorg. Nucl. Chem. 36 (1974) pp 887-898

48. BARTECKI, A., APOSTOLUK, W.
'The extraction of Fe(III) from ammonium chloride solutions with capric acid' Hydrometall. 5 (1980) pp367-379

49. STEFANAKIS, M.I.
'Solvent extraction of iron from aluminium nitrate solutions'
Ph.D. thesis, Imperial College, London (1982)

50. TIKHOMIROV, V.B.
'The mechanism of the extraction of colloidally precipitated iron hydroxide by fatty acids' Proc. Acad. Sci. USSR Phys. Chem. Sect. 139 (1961) pp651-652

51. TANAKA, M., NAKASUKA, N., YAMADA, H.
'Extraction of aluminium with capric acid' J. Inorg. Nucl. Chem. 32 (1970) pp 2791-2793

52. McDOWELL, W.J., HARMON, H.D.
J. Inorg. Nucl. Chem. 31 (1969) pp 1473-1485

53. COTTON, F.A., WILKINSON, G.
'Advanced Inorganic Chemistry' 4th Ed.(1980) Wiley-Interscience New York

54. MONHEMIUS, A.J.
'Precipitation diagrams for metal hydroxides, sulphides, arsenates and phosphates' Trans. I.M.M. 86 (1977) C202-206

55. MONHEMIUS, A.J.
'Hydrometallurgical processing of complex materials' Chemistry and Industry 12 (1981) pp 410-420

56. DIAS, M.J.P.
'A statistical approach to the precipitation of iron as Jarosite' Ph.D. thesis, Imperial College, London (1979)

57. AGATZINI, S.
'A statistical approach to the precipitation of iron as "goethite" ' Ph.D. thesis, Imperial College, London (1981)

58. BERNAL, J.D., DASGUPTA, D.R., MacKAY, A.L.
'The oxides and hydroxides of iron and their structural inter-relationships' Clay Minerals Bull. 4 21 (1959) pp 15-30

59. DUTRIZAC, J.E.
'The physical chemistry of iron precipitation in the zinc industry' Lead-Zinc-Tin '80 TMS-AIME World Symposium on Metallurgy and Environment Control. Ed. Cigan, Mackey and O'Keefe (1980) pp 532-564

60. McANDREW, R.T., WANG, S.S., BROWN, W.R.
'Precipitation of iron compounds from sulphuric acid leach solutions' C.I.M. Bull. 68 (753) (1975) pp 101-110

61. ROBINS, R.G.
'Hydrothermal precipitation in solutions of thorium nitrate, ferric nitrate and aluminium nitrate' J. Inorg. Nucl. Chem. 29 (1967) pp 431-435

62. CHRISTENSEN, A.M.
'Hydrothermal preparation of goethite and hematite from amorphous iron(III) hydroxide' Acta Chemica Scandinavica 22 (1968) pp 1487-1490

63. SMITH, F.G., KIDD, D.J.
'Hematite-goethite relations in neutral and alkaline solutions under pressure' Amer. Miner. 34 (1949) pp 403-412

64. LANGMUIR, D.
'Particle size effect on the reaction goethite=hematite+water' Amer. J. Sci. 271 (1971) pp 147-156

65. VAN DER KRAAN, A.M., MEDEMA, J.
'The nature of fine particles of αFeOOH' J. Inorg. Nucl. Chem. 31 (1969) pp 2039-2044

66. COLLEPARDI, M., MASSIDDA, L., ROSSI, G.
'Aging of iron oxide gels' Trans. I.M.M. 81 (1972) pp C43-46

67. COLLEPARDI, M., MASSIDDA, L., ROSSI, G.
'Effect of pH and salt additions on aging of ferric oxide gels' Trans. I.M.M. 82 (1973) pp C88-91

68. ATKINSON, R.J., POSNER, A.M., QUIRK, J.P.
'Crystal nucleation and growth in hydrolysing iron(III) chloride solutions' Clay and Clay Minerals 25 (1977) pp 49-56

69. MATIJEVÍC, E., BELL, A., BRACE, R., McFADYEN, P.
'Formation and surface characteristics of hydrous metal oxide sols' J.Electrochem. Soc. 120 (1977) pp 893-899

70. MATIJEVÍC, E., SAPIESZKO, R.S., MELVILLE, J.B.
'Ferric hydrous oxide sols -1. Monodispersed iron(III) sulphate particles' J. Coll. Interface Sci. 50 (1975) pp 567-581

71. DUTRIZAC, J.E.
'The behaviour of impurities during jarosite precipitation' Proc. NATO Advanced Research Institute on Hydrometallurgical Process Fundamentals, Cambridge (1982)

72. HAIGH, C.J.
'The hydrolysis of iron in acid solutions' Proc. Aust. Inst. Min. Met. Sept (1967) pp 49-56

73. DAVEY, P.T., SCOTT, T.R.
'Formation of βFeOOH and αFe_2O_3 in the goethite process' Trans. I.M.M. (1975) C83-86

74. DELVAUX, R.
'Lixivation de minerais de zinc grilles selon le procede goethite' Metallurgie XVI 3(1976) pp 154-163

75. DAVEY, P.T., SCOTT, T.R.
'Removal of iron from leach liquors by the 'goethite' process' Hydrometall. 2 (1976) pp 25-33

76. DOUSMA, J., DE BRUYN, P.L.
'Hydrolysis-precipitation studies of iron solutions,I. Model for hydrolysis and precipitation from Fe(III) nitrate solutions' J. Colloid and Interface Sci. 56 (1976) pp 527-539

77. SAPIESZKO, R.S., PATEL, R.C., MATIJEVÍC, E.
'Ferric hydrous oxide sols -2. Thermodynamics of aqueous hydroxo and sulphato ferric complexes' J. Phys. Chem. 81 (1977) pp 1061-1068

78. KIYAMA, M., TAKADA, T.
'The hydrolysis of ferric complexes. Magnetic and spectrophotometric studies of aqueous solutions of ferric salts' Bull. Chem. Soc. Japan 46 (1973) pp 1680-1686

79. DOUSMA, J., DE BRUYN, P.L.
'Hydrolysis-precipitation studies of iron solutions, II. Aging studies and the model for precipitation from Fe(III) nitrate solutions' J. Colloid and Interface Sci. 64 (1978) pp 154-170

80. FRYER, J.R., GILDAWIE, A.M., PATERSON, R.
'Polymeric film precursors in the homogeneous crystallisation of some metal oxides' Nature 252 (1974) pp 574-576

81. MURPHY, P.J., POSNER, A.M., QUIRK, J.P.
'Characterisation of hydrolysed ferric iron solutions' J. Colloid and Interface Sci. 56 (1976) pp 312-319

82. FASIKA, E.J.
'Structural aspects of the oxides and oxyhydroxides of iron' Corrosion Science 7 (1967) pp 833-839

83. WELLS, A.F.
'Structural Inorganic Chemistry' 3rd Ed. Oxford University Press (1962)

84. HAPPEL, J., HNATOW, M., BAJARS, L.
'Base Metal Oxide Catalysts' Marcel Dekker (1977)

85. RICHES, E.E.
'Ferrites: a review of materials and applications' Mills and Boon, London (1972)

86. SNELLING, E.C.
'Soft Ferrites' Iliffe Books Ltd, London (1969)

87. KREBS, H.
'Fundamentals of Inorganic Crystal Chemistry' McGraw-Hill, London (1968)

88. KIRK-OTHMER
'Encyclopedia of Chemical Technology' 2nd Ed. (1965) John Wiley-Interscience Vol 8 p881

89. SMIT, J. (Ed.)
'Magnetic Properties of Materials' McGraw-Hill (1971) pp 20-58

90. CULLITY, B.D.
'Introduction to Magnetic Materials' Addison-Wesley (1972)

91. TARASEVICH, M.R., EFREHOV, B.N.
S. Tratti (Ed.) 'Electrodes of Conductive Metallic Oxides' Pt A Elsevier Scientific Publishing Co (1980)

92. GILLOT, B., BOUTON, F.
'Correlation between IR spectra, X-ray diffraction and distribution of structural vacancies in $Fe^{3+}[\square_\delta Fe^{2+}_{1-3\delta} Fe^{3+}_{(1-x)2\delta} M^{3+}_{x}]O^{2-}_{4}$ type spinels'
J. of Solid State Chemistry 32 (1980) pp 303-310

93. WEAST, R.C. (Ed.)
'CRC Handbook of Chemistry and Physics' 59th Ed. (1978/79)

94. LAGOS, G.
Private communication, Imperial College, London

95. TSEUNG, A.C.C., GOLDSTEIN, J.R.
'The preparation of ultrafine cobalt-iron oxides' J. Materials Sci. 7 (1972) pp 1383-1390

96. SCHUELE, W.J., DEETSCREEK, V.D.
'Preparation, growth and study of ultrafine ferrite particles' J. Appl. Physics 32 (1961) pp 235S-236S

97. HAN, K.N., NARITA, E., LAWSON, F.
'The coprecipitation behaviour of Co(II) and Ni(II) with Fe(III), Cr(III) and Al(III) from aqueous ammoniacal solutions' Hydrometall. 8 (1982) pp 365-377

98. DUCKWORTH, W.E.
'Statistical Techniques in Technological Research' (1968) Methuen and Co. London

99. VOGEL, A.I.
'A Textbook of Quantitative Inorganic Analysis' 3rd Ed. (1961) Longmans, London

100. PERKIN-ELMER
'Analytical Methods for Atomic Absorption Spectrophotometry - Standard Conditions' (1973) P.E. Corp. Norwalk, Connecticut, USA

101. 'Powder Diffraction File of Inorganic Compounds' Publ. Joint Committee on Powder Diffraction Standards, Pennsylvania, USA (1981)

102. BOX, G.E.P., HUNTER, W.G., HUNTER, J.S.
'Statistics for Experimenters' John Wiley and Sons, New York (1978)

103. DAVIES, O.L. (Ed.)
'The Design and Analysis of Industrial Experiments' 2nd Ed. Longman Group Ltd. (1956)

104. GAY, P.
'The Crystalline State' Oliver and Boyd, Edinburgh (1972)

105. PLACKETT, P.L., BURMAN, J.P.
'The design of optimum multifactorial experiments' Biometrika 33 (1946) pp 305-325

106. RYAN, T., JOINER, B., RYAN, B.
'Minitab Student Handbook' Duxbury Press (1976)

107. NAKAMOTO, K.
'Infrared Spectra' 'Coordination Chemistry' A.E. Martell (Ed.) Vol 1, A.C.S Monograph , Van Nostrand Reinhold Co. (1971)

108. COLTHUP, N.B., DALY, L.H., WIBERLY, S.E.
'Introduction to Infrared and Raman Spectroscopy' 2nd Ed. Academic Press (1975)

109. CRABTREE, H.E., RICE, N.M.
'A spectrophotometric study of the organic phase complexes formed in the extraction of cobalt(II) with carboxylic acids' Proc. Int. Solv. Extr. Conf. (1974) Vol I pp 791-822

110. NAKAMOTO, K.
'Infrared Spectra of Inorganic and Coordination Compounds' 2nd Ed. (1970) Wiley-Interscience

111. WILKINSON, F.
'Chemical Kinetics and Reaction Mechanisms' Van Nostrand Reinhold, London (1980) Ch 8

ACKNOWLEDGEMENTS

I would like to sincerely thank my supervisor, Dr A. J. Monhemius for his help, advice and interest in this work over the past few years.

I am also grateful to Prof. A. R. Burkin for his interest and helpful ideas.

I wish to thank Mr J. E. A. Burgess for technical assistance with all aspects of the experimental work, and Mr G. Briers for help with electron microscopy.

I am indebted to the Science and Engineering Research Council for a research award, to the Institution of Mining and Metallurgy for a Bosworth Smith Trust Fund Award, and to Rio Tinto Zinc for a special bursary.

I have enjoyed working in the Hydrometallurgy Group, and would like to thank all members, past and present, for their frienship. Particular thanks are due to Luiz Teixeira, for the autoclave, help and many useful discussions, and to David Brandt and Bas Sajik.

Gorgonzola and Chesney deserve a special mention for hindering the rate of progress. It must be said that Chesney redeemed himself by overseeing the production of this thesis, and now is a very knowledgeable cat.

Finally, I am very grateful to my mother, for proof reading, and to Des for help with Chapter 9, proof reading and general comments. I would like to thank all of my family and friends for their encouragement, especially during the last few months.